DEVELOPING AN INTEGRATED OMICS TECHNOLOGY TO ELUCIDATE BIOLOGICAL MECHANISM OF METAL EXPOSURE

Eugenio Galano

Dottorato in Scienze Biotecnologiche – XXV ciclo
Indirizzo Biotecnologie Industriali e Molecolari
Università di Napoli Federico II

Dottorato in Scienze Biotecnologiche – XXV ciclo
Indirizzo Biotecnologie Industriali e Molecolari
Università di Napoli Federico II

DEVELOPING AN INTEGRATED OMICS TECHNOLOGY TO ELUCIDATE BIOLOGICAL MECHANISM OF METAL EXPOSURE

Eugenio Galano

Dottorando: Eugenio Galano

Relatore: Dott.sa Angela Amoresano

Coordinatore: Prof. Giovanni Sannia

L'uomo saggio non è colui che ha imparato, ma chi rimane aperto al flusso della verità e della conoscenza, con la consapevolezza che il traguardo raggiunto della sapienza non sarà di certo l'arrivo, ma il viaggio.

Gabriele Rolla

INDEX

Summary

About 30% of all annotated proteins reported in the major databases (PDB, NCBInr, and Uniprot) results to be associated with a metal. In some cases the functions of these proteins strongly depend by the interaction with the right metal.
Metal ions, associated with macromolecules, are utilized by biological systems in fundamental processes; therefore cytosolic concentrations of metals are tightly controlled. For a complete characterization of cell chemistry, the understanding of mechanisms by which a metal is sensed, stored, or incorporated as a cofactor is required.
Some metals, such as Ca, Co, Cr, Cu, Fe, K, Mg, Mn, Na, Ni and Zn, are essential, in fact they serve as micronutrients and are used for redox-processes, to stabilize molecules through electrostatic interactions, as components of various enzymes and for regulation of osmotic pressure. Many other metals, in particular heavy metals, have no biological role (e.g. Ag, Al, Cd, Au, Pb and Hg), and are nonessential and potentially toxic to mammalians and microorganisms.
Selenium is a crucial micronutrient for human health. In human Se is a component of several important selenoproteins and enzymes required for different functions, such as antioxidant defense and reduction of inflammation. Several organisms possess the ability to metabolize Se into protein by a specific pathway dedicated to the biosynthesis of proteins which contain the aminoacid selenocysteine (Sec, U), or by a non-specific mechanism.
The improvements in high-throughput technology, has led to born of a large number of new "omics" disciplines with the aim to expand the knowledge acquired. Thus "metallomics" was born; this term, coined by Haraguchi, denotes the ensemble of research activities related to metals of biological interest.
However detailed knowledge of interaction between metals and proteins within organisms is fundamental to prevent diseases related to heavy metals pollutions, or to use some detoxification process to produce more bio-available forms of seleno-containing compounds.
This PhD thesis targeted the characterization of metals involved in relevant biological processes by metallomics and proteomics approaches. Thus the following systems of biotechnological interest have been analyzed in this study: **1) *Escherichia coli* used as model organism for a study of the effects of heavy-metals contamination.** The development of an integrated metallomics-proteomics approach for the investigation of the effects of cadmium exposure on *Escherichia coli* is reported. **2) HRCE (Human Renal Cortical Epithelial) cells for an investigation of the effects to cadmium and lead exposure.** Apoptotic pathway was demonstrated to be induced by either cadmium or lead, with the latter the more toxic for human primary renal cells. **3) *Lactobacillus reuteri* Lb2 BM-DSM 16143 to study the incorporation of selenium into selenocysteines by an integrated ICP-MS based approach.** Characterization of the ability of this probiotic microorganism to recover high concentration of selenium and convert them into selenocysteines residues, within the primary sequence of some proteins, is reported, representing an additional innovative approach to solve human selenium deficiency.

Riassunto

Il rapido aumento di genomi completamente sequenziati, unito ai progressi tecnologici di strumentazioni definite “ad alta produttività”, ha portato alla nascita di nuove discipline "omiche" che si affiancano alle più ben conosciute genomica e proteomica, con l'obiettivo di ampliare le informazioni acquisibili.
Il termine “metalloma” fu coniato dal prof. R.J.P. Williams nel 2001, il quale lo definì “una distribuzione di elementi, un equilibrio di concentrazioni di ioni metallici, il contenuto elementare in un dato compartimento cellulare, cellula o organismo” [1]. Il significato di metalloma fu in seguito esteso all’interezza di tutte le specie metalliche e metalloidi presenti in un tipo di cellula o tessuto [2]. Di conseguenza il termine “metallomica”, inteso come quella disciplina che studia il metalloma, indicò l'insieme delle attività di ricerca riguardanti metalli d’interesse biologico, comprese le interazioni e le connessioni funzionali di ioni metallici e specie metalliche [3].
Il riconoscimento dell'importanza dei metalli nei sistemi biologici e importanti progressi nella strumentazione analitica ha portato alla nascita della nuova area di ricerca chiamata *metalloproteomica,* definita come l’insieme di tutte le proteine ottenute da un determinato genoma che possono legare uno o più metalli [4]. La metalloproteomica rappresenta, infatti, un ampliamento delle conoscenze acquisibili con la proteomica tradizionale. Infatti, tale integrazione ha permesso la creazione di approcci innovativi e nuove strategie analitiche mirate allo studio di specie chimiche metalliche legate a proteine.
Almeno un terzo di tutte le proteine annotate e riportate nei principali database (PDB, NCBInr, UniProt) è associato con un metallo [4]. In alcuni casi, la funzione di queste proteine, chiamate anche “metalloproteine”, ha bisogno del corretto ione metallico come co-fattore [5]. Metalli di transizione come ad esempio Cu, Fe, Zn, con i loro stati di ossidazione multipli, sono i metalli che più abbondantemente si ritrovano associati con proteine.
I metalli rappresentano circa il 75% degli elementi noti; derivano sia da fonti naturali che artificiali e sono ubiquitariamente presenti in natura. Alcuni metalli, come Ca, Co, Cr, Cu, Fe, K, Mg, Mn, Na, Ni e Zn, sono essenziali e servono come micronutrienti e sono utilizzati dagli organismi nei processi ossido-reduttivi, nella stabilizzazione di molecole attraverso interazioni elettrostatiche, nella regolazione della pressione osmotica. Molti altri metalli, invece, non rivestono nessun ruolo biologico (ad esempio Ag, Al, Cd, Au, Pb e Hg), e sono potenzialmente tossici per gli organismi; tali metalli fanno tutti parte della categoria dei metalli pesanti. Tale tossicità è essenzialmente esercitata attraverso lo spiazzamento dei metalli essenziali dai loro siti di legame, causando riduzione o perdita di funzione. Inoltre, qualora presenti oltre certi limiti di concentrazione, tutti i metalli possono causare tossicità con effetti che vanno dall’alterazione della permeabilità delle membrane biologiche, fino a danni a livello del DNA.
Stando ad una rigorosa definizione di “metalli pesanti” basata su caratteristiche chimico-fisiche (densità, peso e numero atomico), ventitré elementi rientrano in questa categoria. In genere, però, quando si parla d’inquinamento da metalli pesanti, ci si riferisce a un numero ridotto di tredici elementi, che sono i maggiori responsabili dei danni ambientali: Ag, As, Be, Cd, Cr, Cu, Hg, Ni, Pb, Sb, Se, Tl e Zn [6]. Essi sono considerati “contaminanti persistenti” giacché non possono essere degradati né distrutti. Sono introdotti nell'ambiente, per cause naturali e antropiche, in forma elementare o di composto. Le principali sorgenti di emissione sono le industrie fondiarie, i siti minerari e i prodotti di combustione. Dall'inizio della rivoluzione

industriale, i metalli pesanti sono stati emessi e rilasciati in ambienti terrestri e acquatici, con numerosi effetti negativi su diversi sistemi biologici, dai batteri fino agli animali e all'uomo [7]. La tossicità dei metalli pesanti, in modo particolare Cd, Hg e Pb, deriva dall'elevata affinità dei cationi metallici per lo zolfo; pertanto i gruppi sulfidrilici (-SH) di proteine e peptidi sono facilmente complessati a tali metalli, soprattutto se sotto forma di ioni bivalenti, alterando la stabilità e l'attività di proteine ed enzimi.
L'inquinamento ambientale a causa di ioni metallici tossici, in particolar modo metalli pesanti, è una problematica molto diffusa che riceve una notevole attenzione poiché coinvolge seriamente la salute umana. L'accumulo di metalli pesanti genera malattie sia in fase acuta sia cronica, con disturbi quali ad esempio squilibri ormonali, carenze nutrizionali, malattie autoimmuni e disturbi neurologici [8]. L'organo principale di accumulo a lungo termine di metalli è il rene [9]. Infatti, il danno renale è stato descritto come il problema principale per i pazienti cronicamente esposti a metalli pesanti [10]. Tali agenti tossici raggiungono il rene in forma complessata con proteine e sono filtrati nel glomerulo renale, riassorbiti e accumulati nelle cellule renali. L'esposizione cronica al cadmio è associata a una progressiva disfunzione tubulare renale. I dati di studi sull'uomo suggeriscono un periodo di latenza di circa dieci anni prima della comparsa clinica del danno renale. I primi sintomi clinici di nefrotossicità si diagnosticano con valori urinali di 2 mg/g di creatinina; in genere i biomarcatori sono la presenza nelle urine di β2-microglobulina, α1-microglobulina e N-acetil-B-glucosaminidasi (NAG). Molti lavori sono attualmente in corso per definire la "concentrazione critica renale" per ciascun metallo, e per determinare marcatori specifici di danno precoce in cellule renali, al fine di poter evitare la compromissione della funzionalità renale e impedire l'effetto tossico cronico.
L'importanza dello studio dei metalli non è dovuta solo al campo dell'inquinamento ambientale, ma riguarda anche funzioni biologiche in cui alcuni metalli rivestono un ruolo essenziale. Tra questi, il selenio (Se) rappresenta un interessante campo di studio: è, infatti, considerato un nutriente essenziale per gli esseri umani, e l'EFSA (*European Food Safety Authority*) nel 2008 ha stabilito in 55mg la dose quotidiana raccomandata per gli esseri umani [11]. Il Se è un componente fondamentale di diverse famiglie proteiche, alcune delle quali ben caratterizzate come iodotirine-5 deiodinasi, glutatione perossidasi (GPX1), e tioredossina reduttasi [12]. Diversi organismi possiedono la capacità di metabolizzare Se in selenoproteine mediante essenzialmente due meccanismi: il primo è un meccanismo specifico dedicato alla biosintesi di proteine che contengono l'amminoacido Selenocisteina (Sec, U), mentre il secondo è un meccanismo non specifico in cui un atomo di zolfo da residui di metionina e cisteina è sostituito con un atomo di selenio in maniera del tutto casuale. L'insufficienza di Se può indurre numerose malattie come malattie cardiache, ipotiroidismo, diminuzione della fertilità, malattie cardiovascolari e anche alcuni tipi di cancro [13]. Negli ultimi anni sono state sviluppate varietà di prodotti biologici selenio-arricchiti, per sopperire alla mancata assimilazione di selenio in paesi in cui il consumo di selenio scende al di sotto delle dosi giornaliere raccomandate. A tale proposito il sistema più ampiamente studiato riguarda il lievito *Saccharomyces cerevisiae* capace di convertire selenio inorganico, potenzialmente tossico e scarsamente biodisponibile, in forme organiche (selenoproteine) [14].

Il presente progetto di dottorato riguarda lo studio degli effetti che alcuni metalli inducono in particolari sistemi biologici; in particolare sono stati valutati i cambiamenti a livello del proteoma indotti dall'esposizione a elevate concentrazioni

di metalli, mediante approcci integrati di metallomica e proteomica. I seguenti sistemi d'interesse biotecnologico sono stati analizzati in questo progetto:
1) *Escherichia coli,* usato come organismo modello per lo studio degli effetti della contaminazione da metalli pesanti (Capitolo II).
2) cellule HRCE (cellule epiteliali renali corticali umane), per lo studio degli effetti dell'esposizione a cadmio e piombo su cellule umane primarie (Capitolo III).
3) *Lactobacillus reuteri* LB2 BM-DSM 16143 per uno studio dell'incorporazione di selenio in proteine (Capitolo IV).

Capitolo II: Sviluppo di una strategia analitica per lo studio degli effetti di metalli pesanti sul batterio *Escherichia coli* usato come sistema modello.

Accurate indagini rivolte allo studio dei meccanismi di come i metalli esercitino i loro effetti tossici in sistemi biologici e come questi ultimi si adattino in risposta a tale stress, sono in costante sviluppo. Tali studi sono condotti su molteplici sistemi biologici, spesso utilizzati come sistemi modello, come ad esempio piante, animali, microbi, e cellule di mammifero [15].
Escherichia coli, un bacillo Gram-negativo, è uno dei modelli più diffusamente utilizzati per lo studio dei danni provocati da stress a causa di metalli, grazie al suo rapido tempo di duplicazione e rapida risposta alle sostanze tossiche. Benché in letteratura siano riportati numerosi lavori sulla regolazione dei processi cellulari in seguito all'esposizione a ioni metallici sia a livello trascrizionale che traduzionali, i meccanismi molecolari di risposta cellulare contro vari ioni metallici non sono ancora completamente compresi.
Pertanto, nel presente progetto, è stato studiato l'effetto, a livello proteomico, dell'esposizione di cadmio, alla dose corrispondente il 50% d'inibizione della crescita, in *E. coli* (ceppo TK12 MG1655). Attraverso il ritrovamento di up- e down-regolazioni di proteine differenzialmente espresse, integrato con dati quantitativi provenienti da analisi ICP-MS, è stato possibile studiare i meccanismi di adattamento cellulare nei confronti del metallo tossico.
Sono state quindi inizialmente allestite diverse colture di *E. coli*, utilizzando concentrazioni crescenti (da 0.05 a 1 mM) di cadmio (Cd) e piombo (Pb), al fine di determinare le dosi tossiche che esercitassero circa il 50% d'inibizione della crescita microbica. Relativamente al Cd tale valore è 0.2 mM, mentre per il Pb non si è riscontrato nessun effetto sulla crescita fino alla concentrazione di 1mM.
Analisi successive sono state condotte per valutare l'effettivo assorbimento dei metalli da parte delle cellule batteriche, attraverso una metodologia sviluppata *ad hoc* che ha previsto l'utilizzo di un forno a microonde per la completa dissoluzione della matrice organica, seguita da un'analisi quantitativa multi-elementare ICP-MS. Sono stati preventivamente effettuati dei prelievi durante le crescite microbiche; da ogni prelievo è stato ottenuto un pellet cellulare, un surnatante contenente il mezzo di coltura e un lavaggio del pellet cellulare effettuato in presenza di EDTA. Tutti i campioni così ottenuti sono stati diluiti in un'apposita soluzione di acido nitrico e perossido di idrogeno e introdotti all'interno di un forno a microonde, utilizzando un programma ottimizzato per ottenere una rapida dissoluzione dei campioni. Infine tutti i campioni sono stati opportunamente diluiti e analizzati mediante ICP-MS.
I dati ottenuti hanno mostrato che *E.coli* è in grado di assimilare alte dosi di entrambi i metalli; infatti, per il cadmio la quantità recuperata dalla biomassa rappresenta circa il 20% della concentrazione inizialmente presente nel terreno di coltura, mentre per il piombo questo valore raggiunge circa il 35%. Inoltre in entrambi i casi, l'assorbimento è avvenuto durante i primi novanta minuti della crescita cellulare,

rimanendo costante durante le successive fasi di crescita. Sfruttando le potenzialità dell'ICP-MS di eseguire analisi quantitative multi-elementari, sono stati monitorati anche altri elementi durante la crescita microbica, al fine di valutare eventuali cambiamenti a seguito dell'esposizione ai metalli. Sono stati monitorati i seguenti elementi: Ag, Al, As, Co, Cr, Cu, Fe, Mn, Ni, Sb, Se, Sn, Zn e V. Per quasi tutti i metalli, nessuna rilevante modifica dei livelli citosolici è stata rilevata dal confronto con il controllo, mentre è stata riscontrata una drastica diminuzione di Zn nel campione esposto a 0.2 mM di Cd, con una concentrazione che è passata da 35 mg/L nel controllo a 2 mg/L. Si può quindi ipotizzare che la presenza di elevati livelli di Cd nel mezzo di coltura, colpisca l'assimilazione dello Zn.

In seguito mediante un approccio di proteomica differenziale sono state valutate variazioni semi-quantitative dell'espressione proteica di *E.coli* in risposta all'esposizione a 0.2mM di Cd. A tal proposito sono state ottenute mappe bidimensionali da estratti proteici che, attraverso l'uso di opportuni software e strumentazioni, sono state confrontate al fine di valutare gli spot differenzialmente espressi presenti nelle mappe proteiche. Gli spot selezionati sono stati successivamente processati, ottenendo miscele peptidiche che sono state identificate mediante un approccio di proteomica *bottom-up,* che ha previsto un'analisi in spettrometria di massa LC-MS/MS e una successiva ricerca in banca dati. Con questa tecnica sono state identificate 21 proteine differenzialmente espresse, 17 delle quali mostravano una diminuzione nei livelli di espressione e 4 invece un aumento (Tabella II.1). I risultati ottenuti rivelano che l'esposizione al cadmio influenza molteplici funzioni cellulari quali: 1) alterazione del macchinario di sintesi proteica evidenziato dalla riduzione dei fattori EF-Tu e EF-Ts, due proteine regolatrici della traduzione; 2) alterazione del metabolismo energetico con diminuzione dei livelli di triptofanasi (tnaA), un enzima coinvolto nel metabolismo degli amminoacidi, e di malato deidrogenasi (MDH) e fosfoglicerato chinasi (PGK); 3) riduzione del trasporto attivo attraverso le membrane cellulari, evidenziato dai bassi livelle delle proteine DppA e OppA; 4) influenza sulla chemiotassi e sul trasporto degli zuccheri con diminuzione di proteine come rbsB, MBP e GBP. Di contro invece è stato riscontrato un aumento di alcune proteine coinvolte nell'efflusso di materiale dal citosol al periplasma, quali ZnuA, lsrB e OmpA. In particolare ZnuA appartiene a una famiglia di proteine che funzionano da recettori iniziali nella captazione di ioni metallici, in particolar modo Zn^{2+}. ZnuA possiede un dominio centrale *metal binding* di lunghezza variabile in differenti specie batteriche che è caratterizzato dalla presenza di un numero elevato di residui di istidina, acidi aspartici e glutammici [16].

In conclusione, i dati ottenuti dalle analisi ICP-MS, insieme con i dati di proteomica, suggeriscono che esiste una forte correlazione tra zinco e cadmio, in particolare portando a una deplezione di zinco in cellule di *E.coli* esposte a cadmio. Inoltre l'assorbimento di cadmio influenza molteplici funzioni biologiche, con conseguente riduzione dei metabolismi primari, a fronte di un aumento di produzione di proteine coinvolte nel meccanismo di secrezione dallo spazio intracellulare verso l'extracellulare.

Capitolo III: Un approccio proteomico per studiare gli effetti di cadmio e piombo sulle cellule primarie renali.

In questo capitolo è riportato uno studio degli effetti dei metalli pesanti cadmio e piombo sia sulla vitalità sia sul proteoma di cellule primarie HRCE (umane epiteliali corticali renali).

Le cellule sono state cresciute in presenza e in assenza (controllo) di concentrazioni elevate di cadmio e piombo (10 µg/mL di $CdCl_2$ e 100 µg/mL di $PbCl_2$ per 24 h) aggiunte nel terreno di coltura.

La vitalità cellulare è stata misurata mediante il saggio di proliferazione cellulare MTT, che ha evidenziato una forte inibizione della vitalità cellulare sia dose- sia tempo-dipendente; gli effetti tossici sono particolarmente evidenti in seguito ad esposizione al cadmio, con un IC_{50} (concentrazione necessaria per inibire il 50% del campione in esame) ottenuto ad una concentrazione di 6 µg/mL, mentre per il piombo l'IC_{50} è pari a 50 µg/mL.

In seguito sono state condotte analisi ICP-MS per stimare la quantità di metalli pesanti nel compartimento intracellulare. A tal proposito sono state prelevate aliquote di terreno di coltura al tempo zero e dopo 24 h. Al termine delle 24 h le cellule sono state staccate dalla piastra e sottoposte a completa dissoluzione utilizzando un sistema a microonde. E' stato quindi possibile stabilire la quantità di cadmio e piombo presente nel mezzo e soprattutto la quantità di metalli presente nelle cellule vive, che è circa lo 0,3% per il Cd e lo 0,7% per il Pb; tale concentrazione potrebbe indicare la dose "sopportata" dalle cellule renali.

E' stata in seguito effettuata un'indagine proteomica sistematica, basata su elettroforesi bidimensionale, analisi d'immagine, identificazione delle proteine e analisi bioinformatica.

Più di 300 spot proteici sono stati analizzati in cerca di variazione rilevante dei livelli di espressione del proteoma, a seguito di esposizione delle cellule a cadmio e piombo; tra questi, 25 sono risultati essere significativi e sono stati di conseguenza tagliati dal gel e analizzati mediante spettrometria di massa. La maggior parte delle proteine identificate è risultata essere coinvolta in due principali processi cellulari: apoptosi e folding proteico. Per il cadmio il 48% di esse ha un ruolo diretto nella morte cellulare apoptotica, mentre per il piombo il valore è del 18%. Invece il 36% delle proteine influenzate dalla presenza piombo è coinvolto nel ripiegamento proteico rispetto al 19% osservato dopo esposizione al cadmio.

Analisi bioinformatiche utilizzando il software *Ingenuity* hanno chiaramente indicato che per entrambi i metalli maggior parte delle proteine interessate hanno un ruolo nella "rete" cellulare che porta alla morte e alla compromissione delle funzioni di mantenimento delle cellule.

La morte, causata da apoptosi, è stata confermata dall'analisi dei nuclei apoptotici, risultati essere di forma anomala in seguito a saggio di colorazione con il reattivo Hoechst 33342.

L'analisi della via apoptotica è stata compiuta sottoponendo estratti cellulari ad analisi Western blot utilizzando gli anticorpi anti-procaspase-3, anti-Bcl-2, anti-procaspase-8. I saggi hanno rilevato l'attivazione della caspasi-3, e una significativa down-regolazione del marcatore anti-apoptotico Bcl-2, mentre non è stata evidenziata nessuna alterazione della caspasi-8.

In conclusione tale studio su cellule primarie, sebbene condotto *in vitro*, può rappresentare un contributo all'identificazione di potenziali biomarker d'inquinamento ambientale da metalli pesanti in cellule renali umane.

Capitolo IV: Incorporazione selettiva di selenio in selenocisteine del batterio probiotico *Lactobacillus r*euteri LB2 BM-DSM 16143 mediante un approccio proteomico assistito da ICP-MS.

Lactobacillus reuteri è un batterio lattico eterofermentante, che colonizza il tratto gastrointestinale e si ritrova comunemente in diversi prodotti lattiero-caseari, carni e in impasti acidi. Tale microorganismo è stato ampiamente descritto come probiotico: infatti, produce composti antimicrobici come la reuterina (β-idrossipropionaldeide), con un ampio spettro di azione [17], efficace ad esempio contro la diarrea nei bambini [18] e con effetti immuno-modulanti (potente TNF-inibitore) sugli esseri umani [19]. Dal momento che *L. reuteri* è un naturale abitante della flora intestinale umana, l'associazione della funzione di probiotico unita alla sua capacità di fissare selenio in proteine, può rappresentare un approccio innovativo per risolvere il problema di carenza di selenio, diventando una valida alternativa all'uso di lievito arricchito in selenio come integratore alimentare in particolari diete.

Nel presente studio *L. reuteri* LB2 BM-DSM 16143 è stato cresciuto in presenza di un'elevata concentrazione di selenito di sodio Na_2SeO_3, la forma più tossica di selenio, alla concentrazione di 4.38 mg/L (equivalente a 2 mg/L di Se).

Sono stati inizialmente eseguiti esperimenti per valutare l'assorbimento di selenio da parte di *L. reuteri* LB2 BM-DSM 16143 durante la crescita; i risultati ottenuti hanno dimostrato la capacità del ceppo di recuperare un'elevata concentrazione di selenio dal mezzo, e di stabilire in quale fase del ciclo cellulare tale assimilazione avvenga. E' stato, infatti, determinato il punto nella crescita microbica corrispondente al massimo di concentrazione intracellulare di selenio, che è risultato essere dopo 6 ore di crescita in fase esponenziale. La concentrazione massima recuperata dalla biomassa è stata all'incirca di 1 mg/L, corrispondente quindi al 50% del selenio somministrato nel mezzo di coltura.

Una volta determinata la capacità del ceppo di internalizzare selenio, è stata valutata la quantità di metallo covalentemente legata a proteine, attraverso frazionamento ottenuto per cromatografia liquida (HPLC e SEC) dell'estratto proteico totale, seguito da rivelazione per ICP-MS. Tali analisi hanno permesso di stabilire che circa la metà del selenio internalizzato è covalentemente incorporato in proteine. Successivi studi sono stati impiegati per determinare e localizzare la destinazione finale del selenio assimilato, utilizzando un approccio innovativo analitico basato sull'integrazione di metallomica e strategie di proteomica. La strategia ha previsto l'utilizzo di un sistema "Laser Ablation" accoppiato a rivelazione ICP-MS per il ritrovamento di selenio da gel elettroforetici sia mono- che bidimensionali (2D-LA-ICPMS). E' stato così possibile risolvere in un campione complesso come un gel bidimensionale, quale proteina contenesse selenio; tali spot proteici sono stati poi analizzati mediante protocolli classici di spettrometria di massa, con l'obiettivo di identificare le proteine d'interesse e di ritrovare i punti i cui era avvenuta la modifica. Sono state identificate le seguenti proteine: due enzimi glicolitici (gliceraldeide 3-fosfato deidrogenasi GAPDH, e piruvato chinasi, PK), due enzimi della via dei pentoso fosfato (fosfochetolasi, PKP, e 6-fosfogluconato deidrogenasi, 6PGD), due enzimi del pathway ADI (arginina deiminasi, ADI, e ornitina carbamiltransferasi, OTCase) e la ribonucleoside idrolasi RihC. In alcuni di questi enzimi (PKP, PK, 6PGD, OTCase e RihC) tutti i residui di cisteina presenti nella sequenza sono stati convertiti in selenocisteina. Invece in GAPDH e ADI solo due cisteine su tre sono state sostituite. In entrambi i casi vi erano due residui di cisteina collocati in maniera prossimale lungo la sequenza amminoacidica, di cui solo uno dei due era modificato;

curiosamente, in entrambi i casi, la cisteina modificata risultata essere la cisteina catalitica (^{153}Cys/^{153}SeCys in GAPDH e ^{398}Cys/^{398}SeCys in ADI).
I dati ottenuti hanno dimostrato la peculiarità di questo ceppo batterico di fissare elevate quantità di selenio, convertendolo in forma organica come selenocisteina (SeCys), mentre nessuna sostituzione metionina/selenometionina è stata riscontrata, che invece è tipica di altri microrganismi ben caratterizzati come ad esempio lieviti.
Inoltre i risultati ottenuti localizzano, senza ambiguità, l'esatta posizione all'interno della sequenza primaria delle proteine in cui la SeCys è inserita; questo è il primo studio che descrive questo evento in un batterio lattico, in particolare localizzando i siti in cui è avvenuta la sostituzione cisteina/selenocisteina.
Tuttavia per una completa caratterizzazione del processo biologico d'incorporazione del selenio in proteine, rimane da chiarire se esso avvenga attraverso un meccanismo geneticamente codificato o non-specifico. Il ritrovamento di un unico se-amminoacido, la selenocisteina, potrebbe significare un processo specifico simile a quanto studiato per determinati batteri.
Questa ipotesi è stata provvisoriamente verificata con studi di genomica, analizzando sequenze geniche delle proteine identificate in cerca dei codoni UGA. Sono state eseguite anche analisi RT-PCR per verificare se la modifica che porta alla sostituzione Cys/SeCys, occorra a livello degli mRNA, senza però individuare la presenza di tali codoni.

In conclusione, il seguente progetto di dottorato ha permesso lo sviluppo di metodologie integrate di proteomica e metallomica, utilizzate per lo studio degli effetti dell'esposizione a metalli su diversi proteomi.

Bibliografia

[1] Williams, R.J.., Chemical selection of elements by cells. *Coordination Chemistry Reviews* **2001**, 216-217, 583-595.
[2] Szpunar, J., Metallomics: a new frontier in analytical chemistry. Analytical and bioanalytical chemistry **2004**, 378, 54-6.
[3] Haraguchi, H., Metallomics as integrated biometal science. *Health* **2004**, 5-14.
[4] Shi, W., Chance, M.R., Metallomics and metalloproteomics. *Cellular and molecular life sciences: CMLS* **2008**, 65, 3040-8.
[5] Szpunar, J., Advances in analytical methodology for bioinorganic speciation analysis: metallomics, metalloproteomics and heteroatom-tagged proteomics and metabolomics. *The Analyst* **2005**, 130, 442-65.
[6] Sparks, D.L., Toxic Metals in the Environment: The Role of Surfaces. *Plant and Soil* **2005**, 193-198.
[7] Gadd, G.M., Metals, minerals and microbes: geomicrobiology and bioremediation. *Microbiology* **2010**, 156, 609-43.
[8] Lynes, M.A., Kang, Y.J., Sensi, S.L., Perdrizet, G.A., Hightower, L.E., Heavy metal ions in normal physiology, toxic stress, and cytoprotection. *Annals of the New York Academy of Sciences* **2007**, 1113, 159-172.
[9] Orlowski, C., Piotrowski, J.K., Biological levels of cadmium and zinc in the small intestine of non-occupationally exposed human subjects. *Hum Exp Toxicol* **2003**, 22, 57-63.
[10] Barbier, O., Jacquillet, G., Tauc, M., Cougnon, M., Poujeol, P., Effect of heavy metals on, and handling by, the kidney. *Nephron Physiol* **2005**, 99, 105-110.
[11] EFSA, Selenium-enriched yeast as source for selenium added for nutritional purposes in foods for particular nutritional uses and foods (including food Scientific

Opinion of the Panel on Food Additives , Flavourings , Processing Aids and Materials in Contact with Food Adopted on 9 July 2008. *Aids* **2008**, 1-42.
[12] Wang, Y.D., Wang, X., Ngai, S.M., Wong, Y.-S., Comparative proteomics analysis of selenium responses in selenium-enriched rice grains. *Journal of proteome research* **2013**, 12, 808-20.
[13] Combs, G. F., Jr. Food system-based approaches to improving micronutrient nutrition: the case for selenium. *Biofactors* **2000**, 12, 39−43.
[14] Rayman, M.P. The use of high-selenium yeast to raise selenium status: how does it measure up? *Brit. J. Nutr*, **2004**, 92, 557–573.
[15] Nandakumar, R., Espirito Santo, C., Madayiputhiya, N., Grass, G., Quantitative proteomic profiling of the Escherichia coli response to metallic copper surfaces. *Biometals: an international journal on the role of metal ions in biology, biochemistry, and medicine* **2011**, 24, 429-444.
[16] Berducci, G., Mazzetti, A.P., Rotilio, G., Battistoni, A., Periplasmic competition for zinc uptake between the metallochaperone ZnuA and Cu,Zn superoxide dismutase. *FEBS Lett.* **2004**, 569**,** 289-292.
[17] Talarico, T.L., Casas, I. A., Chung, T.C., Dobrogosz, W.J., Production and isolation of reuterin, a growth inhibitor produced by *Lactobacillus reuteri*. Antimicrob*. Agents Chemother.* **1988,** 32, 1854–1858.
[18] Whitehead, K., Versalovic, J., Roos, S., Britton, R.A., Genomic and genetic characterization of the Bile Stress Response of Probiotic *Lactobacillus reuteri* ATCC 55730. *Appl. Environ. Microbiol.* **2008,** 74, 1812–1819.
[19] Lin, Y.P., Thibodeaux, C.H., Pena, J.A., Ferry, G.D., Versalovic, J., Probiotic *Lactobacillus reuteri* Suppress Proinflammatory Cytokines via c-Jun. *Inflamm Bowel Dis* **2008,** 14, 1068-1083.

Chapter I: Metallomics as new “omics” discipline

I.1 Introduction

As soon as the first complete genome sequence, of *Haemophilus influenzae*, was published [1] it became clear that the next step would concern the function of the genome products. This was the first brick in the construction of the wall further called proteome. The term ‘proteome’ was used for the first time in 1995, to describe the protein complement of a genome [2]. It was clear that with a bridge between these two sciences the understanding of functional mechanisms of living organisms could be obtained. The concepts of genomics (the study of genes and their function) and proteomics (the study of protein properties on large scale [3]) have become part of the everyday language of life sciences.

The explosive increase of complete genome sequences of a large number of organisms, coupled with the improvements in high-throughput technology, has led to a born of a large number of other “omics” disciplines as metabolomics, metabonomics, transcriptomics and so on, with the aim to expand the tool box of proteomics.

Among macromolecules, inorganic compounds such as metal ions are utilized by biological systems in fundamental processes, so the cytosolic concentration of metals is tightly controlled [4]. For a complete characterization of the chemistry of a cell, the understanding of mechanisms by which a metal is sensed, stored, or incorporated as a cofactor is required (Fig. I.1).

The term “metallome” was coined by Williams as “an element distribution, equilibrium concentrations of free metal ions or as a free element content in a cellular compartment, cell, or organism” [5]. The meaning of the term “metallome” was then extended to the entirety of metal and metalloid species present in a cell or tissue type [6]. The term “metallomics” was coined by Haraguchi to denote the ensemble of research activities related to metals of biological interest [7]. Expanding, metallomics became the study of the metallome, interactions, and functional connections of metal ions and other metal species [8]. The terms “metallome” and “metallomics” mimic the terms “genome” and “genomics”.

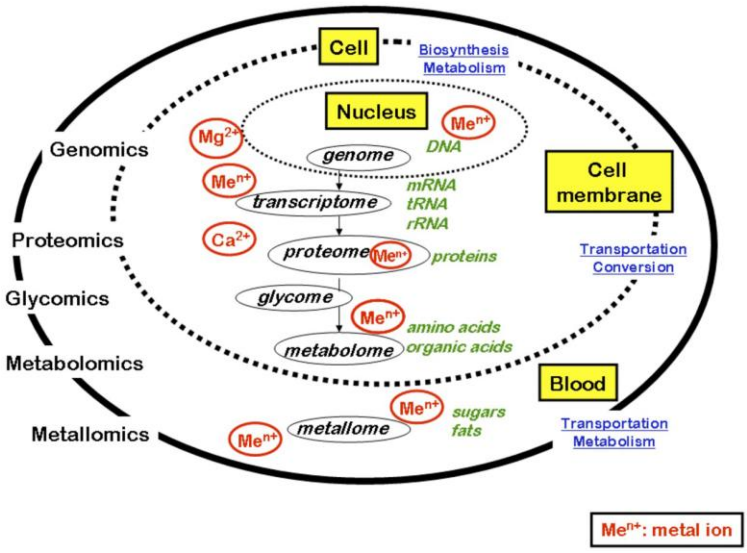

Figure I.1. *A schematic model of the biological system, showing the relationships among genomics, proteomics, metabolomics and metallomics The Mg2+ and Ca2+ions are given as examples because of their large affinities with DNA and proteins, respectively, in the biological cell. Reproduced from ref. [8].*

Metallomics is a discipline with a huge range of application, from the *in vitro* studies on biological catalysis to *in vivo* understanding of effects and interactions of metals and metalloids with organisms, fundamental for bioremediation proposals. However, Lobinski has suggested that an identification of a metal species, even important, without specifying its significance and contribution to the system is not metallomics! [8]

I.1.1 Integration of metallomics with proteomics: metalloproteomics

Metalloproteomics represents an expansion of traditional proteomics, usually considering metal-free moieties, in which the bound metals represent the mainly focus. Beside metalloproteomics is a quite new discipline it represents an advance in analytical methodology [9].

About the 30% of all annotated proteins reported in the major databases (PDB, NCBInr, and Uniprot) result to be associated with a metal [10]. In some cases the function of this proteins, also called metalloproteins, strongly depend by the interaction of the right metal [11]. Transition metals such as e.g. Cu, Fe, Zn, with their multiple oxidation states, are the most abundant bound metals.

Typically metalloproteomics studies are divided in two major groups in which one is represented by covalently bounded metals in which the predominant topic deals with Selenium-containing amino acids, and the second one that is constituted by proteins that have a non covalent interactions with metals, such as metal-binding proteins, metalloenzymes, metal-transport proteins and metal-stress proteins (Fig. I.2). Two of these aspects (Selenium-containing amino acids and metal-stress proteins) will be detailed in the next sections.

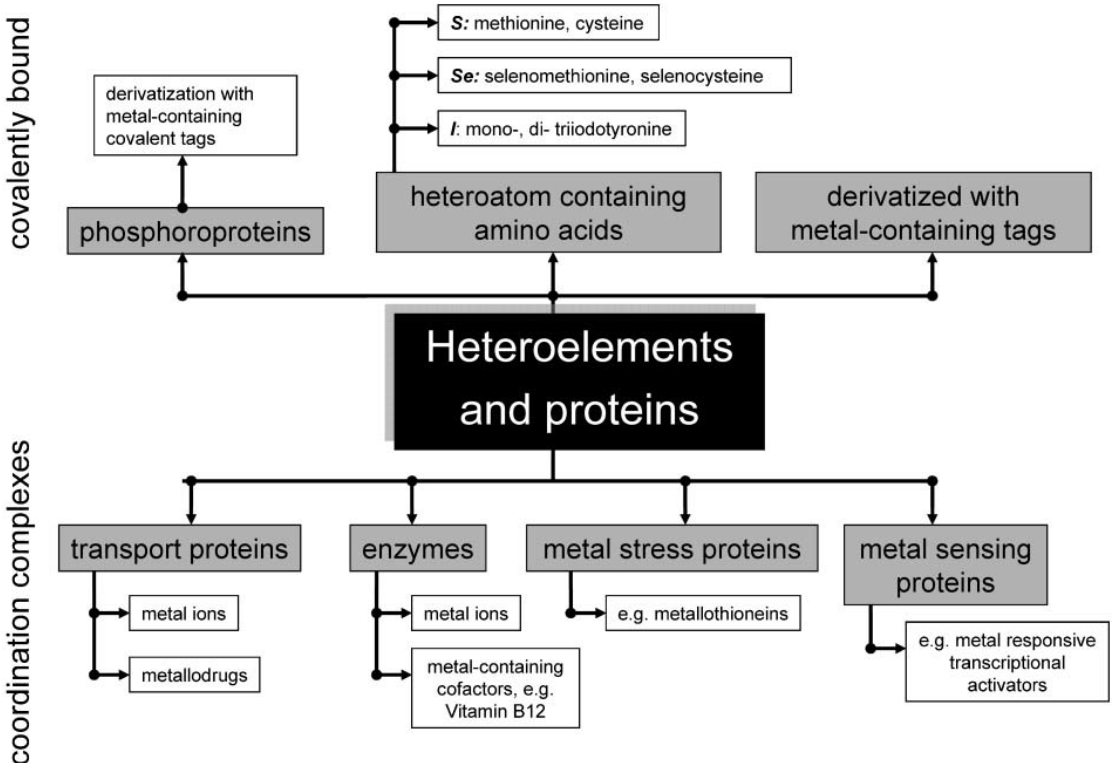

Figure I.2. *A schematic diagram of the bulk of applications in the field of metalloproteomics. Reproduced from ref. [11].*

I.2 Mass Spectrometry Approaches

Mass spectrometry (MS) has progressed to become a powerful analytical tool used in almost every discipline within the life and health sciences, thanks to the evolution in high-throughput technology and the development in instrumentation in terms of reproducibility, sensitivity and resolution.

I.2.1 MS: Principles and instrumentation

Mass spectrometry (MS) is a powerful analytical technique used to identify unknown compounds, to quantify known compounds, and to elucidate the structure and chemical properties of molecules. Moreover, the elucidation of the chemical structures of molecules, such as peptides and other chemical compounds can also be accomplished.

MS has its origins in the early part of the last century, from the experiences of JJ Thomson, who pointed out the formation of electrons and "positive radiation" in a tube under vacuum, which was applied a difference electric potential; thus the dogma in MS is the production of gas phase ions [12.]

The instrument consists of three major components: an **ion source** for producing gaseous ions from the substance being studied; an **analyzer** for resolving the ions into their characteristics mass components according to their mass-to-charge ratio; a **detector system** for detecting the ions and recording the relative abundance of each of the resolved ionic species (Fig. I.3). In addition, a sample introduction system is necessary to admit the samples to be studied to the ion source while maintaining the high vacuum (~10^{-5} to 10^{-8} mm of mercury) is necessary in order to prevent collisions of ions with residual gas molecules in the analyser during the flight from the ion source to the detector.

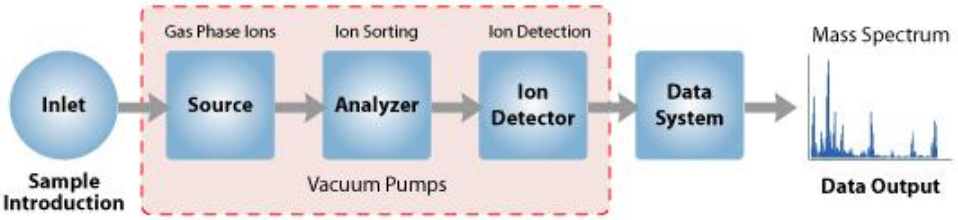

Figure I.3. *A schematic diagram of the components in a mass spectrometer.*

With all the above components, a mass spectrometer should always perform the following processes:

1. Produce ions from the sample in the ionization source.
2. Separate these ions according to their mass-to-charge ratio in the mass analyzer.
3. Eventually, fragment the selected ions and analyze the fragments in a second analyzer.
4. Detect the ions emerging from the last analyzer and measure their abundance with the detector that converts the ions into electrical signals.
5. Process the signals from the detector that are transmitted to the computer and control the instrument using feedback.

Generally mass spectrometers can be distinguished both on the type of ionization systems and on the type of analyser; the latest one is an essential component to define the accessible mass range, sensitivity and resolution of an instrument.

From the beginning to the 1970s mass spectrometry was limited to the analysis of volatile and low-molecular-weight compounds and the most used source were the so

called hard because they impart sufficient energy to analytes, relaxation involves rupture of bonds, producing fragment ions that have mass-to-charge ratios less than that of the molecular ion. In the late 1980’s, thanks to the efforts of John Fenn and Koichi Tanaka (who won the 2002 Nobel prize in Chemistry), two ionization techniques appeared that would spark a huge increase in interest in MS. These were: Matrix Assisted Laser Desorption Ionization (MALDI) [13] and Electrospray Ionization (ESI) [14]. These ionization techniques were revolutionary because they were *soft*, meaning that they transferred whole molecules intact into the gas phase, making possible the analysis of macromolecules such as peptides, proteins, nucleic acids and lipids.

For **MALDI** ion source, analytes needs to be embedded in a solid matrix, generally mixed with a large excess which absorbs energy in the order of 10^6-10^8 W sec^{-2} at the wavelength of the laser (typically 337 nm). A pulsed laser hits clusters of analytes and matrix, leading to intense heating and generating a plume of ejected material that rapidly expands and undergoes cooling, in a pulsed beam fashion. Generation of ions is believed to arise through ion/molecule reactions in the gas phase. Generally, the $[M+H]^+$ ion are preferentially formed in the positive ion mode, and $[M-H]^-$ ion in the negative ion mode. The presence of singly-charged signals in MALDI spectra allows correlating each peak one-to-one with analytes, thus allowing the analysis of complex mixtures. With the tools available on the market at the time, the accuracy of measurement of the mass is 0.01% (± 1 in 10,000 Da) [15].

ESI starts by samples in aqueous solution. Analytes exist as ions in solution because they contain functional groups whose ionization is controlled by the pH of the solution. Sample is dissolved in a polar, volatile solvent and pumped through a narrow, stainless steel capillary, ending with a needle (tip). A high voltage is applied to the tip of the capillary and the sample emerging from the tip is dispersed into a spray of highly charged droplets; this process is aided by a co-axially introduced gas, called nebulising gas, flowing around the outside of the capillary. The charged droplets diminish in volume by solvent evaporation, assisted by a warm flow of nitrogen, known as desolvatation gas, which flows perpendicularly to the front of the ionization source. Once the droplets have reached the Rayleigh limit, ions are desorbed from the droplet generating gas-phase ions in a continuous beam fashion. This technique gives rise to multiply-charged molecular-related ions such as $(M+nH)^{n+}$ in positive ionization mode and $(M-nH)^{n-}$ in negative ionization mode, where the number of charges depends on the chemical-physical characteristics of analytes; thus each analytes could assume more than one charge complicating the form assumed by the signal; for this reason this source is not useful to the analysis of complex mixtures except using pre-fractionation systems. The fact that ionization takes place in solution gives the possibility to couple ESI-ion sources to liquid chromatography. When liquid chromatography and mass spectrometry are coupled (LC-MS), MS analysis of the components of the sample takes place on-line as they elute from the chromatography column. To separate proteins or peptides columns filled with silica particles of diameter of μm with aliphatic side-chain are commercially in use. Aliphatic side-chain length depends on the type of sample that is loaded on the column: four, eight and eighteen carbonium atoms to separate big proteins, little proteins or big peptides and peptides respectively. To reach maximum sensitivity the evolution of instruments sees the nano-scale. Coupling nano-LC at submicroliter flow rates to the highly sensitive micro-scale ES interface the sensitivity enhance of several orders of magnitude [16].

Once generated, gas phase ions must be separated; usually mass analyzers act as mass filters, based on the interactions of charged analytes with electric and magnetic fields. The revolution in biological mass spectrometry was not only due to improvements in ionization techniques, in particular MALDI and ESI, but also from improvements to mass analysers as quadrupoles (Q), ion traps (IT), time-of-flight (TOF), Fourier transform ion cyclotron resonance (FTICR), Orbitrap or combination of these in “hybrid instruments”, that are commonly use in proteomics (Fig. I.4); they differ for their resolution, sensitivity and accuracy and for the types of experiments that are able to perform. TOF analysers are typically used in combination with MALDI (MALDI-TOF MS instruments); however both MALDI sources and TOF analysers can be used in different configurations.

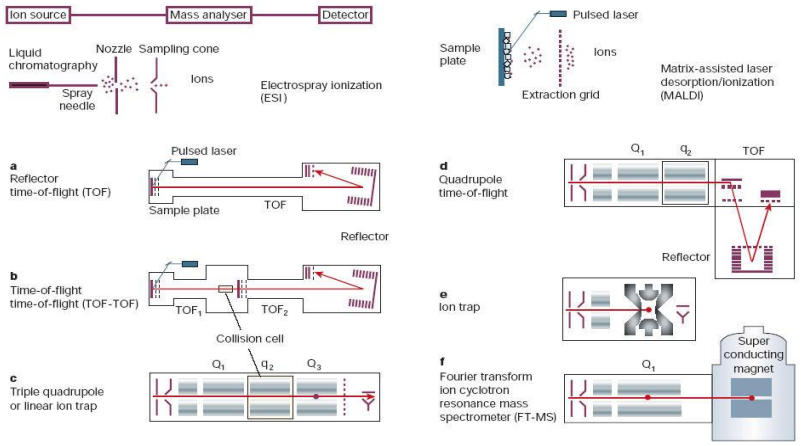

Figure I.4. *Typical mass spectrometers developed for proteomics applications.*

The **TOF** is essentially constituted by a tube of known length, where there is absence of electric field and a high vacuum condition (~10^{-7}-10^{-9} atm). A set of ions is emitted from the source in a very short time; ions are accelerated to a constant kinetic energy and focused towards the "flight tube". Since the kinetic energy is given by $mv^2/2$, where *m* is the mass of the ion (m/z) and *v* its velocity, the lower the ratio m/z, the greater will be its speed. The instrument measures the time that each ion takes to reach the detector placed at the end of the pipe itself; since all the ions have the same kinetic energy, the time used will be solely a function of their m/z ratio. The analysable m/z range of this instrumentation is theoretically unlimited and the union MALDI/TOF ensures a high sensitivity (few femtomoli for each analysis). The resolution is rather limited (about 3000, up to 5000 m/z) and tends to collapse with the increase in size of the analytes.
MALDI ionization process causes a spread of kinetic energy of ions resulting in different points in time and space of ions formation within the ion source. Thereby ions with the same mass obtain different kinetic energies and velocities during their extraction out of the ion source. This results in peak broadening, causing a loss in resolution. This peak broadening has been reduced by the introduction of the “delayed extraction” and of a “reflector” at the end of the linear flight tube [17]. The reflector allows ions to slow down and it reverts their flight path to a second detector. Ions with lower kinetic energy do not penetrate the reflector as deep and thus turn around faster, catching up with ions of slightly greater kinetic energy that penetrate the reflector deeper. Thereby the flight times of ions with identical m/z values, but

different kinetic energy values will be corrected when the ions arrive to the detector. The price of this enormous gain in resolution is given by a loss of sensitivity of about 10 times [15].

Quadrupole (Q) mass analysers have become one of the most widely used types of mass analyser mainly because of their ease of use, small size and relative low cost. A quadrupole mass filter consists of four parallel rods to which fixed DC and alternating RF potentials are applied [18]. Ions drift through the middle of the quadrupole to the mass detector. Ions oscillate in the x,y-plane and the frequency of oscillations depends on their m/z values and on the applied potentials. If the oscillation of an ion is stable, the ion will pass through the rods and reach the detector. All other ions do not have a stable trajectory through the quadrupole mass analyzer and will collide with the quadrupole rods, never reaching the detector. The m/z values of the ions able to move on stable trajectories depend on the amplitude of RF and DC voltages. The RF is varied to bring ions of different m/z into focus on the detector and thus build up a mass spectrum.

I.2.2 Tandem MS and QqTOF

Mass spectrometric analysis produces ions that are separated by m/z and analysed directly. Using a soft ionization method the mass spectrum will yield the molecular weight values of single analytes but little or no structural information. Tandem mass spectrometry (MS/MS) is used to produce structural information about a compound by fragmenting specific analytes inside the mass spectrometer and identifying the fragment ions. Tandem mass spectrometry also enables specific compounds to be detected in complex mixtures on account of their specific and characteristic fragmentation patterns. MS/MS is based on two stages of mass analysis, one to select a precursor or parent ion and the second to analyze fragment or daughter ions, using two different mass analysers, the first mass analyser is used to selectively pass ions into another reaction region, the second mass analyzer is used to record the m/z values of the dissociation products. Generally the reaction region or collision cell is the region into which an inert gas (e.g. nitrogen, argon, and helium) is admitted to collide with the selected ions causing the fragmentation. This process is known as Collisionally Induced Dissociation (CID) or Collisionally Activated Dissociation (CAD) [19]. Inelastic collisions between the precursor ion with a high translational energy and a neutral target gas cause the conversion of part of the translational energy into internal energy of the ion, leading to subsequent decomposition [20]. The CID process is highly dependent on the relative masses of the two species. The overall CID process is assumed to occur by a two-step mechanism, where the excitation of the precursors and their fragmentations are separated in time. Generally fragmentation of a precursor ion can occur if the collision energy is high enough to allow the ion to be excited beyond its threshold of dissociation. All CID processes can be separated into two categories based on the energy of the precursor ion. Low-energy collisions, common in triple quadrupoles (QqQ) and trapping devices, such as quadrupole, ion traps (IT) and Fourier-transform ion cyclotron resonance (FTICR) instruments, occur in the 1–100 eV range of collision energy and, even though the average energy deposited per collision may be lower than in high-energy CID, product ion yields are very high, especially since multiple collisions are allowed by the gas pressure and length of the collision cell in a QqQ or the time chosen for CID in ion traps. High-energy collisions, seen in sector and TOF/TOF instruments, are in the keV; the precursor ion beam, having a kinetic energy of a few keV, can enter the collision cell, usually causing single collisions before mass analysis of the product

ions. Moreover high-energy CID spectra usually show increased side-chain fragmentation [21]. The observed fragmentation pattern depends on various parameters including the amino acid composition and size of the peptide, excitation method, time scale of the instrument, the charge state of the ion, etc [22]. The sequence of peptides can be determined by interpreting the data resulting from fragmenting the peptides in tandem mass spectrometers. In this technique, one peptide species is selected in the first mass spectrometer and is then dissociated by collision with an inert gas, generally argon or nitrogen. The resulting fragments are separated in the second part of the tandem mass spectrometer, producing the tandem mass spectrum (MS/MS spectrum) [23][24]. Several bonds along the backbone can be broken by the collisions (NH-CαH, CαH-CO and CO-NH) originating different fragment ions. Each bond breakage gives rise to two species, one neutral and the other one charged, and only the charged species is monitored by the mass spectrometer. Hence there are six possible fragment ions for each amino acid residue and these are labelled as in the figure (Fig. I.5), with the a, b, and c ions having the charge retained on the N-terminal fragment, and the x, y and z ions having the charge on the C-terminal fragment. The most common ion types are the b and the y ions, which denote fragmentation at the amine bond with charge retention on the N or C terminus, respectively [25]. The most comprehensive model currently available to describe how protonated peptides fragment is the so-called “*mobile proton*” model [22]. According to this model peptides activated under low-energy CID, fragment mainly by charge directed reaction. In fact protonation on the amide nitrogen along the amino acid backbone leads to considerable weakening of the amide bond and leads to cleavage, generating fragment ions. Considering, for example, a doubly protonated tryptic peptide, one proton will be localized on C-terminal Arg or Lys side chain and the second may be localized at one of the amide bonds or the N-terminal. In this case the “*heterogeneous population model*” [26] assumes that, when the second proton is mobilized along the amino acid backbone, it will exist different protonated forms of the precursor ion that can easily fragment giving complementary series.

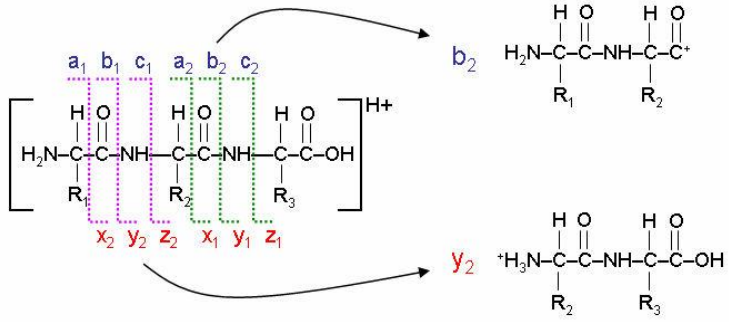

Figure I.5. *Peptides fragmentation scheme.*

Several hybrid geometries have recently been introduced with specific advantages; as an example the quadrupole-time of flight (QqTOF) instrument will be examinated in detail.

QqTOF mass spectrometer

QqTOF mass spectrometers have rapidly been embraced by the scientific community as powerful and robust instruments with unique capabilities. QqTOF tandem mass spectrometer can be described as a triple quadrupole with the last quadrupole section replaced by a TOF analyzer. It combines the high performance of TOF

devices, in both the MS and MS/MS modes, with the widely used techniques of electrospray ionization. QqTOF mass spectrometers are characterized by high sensitivity, high mass accuracy and high mass resolution for both precursor and product ions, and also by the simplicity of operation [27]. This advantage does not inherently apply to the more specialized scan modes as the precursor ion, neutral loss, and multiple reaction monitoring of triple quadrupole systems, and until recently these scan methods could not be performed with any reasonable efficiency. The popularity of the QqTOF has been significantly advanced by the rapid growth of semi-automated instrument control and data processing and by continuing improvements in the core performance characteristics of mass resolution and sensitivity. In the usual QqTOF configuration, an additional RF only quadrupole Q_0 is added to provide collisional cooling and focusing of the ions entering the instrument. So the instrument (Fig. I.6) consists of three quadrupoles, Q_0, Q_1 and q_2, followed by a reflecting TOF mass analyzer with orthogonal injection of ions [28].

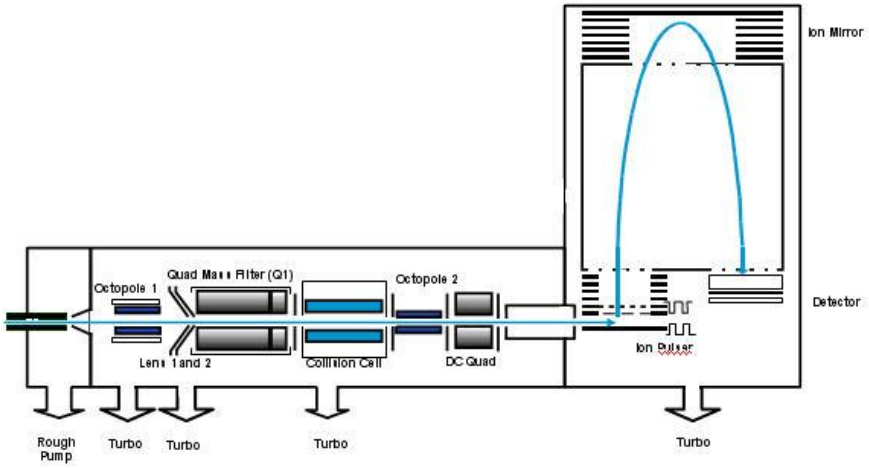

Figure I.6. *Schematic representation of Agilent 6520 Q-TOF mass spectrometer.*

For single MS measurements, the mass filter Q_1 is operated in the RF only mode so that it serves simply as a transmission element, while the TOF analyzer is used to record spectra. The resulting spectra benefit from the high resolution and mass accuracy of the TOF instruments, and also from their ability to record all ions in parallel, without scanning. Both Q_0 and q_2 are operated in the RF only mode: the RF field creates a potential that provides radial confinement of the precursor and/or fragment ions. Since the RF quadrupoles are normally operated at a pressure of several millitorr, they provide both radial and axial collisional damping of ion motion. Ions are thermalised in collisions with neutral gas molecules, reducing both the energy spread and the beam diameter and resulting in better transmission into and through both the quadrupole and TOF analyzers.
For MS/MS, Q_1 is operated in the mass filter mode to transmit only the parent ion of interest. The ion is then accelerated to an energy of between 20 and 200 eV before it enters the collision cell q_2, where it undergoes collision induced dissociation (CID) with neutral gas molecules (usually Ar or N_2). The resulting fragment ions are collisionally cooled and focused by RF fields. This step is even more important in QqTOF instruments than it is in triple quadrupoles because the TOF analyzer is much more sensitive to the “quality” of the incoming ion beam than is Q_3 in a triple quadrupole instrument. Both sensitivity and resolution benefit from the additional collisional focusing in the pressurized collision cell. After leaving the collision cell,

ions are re-accelerated to the required energy (usually several tens of eV per unit charge), and focused by ion optics into a parallel beam that continuously enters the ion modulator of the TOF analyzer. Initially the modulator region is field-free, so ions continue to move in their original direction in the gap. A pulsed electric field is applied at a frequency of several kHz across the modulator gap, pushing ions in a direction orthogonal to their original trajectory into the accelerating column, where they acquire their final energy of several keV per charge. From the accelerating column, ions arrive in the field-free drift space, where TOF mass separation occurs. The ratio of velocities (or energies) in the two orthogonal directions is selected such that ions reach the ion mirror and then the TOF detector naturally, without requiring an additional deflection in the drift region, which could affect the mass resolution [29].

I.2.3 ICP-MS

Among the different detection strategies developed for proteomics and above described, recent developments in ICP-MS could expand the “tool-box” for protein analysis; in fact, the use of **ICP** (Inductively Coupled Plasma) for ionization of peptides and proteins allows for a very sensitive and robust determination of a desired element (other than C, H, O or N) in the proteins of interest. ICP-MS, also termed element MS, is an established tool for quantitative element trace analysis and for speciation of elements in biological samples.

ICP-MS was developed in the late 1980's to combine the easy sample introduction and quick analysis of ICP technology with the accurate and low detection limits of a mass spectrometer.

The source is characterized by a plasma torch consisting of three concentric tubes, usually made of quartz, with the final end placed in a metal coil powered by a radiofrequency generator that generates an intense magnetic field. To produce the plasma is used an argon flow of about 14-18 liters per minute; therefore free electrons and Ar^+ ions are produced. The electrons due to the magnetic field induced undergo accelerations in the direction variable as a function of frequency variations, and, collide with argon atoms, produce additional ions Ar^+ and electrons; when the production of new electrons will be balanced by a combination of ions Ar^+ with the electrons, a dynamic equilibrium will reach and Ar atoms will form again. The plasma produced in this way is able to reach a temperature of the order of 7000-10000 K. [30]. The argon ICP is a highly efficient ion source. Most metals are ionized at 80 to >95% efficiency, while a few high ionization potential metals such as mercury have ionization efficiencies as low as 40%. Even nonmetals such as sulfur, phosphorus, silicon, and all of the halogens except fluorine are sufficiently ionized to allow for highly sensitive measurement. Only five elements cannot be directly measured by ICP-MS: hydrogen, helium, fluorine, neon, and argon. The first four are not ionized because their first ionization potentials are higher than that of argon, and the last is not measurable in argon plasma.

Two supplementary argon streams are introduced in the torch, typically at one liter per minute flow, an auxiliary of the two outer tubes in order to keep the plasma away from the walls of the torch and a third flow introduced by the central tube to create a zone with minor temperature. The ICP torch is designed to allow the injection of the sample directly in the heart of the plasma. The sample is aspirated, and atomized, enters the through the plasma torch. The aerosol of the sample arriving in the plasma, collide with electrons, atoms and Ar^+ ions and is atomized and ionized. The ions formed are predominantly mono charge (M^+), even though they may form double charged (M^{2+}) species. Moreover, some of these ions can recombine with other

species in plasma producing molecular species stable or metastable. For the analysis we prefer to have the form mono cation M^+, therefore choose the experimental conditions that increase the production to the detriment of other species. Because atomization/ionization occurs at atmospheric pressure, the interface between the ICP and MS components becomes crucial in creating a vacuum environment for the MS system. The interface consists of two cones with the tip pointing toward the plasma. The region between the two cones is maintained at a pressure of 2 mbar using a rotary pump. When the sample expands in this region it forms a supersonic jet, the central part of which flows through the orifice of smaller diameter of the second cone. Immediately behind the cone is placed a negatively charged electrode call *lens extraction*, (from -100 to -200 V), which attracts and accelerates the positive ions moving towards a series of focusing lenses. Ionic lenses have the task of focusing the beam of ions within the analyzer mass, i.e. in practice to restrict the energy range of ions before being analyzed by mass spectrometry. The sample ions pass into the MS system at high speeds, expanding in the vacuum system. The entire mass spectrometer must be kept in a vacuum so that the ions are free to move without collisions with air molecules. Since the ICP is maintained at atmospheric pressure, a pumping system is needed to continuously pull a vacuum inside the spectrometer. In order to most efficiently reduce the pressure several pumps are typically used to gradually reduce pressure to 10^{-5} mbar before the ion stream reaches the quadrupole. This allows the passage of ions of time thanks an oscillation frequency. The ions transmitted by the mass analyzer are revealed an electron multiplier. It is a cone which has a high voltage applied to it opposite in charge to that of the ions being detected. Ions leaving the quadrupole are attracted to the interior cone surface. When they strike the surface additional secondary electrons are emitted which move farther into the tube emitting additional secondary electrons. As the process continues even more electrons are formed, resulting in as many as 10^8 electrons at the other end of the tube after one ion strikes at the entrance of the cone. One of the great advantages to ICP-MS is extremely low detection limits for a wide variety of elements.

A problem that has limited the applicability of ICPMS was represented by polyatomic interferences such as for the accurate determination of selenium; Major isotopes of selenium (^{80}Se, ^{78}Se and ^{76}Se) are all subject to severe Ar_2^+ interferences. Other Se isotopes of lower abundance (^{82}Se or ^{77}Se) can also be interfered by molecular ions from halogens (BrH^+, ClO^+) present in the sample [31].

Thus several strategies were adopted by suppliers for abolish the problem of the polyatomic interferences. Dynamic reaction cell (DRC) and Axial field technology (AFT) were introduced by Perkin-Elmer on their instruments; Collisional reaction interface (CRI) or mini- Collison/Reaction Cell, used in the Bruker ICP-MS Aurora M90; Collision cell technology with kinetic energy discrimination of Thermo Scientific's XSeries2 instrument; Octopole reaction system (ORS) implemented by Agilent's 7500 series. In particular the ORS system adopted by Agilent is both a collision/reaction cell, depending on which gas is pressurized into the Octapole [32]. In fact the ORS uses only helium or hydrogen; the cell is positioned between the ion lens assembly and the mass analyzer quadrupole. H_2-cell mode is usually used for the reduction of plasma-based species (e.g., Ar^+, ArO^+ and Ar_2^+) by ion-molecule reactions. As polyatomic interfering ions are larger than monoatomic analytes ions, they collide more frequently with He gas and lose more kinetic energy. A potential energy barrier (bias voltage) is set between the octopole (cell) and the quadrupole (mass analyzer) to exclude the low energy ions from entering the mass analyzer.

Ions with sufficient energy can overcome the bias voltage and pass the mass analyzer for subsequent separation and detection. One additional benefit of using He is the absence of newly formed interfering species because of its inert nature.

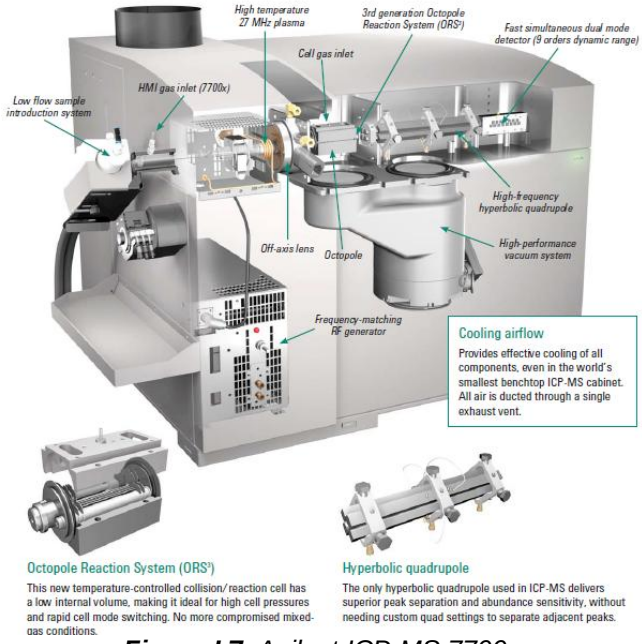

Figure I.7. *Agilent ICP-MS 7700*

With a traditional molecular mass spectrometry approach, a comprehensive study of metalloproteins is not sufficient because of the lost of information regarding metals. For this reason nowadays parallel information about the metal/metalloid associated with protein are obtained by complementary detection systems based on the integration of elemental and molecular mass spectrometry. Inductively coupled plasma and electrospray ionisation mass spectrometry (ICP-MS and ESI-MS) have been defined the ‘‘dream team’’ in metalloproteomics [33].

I.3 Metals and environment

Metals constitute about 75% of the known elements; they are derived from both natural and anthropogenic sources and they are ubiquitously found in nature. Since the beginning of the industrial revolution, metals have been emitted to and deposited in the environment, in particular in terrestrial and aquatic habitats being associated with adverse effects on several biological systems, from bacteria to animals and humans [34]. Metals have traditionally been classified into categories such as light, heavy, semimetal (i.e. metalloids), toxic, and trace, depending on several chemical and physical criteria such as density, weight, atomic number, and degree of toxicity [35]. Thirteen trace metals and metalloids (Ag, As, Be, Cd, Cr, Cu, Hg, Ni, Pb, Sb, Se, Tl, Zn) are considered priority pollutants [36]; they originate from natural sources such as rocks and metalliferous minerals, and anthropogenic inputs from e.g. agriculture, metallurgy, energy production, microelectronics, mining, sewage sludge and waste disposal [37]. The input of metals in the ecosystem can happen in different ways, by atmospheric deposition, volatile distribution such as for both metals and metalloids As, Hg, Se and Sb, or transported as particulates for Cu, Pb and Zn [38].
Although metals represent a great source of pollution, they are also essential nutrients for plants and microbes and important solid components that can have a fundamental effect on soil biogeochemical processes, e.g. clays, minerals, oxides [39]. In fact metals have been adopted by biological systems because of their

catalytic versatility; the unique properties of metal ions have been exploited by nature to perform a wide range of tasks. These include roles as structural components of biomolecules, signaling molecules, and catalytic cofactors in reversible oxidation-reduction and hydrolytic reactions and in structural rearrangements of organic molecules and electron transfer chemistry. Indeed, the role performed by metal ions cannot be performed by any other entity, so they play a crucial role in the life processes of microorganisms [40].
Some metals, such as Ca, Co, Cr, Cu, Fe, K, Mg, Mn, Na, Ni and Zn, are essential, serve as micronutrients and are used for redox-processes, for to stabilize molecules through electrostatic interactions, as components of various enzymes and for regulation of osmotic pressure. Many other metals have no biological role (e.g. Ag, Al, Cd, Au, Pb and Hg), and are nonessential and potentially toxic to microorganisms. Toxicity of nonessential metals can occurs through the displacement of essential metals from their native binding sites or through ligand interactions. In addition, when present above certain threshold concentrations, both essential and nonessential metals can exert toxicity such as damage cell membranes, alter enzyme specificity, disrupt cellular functions and damage the structure of DNA. Although metals exhibit a range of toxicities towards microbes, many of them have developed survival mechanisms, leading to the use of microbes in the field of bioremediation of metal-contaminated sites and treatment of industrial wastes. The mechanisms include redox transformations, the production of metal-binding peptides and proteins (e.g. metallothioneins, phytochelatins), organic and inorganic precipitation, active transport, efflux and intracellular compartmentalization, while cell walls and other structural components have significant metal-binding abilities [34].
The microbial survival strategies are an important research area, because there’s a need of understanding, at a molecular level, of how some organisms defend themselves against metals, in order to increase the success of bioremediating contaminated soils. Looking at the literature, the most detailed research has been done for As, Hg, Cd, Cu, Co, Zn, Pb, Ag, Ni and Te, for which resistance genes have been sequenced and mechanisms proposed [41] [42].

I.3.1 Heavy metals pollution

Heavy metals are rigorously defined as metallic elements that have a specific gravity that is at least 5 times the specific gravity of water (where the specific gravity of water is 1 at 4°C) [43]. According to this definition, some well-known toxic metallic elements with a specific gravity that is 5 or more times that of water are As, 5.7; Cd, 8.65; Fe, 7.9; Pb, 11.34; and Hg, 13.546. The major drawback of this way to classify the heavy metals is that it encompasses a heterogeneous array of elements with diverse chemical and biological properties [44]. With the assumption that heaviness and toxicity are related (in fact the expression 'heavy metals' is often used where there are connotations of toxicity), other metals such as metalloids enter in this classification, expanding the list at 23 elements (Ag, As, Au, Bi, Cd, Ce, Co, Cr, Cu, Fe, Ga, Hg, Mn, Ni, Pb, Pt, Sb, Sn, Te, Tl, U, V, and Zn). In small quantities, certain heavy metals are nutritionally essential for a healthy life; some of these are referred to as the trace elements (e.g., Cu, Fe, Mn, and Zn).
Heavy metals become toxic when they are not metabolized by the body and accumulate in the soft tissues. Heavy metals may enter the human body through food, water, air, or absorption through the skin when they come in contact with humans in agriculture and in manufacturing, pharmaceutical, industrial, or residential settings. Heavy metal toxicity can result in damaged or reduced mental and central

nervous function, lower energy levels, and damage to blood composition, lungs, kidneys, liver, and other vital organs. Long-term exposure may result in slowly progressing physical, muscular, and neurological degenerative processes that mimic Alzheimer's disease, Parkinson's disease, muscular dystrophy, and multiple sclerosis.
The Agency for Toxic Substances and Disease Registry (ATSDR) in Atlanta, Georgia, (a part of the U.S. Department of Health and Human Services) was established by congressional mandate to perform specific functions concerning adverse human health effects and diminished quality of life associated with exposure to hazardous substances. The ATSDR is responsible for assessment of waste sites and providing health information concerning hazardous substances, response to emergency release situations, and education and training concerning hazardous substances (ATSDR Mission Statement, November 7, 2001). In cooperation with the U.S. Environmental Protection Agency, the ATSDR has compiled a Priority List of Hazardous Substance for 2001 in which the heavy metals As (1), Pb (2), Hg (3), and Cd (7) appear on the top of this list (Tab. I.1).

2011 Rank	Substance Name	Total Points	2007 Rank	CAS #
1	ARSENIC	1665.5	1	007440-38-2
2	LEAD	1529.1	2	007439-92-1
3	MERCURY	1460.9	3	007439-97-6
4	VINYL CHLORIDE	1361.1	4	000075-01-4
5	POLYCHLORINATED BIPHENYLS	1344.1	5	001336-36-3
6	BENZENE	1332.0	6	000071-43-2
7	CADMIUM	1318.7	7	007440-43-9
8	BENZO(A)PYRENE	1305.7	9	000050-32-8
9	POLYCYCLIC AROMATIC HYDROCARBONS	1282.3	8	130498-29-2
10	BENZO(B)FLUORANTHENE	1252.4	10	000205-99-2
11	CHLOROFORM	1207.5	11	000067-66-3

Table I.1. *First 11 positions from the ATSDR (Agency for Toxic Substances and Disease Registry) 2011 Priority List of Hazardous Substance. The hazard potential of each candidate substance is ranked according to the following algorithm: Total Points (max 1800 points) = NPL Frequency (600 points) + Toxicity (600 points) + Potential for human exposure (600 points).*

I.3.2 Selenium and Selenoproteins

Selenium (Se) belonging to the chalcogen family (oxygen group element, Group VIA in the periodic table of elements) with chemical properties similar to the adjacent sulphur (S) and tellurium (Te). Selenium displays metalloid characteristics and it occurs in several different oxidation states as selenide (Se^{2-}), elemental selenium (Se^{0}), selenite (Se^{4+}), and selenate (Se^{6+}) [46]. Se was discovered in 1817 by the Swedish physician and chemist Jöns Jakob Berzelius. He named it after the Greek moon goddess Selene (Se). Se had a huge spread in interest 60 years ago since it has been recognized as an essential trace element for many life forms including man. Pinsent was the first one to report, in the 1954, that Se is essential for the enzyme activity of ‘formic dehydrogenase’ in *Escherichia coli* [47]. A great surprise to the scientific community was the discovery that Se was co-translationally incorporated into protein in form of selenocysteine (Sec, U), that was after

established as the 21st proteinogenic amino acid [48]. This mechanism was first described in *Escherichia coli* and then well characterized also in mammalian cells [49].
Nowadays is well known that Se is a crucial micronutrient for human health [50]. It was established from the EFSA (European Food Safety Authority) in the 2008 a recommended intake for humans: 55 μg/day. Inadequate Se consumption is related to poor health, decreased fertility, cardiovascular disease and also to some types of cancer, so Se is also considered as an anticarcinogenic agent [51][52]. In human Se is a component of several important selenoproteins and enzymes required for different functions such as antioxidant defense and reduction of inflammation [1]; one of the most significant for human is Glutathione peroxidase (GPx1), which is the third defense against ROS (Reactive Oxygen Species), after Superoxide dismutase and Catalase [53].
In some organisms (prokaryotes, eukaryotes and archaea) Se can be metabolized in a specific pathway dedicated to the biosynthesis of proteins which contain the amino acid Sec. The common features to all organisms are the UGA-Sec codon, the specific tRNA (^{SecSer}tRNA), the SECIS element, and several protein factors. The codon-defining of selenocysteine is the TGA codon that is normally interpreted as a stop signal by the cell’s protein biosynthesis machinery; so Sec insertion requires additional signals, allowing the reinterpretation of the stop signal as a Sec incorporation command. This signaling is achieved via the interaction of several proteins with a special messenger RNA (mRNA) secondary structure, known as the SECIS (SElenoCysteine Insertion Sequence) element. This element is a RNA stem-loop structure that in eukaryotes is located within the 3’-untranslated region (UTR) of the mRNAs, while in prokaryotes it is found within the coding sequence [54]. In fig I.8 mechanism of Sec biosynthesis proposed by Gromer and co-workers [55] for humans is illustrated.

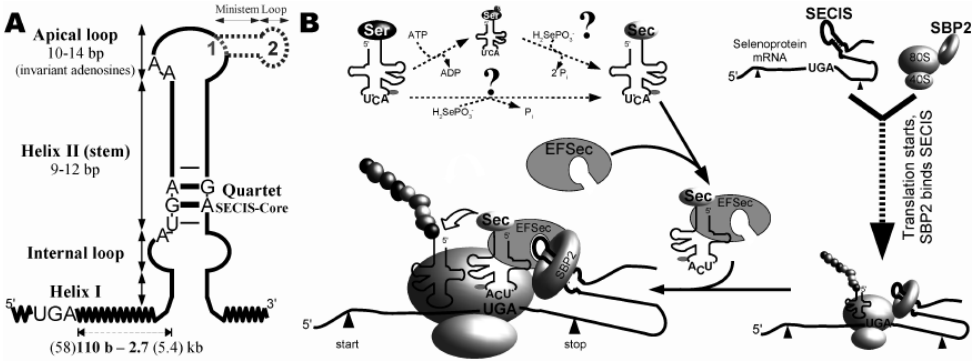

Figure I.8. *Selenoproteins biosynthesis in humans. Reproduced from ref. [55].*

Despite specific incorporation of Sec during translation, some organisms (yeasts, fungi and plants) can introduce Se into protein trough a non-specific mechanism; in that case the Se-amino acids produced are selenomethionine (Sem) and alkylated forms of Sec named Se-methyl selenocysteine (MeSeCys) and γ-glutamyl-Se-methylselenocysteine [57]. As concern Sem, an unselective substitution of methionine for selenomethionine in $tRNA_{Met}$ and, therefore, in the total body protein pool, occurs, due the fact that $tRNA_{Met}$ cannot distinguish between Met and Sem [56][57]. The non-specific incorporation of selenomethionine is also underlined by the fact that thus far, there is no evidence for a specific $tRNA_{Sem}$ in any organism.
It must be underlined that only Sec-containing proteins are called true selenoproteins because of the nonspecific nature of Se utilization in Sem-containing proteins [58].

I.4 References

[1] Fleischmann, R.D., Adams, M.D., White, O., Clayton, R.A., Kirkness, E.F., Kerlavage, A.R., Bult, C.J., Tomb, J.F., Dougherty, B.A., Merrick, J.M., Whole-genome random sequencing and assembly of Haemophilus influenzae Rd. *Science* **1995**, 269, 496-512.

[2] Wasinger, V.C., Cordwell, S.J., Cerpa-Poljak, A., Yan, J.X., Gooley, A.A., Wilkins, M.R., Duncan, M.W., Harris, R., Williams, K.L., Humphery-Smith, I., Progress with gene-product mapping of the Mollicutes: Mycoplasma genitalium. *Electrophoresis* **1995**, 16, 1090-4.

[3] Blackstock, W.P., Weir, M.P., Proteomics: quantitative and physical mapping of cellular proteins. *Trends in biotechnology* **1999**, 17, 121-7.

[4] Outten, C.E., O’Halloran, T.V., Femtomolar sensitivity of metalloregulatory proteins controlling zinc homeostasis. *Science* **2001**, 292, 2488-92.

[5] Williams, R.J.., Chemical selection of elements by cells. *Coordination Chemistry Reviews* **2001**, 216-217, 583-595.

[6] Szpunar, J., Metallomics: a new frontier in analytical chemistry. Analytical and bioanalytical chemistry **2004**, 378, 54-6.

[7] Haraguchi, H., Metallomics as integrated biometal science. *Health* **2004**, 5-14.

[8] Lobinski, R., Becker, J.S., Haraguchi, H., Sarkar, B., Metallomics: Guidelines for terminology and critical evaluation of analytical chemistry approaches (IUPAC Technical Report). *Pure and Applied Chemistry* **2010**, 82, 493-504.

[9] Bettmer, J., Metalloproteomics: a challenge for analytical chemists. *Analytical and bioanalytical chemistry* **2005**, 383, 370-1.

[10] Shi, W., Chance, M.R., Metallomics and metalloproteomics. *Cellular and molecular life sciences: CMLS* **2008**, 65, 3040-8.

[11] Szpunar, J., Advances in analytical methodology for bioinorganic speciation analysis: metallomics, metalloproteomics and heteroatom-tagged proteomics and metabolomics. *The Analyst* **2005**, 130, 442-65.

[12] Cooks, R,G,, Chen, G., Wong, P., Wollnik, H. Mass spectrometers. *Encyclopedia of Applied Physics* **1997**, 19, 289-97.

[13] Karas, M., Hillenkamp, F., Laser desorption ionization of proteins with molecular masses exceeding 10,000 daltons. *Anal. Chem.* **1988**, 60, 2299-301.

[14] Whitehouse C. M., Dreyer R. N., Yamashita M., Fenn J. B. Electrospray interface for liquid chromatographs and mass spectrometers. *Anal Chem.* **1985**, 57, 675–9.

[15] Caprioli, R., Sutter, M., Mass spectrometry tutorial **1995**, www.mc.vanderbilt.edu/msrc/tutorials/index.php

[16] Van Bramer, S.E., An Introduction to Mass Spectrometry **1998**.

[17] Cornish, T.J., Cotter, R.J., A curved-field reflectron for improved energy focusing of product ions in time-of-flight mass spectrometry *Rapid Commun. Mass Spectrom.,* **1993**, 11, 1037-40.

[18] Dawson, P.H., Quadrupole Mass Spectrometry and its applications *Elsevier Scientific Publishing Company*, **1976**.

[19] McLuckey, S.A., Goeringer, D.E., Glish, G.L., Collisional activation with random noise in ion trap mass spectrometry *Anal Chem.* **1992**, 64, 1455-60.

[20] Levsen, K., Fundamental Aspects of Organic Mass Spectrometry Verlag Chemie, **1978**.

[21] Sleno, L., Volmer, D.A., Ion activation methods for tandem mass spectrometry *J Mass Spectrom*., **2004,** 39, 1091-112.

[22] Paizs, B., Suhai, S., Fragmentation pathways of protonated peptides. *Mass Spectrom Rev.*, **2005**, 24, 508-48.
[23] Biemann, K., Contributions of mass spectrometry to peptide and protein structure. *Biomed Environ Mass Spectrom*, **1988**, 16, 99–111.
[24] Papayannopoulos, I.A., The interpretation of collision induced dissociation tandem mass spectra of peptides *Mass Spectrom Rev*, **1995**,14, 49–73.
[25] Roepstorff, P., Fohlmann, J., Proposal for a common nomenclature for sequence ions in mass spectra of peptides. *Biomed Mass Spectrom*, **1984**, 11, 601.
[26] Burlet, O., Yang, C.Y., Kaskell, S.J., Influence of cysteine to cysteic acid oxidation on the collision-activated decomposition of protonated peptides: Evidence for intraionic interactions. *J Am Soc Mass Spectrom*, *1992*, 3, 337–344.
[27] Morris, H.R., Paxton, T., Panico, M., McDowell, R., Dell, A., A novel geometry mass spectrometer, the Q-TOF, for low-femtomole/attomole-range biopolymer sequencing *J Protein Chem.,* **1997**, 16, 469-79.
[28] Shevchenko, A., Chernushevich, I., Ens, W., Standing, K.G., Bruce Thomson, B., Wilm, M., and Mann, M., Rapid “de Novo” Peptide Sequencing by a Combination of Nanoelectrospray , Isotopic Labeling and a Quadrupole/Time-of-flight Mass Spectrometer. *Rapid Commun Mass Spectrom.* **1997**, 11, 1015-1024.
[29] Coles, J.N., Guilhaus, M., Resolution limitations from detector pulse-width and jitter in a linear orthogonal-acceleration time-of-flight mass spectrometer. *J Am Soc Mass Spectrom*, **1994**, 5, 772–778.
[30] B’Hymer, C., Brisbin, J.A., Sutton, K.L., and Caruso, J.A., New approaches for elemental speciation using plasma mass spectrometry *Am. Lab.*, **2000**, 32, 17-39.
[31] Hinojosa Reyes, L., Marchante Gayón, J.M., García Alonso, J.I., Sanz-Medel, A., Determination of selenium in biological materials by isotope dilution analysis with an octapole reaction system ICP-MS. *Journal of Analytical Atomic Spectrometry* **2003**, 18, 11-16.
[32] Yip, Y.-chung, Sham, W.-cheong, Applications of collision/reaction-cell technology in isotope dilution mass spectrometry. *TrAC Trends in Analytical Chemistry* **2007**, 26, 727-743.
[33] Wind, M., Lehmann, W.D., Element and molecular mass spectrometry — an emerging analytical dream team in the life sciences. *Cancer Research* **2004**, 20-25.
[34] Gadd, G.M., Metals, minerals and microbes: geomicrobiology and bioremediation. *Microbiology* **2010**, 156, 609-43.
[35] Roberts, D., Earth, W., Associates, S., Speciation of Metals in Soils. *Soil Science* **2005**, 619-654.
[36] Sparks, D.L., Toxic Metals in the Environment: The Role of Surfaces. *Plant and Soil* **2005**, 193-198.
[37] Gilmour, C., Riedel, G., Biogeochemistry of trace metals and metalloids. *Encyclopedia of Inland Waters* **2009**, 7–15.
[38] Adriano, D. C., *Trace Elements in the Terrestrial Environment: Biogeochemistry, Bioavailability and Risks of Metals* **2001**.
[39] Huang, P. M., Wang, M. C., Wang, M. K., Mineral–organic–microbial interactions. In *Encyclopedia of Soils in the Environment* **2004**, 486–499.

[40] Ma, Z., Jacobsen, F.E., Giedroc, D.P., Coordination chemistry of bacterial metal transport and sensing. *Chemical reviews* **2009**, 109, 4644-81.
[41] Osman, D., Cavet, J. S., Copper homeostasis in bacteria. *Adv Appl Microbiol* **2008**, 65, 217–247.
[42] Silver, S., Phung, L. T., Heavy metals, bacterial resistance. *Encyclopedia of Microbiology*, **2009**, 220–227.
[43] Fergusson, J.E., The Heavy Elements: Chemistry, Environmental Impact and Health Effects, *Pergamon Press,Oxford*, **1990**, 345.
[44] Nieboer, E., Richardson, D.H.S., The replacement of the nondescript term ‘heavy metal’ by a biologically significant and chemically significant classification of metal ions. *Environ Pollut*, **1980**, 1, 3–26.
[45] Duffus, J.H., "Heavy metals" A meaningless term? *Pure Appl. Chern*. **2002**,74, 793-807.
[46] White, P.J., Bowen, H.C., Parmaguru, P., Fritz, M., et al., Interactions between selenium and sulphur nutrition in Arabidopsis thaliana. *Journal of experimental botany*, **2004**, 55, 1927-37.
[47] Pinsent, J., The need for selenite and molybdate in the formation of formic dehydrogenase by members of the coli-aerogenes group of bacteria. *Biochem J*, **1954**, 57, 10-6.
[48] Gunzler, W.A., Steffens, G.J., Grossmann, A., Kim, S.M.A., Otting, F., Wendel, A., and Flohe, L. The amino acid sequence of bovine glutathione peroxidase. *Hoppe-Seyler’s. Z. Physiol. Chem*., **1984**, 365, 195–212.
[49] Lu, J., Holmgren, A., Selenoproteins. *The Journal of biological chemistry,* **2009**, 284, 723-7.
[50] Rayman, M.P. The use of high-selenium yeast to raise selenium status: how does it measure up? *Brit. J. Nutr*, **2004**, 92, 557–573.
[51] Calomme, M., Hu, J., Van Den Branden, K., and Vanden Berghe, D.A., Seleno-Lactobacillus An Organic Selenium Source. *Biological Trace Element Research* **1995**, 47, 379-383.
[52] Alzate, A., Fernández-Fernández, A., Pérez-Conde, M.C., Gutiérrez, A.M., Cámara, C., Comparison of biotransformation of inorganic selenium by Lactobacillus and Saccharomyces in lactic fermentation process of yogurt and kefir. *Journal of agricultural and food chemistry* **2008**, 56, 8728-36.
[53] Matés, J.M., Effects of antioxidant enzymes in the molecular control of reactive oxygen species toxicology. *Toxicology* **2000**, 153, 83-104.
[54] Su, D., Li, Y., and Gladyshev, V.N. Selenocysteine insertion directed by the 3'-UTR SECIS element in Escherichia coli. *Nucleic Acids Res* **2005**, 33, 2486-2492.
[55] Gromer S., Eubel J. K., Lee B. L., Jacob J. Human selenoproteins at a glance. *Cell. Mol. Life Sci.* **2005**, 62, 2414–2437.
[56] Birringer M., Pilawa S., Flohé L. Trends in selenium biochemistry. *Nat. Prod. Rep.* **2002**, 19, 693–718.
[57] Suzuki, K.T., Metabolomics of Selenium: Se Metabolites Based on Speciation Studies. *Toxicology* **2005**, 51, 107-114.
[58] Lopez Heras, I., Palomo, M., Madrid, Y., Selenoproteins: the key factor in selenium essentiality. State of the art analytical techniques for selenoprotein studies. *Analytical and bioanalytical chemistry* **2011**, 400, 1717-27.

Chapter II: Development of a strategy to study effects of heavy-metals contamination on model system *Escherichia coli*

II.1 Introduction

Here a development of an integrated metallomics-proteomics approach for the investigation of the effects of heavy metals exposure on *Escherichia coli* as model organism is reported.
Different culture conditions were tested at different concentrations of heavy-metals in liquid media (Cd, and Pb), in order to determine the toxic doses of pollutants that exerted approximately 50% inhibition of growth.
A microwave assisted digestion procedure was developed for the dissolution of biological samples before ICP-MS determination of their elemental composition. The developed methodology was applied to the evaluation of quantitative changes of the heavy-metals levels in the medium during the growth, in order to understand critical toxic levels for each metal.
An evaluation of the effects of cadmium on proteome of *E. coli* cultures was performed by using a classical proteomics approach based on 2D-PAGE, image analysis and identification of differentially expressed proteins.

II.1.1 Microbial heavy-metal resistance

Environmental pollution due to the presence of heavy metals is one of the most studied problems because the current harmful effects are still difficult to predict. Their presence and relative concentration means that heavy metals are a major source of toxicity to humans and to the entire environment in general [1].
The toxicity of heavy metals is not only due to high concentrations, but also to secondary processes; some pollutants, in fact, may induce a process of oxidation - reduction cycle, generating reactive oxygen and nitrogen species (ROS = Reactive Oxygen Species). If these species are not extinguished by cellular mechanisms, may promote a state of oxidative stress, which in some cases can also lead to cell death [2].
Living organisms, such as gram-negative *Escherichia coli*, are usually used as bio-indicator to study cellular responses to environmental signals, identifying molecules involved in defense mechanisms [3].
Metals play an important role in life processes of living organisms. Some metals, such as calcium, cobalt, chromium, copper, iron, potassium, magnesium, manganese, sodium, nickel and zinc, are essential, serve as micronutrients and are used for redox-processes, to stabilize molecules through electrostatic interactions, as components of various enzymes and for regulation of osmotic pressure [4]. Many other metals have no biological role (e.g. silver, aluminum, cadmium, gold, lead, mercury and arsenium), and are nonessential and potentially toxic to microorganisms [4]. Toxicity of nonessential metals occurs through the displacement of essential metals from their native binding sites or through ligand interactions. For example, Hg^{2+}, Cd^{2+} and Ag^{2+} tend to bind to SH groups, and thus inhibit the activity of sensitive enzymes [5]. In addition, at high levels, both essential and nonessential metals can damage cell membranes, alter enzyme specificity, disrupt cellular functions and damage the structure of DNA [6].
The investigation of microbial resistance mechanisms towards heavy metals is essential for the potential applications of microorganisms in bioremediation.
Research carried out since the early 1970s identified several microorganisms as being resistant to certain metals. These reports included mostly aerobic microorganisms, with prominent examples being resistance in *Staphylococcaus* sp., *Escherichia coli*, *Pseudomonas aeruginosa*, and *Bacillus* sp [7][8][9][10].

Six generic metal resistance mechanisms exist: metal exclusion by permeability barrier, intra- and extra-cellular sequestration of the metal by protein binding, active efflux transport systems away from the cell, enzymatic detoxification of the metal to a less toxic form, and reduction in the sensitivity of cellular targets to metal ions [11].
The main process for regulating intracellular metal concentration is with membrane transport mechanisms. Under normal conditions, both nonessential and essential metal ions are transported into an organism by nonspecific uptake systems. However, in cases where metal ions are in excess, synthesis of specific ion efflux systems can occur to exclude nonessential metals. An example is the exclusion of the toxic metal arsenate As(V) during the uptake of essential phosphates. The cell discriminates against As(V) by inducing a more specific system that takes up phosphate with 100-fold greater specificity than normal mechanisms [12].
The presence of metal ions can up-regulate genes to initiate metal resistance by enzymatic detoxification [13]. The most prominent example is Hg(II) resistance coded for by the *mer* (mercury) operon. Mercury is highly toxic because of its affinity for thiols [14]. It inactivates thiols that are part of enzymes and other essential cellular proteins. Bacteria have adapted to the presence of Hg(II) by evolving a set of genes that form a resistance operon. The gene products of this operon not only detoxify Hg(II) but are also involved in transport and self-regulation [15].
However, all toxic metals share the common feature of essential trace elements such as copper, zinc and iron, in relation with cellular uptake that altered the homeostasis of cells. Many cellular efforts are in fact devoted by the cells to maintain an optimal bioavailable concentration of metals through extensive regulatory and protein-coding machinery. This complexity to support a right homeostasis is reflected by the large number of heavy-metal-binding protein dedicated to transport of specific metals, as reported for iron, zinc, manganese, copper, nichel and cobalt in figure II.1. Stress response represented by the presence of toxic metal ions can alter the maintaining of a constant state of the homeostasis using the same transport mechanism, leading to a depletion of a particular metal ion (e.g., zinc) with a toxic one (cadmium) [16].

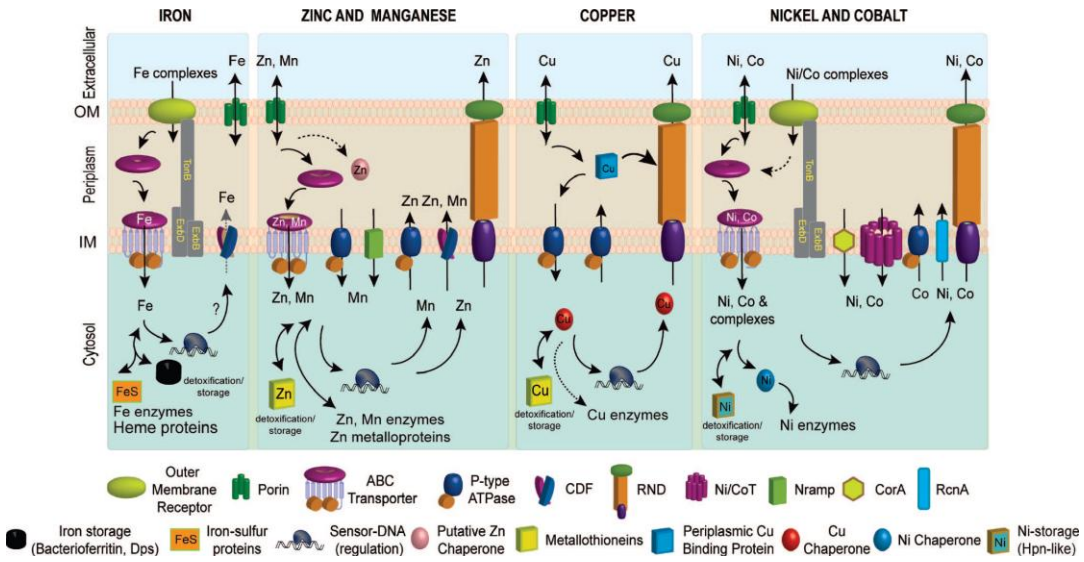

Figure II.1. *Schematic metal homeostasis models for iron, zinc and manganese, copper, and nickel and cobalt, shown specifically in Gram-negative bacteria. Reproduced from ref. [16].*

The understanding of the genetic basis of metal resistance is rapidly increasing the ability to use these systems for environmental applications. Improvements in genetic manipulation techniques make it possible to create super accumulator bacteria that can help decontaminate polluted soils and water [4]. The understanding of how microorganisms resist to metals, can increase the success of bioremediating contaminated environments.

II.2 Materials and Method

Bacterial Strain

All experiments were carried out using as host *E. coli* strain TK12 MG1655.

Effect of Metal Ions on Growth Inhibition

Cells were grown in 5 mL Luria-Bertani (LB) broth (10 g/L tryptone, 5 g/L NaCl and 5 g/L yeast extract, pH 7.2) at 37 ºC, 250 rpm for overnight. Then 50 µL of overnight cultures were transferred into 5 mL broth and grown until OD reached 0.5. Cells were adjusted to equal OD = 0.05 in LB broth. Aliquot of sample (100 µL) was seeded onto a 96 well sterile microplate and 100 µL of LB broth containing an increasing range of metal-ion concentrations of Cd^{2+} ($CdCl_2$) and Pb^{2+} ($PbCl_2$). The concentrations chosen for metals exposure were: 0.05, 0.1, 0.2, 0.4, 0.8 and 1mM for both Cd and Pb.

Plate was further incubated at 37ºC with moisture for 30 hours. The growth rate was determined by monitoring the absorbance at 600 nm by microplate reader. The concentrations of metal ions those gave rise approximately 50% growth inhibition were selected for further experiments.

Microwave Acid digestion and ICP-MS analysis

For metals analysis, an appropriate method consisting of a mineralization procedure using a microwave digestion oven coupled with high sensitive ICP-MS quantitative analysis was setting up.

Aliquots of each sample (1 mL of growth medium, 0.5 OD of pellet and 1 mL of wash of each pellet) were introduced into the digestion vessels. Wet oxidation was induced using concentrated, 6 mL of ultra-high purity nitric acid with the addition of a 2 mL of concentrated hydrogen peroxide. Oxidation was carried out in an hermetically sealed PTFE reactor introduced inside a microwave oven and irradiated at 1400 W, using a high-pressure microwave digestion oven (Ethos EZ, from Milestone). Temperature control was used as opposed to pressure control. Samples were ramped to 220 °C over 15 minutes and held at 220 °C for 20 minutes before cooling to below 50 °C before venting the vessel for 30 minutes. Both pressure and temperature were monitored by direct measurement throughout the digestion to ensure that samples attained the critical temperature of 220 °C, at which biological components are digested. Then, the sample digests were diluted 100x with bidistilled water, and an aliquot of each sample was used for ICP-MS determination. The analyses were carried out in triplicate on an Agilent 7700 ICP-MS, equipped with a frequency-matching RF generator and 3rd generation Octopole Reaction System (ORS3), operating with helium as cell gas. The parameters were set as follows: RF power 1550 W, plasma gas flow 14 L min $^{-1}$; carrier gas flow 0.99 L min $^{-1}$; He gas flow 4.3 mL min $^{-1}$. ^{103}Rh was used as an internal standard (50 µg L^{-1} final concentration).

Multi-element calibration standards were prepared in 5% HNO_3 at 4 different concentrations (1, 10, 50, and 100 μg L^{-1}).

Preparation of Protein Samples for Proteomic Analysis

Cells were grown at 37 ºC for overnight in 5 mL LB. Cells were subsequently inoculated in 200 mL LB and incubated at 37ºC for 2 hours. Metal solution was then added to the culture to yield the final concentrations of 0.2 mM cadmium. After 2 hours, cells were collected, washed, and resuspended in Tris buffer. Cells were disrupted by using a French press. Collection of whole cell lysate was performed by centrifugation at 13,000 rpm for 30 min at 4 °C. Bradford's method was used for quantification of protein amounts using bovine serum albumin as a standard.

Two-Dimensional Gel Electrophoresis (2-DE)

The first dimensional electrophoresis (isoelectric focusing, IEF) was carried out on non-linear wide-range immobilized pH gradients (pH 4-7; 7 cm long IPG strips; GE Healthcare, Uppsala, Sweden) and achieved using the Ettan IPGphor system (GE Healthcare, Uppsala, Sweden). 150 μg of protein extracts were precipitated with methanol/chloroform according to Wessel [17] and solubilized in 125 μL of rehydratation buffer and 0,2% (v/v) carrier ampholyte for 12h, at 50 mA, at 20° C. The strips were then focused according to the following electrical conditions at 20°C: 500 V for 30 min, 1000 V for 30 min, 5000 V for 10h, until a total of 15000 Vt was reached. After focusing, IPG strips were equilibrated for 15 min in 6 M urea, 30% (V/V) glycerol, 2% (w/V) SDS, 0.05 M Tris-HCl, pH 6.8, 1% (w/V) DTT, and subsequently for 15 min in the same urea/SDS/Tris buffer solution but substituting the 1% (w/V) DTT with 2.5% (w/V) iodoacetamide. The second dimension was carried out on 12.5% (w/w) polyacrylamide gels (10 cm x 8 cm x 1 mm) at 25 mA/gel constant current, until the dye front reached the bottom of the gel, according to Laemmli [18]. Gels were stained overnight with colloidal Coomassie Brilliant Blue and destained with MilliQ grade water.

Image analysis

Gel images were acquired with an Epson expression 1680 PRO scanner. Computer-aided 2-D image analysis was carried out using the ImageMaster™ 2D Platinum software. Relative spot volumes (%V) (V=integration of OD over the spot area; %V = V single spot/V total spot) were used for quantitative analysis in order to decrease experimental errors. The normalized intensity of spots on three replicate 2-D gels was averaged and standard deviation was calculated for each condition. A few initial reference points (landmarks) were affixed for gels alignment, representing the first step of the images analysis. Landmarks are positions in one gel that correspond to the same position in the other gels. Then, the software automatically detects spots, which represent the proteins on the gels. The software "matches" the gels and the corresponding spots are paired. The pair is the association between spots that represent the same protein in different gels.

Quantification of intensity of each spot was performed in term of spot volume (area x intensity). Then, determination of differentially expressed proteins was achieved by comparing the ratio of % volume values between control and treated sample gel; spots that exhibit a variation of ± 20% were considered not affected by metals exposure.

Protein identification

Spots selected by image analysis were further excised from the gels destained by repetitive washes with 0.1 M NH_4HCO_3, pH 7.5, containing 40% acetonitrile. Enzymatic digestion was carried out with 100 ng of trypsin in 50 µL of 10 mM ammonium bicarbonate buffer, pH 7.8. Gel pieces were incubated at 37 °C overnight. Peptides were then extracted by washing the gel particles with 10 mM ammonium bicarbonate and 1% formic acid in 50% acetonitrile at room temperature. The resulting peptide mixtures were filtrated using 0.22 PVDF filter from Millipore.

The peptide mixtures were analyzed using a CHIP MS 6520 QTOF equipped with a capillary 1200 HPLC system and a chip cube (Agilent Technologies, Palo Alto, Ca). After loading, the peptide mixture (8 µL in 0.1% formic acid) was first concentrated and washed at 4 µL min^{-1} in 40 nL enrichment column (Agilent Technologies chip), with 0.1% formic acid in 2% acetonitrile as eluent. The sample was then fractionated on a C18 reverse-phase capillary column (75µm x 43mm in the Agilent Technologies chip) at flow rate of 400 nL min^{-1} with a linear gradient of eluent B (0.1% formic acid in 95% acetonitrile) in A (0.1% formic acid in 2% acetonitrile) from 7 to 60 % in 50 min. Peptide analysis was performed using data-dependent acquisition of one MS scan (mass range from 300 to 2000 m/z) followed by MS/MS scans of the three most abundant ions in each MS scan. Raw data from nanoLC–MS/MS were analyzed using Qualitative Analysis software and MSMS spectra were searched against non-redundant protein databases Uniprot/Sprot, with the taxonomy restriction to *Escherichia coli*, using in house MASCOT software (www.matrixscience.com). The Mascot search parameters were: “trypsin” as enzyme allowing up to 3 missed cleavages; carbamidomethyl on cysteine residues as fixed modification; oxidation of methionine and formation of pyroGlu N-term on glutamine were selected as variable modifications; 20 ppm on MS and 0.6 Da on MS/MS tolerances. For protein identifications only peptides with an individual ions scores > 20 was used.

II.3 Results and discussion

II.3.1 Screening of lethal doses of pollutants

Different cultures were tested at different concentrations of heavy-metals in liquid media (Cd, and Pb), in order to determine the toxic doses of pollutants that exerted approximately 50% inhibition of growth. The metal chloride was used in order to prefer bio-adsorption of metal on the cell surface to its intracellular uptake [19].

As reported in figure II.2 (left panel) 0.2 mM of $CdCl_2$ gave rise approximately 50% growth inhibition. Thus this value was selected for further experiments. As for lead, any variation during microbial growth up to 1mM concentrations was observed; in fact in literature is reported that the minimal inhibitory concentration (MIC) determined for *E.coli* is 5 mM [20].

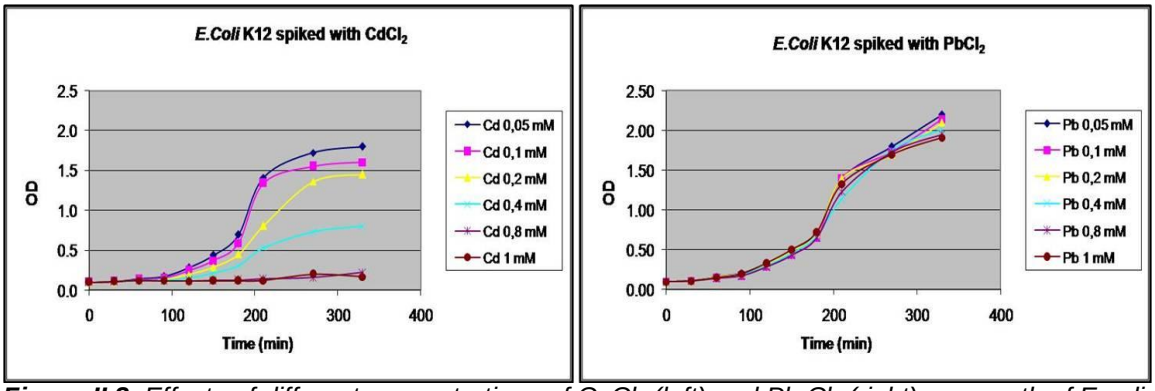

Figure II.2. *Effects of different concentrations of $CaCl_2$ (left) and Pb Cl_2 (right) on growth of E.coli strain TK12 MG1655 in multiwell plate.*

II.3.2 Effects on lag time

In literature is reported that heavy metal concentrations above trace levels result in prolonged lag time and/or reduced growth rate, and the duration of the lag is observed to be dependent on the metal concentration [21]. In fact, in cadmium treatment an extension of lag time was found (Fig. II.3). The prolonged lag phases was proposed due to several causes, such as: the decline in cell viability; the heavy metal penetrating into the periplasm or cytoplasm to react with intracellular components; a detoxification process, which becomes longer as the amount of ions to inactivate is higher; the time necessary for acclimation; a physiological adaptations of the bacteria to the environmental conditions [21].

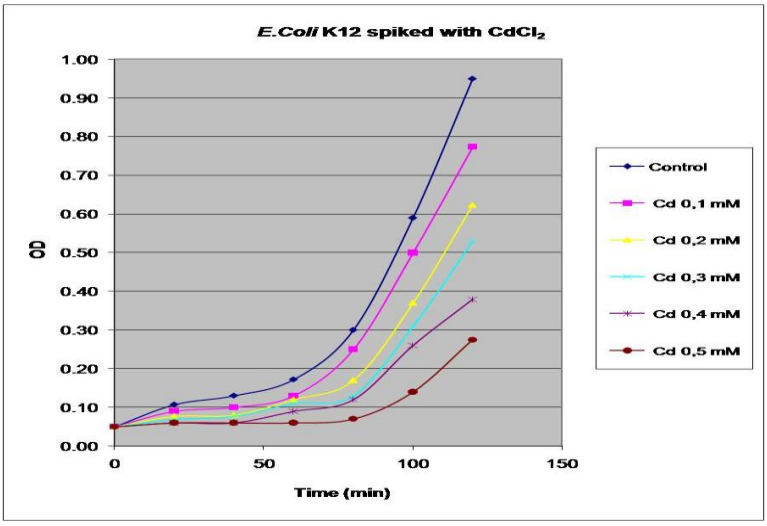

Figure II.3. *Effects on lag time of different concentrations of $CaCl_2$ on initial growth phase of E.coli strain TK12 MG1655.*

II.3.3 Metallomic approach

The ICP-MS data collected (Fig. II.4) show that cadmium and lead were internalized with high efficiency; in fact for cadmium the uptake is about 20% against the percentage of about 35% for lead. In both cases the uptake happens during the first 90 minutes of cellular growth, and both the cellular and the extracellular concentration of metals do not change during further times. It was been measured also the absorption of metal ions upon cellular surface by washing pellet several

times with bidistilled water; the result is that for lead we found an 8% of total lead administered, while about 1% is present in cadmium treatment.

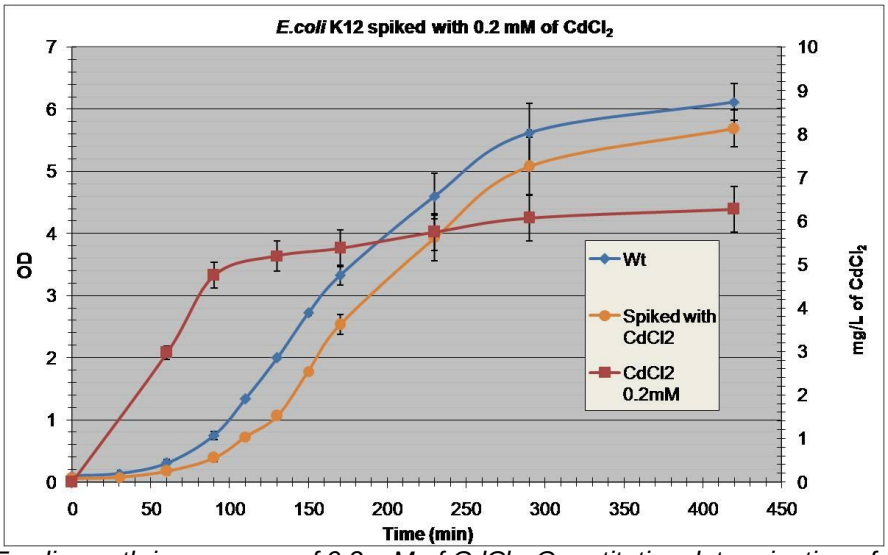

Figure II.4. *E.coli growth in presence of 0.2 mM of $CdCl_2$. Quantitative determination of Cadmium by ICP-MS during microbial growth.*

II.3.4 Multielemental ICP-MS analysis and PCA statistical analysis

By using the capability of ICP-MS to perform multi-elemental analysis at the same time, several essential elements were also monitored in a control microbial growth and a Cd exposure condition. These elements were Ag, Al, As, Co, Cr, Cu, Fe, Mn, Ni, Sb, Se, Sn, Zn and V. For almost all metals (like for example Fe and Ni showed in Fig. II.5), no changes were detected between comparison of the intracellular concentrations in control sample and in lead-spiked sample; on the contrary a high decrease of intracellular Zn (from 35 mg/L estimated in control to 2 mg/L in cadmium-spiked sample, Fig. II.5) was detected in the microbial growth in presence of Cd. It was calculated by Outten and coworkers [22] the total zinc content, from metal-depleted media, in *Escherichia coli* cells, that is around 2*105 Zn atoms per cell, corresponding to 0.2 mM (about 13 mg/L); these value suggest that the presence of high levels of Cd in liquid media, affects the Zn uptake.

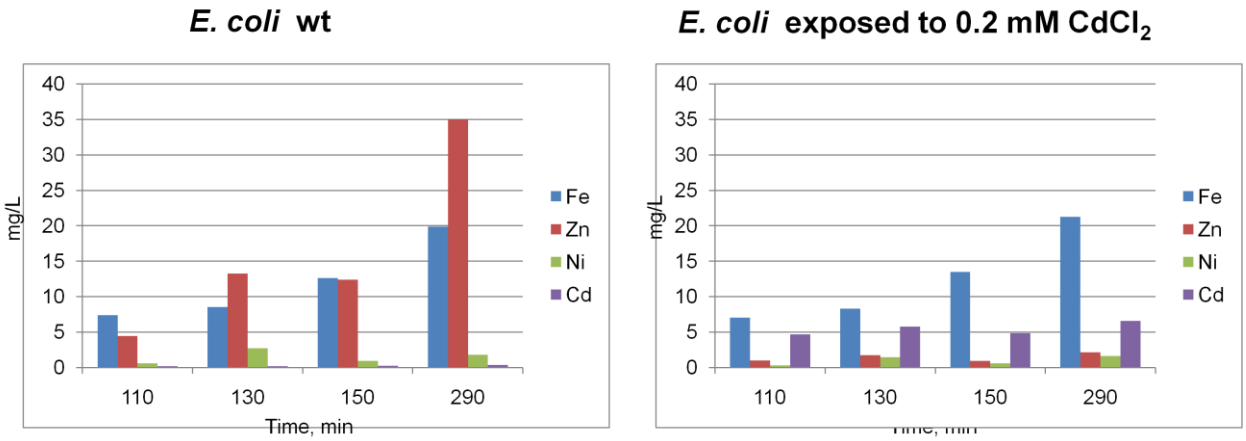

Figure II.5. *Metals quantification by ICP-MS analysis during E.coli growth in control condition (left) and with addition of 0.2 mM of $CdCl_2$ in liquid medium. Four metals are illustrated; while for Fe and Ni seems to be no variation in concentration, a drastic decrease of Zn is notable in Cd exposure.*

The high-throughput data file resulting from ICP-MS analysis was subjected to multivariate statistical analysis. To this aim, the principal component analysis (PCA) was performed by using the XLSTAT software. PCA is a multivariate analysis method that highlights inherent clustering behavior based on the similarity of the data profiles, thus representing a common tool to visualize an overall trend of the data obtained, and to underline differences between complex data set. The PCA enables a reduction in data complexity and description of a given multidimensional system by means of a small number of new variables, which are the result of a composition of 16 (metals) original variables. New variables are extracted, as long as it is believed that the explained variance is sufficiently large compared to the total variance. The biplot forming by new variables named F1 and F2 account for approx. 70% of the total variance (Fig. II.6). More interestingly, this analysis showed that the individual elementals monitored have a common feature; in fact most of divalent ions were in the most populated cluster of the biplot diagram. In particular Zn and Cd resulted to be very closed in the plot region; this finding could be related to the same transport mechanism necessary for the uptake of these metals from the medium.

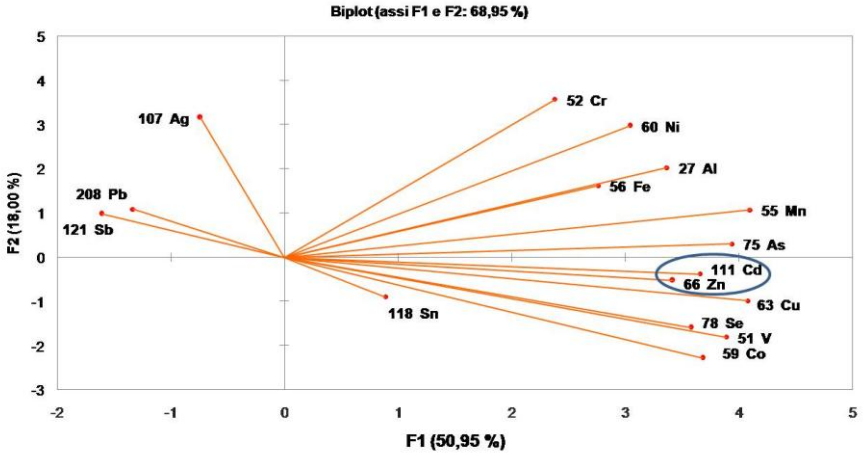

Figure II.6: *PCA statistical analysis of metals present in a Cd-spiked liquid medium of E.coli during microbial growth*

II.3.5 Classical proteomic approach

Significant changes of differentially expressed proteins in response to toxic doses of cadmium 0.2 mM were detected; this alteration implied the involvement of a cellular processes network.

Semi-quantitative changes in the proteins expression were observed by 2D-PAGE, Image Analysis and Mass Spectrometry analysis.

After comassie staining, the two gel maps were compared; 85 spots were properly matched and, considering a tolerance of 20% of the volumes comparison, 21 spots were found to be differentially expressed, of which 17 were down - regulated and 4 up – regulated (Fig. II.7 and Table II.1).

Thus, these spots were excised from the gel and *in situ* hydrolyzed with trypsin. The peptide mixtures were then analyzed through nLC-MS/MS using an Agilent CHIP MS 6520 QTOF.

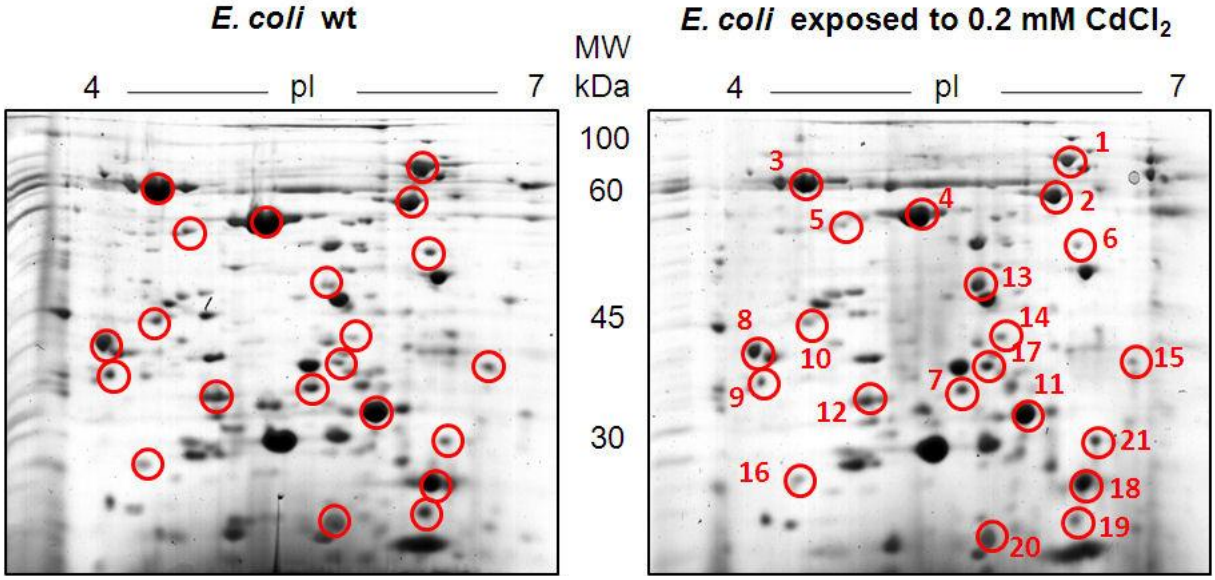

Figure II.7: *Master map representing protein profiles of E. coli strain TK12 MG1655 grown in the absence (left) and presence of 0.2 mM $CdCl_2$ (right). Numbers of protein spot denoted as identified protein represented in table II.1.*

Spot No.	Δ volume (%)	Nominal mass (Da)	Description	SwissProt Accession No.	Protein Score	N° of Peptides	Sequence Coverage (%)
1	-75	60483	Periplasmic dipeptide transport protein	P23847	47	3	10
2	-72	60975	Periplasmatic oligopeptide-binding	P23843	1736	54	82
3	-51	57464	60 kDa chaperonin	P0A6F5	757	28	58
4	-67	53139	Tryptophanase	P0A853	115	8	17
5	-52	51265	Flagellin	P04949	2199	40	96

6	-78	42928	3-oxoacyl-[acyl-carrier-protein] synthase 1	P0A953	89	4	16
7	-56	45683	Enolase	P0A6P9	209	7	30
8	-48	43427	Elongation factor Tu 1	P0CE47	634	20	52
9	-64	41264	Phosphoglycerate kinase	P0A799	620	23	59
10	-61	43360	Maltose-binding periplasmic	P0AEX9	336	14	41
11	-55	42128	Alcohol dehydrogenase	Q46856	1348	36	84
12	-59	32504	Malato-dehydrogenase	B6I1V4	923	23	86
13	+109	36776	Autoinducer 2-binding protein lsrB	B1XEA	209	11	38
14	+64	37292	Outer membrane protein A	P0A910	120	4	14
15	-54	35690	D-galactose-binding periplasmic	P0AEE5	571	23	58
16	-45	30518	Elongation factor Ts	P0A6P1	90	3	13
17	+43	33870	High-affinity zinc uptake sistem ZnuA	P39172	166	8	37
18	-45	30931	D-Ribose-binding periplasmatic	P02925	459	19	66
19	-39	31021	D-tagatose-1,6-bisphosphate aldolase subunit gatY	P0C8J6	363	15	57
20	-34	31147	2,5-diketo-D-gluconic acid reductase A	Q46857	298	12	49
21	+32	26619	Uncharacterized protein YggE	P0ADS6	81	4	11

Table II.1. *List of the proteins identified by nanoLC-MS/MS. Spot numbers refer to figure II.7. Variation in fold expression are given by the comparison of each spot with the control. +/- indicates increment/decrement with respect to the control.*

Analysis of proteins for which translational levels were found to be decreased (Table II.1) reveals that the exposure to cadmium affects many cellular functions. Alteration on the protein biosynthesis machinery was displayed through EF-Tu and EF-Ts, two proteins involved in translation; this adaptation may comprise a general response to stress or may merely be a function of lower growth rates in the presence of a toxic

agent. In addition the reduction of Tryptophanase (tnaA), a protein involved in metabolism of amino acids, suggests that the cell is less catabolic in nature.
A decrease of Malate dehydrogenase (MDH) and Phosphoglycerate kinase (pgk) levels up to 59% and 64% respectively was found; this can explain the decrease of biomass observed in the Cd treated cells.
Reduction of several proteins involved in active transport through biological membranes, Dipeptide binding protein (DppA), oligopeptide transport periplasmic binding protein (OppA) was found. Even the chemotaxis and the transport of sugars was affected as a decrease of D-Ribose-binding periplasmatic (rbsB)**,** Maltose-binding periplasmatic (MBP) and D-Galactose-binding periplasmatic (GBP) were found. It has been believed that importing of amino acid and other carbon sources *via* periplasmic binding proteins is essential for *E.coli* cells during energy crisis [23]. Therefore, using this low-energy requiring transport system may in turn result in a rapid consumption of such transporters [24]. Moreover GBP possess a metal-binding site, structurally similar to that of EF-hand proteins; in literature is reported that GBP possess relative affinities for various metals which bind to the lone calcium-binding site of EF-hand loop. In order of affinity the metals are: $Ca^{2+} > Tb^{3+} > Pb^{2+} > Cd^{2+} > Sr^{2+} > Mg^{2+} > Ba^{2+}$ [25]
Other proteins identified are involved in microbial mobility such as Flagellin (fliC), and protein folding as 60 KDa Chaperonin (groL). Flagellin is a component of flagellar filament which provides motility to the bacteria. Potential benefits of motility include increased efficiency of nutrient acquisition and avoidance of toxic substances [26]. It has been reported that synthesis of Flagellin gets repressed by various antibiotics belonging to different groups having different mode of actions. In addition Shoeb and coworkers have demonstrated that Flagellin represent a mechanism of tolerance against nickel in *Bacillus cereus* protein [27].
About up-regulated proteins, it is worth noting that the presence of Cd rendered the up-regulation of zinc-binding transport protein (ZnuA). This protein belongs to the TroA superfamily of periplasmic metal binding proteins, which function as initial receptors in the ABC uptake of Zn^{2+}. ZnuA possesses a central domain of variable length in different bacterial species which is characterized by the presence of a high number of histidine and acidic residues whose function is not yet known. Some studies have suggested that this loop could enhance zinc binding ability and its subsequent transfer to the primary binding site of ZnuA [28].
It was established that cadmium induces the accumulation of proteins involved in zinc transport, i.e., ZnuA and ZnuB and it was suggested by that cadmium alters zinc homeostasis in bacteria [29]. These proteins could be involved in the chelation of excess cytosolic metal ions which may generate tolerance or perhaps represent compensatory alterations which preserve cation metabolism in the presence of excess Zn(II), Cd(II), Co(II) or Ni(II) [30].
An increase of ZnuA might be attributable to zinc deficiency once substitution of zinc ions by cadmium occurs. Therefore, compensation by increase regulating of zinc uptake via ZnuABC system took place [31].
In addition an increase in expression levels of other proteins involved in transport machinery was found, Autoinducer 2-binding protein (lsrB) and Outer membrane protein A (OmpA). These findings can be explained with the required to efflux metal xenobiotics from the cells when a certain toxic level is reached.
A strong up-regulation of Autoinducer 2-binding protein (lsrB) was found. LsrB is a part of the ATP binding cassette (ABC) transporter complex. Furthermore, consistent

with tolerance to cations, OmpA, an outer-membrane porins, was found to be over-expressed. Porin are membrane proteins which in a multimeric form constitutes a water-filled transmembrane channel. This pore allows the passage of ions and numerous other, non-specific molecules through the membrane [32].
Moreover translational level of Uncharacterized protein YggE was found to be increased; YggE is involved cellular response to stress represented by reactive oxygen species; Kim and coauthors has recently demonstrated by DNA microarray analysis that *yggE* gene, together with *yfiD*, *yggB*, were up-regulated in a superoxide dismutase (SOD)-deficient *Escherichia coli* strain IM303 cultivated under the oxidative stress [33].

II.4 Conclusion

This work details the investigation of metal-ion tolerance in *E. coli*, looking in particular at the effects on proteome after exposure to a dose of cadmium that was found to exert approximately 50% inhibition of microbial growth. Metallomics data together with proteomics and statistical analysis suggest that a strong correlation between zinc and cadmium take place, in particular with a depletion of zinc in cadmium-treated *E.coli* cells, coherent with an increase of cadmium into cells.
In addition cadmium seems to affect many molecular functions, in particular a strong decrease of biosynthesis machinery and in general energy metabolism, despite an over-expression over proteins involved in transport mechanism trough membrane.
Many of the identified proteins possess a metal-binding domain and for some of them in literature are reported the capability to bind unspecifically many divalent metal ions, as for example for ZnuA which level could be increased in order to efflux cadmium from the intracellular space to the extracellular.

Acknowledgements

Author thanks Dr. Pamela Di Pasquale for supplying *E.coli* samples.

II.6 References

[1] Haferburg, G., Kothe, E., Microbes and metals: interactions in the environment. *Journal of basic microbiology* **2007**, 47, 453-67.
[2] López-Barea, J., Gómez-Ariza, J.L., Environmental proteomics and metallomics. *Proteomics* **2006**, 6 Suppl 1, S51-62.
[3] González-Fernández, M., García-Barrera, T., Jurado, J., Prieto-Álamo, M.J., et al., Integrated application of transcriptomics, proteomics, and metallomics in environmental studies. *Pure and Applied Chemistry* **2008**, 80, 2609-2626.
[4] Bruins, M.R., Kapil, S., Oehme, F.W., Microbial resistance to metals in the environment. *Ecotoxicology and environmental safety* **2000**, 45, 198-207.
[5] Nies, D.H., Microbial heavy-metal resistance. *Applied microbiology and biotechnology* **1999**, 51, 730-50.
[6] Poole, R. K., Gadd, G. M., Metals: Microbe Interactions. *IRL Press, Oxford*.**1989**, 1-37.
[7] Schwarz, S.T., Hobel, H., Plasmid and resistance to antimicrobial agents and heavy metals in *Staphylococcus hyicus* from pigs and cattle. *J. Vet. Med. Educ.* **1989**, 36, 669-673.
[8] Harnett, N.M., Gyles, C.L., Resistance to drugs and heavy metals, colicin production and biochemical characteristics of selected bovine and porcine *E. coli* strains. *Appl. Environ. Microbiol.* **1984** ,48, 930-945.

[9] Marques, A.M., Congregado, F., Simon-Pujol, D.M., Antibiotic and heavy metal resistance of *Pseudomonas aeruginosa* isolated from soils. *J. Appl. Bacteriol.* **1979**, 41, 341-350.
[10] Belliveau**,** B**.**H**.**, Starodub**,** M**.**E**.**, Trevors**,** J**.**T**.,** Occurrence of antibiotic and metal resistance and plasmids in Bacillus strains isolated from marine sediment. *Can J Microbiol*. **1991**, 37, 513-520.
[11] Silver, S., Phung, L. T., Bacterial heavy metal resistance: new surprises. *Annu*. *Rev*. *Microbiol*. **1996**, 50, 753-789.
[12] Nies, D.H., Silver, S., Ion efflux systems involved in bacterial metal resistances. *J Indust Microbiol.* **1995**, 14, 186-199.
[13] Silver, S., Walderhaug, M., Gene regulation and chromosomedetermined inorganic ion transport in bacteria. *Microbiol*. *Rev*. **1992**, 56, 195-228.
[14] Misra, T. K., Bacterial resistance to inorganic mercury salts and organomercurials. *Plasmid* **1992**, 27, 4-16.
[15] Weiss, A., Murphy, S., Silver, S., Mercury and organomercurial resistance determined by plasmids in *Staphylococcus aureus*. *J*. *Bacteriol*. **1977**, 132, 197-208.
[16] Ma, Z., Jacobsen, F.E., Giedroc, D.P., Coordination chemistry of bacterial metal transport and sensing. *Chemical reviews* **2009**, 109, 4644-81.
[17] Wessel, D., Flügge, U.I., A method for the quantitative recovery of protein in dilute solution in the presence of detergents and lipids. *Anal Biochem*. **1984**, 138, 141-143.
[18] Laemmli, U.K. Cleavage of structural proteins during the assembly of the head of bacteriophage T4. *Nature* **1970**, 227, 680-685.
[19] Kotrba, P., Pospisil, P., De Lorenzo, V., Ruml, T., Enhanced metallosorption of *Escherichia coli* cells due to surface display of beta- and alpha-domains of mammalian metallothionein as a fusion to LamB protein. *J Recept Signal Transduct Res.* **1999**, 19, 703-715.
[20] Mergeay, M., Nies, D.H., Schlegel, H.G., Gerits, J., Charles, P.,, Van Gijsegem, F., Alcaligenes eutrophus CH34 is a facultative chemolithotroph with plasmid-bound resistance to heavy metals. *J Bacteriol.* **1985**, 162, 328-334.
[21] Sengör, S.S., Barua, S., Gikas, P., Ginn, T.R., Peyton, B., Sani, R.K., Spycher, N.F., Influence of heavy metals on microbial growth kinetics including lag time: mathematical modeling and experimental verification. *Environ Toxicol Chem*. **2009**, 28 2020-2029.
[22] Outten, C.E., O'Halloran, T.V., Femtomolar sensitivity of metalloregulatory proteins controlling zinc homeostasis. *Science* **2001**, 292, 2488-2492.
[23] Wang, A., Crowley, D.E., Wang, A., Crowley, D.E., Global Gene Expression Responses to Cadmium Toxicity in Escherichia coli Global Gene Expression Responses to Cadmium Toxicity in Escherichia coli. *J Bacteriol.* **2005** May; 187, 3259–3266.
[24] Easton, J.A., Thompson, P., Crowder, M.W., Time-dependent translational response of *E. coli* to excess Zn(II). *Journal of biomolecular techniques* **2006**, 17, 303-307.
[25] Vyas, M.N., Jacobson, B.L., Quiocho, F.A., The calcium-binding site in the galactose chemoreceptor protein. Crystallographic and metal-binding studies. *The Journal of Biological Chemistry* **1989**, 264, 20817-20821.
[26] Ottemann, K.M., Miller, J.F., MicroReview Roles for motility in bacterial – host interactions. *Molecular Microbiology* **1997**, 24, 1109-1117.

[27] Shoeb, E., Ahmed, N., Warner, P. J., Morgan, S. Azim, M., Identification of a unique mechanism of tolerance against nickel in *Bacillus cereus* isolated from heavy metal contaminated sites. *Internet J Microbiol*. **2010**, 9, 1.
[28] Berducci, G., Mazzetti, A.P., Rotilio, G., Battistoni, A., Periplasmic competition for zinc uptake between the metallochaperone ZnuA and Cu,Zn superoxide dismutase. *FEBS Lett.* **2004**, 569**,** 289-292.
[29] Petrarca, P., Ammendola, S., Pasquali, P., Battistoni, A., The Zur-regulated ZinT protein is an auxiliary component of the high-affinity ZnuABC zinc transporter that facilitates metal recruitment during severe zinc shortage. *Journal of bacteriology* **2010**, 192, 1553-64.
[30] Brocklehurst, K.R., Morby, A.P., Metal-ion tolerance in *Escherichia coli*: analysis of transcriptional profiles by gene-array technology. *Microbiology* **2000**, 146, 2277-82.
[31] Rensing, C., Ghosh, M., Rosen, B.P., Families of soft-metal-ion-transporting ATPases. *Journal of bacteriology* **1999**, 181, 5891-5897.
[32] Ried, G., Hindennach, I., Henning, U., Role of lipopolysaccharide in assembly of *Escherichia coli* outer membrane proteins OmpA, OmpC, and OmpF. *J. Bacteriol.* **1990**, 172, 6048-6053.
[33] Kim, S., Nishioka, M., Hayashi, S., Honda, H., et al., The Gene yggE Functions in Restoring Physiological Defects of Escherichia coli Cultivated under Oxidative Stress Conditions. *Appl. Environ. Microbiol.* **2005**, 71, 2762-2765.

Chapter III: A proteomic approach to investigate the effects of cadmium and lead on human primary renal cells

III.1 Introduction

In this chapter an investigation of the effects of cadmium and lead on the viability of primary HRCE (Human Renal Cortical Epithelial) cells, is reported.
HRCE cells were grown in presence and in absence (control) of high doses of cadmium and lead (10 mg/L of $CdCl_2$ and 100 mg/L of $PbCl_2$ for 24h).
Viability of the cells was measured by MTT assay. DNA fragmentation was analyzed by Hoechst staining. For measurement of caspases levels, the whole lysates were subjected to Western blot analyses by using anti-procaspase-3, anti-Bcl-2, and anti-procaspase-8.
A severe dose- and time-dependent inhibition of cell viability was induced by either heavy metals. Cadmium and lead induce the activation of caspase-3 in a time dependent manner. Cell mortality is due to apoptotic death, as demonstrated by the activation of caspase-3 and down-regulation of the anti-apoptotic marker Bcl-2, whereas no apparent activation of caspase-8 was evidenced. ICP-MS analyses were performed to estimate the amount of heavy metals in the intracellular compartment.
Since little is known about the mechanism of apoptosis by heavy metal toxicity, a systematic proteomic investigation, based on 2D-PAGE, image analysis, protein identification and bioinformatics analyses was employed. Several proteins, particularly affected in their expression levels by metals exposure, were identified. The majority of them resulted to be involved in apoptotic pathways, protein folding and energetic metabolism. This study merely represents a contribution to the identification of potential biomarkers of heavy metal environmental pollution.

III.1.1 Metals and apoptosis

Apoptosis, is as programmed cell death which is an tightly regulated process found in all multicellular organisms, activated by various apoptotic pathways [1] [2]. It is not only implicated in regulatory mechanisms of cells, but has been attributed to a number of diseases, i.e. inflammation, malignancy, autoimmunity and neurodegeneration.
Depending on the use of different initiating caspases, signal-induced apoptosis can be divided into two types: receptor-mediated (also named extrinsic pathway) and mitochondrial-mediated (intrinsic) apoptosis (the latter is illustrated in fig. III.1) [3] [4].
Intrinsic pathway is initiated from within the cell and it is often activated in response to cell stress signals with the activation of procaspase 9, while extrinsic pathway begins outside the cell through activation of pro-apoptotic receptors on the cell surface, leading to the activation of procaspase 8 [5]. Both caspase 8 and caspase 9 use the same executive caspases, caspase 3, to complete the apoptotic process.
Many metal ions (arsenium, cadmium, chromium, nickel, lead, mercury, vanadium) can induce apoptosis, generating reactive oxygen species (ROS) that can compromise the normal function of mitochondria. Metals can also enter the endoplasmic reticulum through the calcium channels, releasing calcium into cytosol where calcium act as a second message to trigger the apoptotic cascade [2]. Thus accumulation of Ca^{2+}, up-regulation of caspase-3, down-regulation of the antiapoptotic proteins Bcl-2 (B-cell lymphoma 2), could be indications of metal-induced apoptosis.
More in detail, mitochondria can trigger apoptotic cell death by at least three general mechanisms: disruption of electron transport, release of proteins that lead to the activation of caspase family proteases and alteration of the mitochondrial inner transmembrane redox potential ($\Delta\Psi m$) [4].

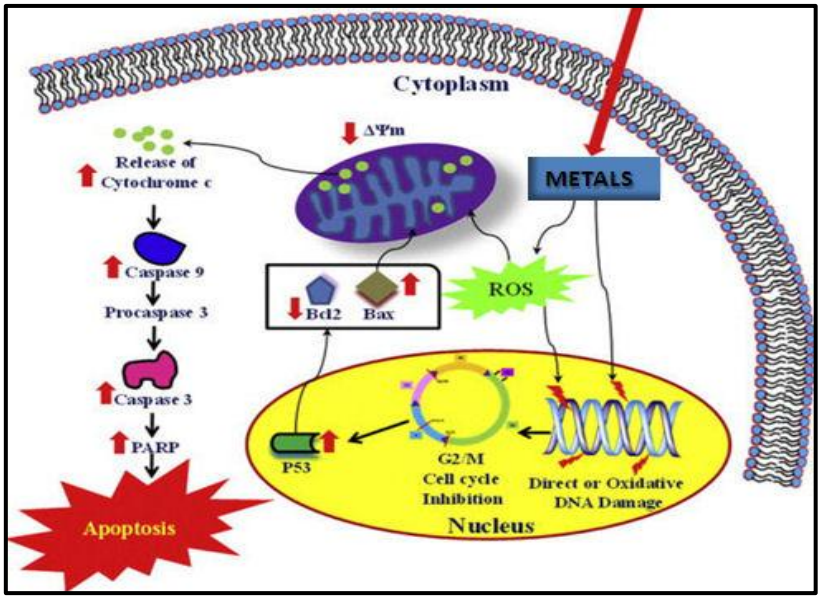

Figure III.1. *Intrinsic apoptosis pathway linked with ROS formation. Reproduced by ref [6] with some modifications.*

Acknowledgements
Author thanks prof. R. Piccoli's research group for the fruitful collaboration.

III.2 References

[1] Rana, S.V.S., Metals and apoptosis: recent developments. *Journal of trace elements in medicine and biology* **2008**, 22, 262-284.
[2] Chen, F., Shi, X., Intracellular signal transduction of cells in response to carcinogenic metals. *Crit. Rev. Oncol. Hematol.* **2002**, 42, 105-121
[3] Ashkenazi, A. and Dixit, V.M., Death Receptors: Signaling and Modulation. *Science* **1998**, 281, 1305-1308.
[4] Green, D.R. and Reed, J.C., Mitochondria and Apoptosis. *Science* **1998**, 281, 1309-1312.
[5] Lessene, G., Czabotar, P.E., Colman, P.M., BCL-2 family antagonists for cancer therapy. *Nature reviews. Drug discovery* **2008**, 7, 989-1000.
[6] Saquib, Q., Attia, S.M., Siddiqui, M. a, Aboul-Soud, M. a M., et al., Phorate-induced oxidative stress, DNA damage and transcriptional activation of p53 and caspase genes in male Wistar rats. *Toxicology and applied pharmacology* **2012**, 259, 54-65.

In section III-3 following paper, "**A proteomic approach to investigate the effects of cadmium and lead on human primary renal cells**" describe results achieved.

III.3 Submitted paper

PROTEOMICS

PROTEOMICS

A proteomic approach to investigate the effects of cadmium and lead on human primary renal cells

Journal:	*PROTEOMICS*
Manuscript ID:	Draft
Wiley - Manuscript type:	Research Article
Date Submitted by the Author:	n/a
Complete List of Authors:	Galano, Eugenio; University of Naples "Federico II", Department of of Chemical Sciences; National Institute of Biostructures and Biosystems (INBB), Arciello, Angela; University of Naples "Federico II", Department of of Chemical Sciences; National Institute of Biostructures and Biosystems (INBB), Monti, Daria Maria; University of Naples "Federico II", Department of of Chemical Sciences; National Institute of Biostructures and Biosystems (INBB), Piccoli, Renata; University of Naples "Federico II", Department of of Chemical Sciences; National Institute of Biostructures and Biosystems (INBB), Amoresano, Angela; University of Naples "Federico II", Department of of Chemical Sciences; National Institute of Biostructures and Biosystems (INBB),
Key Words:	Apoptosis, Image analysis, Liquid chromatography-tandem mass spectrometry

Wiley - VCH

A proteomic approach to investigate the effects of cadmium and lead on human primary renal cells

Eugenio Galano[1,2,°], Angela Arciello[1,2,°], Daria Maria Monti[1,2], Renata Piccoli[1,2] and Angela Amoresano[1,2]

[1]Department of of Chemical Sciences, University of Naples "Federico II", Italy
[2]National Institute of Biostructures and Biosystems (INBB), Rome, Italy.

° These authors equally contributed to the paper

Correspondance: Dr Eugenio Galano, Department of Chemical Sciences, University of Napoli "Federico II", Monte Sant'Angelo, via Cinthia 4, 80126, Naples, Italy.
Email: eugenio.galano@unina.it Phone: +39 081 679950

Keywords: Apoptosis, heavy metals, proteomics

Abbreviations
HRCE, Human Renal Cortical Epithelial cells
ICP-MS, Inductively Coupled Plasma-MS
nanoLC-MS/MS, nano Liquid Chromatography tandem Mass Spectrometry

Abstract
Heavy metals are strongly poisonous for the environment, but their impact on living cells and organisms is poorly understood at a molecular level. We investigated the effects of cadmium and lead on the viability of primary HRCE cells. A severe dose- and time-dependent inhibition of cell viability was induced by either heavy metals. Cell mortality is due to apoptotic death, as demonstrated by the activation of caspase-3 and down-regulation of the anti-apoptotic marker Bcl-2, whereas no apparent activation of caspase-8 was evidenced. ICP-MS analyses were performed to estimate the amount of heavy metals in the intracellular compartment. To gain insights a systematic proteomic investigation was performed, based on 2D-PAGE, image analysis, protein identification and bioinformatics analyses. Among more than 300 protein spots analyzed, 27 proteins particularly affected in their expression levels by metal exposure were identified. The majority of them resulted to be involved in apoptotic pathways, protein folding and energetic metabolism. The emerging scenario reveals that cellular protein patterns are strongly modified in response to metal exposure, leading to massive protein unfolding, ER stress, and cell death. By this integrated workflow, our study represents a contribution to the identification of potential biomarkers of heavy metal environmental pollution.

1 Introduction

Copper, lead, manganese, cadmium, molybdenum, mercury, arsenic, often referred to as "heavy metals", are poisonous for natural world, animals and humans [1]. Among the heavy metals, some actively participate to biological processes. This is the case of iron, cobalt, copper, manganese, molybdenum and zinc. Other metals, such as lead, cadmium, mercury and arsenic, not involved in biological functions, are harmful even at very low concentrations. Exposure to lead, cadmium, mercury and arsenic, in fact, is the primary cause of work related diseases, therefore these metals have been extensively considered and their effects on human health monitored and controlled by international organisms [2, and references therein]. Nowadays, environment, food and water are often contaminated by a range of chemicals and

heavy metals, such as lead, cadmium, arsenic, chromium and mercury, with a consequent deep impact on human health. Therefore, despite remediation procedures, heavy metal exposure and contamination still remains a challenging task [3]. Different are the ways of heavy metals intake. Smoking is a major source of cadmium exposure; exposition to mercury takes place via food, fish being a major source. Air, food and drinking water are the main via of population intake of lead and arsenic [4].

Various studies have confirmed that heavy metals activate signaling pathways and the carcinogenic effect of metals has been mainly related to activation of redox-sensitive transcription factors. As discussed by Valko and coworkers [5], iron, copper, chromium, vanadium and cobalt undergo redox-cycling reactions. On the other hand, mercury, cadmium and nickel toxicity is demonstrated by depletion of glutathione and binding to sulfhydryl groups of proteins. Disruption of metal ion homeostasis may lead to oxidative stress, increasing lipid peroxidation, protein modification and other effects, all symptomatic for numerous diseases, involving cancer, cardiovascular diseases, diabetes, atherosclerosis, neurological disorders (Alzheimer's disease, Parkinson's disease), chronic inflammation and others [6]. Because of its ability to reabsorb and accumulate divalent metals, the kidneys are the first target organs of heavy metal toxicity [7]. Free divalent cations of Cd and Pb, as discussed above, also bind to protein sulfhydryl groups affecting protein structure and function; furthermore, they may also affect enzymatic reactions in which calcium plays a role.

Cadmium and lead toxicity may cause nephropathies even at low doses, especially in the case of cadmium. It has been demonstrated that cadmium induces apoptosis in human embryonic cells (HEK 293) both through caspase-independent and -dependent pathways that involve mitochondria [8]. Moreover, it has been reported that cadmium induces apoptosis also in human hepatocellular carcinoma cell lines (HepG2 and PLC/PRF/5) in a time- and concentration-dependent manner [9]. In particular, it was well demonstrated that lead and cadmium have a direct effect on the kidneys, being particularly nephrotoxic even at physiological levels [10]. However, the molecular mechanism at the basis of cadmium and lead toxicity, recognized as environmental toxicants and carcinogens, is still unknown, even if many efforts have been applied so far using different analytical procedures. Jeon and coworkers [11] identified by a proteomic approach proteins involved in the adaptive responses to cadmium of U937 cells. More recently, a comparative proteomic analysis between a zinc- and cadmium-resistant human epithelial cell line (HZR, high zinc-resistant HeLa cells) and the parental HeLa cells has been carried out [12].

Here, a proteomic approach, based to 2D-PAGE, image analysis and protein identification by nanoLC-MS/MS, was employed to define the toxic effect and alterations in protein levels caused by exposure of primary human renal cortical epithelial (HRCE) cells to cadmium or lead, in order to gain insights at a molecular level on cellular responses. Moreover, ICP-MS analyses were performed to establish the presence of heavy metals in the intracellular compartment and to determine their amount after 24 h exposure. A comparison of the two proteomes provided a list of proteins significantly altered in their expression levels by heavy metals exposure (Cd or Pb). To the best of our knowledge, for the first time an integrated workflow, based on bioinformatics analysis, Western blotting and fluorescence analytical tools, was exploited strongly indicating that heavy metals activate the apoptotic pathway.

2 Material and Methods

2.1 Materials

Trypsin, DTT, iodoacetamide, puromycin and α-cyano-4-hydroxycinnamic acid were purchased from Sigma-Aldrich. The chemiluminescence detection system (SuperSignal® West Pico) was from Pierce. HRCE cells (Innoprot) were cultured in basal medium, supplemented with 2% foetal bovine serum, epithelial cell growth

supplement and antibiotics, all from Innoprot, in a 5% CO_2 humidified atmosphere at 37ºC. Antibodies were purchased from Cell Signal Technology.

2.2 Analysis of apoptotic pathway

Cells were plated at a density of $2x10^4$ cells/cm^2 in complete medium for 24 h and then treated for 24 h with 10 µg/mL $CdCl_2$ or with 100 µg/mL $PbCl_2$. At the end of incubation, both untreated and treated cells were analyzed. To prepare cell lysates, HRCE cells were scraped off in phosphate buffer, centrifuged at 1,000 g for 10 min and resuspended in lysis buffer (1% NP-40 in PBS, pH 7.4) containing protease inhibitors. After 30 min incubation on ice, lysates were centrifuged at 14,000 g for 30 min at 4°C. Upon determination of total protein concentration in the supernatant by the Bradford assay, samples were analyzed by SDS-PAGE. To detect apoptotic nuclei, cells were seeded on glass coverslips in 24-well plates and grown to semi-confluency. Cells were incubated for 24 h with $CdCl_2$ (10 µg/mL) or $PbCl_2$ (100 µg/mL) in complete medium, after which nuclei were stained with 1 µg/mL Hoechst 33342 for 10 min at 37°C. Cells were then washed with PBS, fixed for 10 min at RT with 2% paraformaldehyde in PBS and mounted in 50% glycerol in PBS. In a parallel experiment, cells were treated with puromycin (10 µg/mL) for 4 h as a control of apoptotic death. Samples were examined using a Leica 6000 UV microscope and a Leica TCS SP5 confocal microscope, equipped with a Leica application suite software. All images were taken under identical conditions.

2.3 ICP-MS analysis

Cells were plated and treated with $CdCl_2$ (10 µg/mL) or with $PbCl_2$ (100 µg/mL) as described above and, after 24 h, the medium of treated and untreated cells was withdrawn and cells were extensively washed with PBS. Metal content was determined by ICP-MS analyses. The total metal amount was calculated by analyzing unconditioned medium supplemented with 10 µg/mL $CdCl_2$ or with 100 µg/mL $PbCl_2$. The amount of extracellular metals was obtained by the sum of the metal content of the conditioned medium and PBS wash, while the intracellular amount was measured by analyzing the cellular content. In particular, the cell pellet (1.9 and $1.2x10^6$ cells for untreated and treated cells, respectively) was resuspended in 1 mL Milli-Q water, transferred in a Teflon vessel and treated with 6 mL HNO_3 (67-69% ultrapure) and 2 mL 30% H_2O_2 in a microwave oven (Milestone Ethos 900-Mega II). Mineralization was achieved with the following microwave oven program: 20 min to reach 220°C at 1400 W; 15 min at 220°C and 1400 W; ventilation for 30 min. The solution was then transferred into polystyrene liners, an aliquot of each sample was diluted 1:10 (v/v) with Milli-Q water and finally analyzed with an Agilent 7700 ICP-MS from Agilent Technologies, equipped with a frequency-matching RF generator and 3rd generation Octopole Reaction System (ORS^3), operating with helium gas in ORF. The following parameters were used: radiofrequency power 1550 W, plasma gas flow 14 L/min; carrier gas flow 0.99 L/min; He gas flow 4.3 mL/min. ^{103}Rh was used as an internal standard (50 µg/L final concentration). Multi-element calibration standards were prepared in 5% HNO_3 at 4 different concentrations (1, 10, 50, and 100 µg/L).

2.4 Cytotoxicity assays

Cells were seeded in 96-well plates (100 µL/well) at a density of $5x10^3$/well. Heavy metals to be tested were added to the cells 24 h after seeding for time- and dose-dependent cytotoxic assays. At the end of incubation, cell viability was assessed by the MTT assay. MTT reagent, dissolved in DMEM in the absence of phenol red (Sigma-Aldrich), was added to the cells (100 µL/well) to a final concentration of 0.5 mg/mL. Following 4 h incubation at 37°C, the culture medium was removed and the resulting formazan salts were dissolved by adding isopropanol containing 0.1 N HCl (100 µL/well). Absorbance values of blue formazan were determined at 570 nm using

an automatic plate reader (Microbeta Wallac 1420, Perkin Elmer). Cell survival was expressed as percentage of viable cells in the presence of the heavy metal under test, with respect to control cells grown in the absence of metal.

2.5 2D-PAGE

The first dimensional electrophoresis was carried out on non-linear wide-range immobilized pH gradients (pH 4-7; 7 cm long IPG strips; GE Healthcare) and achieved using the Ettan IPGphor system (GE Healthcare). 200 µg of protein extracts were precipitated with methanol/chloroform according to Wessel [13] and solubilized in 125 µL of rehydratation buffer and 0.2% (v/v) carrier ampholyte for 12 h, at 50 mA, at 20°C. The strips were then focused according to the following electrical conditions at 20°C: 500 V for 30 min, 1,000 V for 30 min, 5,000 V for 10 h, until a total of 15,000 V was reached. After focusing, analytical and preparative IPG strips were equilibrated for 15 min in 6 M urea, 30% (v/v) glycerol, 2% (w/v) SDS, 0.05 M Tris-HCl, pH 6.8, 1% (w/v) DTT, and subsequently for 15 min in the same urea/SDS/Tris buffer solution but substituting the 1% (w/v) DTT with 2.5% (w/v) iodoacetamide. The second dimension was carried out on 12.5% (w/w) polyacrylamide gels (10x8cmx1mm) at 25 mA/gel constant current and 10°C until the dye front reached the bottom of the gel, according to Laemmli [14] and Hochstrasser [15]. MS-preparative gels were stained overnight with colloidal Coomassie Brilliant Blue and destained with MilliQ grade water.

2.6 Image analysis

Gel images were acquired with an Epson expression 1680 PRO scanner. Computer-aided 2-D image analysis was carried out using the ImageMasterTM 2D Platinum software. Relative spot volumes (%v) (v = integration of OD over the spot area; %v = v single spot/v total spot) were used for quantitative analysis in order to decrease experimental errors. The normalized intensity of spots on three replicate 2-D gels was averaged and standard deviation was calculated for each condition. A few initial reference points were affixed for gels alignment, the first step of the images analysis. Landmarks are positions in one gel that correspond to the same position in the other gels. Then, the software automatically detects spots, which represent the proteins on the gels. The software “matches” the gels and the corresponding spots which are paired. The pair is the association between spots that represent the same protein in different gels. Pairs are automatically determined using ImageMaster powerful gel matching algorithm. The pairs were also evaluated by 3-D spots view. Differences in spot intensity between the gels are identified by relative quantification; spots that exhibit a variation of ± 20% were considered not affected by metals exposure.

2.7 Peptide analysis and protein identification

Spots selected by image analysis were excised from the gels and destained by repetitive alternate washes with 0.1 M NH_4HCO_3, pH 7.5 and ACN. Enzymatic digestion was carried out with 100 ng of trypsin in 50 µL of 10 mM NH_4HCO_3 buffer, pH 7.8. Gel pieces were incubated at 37°C overnight. Peptides were then extracted by washing the gel particles with 10 mM NH_4HCO_3 and 1% formic acid in 50% ACN at room temperature. The resulting peptide mixtures were filtrated using 0.22 PVDF filter from Millipore. The peptide mixtures were analysed by nanoLC-chip MS/MS**,** using a CHIP MS 6520 QTOF equipped with a capillary 1200 HPLC system and a chip cube (Agilent Technologies). After loading, the peptide mixture (8 µL in 0.1% formic acid) was first concentrated and washed at 4 µL/min in 40 nL enrichment column (Agilent Technologies chip), with 0.1% formic acid in 2% ACN as eluent. The sample was then fractionated on a C18 reverse-phase capillary column (75 µm x 43 mm in the Agilent Technologies chip) at flow rate of 400 nL/min with a linear gradient of eluent B (0.1% formic acid in 95% ACN) in A (0.1% formic acid in 2% ACN) from 7 to 60 % in

50 min. Eluted peptides were ionized to charge states 1+, 2+ or higher by the electrospray source. Doubly and triply charged peptides were selected and analyzed using data-dependent acquisition of one MS scan (mass range from 400 to 2,000 m/z) followed by MS/MS scans of the three most abundant ions in each MS scan. Collision energy (CE) applied during peptide fragmentation is calculated by the sequent empirical equations: CE= 4V/100Da -2,4V. Raw data from nanoLC–MS/MS were analyzed and converted in mzData (.XML) file format using Qualitative Analysis software (Agilent MassHunter Workstation Software, version B.02.00) and MS/MS spectra were searched against non-redundant protein databases UniprotSprot (Sprot_40.21.fasta, 533049 sequences; 189064225 residues), with the taxonomy restriction to *Homo sapiens* (20252 sequences), using in house MASCOT software (www.matrixscience.com) version: 2.1.04. The Mascot search parameters were: "trypsin" as enzyme allowing up to 3 missed cleavages, carbamidomethyl on cysteine residues as fixed modification, oxidation of methionine and formation of pyroGlu N-term on glutamine were selected as variable modifications, 20 ppm MS/MS tolerance and 0.6 Da peptide tolerance. By data analysis, threshold provided to evaluate quality of matches for MS/MS data was found to be 25. No single peptide identification, even if unique, and peptide with a score lower than 25, were accepted.

2.8 Bioinformatic analysis

Differentially expressed proteins were listed and uploaded into IPA (Ingenuity Systems, www.ingenuity.com) [16], to highlight direct relationships between candidate proteins using networks and canonical pathways. Two sets of data were created, inferred to the protein identified after Cd(+2) and Pb(+2) exposure. Both sets of data, containing a list of protein IDs from UniprotK databases, were uploaded into IPA software online. Ingenuity Knowledge Base, the core behind IPA, provide a wide range of high-quality detailed information, including direct and indirect protein interaction networks, thus aiding generation of hypotheses for a comprehensive analysis of large number of data.

3 Results

3.1 Effects of heavy metals on cell viability

The effects of cadmium and lead on cell viability were analyzed by using a primary human cell line derived from kidney. The viability of cells treated for 48 h with increasing concentrations of $CdCl_2$ or $PbCl_2$ was tested by the MTT reduction assay, as an indicator of metabolically active cells. In Fig. 1A and B, the results of dose-response experiments are shown. The values are the average of 3 independent experiments, each carried out with triplicate determinations. We observed a dose-dependent inhibition of cell viability associated to the treatment with either heavy metals, with cadmium the most effective. The IC_{50} value, i.e. the metal concentration determining 50% inhibition of cell viability, was found to be 6 µg/mL for $CdCl_2$ and 50 µg/mL for $PbCl_2$.

The results of time-course experiments are shown in Fig. 1C, where the experimental points represent the average of at least 3 independent experiments, each carried out with triplicate determinations. Cells were treated with $CdCl_2$ (10 µg/mL) or with $PbCl_2$ (100 µg/mL) for a length of time ranging from 2 to 72 h and then analyzed by MTT assays. In both cases we observed a time-dependent inhibition of cell viability. Cadmium resulted to be significantly more effective than lead, considering that it was tested at a concentration 10 times lower.

HRCE cells treated for 24 h with the heavy metals were stained with the fluorescent apoptotic marker Hoechst 33342, which binds to the highly condensed chromatin present in the nuclei of apoptotic cells [17, 18]. Fluorescence microscopy images (Fig. 2A) indicated that the nuclei of treated cells were prominently stained with the

dye and often appeared abnormal in shape (Fig. 2C, D), similarly to the cells treated with puromycin (Fig. 2B), an apoptosis inducing agent.
To analyze the apoptotic pathway induced by heavy metals, we treated HRCE cells with $CdCl_2$ (10 µg/mL) or with $PbCl_2$ (100 µg/mL) for 48 h. Cell lysates were then prepared and analysed by Western blotting using an anti-caspase-3 antibody, followed by densitometric analyses (Table 1). Endogeneous alpha-actin, measured with an anti-actin antibody, was used as an internal standard. As shown in Fig. 3, a decrease of the immunopositive signals corresponding to procaspase-3 was observed in cells treated with $PbCl_2$ (lane 2) or with $CdCl_2$ (lane 3) with respect to the untreated cells. We also observed a significant decrease of Bcl-2 immunopositive signals, whereas procaspase-8 level was found to be unchanged upon $PbCl_2$ treatment, or slightly increased following $CdCl_2$ exposure. Our results indicate that both Cd(+2) and Pb(+2) down-regulate Bcl-2 and induce caspase-3 activation, with Cd(+2) being the most effective agent.

3.2 Heavy metals quantification by ICP-MS
The multielemental analysis on different samples was performed by ICP-MS. The standard addition approach for calibration on 3 concentration levels was used in order to keep matrix induced variations under control. A minimum of three replicates of each calibration standard was run. Reagent blanks were run together with matrices.
After treatment with $CdCl_2$ or $PdCl_2$ for 24 h, the amount of metals recovered in the cell conditioned medium, as well as in the cell wash and cell lysate, was determined by ICP-MS (Table 2). The extracellular and intracellular amount of metals was calculated as described in the Methods section and expressed as percentage of the total amount determined. We found that low amounts of metals were internalized in the cells, as about 0.3% of Cd and 0.7% of Pb were detected in the cell lysate.

3.3 Proteomic analyses
Protein extracts from HRCE cells untreated (Fig. 4A), or exposed for 24 h to 10 µg/mL of $CdCl_2$ (B) or to 100 µg/mL of $PbCl_2$ (C), were fractionated by 2D-GE and stained with colloidal Coomassie Blue. The gels were run in triplicate and the bidimensional maps were compared using the ImageMaster 2D Platinum 6.0 software. All spots that exhibited a variation higher than 20% when compared to the control were considered significant. More than 300 most relevant protein spots were visualized and compared (Fig. 4). Among these, 25 spots resulted to be significantly altered following exposure to heavy metals. Upon $PbCl_2$ treatment, nine protein spots showed an increased signal volume, whilst 13 displayed a significant decrease. As for cadmium exposure, 18 spots showed a decreased volume upon $CdCl_2$ treatment.
The 25 selected spots were excised from the gels, digested with trypsin and the resulting peptide mixtures were analyzed by nanoLC-MS/MS experiments. The peptide mixtures were fractionated by nanoHPLC and sequenced by MS/MS generating sequence information on individual peptides. MS/MS spectra were used to search for a non-redundant sequence against UniprotSprot databases using the in-house MASCOT software, taking advantage of the specificity of trypsin and of the taxonomic category of the samples. The number of measured masses matching within the given mass accuracy was recorded and the proteins showing the highest number of peptide matches were examined leading to the identification of the protein components. As further selection criteria, only the proteins identified by MASCOT search with at least 2 peptides with an individual ion score higher than 25 and found exclusively in the replicates were selected. The list of the 27 proteins identified by this approach is reported in Table 3. The data associated with protein identifications are reported in supplementary material (Table S1).
As shown in Table 3, most of the proteins were affected by both metals, whereas others were influenced either by lead or cadmium. Upon lead exposure, some

proteins were found to be up-regulated and others down-regulated, whereas following cadmium exposure all the affected ones were down-regulated. Among these, some resulted undetectable being under the staining detection limit.
On the basis of literature information, the identified proteins were classified into functional groups, generating a sets of data for each metal, as shown in Fig. 5A and B relative to Pb(+2) and Cd(+2) exposure, respectively. The majority of the proteins, whose levels were significantly affected by the exposure to Cd(+2) or Pb(+2), resulted to be involved in specific functions, such as apoptotic pathways, energetic metabolism and protein folding. This is particularly true for cadmium treatment, as about 50% of the identified proteins were implicated in apoptosis. Other altered proteins were found to be involved in protein synthesis and cytoskeleton formation.

3.4 IPA canonical network
Differentially expressed proteins were listed and uploaded into IPA (Ingenuity Systems). Two different networks were generated by IPA software, as reported in Fig. 6A and B, corresponding to Pb(+2) and Cd(+2) exposure, respectively. For Pb treatment, the predicted top functions in which the listed proteins seem to be involved are cell death and cellular function and maintenance, with 17 proteins identified out of 35 proteins that form the predicted group with a total score of 46. The predicted effects illustrated by IPA for Cd exposure are related to cell death and development, involving 17 proteins out of 33 with a score of 49.

4 Discussion
Although essential in many cellular processes, metals become toxic when they are present in excess inducing severe impairment of cell functions. Cadmium is an important environmental pollutant that causes damage to various organs, especially to renal proximal tubular cells [19], and is a human carcinogen. Although exposure to high concentrations of lead is less common than in the past, lead pollution is still a cause of nephrotoxicity.
The effects of heavy metals have been studied in a variety of living cells and organisms, ranging from bacteria or fungi [20] to invertebrates (*C. Elegans*) [21], plants [22], mammalian cells [23] [24, 25] and animal models [26 and references therein], with the ultimate goal of investigating tolerance mechanisms and identifying potential biomarkers for detecting heavy metal toxicity. It emerges that metals induce oxidative stress and apoptosis and that specific responses to metal exposure are elicited by different organisms.
In the present report, the effects of heavy metals cadmium and lead on the viability of primary HRCE cells were investigated, as well as their impact on cell proteome. Due to its origin, this cell line seemed to be particularly appropriate as a model system to study the toxicity of heavy metal pollution in human living cells.
We showed that the viability of human cultured cells, exposed either to cadmium or lead, is severely impaired. The toxic effects are particularly evident with cadmium, as at a concentration as low as 6 µg/mL after 48 h exposure about 50% of cells are strongly affected in their metabolic activity, whereas, at the same concentration of lead, 15-20% of the exposed cells is impaired. For both metals the toxic effect is dose- and time-dependent.
Death is caused by apoptosis, as demonstrated by the presence of Hoechst positive nuclei, often abnormal in shape. The analysis of the apoptotic pathway revealed the activation of caspase-3 by procaspase-3 cleavage (Table 1), as well as a significant down-regulation of the anti-apoptotic marker Bcl-2, whereas no apparent activation of the caspase-8 associated pathway was evidenced. In line with the data on the effects of heavy metals on cell viability, cadmium was found to be more toxic than lead in inducing apoptosis (Fig. 5). According with our results, *in vitro* experiments on human cell lines [23, 24] showed increased DNA fragmentation and caspase-3 activation, as

well as *in vivo* studies [26] demonstrated apoptotic cell death in proximal renal tubules of experimental animals following cadmium exposure.

We performed a systematic proteomic investigation of the effects of heavy metals on the proteome of cultured renal cells. More than three hundred protein spots were analyzed in search of significant variation in protein levels as a consequence of cell exposure to heavy metals. We found that 25 protein spots showed a significant difference in volume with respect to the corresponding spots of untreated cells. All the spots were analyzed by nanoLC-MS/MS and 27 proteins particularly affected in their expression levels by metal exposure were identified (Table 3). It is interesting to notice the down-regulation effect of cadmium on all the affected proteins, whereas a positive or negative effect on protein expression levels is elicited by lead.

The analysis of the functional role of the identified proteins revealed that a significant number of them (48%) play a direct role in apoptotic cell death in the case of cadmium, whereas a slighter effect (18%) was observed for lead. On the other hand, 36% of the proteins affected by lead is involved in protein folding versus 19% observed after cadmium exposure.

Analyses by Ingenuity software clearly indicated that for both metals most of the affected proteins are included in the cellular network “cell death and cellular function and maintenance” (Fig. 6).

Among these, we found that PARK7 is down-regulated by cadmium treatment, while it is unaffected by lead. PARK7 is an anti-apoptotic agent, as it protects cells against oxidative stress and cell death, acting during apoptosis or autophagy phenomena. In response to oxidative stress, PARK7 translocates to the mitochondrion and then to the nucleus. Ren et al. [27] have reported that in PARK7 knockdown H1299 cells caspase-3 activation is accelerated and cell death is induced by UV exposure, suggesting that PARK7 protects cells against UVB-induced cell death, in association with mitochondrial Bcl-X_L.

It is well known that environmental changes, including metals and oxidative stress, cause alterations in the pattern of cellular stress protein expression. Among the proteins whose levels are affected by metal exposure, we identified proteins involved in protein folding. We found that PDIA3 and HSPA5 (also named GRP78), both acting in the endoplasmic reticulum (ER), were down-regulated following cadmium and lead exposure. Transitional endoplasmic reticulum ATPase (TER ATPase, also named VCP) was also found to be affected in the same way by both heavy metals. The functional role and subcellular localization of these proteins collectively indicate that heavy metal exposure of HRCE cells induce massive protein unfolding and ER stress by decreasing chaperone levels. To be connected to ER stress are also the decreased levels of HSPD1 and HSPA9 (also named GRP75), that contribute to protein folding within the ER.

Cadmium has been reported to interfere with protein folding, leading to accumulation of misfolded proteins in ER [28] with an apparent different mechanism, in that a concomitant induction of heat shock protein GRP78 and ER stress response were observed in a renal epithelial cell line as a protection strategy against cadmium cytotoxicity.

Interestingly, we also identified proteins involved in the control and arrangement of the cytoscheleton. Tubulins and myosin appeared to be significantly decreased upon cadmium treatment. A possible explanation could be that cadmium binds to tubulin and myosin sulphydryl groups with a consequent decrease of the functional protein [29]. These proteins are instead up-regulated by lead.

Annexin A1 (ANXA1) levels were found to be increased by lead and decreased by cadmium. Annexins are eukaryotic multifunctional proteins that bind membranes in a calcium-dependent manner. It has been reported [30] that cadmium has a dual effect on annexin A1 expression in arterial endothelial cells, as it was up-regulated after 6 h of metal exposure and down-regulated after 24 h. In the same paper, Vimentin (VIM),

which is part of the intermediate filaments, was also reported to be affected by cadmium treatment. Accordingly, our findings demonstrate a decrease of VIM upon treatment with both cadmium and lead.
Finally, proteins involved in cell metabolism are also affected by metal exposure. Enolase 1 (ENO1), the major glycolytic enolase in non-muscle and neuronal cells, was found to be increased upon lead exposure, being unaffected by cadmium. No alteration of ENO1 by cadmium was evidenced in urothelial cells by Aimola et al. [25].
In conclusion, our results, obtained with a proteomic approach, provided an array of interconnecting signals activated in renal cells exposed to toxic heavy metals. The emerging complex scenario reveals that the cellular protein pattern has been modified in response to metal exposure. A list of proteins whose levels appeared to be significantly altered was provided following their identification. Although the physiopathological conditions that occur *in vivo* when renal cells are exposed to poisonous agents can be hardly reproduced by an *in vitro* cell model, primary cells may represent a suitable choice. Therefore, the identified proteins might represent potential biomarkers for human renal cells exposure to cadmium or lead, making our study a contribution to the prediction of mammalian toxic responses to heavy metal environmental pollution.

Acknowledgments
This work was supported by Programma Operativo Nazionale "Ricerca e Competitività 2007-2013" PON01_01802" and PON01_00117. We thank Dr. Francesco Itri for help in Western blot analyses.
The authors have declared no conflict of interest.

5 References

[1] Wirth, J. J. and Mijal, R. S., Adverse effects of low level heavy metal exposure on male reproductive function. *Syst Biol Reprod Med*. 2010, *56*, 147-167.
[2] Järup, L., Hazards of heavy metal contamination. *Br Med Bull*. 2003, *68*, 167-182.
[3] Monachese, M., Burton, J. P., Reid, G., Bioremediation and human tolerance to heavy metals through microbial processes: A potential role for probiotics? *Appl Environ Microbiol*. 2012, *78*, 6397-404.
[4] Ritter, L., Solomon, K., Sibley, P., Hall, K., Keen, P., Mattu, G., Linton, B., Sources, pathways, and relative risks of contaminants in surface water and groundwater: a perspective prepared for the Walkerton inquiry. *J Toxicol Environ Health A*. 2002, *65*, 1-142.
[5] Valko, M., Morris, H., Cronin, M. T., Metals, toxicity and oxidative stress. *Curr Med Chem*. 2005, *12*, 1161-208.
[6] Jomova, K., Valko, M., Redox cycling mechanisms in the colon. *Medical hypotheses* 2012, *79*, 418-419.
[7] Barbier, O., Jacquillet, G., Tauc, M., Cougnon, M., Poujeol, P., Effect of heavy metals on, and handling by, the kidney. *Nephron Physiol*. 2005, *99*, 105-110.
[8] Mao, W. P., Ye, J. L., Guan, Z. B., Zhao, J. M., Zhang, C., Zhang, N. N., Jiang, P., Tian, T., Cadmium induces apoptosis in human embryonic kidney [HEK] 293 cells by caspase-dependent and -independent pathways acting on mitochondria. *Toxicol In Vitro*. 2007, *21*, 343-354.
[9] Shimoda, R., Nagamine, T., Takagi, H., Mori, M., Waalkes, M. P., Induction of apoptosis in cells by cadmium: quantitative negative correlation between basal or induced metallothionein concentration and apoptotic rate. *Toxicol Sci*. 2001, *64*, 208-215.
[10] Sabath, E., Robles-Osorio, M. L., Renal health and the environment: heavy metal nephrotoxicity. *Nefrologia*. 2012, *32*, 279-286.

[11] Jeon, H. K., Jin, H. S., Lee, D. H., Choi, W. S., Moon, C. K., Oh, Y. J., Lee, T. H., Proteome analysis associated with cadmium adaptation in U937 cells: identification of calbindin-D28k as a secondary cadmium-responsive protein that confers resistance to cadmium-induced apoptosis. *J Biol Chem*. 2004, *279*, 31575-31583.
[12] Rousselet, E., Martelli, A., Chevallet, M., Diemer, H., Van Dorsselaer, A., Rabilloud, T., Moulis, J. M., Zinc adaptation and resistance to cadmium toxicity in mammalian cells: molecular insight by proteomic analysis. *Proteomics*. 2008, *8*, 2244-2255.
[13] Wessel, D., Flügge, U. I., A method for the quantitative recovery of protein in dilute solution in the presence of detergents and lipids. *Anal Biochem*. 1984, *138*, 141-143.
[14] Laemmli, U. K., Cleavage of structural proteins during the assembly of the head of bacteriophage T4. *Nature* 1970, *227*, 680-685.
[15] Hochstrasser, D. F., Patchornik, A., Merril, C. R., Development of polyacrylamide gels that improve the separation of proteins and their detection by silver staining. *Anal Biochem*. 1988, *173*, 412-423.
[16] Jiménez-Marín, A., Collado-Romero, M., Ramirez-Boo, M., Arce, C., Garrido, J. J., Biological pathway analysis by ArrayUnlock and Ingenuity Pathway Analysis. *BMC Proc*. 2009, *3*, S6.
[17] Cecchi, C., Pensalfini, A., Stefani, M., Baglioni, S., Fiorillo, C., Cappadona, S., Caporale, R., Nosi, D., Ruggiero, M., Liguri, G., Replicating neuroblastoma cells in different cell cycle phases display different vulnerability to amyloid toxicity. *J. Mol. Med*. 2008, *86*, 197-209.
[18] Downs, T. R., Wilfinger, W. W., Fluorometric quantification of DNA in cells and tissue. *Anal. Biochem*. 1983, *131*, 538-547.
[19] Goering, P. L., Waalkes, M. P., Klaassen, C. D., Toxicology of cadmium. *Toxicology of Metals: Biochemical Aspects (Handbook of Experimental Pharmacology)* 1995, *115*, 189–214.
[20] Cherrad, S., Girard, V., Dieryckx, C., Gonçalves, I. R., Dupuy, J. W., Bonneu, M., Rascle, C., Job, C., Job, D., Vacher, S., Poussereau, N., Proteomic analysis of proteins secreted by Botrytis cinerea in response to heavy metal toxicity. *Metallomics* 2012, *4*, 835-46.
[21] Hunt, P. R., Olejnik, N., Robert, R. S., Toxicity ranking of heavy metals with screening method using adult Caenorhabditis elegans and propidium iodide replicates toxicity ranking in rat. *Food Chem Toxicol*. 2012, *50*, 3280-3290.
[22] Kumar, A., Prasad, M. N., Sytar, O., Lead toxicity, defense strategies and associated indicative biomarkers in Talinum triangulare grown hydroponically. *Chemosphere* 2012, *89*, 1056-1065.
[23] Nemmiche, S., Chabane-Sari, D., Kadri, M., Guiraud, P., Cadmium-induced apoptosis in the BJAB human B cell line: Involvement of PKC/ERK1/2/JNK signaling pathways in HO-1 expression. *Toxicology* 2012, *300*, 103-11.
[24] Culbreth, M. E., Harrill, J. A., Freudenrich, T. M., Mundy, W. R., Shafer, T. J., Comparison of chemical-induced changes in proliferation and apoptosis in human and mouse neuroprogenitor cells. *Neurotoxicology* 2012, [Epub ahead of print].
[25] Aimola, P., Carmignani, M., Volpe, A. R., Di Benedetto, A., Claudio, L., Waalkes, M. P., Van Bokhoven, A., Tokar, E. J., Claudio, P. P., Cadmium induces p53-dependent apoptosis in human prostate epithelial cells. *PLoS One* 2012, *7*, e33647.
[26] Hamada, T., Tanimoto, A., Sasaguri, Y., Apoptosis induced by cadmium. *Apoptosis* 1997, *2*, 359–367.
[27] Ren, H., Fu, K., Wang, D., Mu, C., Wang, G., Oxidized DJ-1 interacts with the mitochondrial protein BCL-XL. *J Biol Chem.* 2011, *286*, 35308-35317.

[28] Liu, F., Inageda, K., Nishitai, G., Matsuoka, M., Cadmium induces the expression of Grp78, an endoplasmic reticulum molecular chaperone, in LLC-PK1 renal epithelial cells. *Environ. Health Perspect*. 2006, *114*, 859–864.
[29] Hertelendi, Z., Tóth, A., Borbély, A., Galajda, Z., van der Velden, J., Stienen, G. J., Edes, I.,Papp, Z., Oxidation of myofilament protein sulfhydryl groups reduces the contractile force and its Ca2+ sensitivity in human cardiomyocytes. *Antioxid Redox Signal*. 2008, *10*, 1175-1184.
[30] Bernhard D, Rossmann A, Henderson B, Kind M, Seubert A, Wick G., Increased serum cadmium and strontium levels in young smokers: effects on arterial endothelial cell gene transcription. *Arterioscler Thromb Vasc Biol*. 2006, *26*, 833-838.

Table 1: Quantitative analysis of apoptotic marker levels in HRCE cells untreated or treated with $CdCl_2$ (10 µg/mL) or $PbCl_2$ (100 µg/mL) for 48 h. For each sample, the protein intensity level was normalized to endogenous alpha-actin and compared to that of untreated cells. The data represent the means ± standard deviation of protein levels determined in three independent experiments.

Sample	**Procaspase-3 (%)**	**Bcl-2 (%)**	**Procaspase-8 (%)**
Untreated cells	100	100	100
Cells treated with $PbCl_2$	68 ± 5	77 ± 6	109 ± 10
Cells treated with $CdCl_2$	45 ± 4	47 ± 3	127 ± 8

Table 2: Quantitative ICP-MS analysis of HRCE cells treated with $CdCl_2$ (10 µg/mL) or $PbCl_2$ (100 µg/mL) for 24 h. Quantifications were acquired in triplicate. Intracellular metal concentrations were normalized to the total protein content.

Sample	**Cd(+2) (%)**	**Pb(+2) (%)**
Total amount	100 ± 4.5	100 ± 0.6
Cell conditioned medium	88.9 ± 0.4	92.7 ± 2.6
Cell washing	9.6 ± 2.4	6.5 ± 2,1
Cell lysate	0.276 ± 0.002	0.691 ± 0.006

Table 3: List of the proteins identified by nanoLC-MS/MS. Spot numbers refer to Fig. 4. Variation in fold expression are given by the comparison of each spot with the control. +/- indicates increment/decrement with respect to the control; =, no change in the expression level; ud, undetectable spot in the 2D maps. MW, Score, Number of peptides, Peptide sequences and Sequence coverage are reported in supplementary material (Table S1).

No. protein spots	Protein Code	Protein Name	UniProt accession	Fold change after $PbCl_2$ treatment	Fold change after $CdCl_2$ treatment
1	PARK7	Protein DJ-1	Q99497	=	- 0,4
2	EF1D	Elongation Factor 1-Delta	P29692	- 0,6	ud
3	TUBB	Tubulin Beta Chain	P07437	+ 0,7	ud
4	MLC-3	Myosin Light Polypeptide 6	P60660	+ 2,5	ud
5	S100A11	Protein S100-A11	P31949	+ 0,3	- 0,4
6	VCP	Transitional Endoplasmic Reticulum ATPase	P55072	- 0,7	- 0,8
7	CALD1	Caldesmon	Q05682	- 0,7	- 0,6
8	HSPA9	Stress-70 Protein, Mitochondrial	P38646	- 0,7	=
9	CCT5	T-complex Protein 1 Subunit Epsilon	P48643	- 0,7	- 0,3
	HSPD1	60kDa Heat Shock Protein, Mitochondrial	P10809	- 0,7	- 0,3
10	HSPA5	78 kDa Glucose-regulated protein	P11021	- 0,7	- 0,5
11	LYS	Lysozyme C	P61626	- 0,8	- 0,6
12	CCT2	T-complex Protein 1 Subunit Beta	P78371	- 0,6	- 0,7
13	ENO1	Alpha-Enolase	P06733	+ 0,3	=
14	EF1B	Elongation Factor 1-Beta	P24534	+ 0,6	- 0,8
15	DDAH-2	N[G], N[G]-Dimethylarginine Dimethylaminohydrolase 2	O95865	+ 2,5	- 0,5
16	ANXA1	Annexin A1	P04083	+ 0,5	- 0,3
17	TPI1	Triosephosphate Isomerase	P60174	=	- 0,6
18	HSPB1	Heat Shock Protein Beta-1	P04792	+ 0,6	=

19	NME1	Nucleoside Diphosphate Kinase A	P15531	=	- 0,6
20	UCH-L1	Ubiquitin Carboxyl-terminal hydrolase isozyme L1	P09936	=	0,5
21	TUBB2C	Tubulin Beta-4B Chain	P68371	+ 1,1	ud
22	VIM	Vimentin	P08670	- 0,4	- 0,4
23	PDIA3	Protein Disulfide-Isomerase A3	P30101	- 0,5	- 0,5
24	LGALS1	Galectin-1	P09382	=	- 0,5
25	PP17	Perilipin-3	O60664	- 0,6	=
	ACTB	Actin, Cytoplasmic	P60709	- 0,6	=

Figure 1: Dose-response curves upon treatment of HRCE cells with $CdCl_2$ (A) or $PbCl_2$ (B) for 48 h. Cell viability was expressed as the percentage of MTT reduction with respect to control cells, tested under the same conditions but in the absence of metal. (C) Time-course of the effects of $CdCl_2$ (10 µg/mL) and $PbCl_2$ (100 µg/mL) on the viability of HRCE cells determined by the MTT assay for different lengths of time in the range 2-72 h. Error bars correspond to the s.d. values of three independent experiments. *P* values < 0.01.

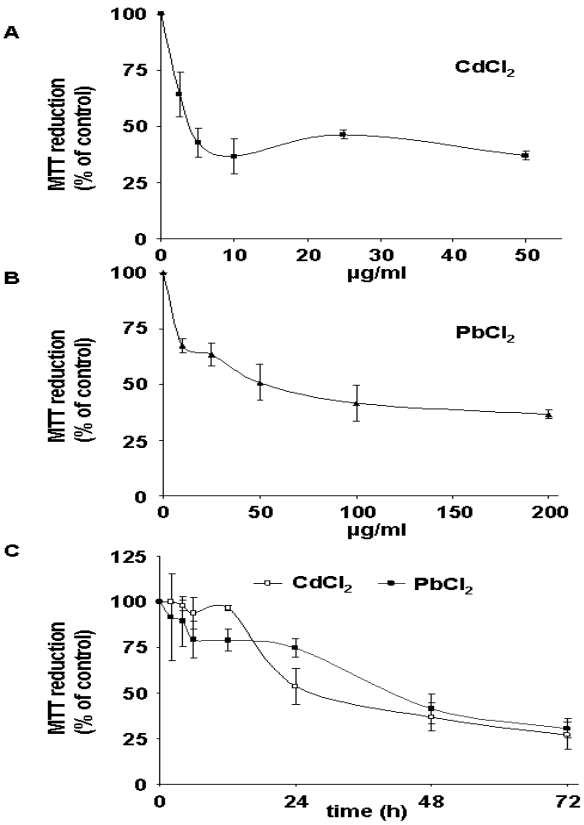

Figure 2: Hoechst staining of HRCE cells untreated (A) or treated with 10 µg/mL puromycin for 4 h (B), 10 µg/mL $CdCl_2$ for 24 h (C), 100 µg/mL $PbCl_2$ for 24 h (D). All images were acquired at the same magnification.

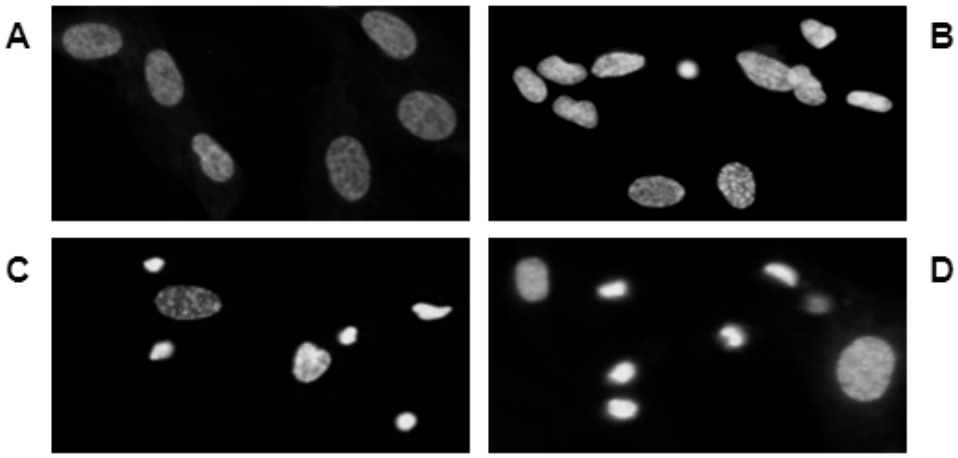

Figure 3: Analysis of apoptotic markers in HRCE cells untreated or treated with $CdCl_2$ (10 µg/mL) or $PbCl_2$ (100 µg/mL). Western blot analyses were performed using anti-procaspase-3, anti-Bcl-2, anti-procaspase-8 and anti-alpha-actin antibodies. Lane 1, cell lysate of untreated cells; lane 2, lysate of cells treated with $PbCl_2$; lane 3, lysate of cells treated with $CdCl_2$.

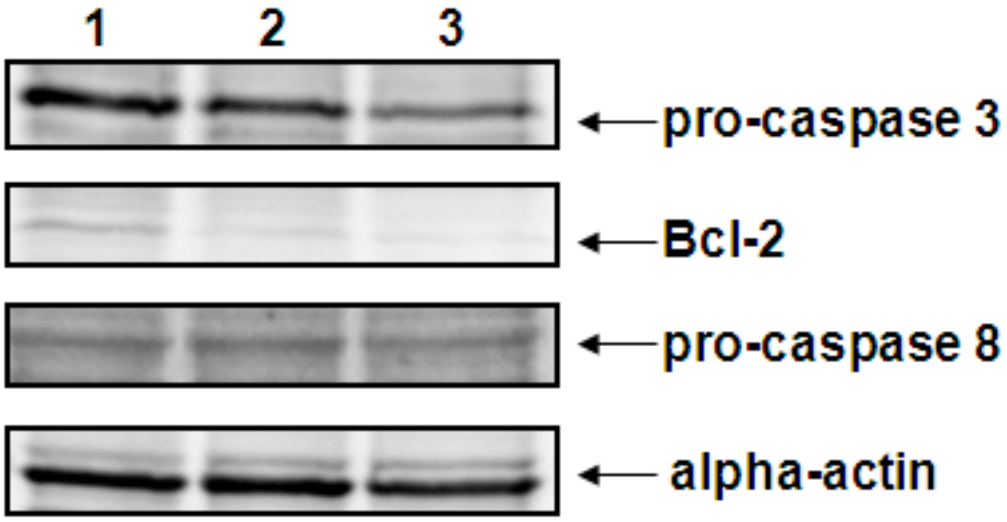

Figure 4: Protein 2D maps of HRCE cells grown in control (A) and stimulated conditions (100 µg/mL $PbCl_2$ and 10 µg/mL $CdCl_2$ for B and C, respectively) in the acidic (4–7) pI range. Numbers and circles indicate differentially expressed protein spots submitted to proteomic analyses.

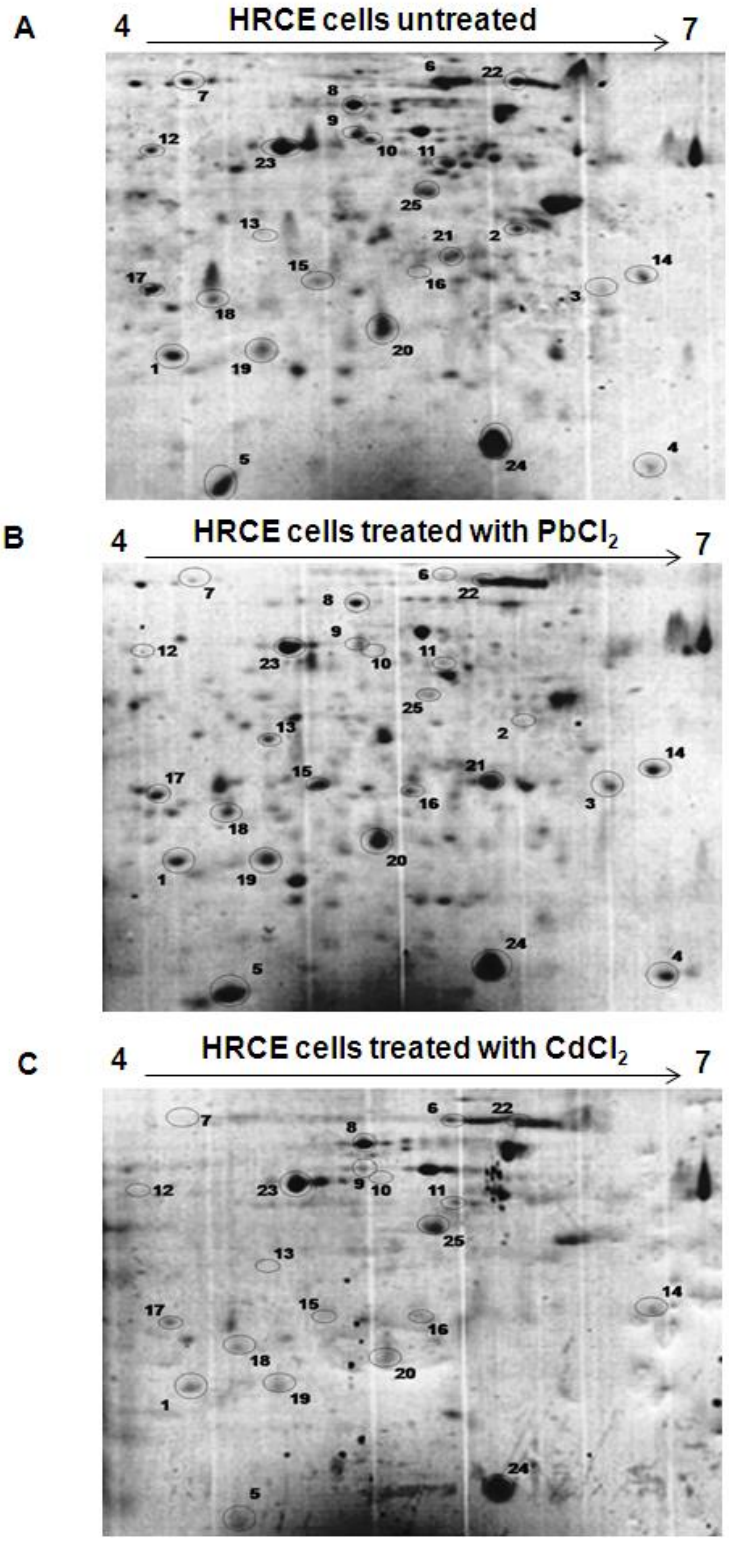

Figure 5: Schematic representation of multiple cellular functions in which the identified proteins are involved.

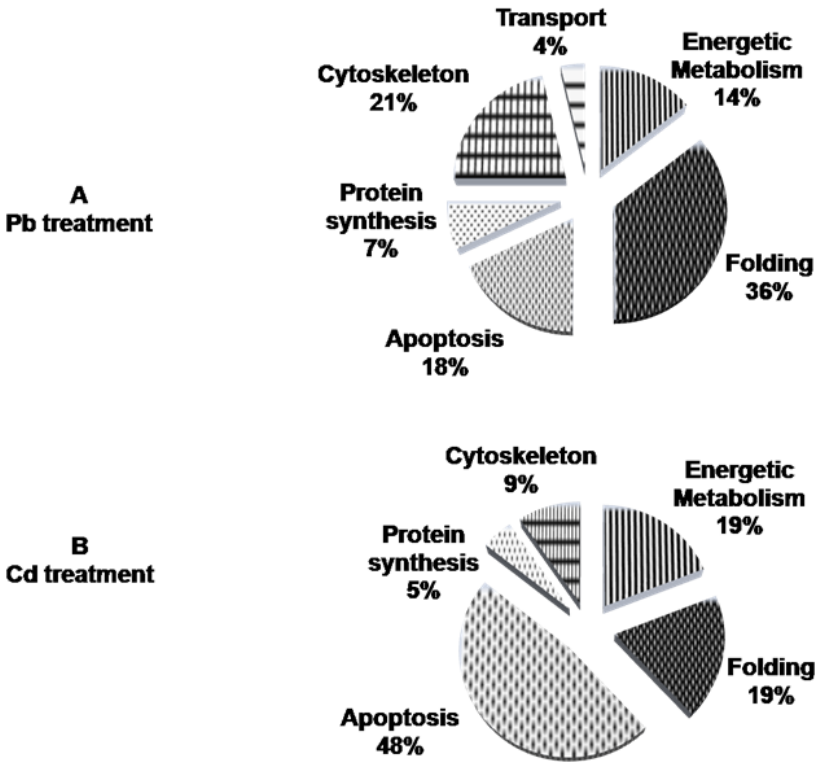

Figure 6: Canonical pathways identified by Ingenuity Pathway Analysis performed on differentially expressed proteins generated from 2D-GE nanoLC-MS/MS analysis after 24 h exposure to 100 µg/mL $PbCl_2$ (A) or 10 µg/mL $CdCl_2$ (B). Solid lines indicate direct interactions, dashed lines indicate indirect interactions. Arrows indicate activation, bars inhibition. Squares indicate proteins identified by nanoLC-MS/MS.

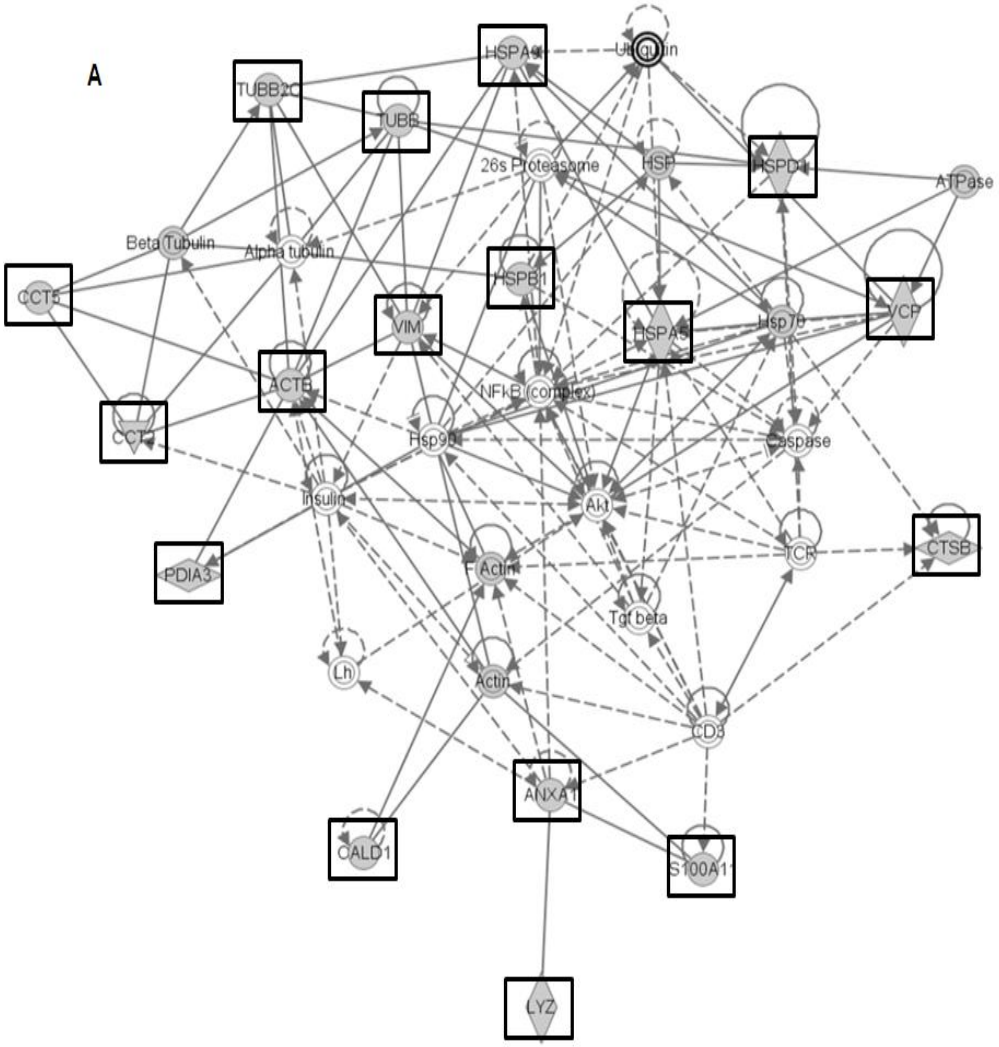

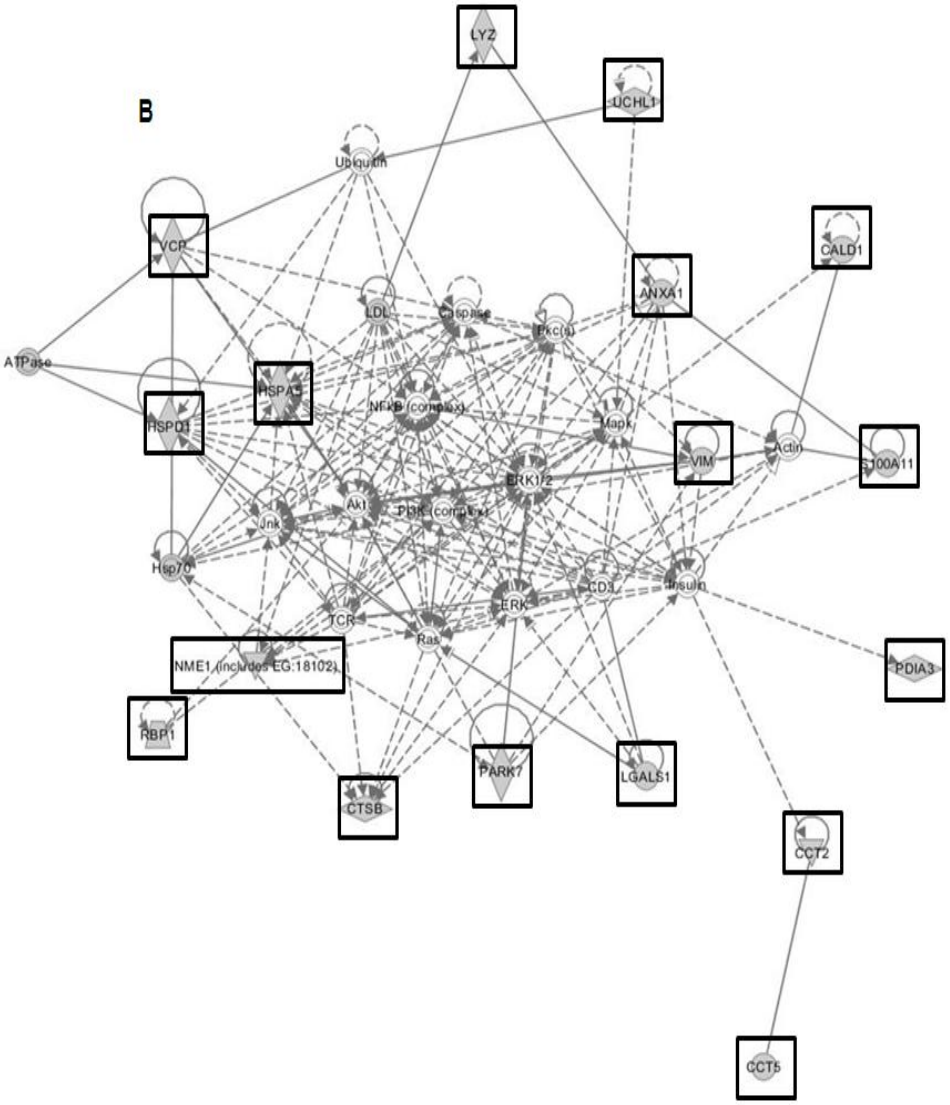
B
LYZ
UCHL1
Ubiquitin
VCP
CALD1
ANXA1
LDL
Caspase
Pkc(s)
ATPase
HSPA5
HSPD1
NFkB (complex)
Mapk
VIM
Actin
S100A11
ERK1/2
Akt
Jnk
PI3K (complex)
Hsp70
CD3
Insulin
ERK
TCR
Ras
PDIA3
NME1 (includes EG:18102)
RBP1
PARK7
LGALS1
CTSB
CCT2
CCT5

Chapter IV: Probiotic *Lactobacillus reuteri* Lb2 BM-DSM 16143 selective incorporation of selenium into selenocysteines proved by inductively coupled plasma mass spectrometry (ICP-MS) - assisted proteomics approach

IV.1 Introduction

Selenium (Se) is an essential nutrient for humans as being a crucial component of several family proteins, some of them well characterized such as iodothyrine 5-deiodinase, glutathione peroxidase (GPX1), and thioredoxin reductase [1].
Moreover selenium is of special interest because of its favorable nature for humans since its deficiency seriously affect human health by leading to heart diseases, hypothyroidism and a weakened immune system [2].
In this chapter an investigation of selenium incorporation into proteins in probiotic *Lactobacillus reuteri* Lb2 BM-DSM 16143 is reported.
ICP MS based experiments on selenium uptake by *L. reuteri* Lb2 BM-DSM 16143 during growth demonstrated the ability of the strain to recover high concentration of selenium from the medium.
Further studies were employed to determine and localize the final destination of the assimilated selenium. Thus an innovative analytical approach based on the integration of metallomics and proteomics strategies was used for an in depth investigation on protein selenization mechanism.
Our data demonstrated that in this *L. reuteri* strain all the Se fixed into proteins was incorporated as selenocysteine (SeCys), while methionine/selenomethionine substitution, that is typical of other microorganisms such as yeasts, did not occur.
Moreover our results unambiguously localize the exact position within the primary sequence of proteins in which SeCys was inserted.
Even if we demonstrated that in this *L. reuteri* strain Se insertion into proteins exclusively occurs as selenocysteine with a Cys/SeCys replacement, although the insertion mechanism still remains to be established. Since in GAPDH and ADI there is a specific substitution of only two of the three Cys, it can be suggested that the insertion of SeCys can be genetically encoded, according to the mechanism used by other bacteria. This hypothesis was tentatively verified via genomic studies by analyzing gene sequences of the identified proteins searching for UGA codon. Also RT-PCR analyses were performed in order to verify if the modification leading to Cys/SeCys substitution occurs at mRNA level.

IV.2 Selenium incorporation

Up to now, two possible mechanisms for selenium incorporation are well known. The first pathway is based on the non-specific incorporation of a seleno-amino acid into a protein in which enzymes involved in the sulfur metabolism also accept the corresponding selenium analogues, being the SeMet the most preferred Se-amino acid [3]. The second pathway corresponds to the specific incorporation of selenium into proteins in form of genetically encoded selenocysteine (Sec) [4]. It is well characterized that specific insertion of Sec needs four gene products: SelA (selenocysteine synthase), SelB (a special translation factor that recognizes selenocystyl-$tRNA^{Sec}$), SelC (Sec-specific tRNA) and SelD (selenophosphate synthase) [5].
However, quite a few bacteria that do not make Sec still have the selD gene (even called “orphan selD”) in their genome, in absence of selA, selB and selC genes. It was recently proposed that orphan SelD could have an alternative role in some bacterial and archaea cells [6]. SelD generates the activated form of selenium, selenophosphate, using ATP as the energy source, and is required also in a fundamentally different system, tRNA modification with selenouridine [7][8]. In fact

Zhang and co-workers proposed that selenophosphate is used to modify U34 of $tRNA^{Lys}$, $tRNA^{Glu}$ and $tRNA^{Gln}$ in some bacteria, requiring also the presence of SelU (ybbB), the latter coding for 2-selenouridine synthase [9].
On the other hand, Haft has reported that prokaryotic cells can use selenophosphate in biosynthesis of Se-containing molybdoenzymes, a reaction thought to involve a redox enzyme as a source of reduced Se. In this mechanism the contribution of Se does not derive from SeCys but through some unknown mechanism, as there are a few known examples of molybdenum hydroxylases [6].
However, the question of selenium essentiality in some organisms lacking of UGA codon and the complete set of selABCD proteins, is still controversial and remains unresolved [10]. To date, there is no direct evidence for the specific incorporation of SeCys in *Lactobacillus* species, thus the present investigation on the presence of SeCys-containing proteins is of high interest in particular concerning nutraceutical applications.

IV.3 Selenium-enriched foods for particular nutritional uses

On the basis of positive opinion given by European Community as regarding the use of selenium-enriched yeast as source of selenium in nutritional purposes [11], several alternative selenium-enriched organisms has been proposed. In particular many selenium-enriched vegetables (garlic, onion, ramp, cabbage, sprout, and broccoli) were selected to be used for the great ability of plants to hyper-accumulate inorganic forms of selenium and to convert them into organic forms [12][13][14][15][16][17]. Major Se-species reported in these selenized vegetables are Se-methyl-selenocysteine and γ-glutamyl-Semethyl-selenocysteine [1].
However a complete characterization of the total set of selenium-containing molecules (both organic and inorganic) present in a sample to assure the viability or safety of the proposed products is needed in order to obtain the approval by the EFSA. Thus a lot of efforts were devoted to analytical studies that help to elucidate both the speciation and the amounts of the different forms of selenium in several organisms. For this reason the work discussed in this chapter would represent a starting point to candidate the use of *Lactobacillus reuteri* Lb2 BM-DSM 16143 *to* be used for nutritional purposes in certain categories of foods as a safety source of selenocysteine for humans and animals. A rapid comparison with a well characterized selenium-enriched yeast, can be given by the fact that in yeast the predominant form of seleno-amino acid is selenomethionine, with an amount of approximately 60-85% of total selenium species, while selenocysteine is only approximating to 2-4%. The data obtained in this work rather suggest that *Lactobacillus reuteri* Lb2 BM-DSM 16143 peculiarly fix selenium only into selenocysteine-containing proteins with an amount of approximately 50% of total selenium species. Moreover as for the use of Se-enriched food for human and animal uses, it must be underlined that following absorption, selenomethionine need to be metabolized and finally converted into selenocysteine though the pathways of methionine metabolism to be fixed as selenoproteins, while selenocysteine from *Lactobacillus reuteri* could be more rapidly metabolized and then inserted into proteins.

In section IV-4 following paper, "**Probiotic Lactobacillus reuteri Lb2 BM-DSM 16143 selective incorporation of selenium into selenocysteines proved by inductively coupled plasma mass spectrometry (ICP-MS) - assisted proteomics approach**" describe results achieved.

IV.4 Submitted paper

Manuscript Title:	Probiotic Lactobacillus reuteri Lb2 BM-DSM 16143 selective incorporation of selenium into selenocysteines probed by inductively coupled plasma mass spectrometry (ICP MS) - assisted proteomics approach
Manuscript No:	MCP/2013/027607
Manuscript Type:	Research Article
Date Submitted by the Author:	17 Jan 2013
Complete List of Authors:	Eugenio Galano, Erika Mangiapane, Juliusz Bianga, Angelo Palmese, Enrica Pessione, Joanna Szpunar, Ryszard Lobinski, and Angela Amoresano
Keywords:	2-D Gel Electrophoresis; Mass Spectrometry; Prokaryotes*; Protein Identification* ; Tandem Mass Spectrometry; ICP-MS; Lactobacillus; Se/S substitution ; Selenated proteins; Selenocysteine

Probiotic *Lactobacillus reuteri* Lb2 BM-DSM 16143 selective incorporation of selenium into selenocysteines proved by inductively coupled plasma mass spectrometry (ICP MS) - assisted proteomics approach

Eugenio Galano[1,2,*], Erika Mangiapane[3], Juliusz Bianga[4], Angelo Palmese[1], Enrica Pessione[3], Joanna Szpunar[4], Ryszard Lobinski[4] and Angela Amoresano[1,2]

[1]Department of Chemical Sciences, University of Naples "Federico II", Italy
[2]National Institute of Biostructures and Biosystems (INBB), Rome, Italy.
[3]Department of Life Sciences and Systems Biology, University of Turin, Italy
[4]LCABIE UMR5254, Technopôle Hélioparc Pau Pyrénées, France

***Corresponding author:**
E. Galano, Department of Chemical Sciences, University of Napoli "Federico II", Monte Sant'Angelo, via Cinthia 4, 80126, Naples, Italy. Phone: +39 081 679950, Fax: +39 081 674313 Email: eugenio.galano@unina.it

Running title
Selenocysteines in *L. reuteri* by ICP-MS and proteomics

Keywords
Selenated proteins, Selenocysteine, Lactobacillus, Mass Spectrometry, Se/S substitution

Summary
Selenium (Se) can be efficiently metabolized by the well-known probiotic *Lactobacillus reuteri*. An analytical approach was developed to study the incorporation of Se into *L. reuteri* Lb2 BM-DSM16143 proteins. Se-enriched proteins were detected in 2D gels by laser ablation inductively coupled plasma mass spectrometry (ICP MS) without the use of radioactive isotopes. The Se-containing spots were analyzed by capillary HPLC with the parallel ICP MS and electrospray Orbitrap MS/MS detection. The method allowed the localization of the Se-amino acids and the demonstration that all selenium was incorporated as selenocysteine in 7 most abundant proteins. This way of incorporation differs from the one used by yeasts and plants where the Se/S replacement in methionine is privileged.

Introduction
In recent years selenium (Se) has received great attention since it has been defined essential for human health. Severe Se deficiency is linked to oxidative stress and ageing process (1), a high risk of death in HIV patients (2) and irreversible brain injury (seizures, Parkinson's disease) (3).
Se occurs in nature principally in four inorganic chemical forms: the highly toxic selenide (Se^{2-}) (4), the moderately toxic selenate (SeO_4^{2-}) and selenite (SeO_3^{2-}) and elemental selenium (Se^0) which is essentially non-toxic and can be stored by several bacterial species as nanoparticles on the cell surface (5,6,7). Inorganic selenium can be converted by biological systems (microorganisms, plants, animals and humans) into seleno-amino acids which are then incorporated into proteins. The two most common selenoamino acids are selenomethionine (SeMet) and selenocysteine (SeCys). The former is synthesized *via* a route similar to the sulfur metabolic pathway, and inserted non-specifically in substitution of Met, with no alteration of protein structure (8, 9). The

insertion of SeCys is genetically encoded by the UGA (TGA) codon and requires a SECIS element downstream of such codon, a specific $tRNA^{[Ser]Sec}$ and accessory proteins (10).

True selenoproteins (containing SeCys) are synthesized by several bacteria according to this pathway. Among Gram negative, *E. coli* produces three forms of selenated formate dehydrogenase (FdhN, FdhO, FdhH) (11). Among Gram-positives, all the selenoproteins experimentally known were found exclusively in strictly anaerobic bacteria belonging to the clostridial clade. Examples include glycine reductase from *Clostridium sticklandii* (12) and *Eubacterium acidaminophilum* (13), proline reductase in *C. sticklandii* (14), xanthine dehydrogenase in *C. acidiurici* (15) and several antioxidant defense proteins (16). *Enterococcus faecalis* is the only member of the *Firmicutes/Lactobacillales* subdivision containing a SeCys-decoding trait (SelD) (17).

Lactobacillus reuteri species has widely been described as a probiotic: it produces antimicrobial compounds, such as reuterin, with a broad spectrum of action (18), it is effective against diarrhea in children (19) and possesses immunomodulatory (potent TNF-inhibitory activity) effects in humans (20). Since *L. reuteri* species are native inhabitants of human microbiota, the association of the probiotic feature *L. reuteri* Lb2 BM-DSM 16143 with its ability to fix selenium into proteins, represents an additional innovative approach to solve human selenium deficiency.

This is the first study in which a member of *Firmicutes/Lactobacillales* subdivision, *Lactobacillus reuteri* Lb2 BM-DSM 16143, is analyzed for its ability to fix selenium into proteins as selenocysteine. The objective of this research was to investigate the selenium speciation according to the selenium metabolism of this strain. For this purpose an innovative analytical approach was developed. It combined the location of the most abundant Se-containing proteins in 2D gel by laser ablation inductively coupled plasma mass spectrometry imaging (LA-ICP MSI) and their identification by capillary HPLC with the parallel ICP MS and electrospray Orbitrap MS/MS detection.

Experimental Procedures

Culture conditions

Cultures were grown in closed 250-mL screw cap bottles, at 37°C without shaking. *L. reuteri* Lb2 BM-DSM 16143 was grown in a stimulated condition (MRS medium (Difco) supplemented with 4.38 mg L^{-1} sodium selenite corresponding to 2 mg L^{-1} selenium). Two biological replicates were performed. For the recovery of the soluble protein extract 1 mL of pre-cultured bacteria was added to the culture medium and after 6 h of growth 50 mg (dry weight) of material was harvested.

Microwave-assisted digestion and ICP-MS analysis

Three types of samples were collected at different times during the cell growth: i) pellet: a volume of the culture,to detect cell incorporation of Se, was taken and centrifuged (10,000 *g*, 4°C, 15 min); ii) supernatant, to evaluate non-uptaken Se: 1 mL of the culture broth was centrifuged at 10,000 *g*, 4°C, 15 min in order to separate the biomass and to recover the supernatant, and iii) wash supernatant,to recover surface-associated Se(0) deposits (5), was obtained after washing of the harvested biomass with 1 mL 50 mM EDTA to remove residues of Se from the cell wall, and centrifugation at 10,000 *g* (4°C, 15 min).

Each sample (pellet resuspended in 1 mL water; 1 mL of supernatant; 1 mL of EDTA wash) was microwave (Milestone Ethos 900-Mega II) digested in a Teflon vessel , with a mixture of 6 mL of 69 % HNO_3 and 2 mL of 30 % H_2O_2 (both SpS™ grade Super Purity

Solvent from Romil, Cambridge, UK). Mineralization was achieved with the following oven program: 20 min to reach 220°C at 1400 W; 15 min at 220°C and 1400 W; cooling for 30 min. The sample digests were then made up to a volume of 10 mL with water and stored at 4°C prior to ICP-MS analysis. Samples were analyzed after 10-fold dilution. The analyses were carried out in biological duplicate and technical triplicate on a 7700 ICP-MS (Agilent, Hachi-oji, Japan), equipped with a frequency-matching RF generator and 3rd generation Octopole Reaction System (ORS^3), operating with helium as cell gas. The parameters were set as follows: radiofrequency power 1550 W, plasma gas flow 14 L min^{-1}; carrier gas flow 1.0 L min^{-1}; He gas flow 4.6 mL min^{-1}. Internal standard was added to all the samples and calibration points. Multi-element calibration standards were prepared in 5% HNO_3 at 4 concentrations (1, 10, 50, and 100 µg L^{-1}).

Soluble protein extracts

A 50-mg amount of biomass was collected by centrifugation and washed in 50 mL 0.85% NaCl. The obtained pellets were resuspended in 3mL 50mM Tris–HCl, pH 7.3, EDTA-free protease (Complete, Roche), sonicated and clarified clarified by centrifugation (4000 *g*, 20 min, 4°C). To recover the highest amount of proteins, the pellet was resuspended, sonicated and centrifuged again and the two supernatants were combined. Samples were supplemented with 15 µL mL^{-1} of Nuclease Mix (GE Healthcare) and centrifuged (100,000 *g*, 1 h, 4°C) in a Beckman L8–60M Ultracentrifuge (Type 60 rotor). The supernatants were dialyzed against four volumes of water. Protein extracts were quantified using the QuantiPro^{TM} BCA Assay Kit (Sigma-Aldrich).

Gel electrophoretic separations

For 1D-SDS-PAGE different amounts of soluble protein extract (20, 40, 80 and 100 µg) were separated on a 12% T SDS-PAGE after protein precipitation in acetone. For 2D-SDS-PAGE aliquots of 100 µg and 400 µg for each samples were precipitated using the 2-D Clean-Up Kit (GE Healthcare). After precipitation the samples were resuspended in 340 µL of Rehydration buffer (GE Healthcare) supplemented with 1.7 µL of IPG buffer. Isoelectrofocusing was carried out using 4-7 18 cm Immobiline™ DryStrip gels strips (GE Healthcare Bio-Sciences, Uppsala, Sweden) in a IEF-SYS (Biostep, Jahnsdorf, Germany) under a constant current of 3 mA. The strips were then focused according to the following electrical conditions: 500 V for 1 h, 1000 V for 1 h, 5000 V for 3 h, hold at 5000, 6000 for 3 h and hold at 6000 for 5h until a total of 15000 Vt was reached. After focusing IPG strips were reduced in equilibration buffer (6 M urea, 30% (V/V) glycerol, 2% (w/V) SDS, 0.05 M Tris-HCl, pH 6.8) 1% (w/v) with DTT, and subsequently alkylated with 2.5% (w/v) iodoacetamide. SDS-PAGE was done in electrophoresis unit TV100 (Biostep, Jahnsdorf, Germany) cell. Tris glycine was used as running buffer. 4 For 1D-SDS-PAGE 4% acrylamide gels were used as stacking and 12% of acrylamide gels , pH 8.8, were used as separating gels Aliquots of cell extracts were precipitated with acetone and resuspended in Laemmli loading dye and loaded on gel (21). Migration was performed under 120 V and 160 V for 1D and 2D respectively. After electrophoresis gels were stained with Coomassie blue; after staining, gels were washed with a destaining solution containing 10% acetic acid and 10% methanol and finally with water and put on Whatman 3MM Chromatography paper, covered with Saran film. Gels were dried for 1h at 80°C using a vacuum dryer Hoefer Slab Gel Dryer GD 2000 (Amersham Biosciences). Strips scanned by LA – ICP MS were kept in fixing buffer (30% ethanol 10% glycerol) for 30 min and were dried under laminar flow for 4 h.

LA-ICP-MS Analyses

New Wave Research (Freemont, California, USA) UP-213 laser coupled with Agilent 7500cs ICP-MS (Agilent, Tokyo, Japan). The laser was operated in a focused spot mode at the repetition rate of 20 Hz, fluence of 3.80 J cm^{-2}, spot size of 250 µm and 50 and 100µm s^{-1} scan speed for gels and strips respectively. Ablation was carried with a He gas flow of 500 mL min^{-1} and mixed in a T-connector with aerosol obtained using a Micromist nebulizer and a double pass Scott spray chamber from a 2% nitric acid solution. ICP-MS was used in the collision cell mode using 3.6 mL min^{-1} of H_2 as the collision/reaction gas. All the parameters were tuned using as standard the glutathione peroxidase 1 (GPx1) from bovine (Sigma-Aldrich). To obtain two-dimensional (2D) images of selenium distribution, 2D gel was systematically screened (line by line), with a distance between lines of 0.800 mm. The number and the length of lines depend by the dimensions of the area of gel of interest. LA-ICP-MS data files for each analysis were converted into Excel files used to produce both electropherograms and 2D gel images. Finally, the images were plotted using programming script in MATLAB 7.9.0 computing software.

In gel protein hydrolysis

The most abundant selenium-containing spots were excised from a gel obtained in the identical conditions in parallel and *in situ* digested with trypsin. Before adding the enzyme, the excised pieces of gel were washed twice with 200 µL of 200 mM ammonium bicarbonate, 40% acetonitrile at 37 °C. Washing solution was discarded and the pieces of gel were dried under a nitrogen flow. Protein digestion was performed with 20 µL of 20 µg mL^{-1} solution of trypsin (Proteomics Grade from Sigma-Aldrich) and 50 µL of 40 mM ammonium bicarbonate, 9% acetonitrile, overnight at 37°C. Then, samples were transferred to 10 kDa cutoff Vivacon 500 centrifugal filter (Sartorius AG, Goettingen, Germany) and centrifuged at 7000 *g* for 20 min.

Capillary HPLC with the parallel ICP-MS and electrospray LTQ Orbitrap MS/MS

An Agilent 1260 Infinity HPLC system comprising a capillary and isocratic binary pump was used. HPLC-grade H_2O 0.1 % formic acid (FA) and 0.1 % FA in acetonitrile (ACN) were used as mobile phases A and B, respectively. ACN and FA was from Sigma (USA), water from a Milli-Q water purification system. After loading, the peptide mixture (8 µL) was first concentrated on an ZORBAX 300SB C18 (5µm 35 x 0.5mm) enrichment column (Agilent). Then, the analytes were eluted in back flush and separated on a ZORBAX 300SB C18 (3.5µm 100 x 0.3mm) column at flow rate of 4 µL min^{-1}. Peptides were eluted using a gradient: 0–2 min 2% B linear, 2–5 min 2–10% B linear, 5–35 min 10–25% B linear, 35–40 min 25-40% B linear, 40-45 min 40-97% B linear, 45-50 min 97% B isocratic, 50–55 min 97–2% linear.

The ICP MS detection was done using an Agilent 7700cs ICP-MS (Agilent, Tokyo, Japan), via a total consumption nebulizer (22). 5% of O_2 was added to the plasma gas. ICP-MS was used in the collision cell mode using 10 mL min^{-1} of He as the collision/reaction gas. A tryptic digest of a bovine glutathione peroxidase 1 (GPx1) (Sigma-Aldrich) was used to check the performance of the system.

The peptides were identified using a Velos Orbitrap (Thermo Electron, Bremen, Germany) using HCD data dependent analysis, operated in positive ion mode with the following parameters: heater temperature 50°C, sheath gas pressure 5 psi, spray voltage 3.80 kV, capillary temperature 280°C and S-Lens RF 67 %. Data were acquired in both MS and MS/MS mode, range 300-1200 m/z at a rate of 3 spectra/s. All samples were measured in a data dependent acquisition mode. Moreover selected precursor ions to be

fragmented were set. The peptide masses are measured with a resolution of 60,000 in the Orbitrap. Double and triple charged peptide were fragmented by HCD with a resolution of 30,000 with a normalized fragmentation energy of 40%.

Protein identification

The raw data were processed using the Xcalibur software version: 2.1.0 build 1139, while MassMatrix file conversion tool version: 3.0 was used to convert the raw data in common spectral file formats (.mgf mascot generic file). MASCOT software (www.matrixscience.com) version: 2.4.0 was used for the protein identification against NCBInr database (NCBInr_20120920.fasta; 21582400 sequences; 7401135489 residues), with the taxonomy restriction to *Other Firmicutes* (2926062 sequences). The Mascot search parameters were: "trypsin" as enzyme allowing up to 3 missed cleavages, carbamidomethyl and selenocysteine on cysteine residues, oxidation of methionine and formation of pyroGlu N-term on glutamine were selected as variable modifications. The parent peptide mass accuracy was set at 10 ppm and for MS/MS fragments obtained by HCD 0.6 Da tolerance was allowed. By data analysis, threshold provided to evaluate quality of matches for MS/MS data was found to be 41. No single peptide identification, even if unique, and peptide with a score lower than 41, was accepted.

Results

Selenium uptake by L. reuteri Lb2 BM-DSM 16143 during growth

The ICP-MS analyses were performed on three different samples recovered from cultures of *L. reuteri* Lb2 BM-DSM 16143 grown in MRS medium fortified with 2 mg L^{-1} selenium, as described in Materials and Methods section. Since preliminary results (data not shown) indicated that there was no uptake of Se from the medium during the lag phase, attention was focused only on the exponential growth phase. Figure 1 reports Se concentration (expressed in µg L^{-1}) for each sample during *L. reuteri* growth. It reveals that all the selenium added to the medium before the inoculum (2 mg L^{-1}) was completely dissolved and therefore bio-available for the strain. After 2 h growth a slight decrease of Se in the medium is visible, even if a significant uptake occurred only 4 hours after the inoculum. The maximal internalized Se concentration was about 1150 µg L^{-1} after 5 h growth (middle exponential phase), while about 600 µg L^{-1} Se was not internalized. The increase of Se concentration in the pellet was consistent with the progressive decrease in the supernatant. Virtually no Se was measured in the EDTA wash during the *L. reuteri* growth. It is worth noting that the sum of selenium quantified in the three samples analyzed equaled the one added to the medium. This means that there was no Se loss during the experimental steps validating the protocol.

Detection of selenium-containing proteins by LA-ICPMS

In order to locate rapidly and precisely the selenium-containing proteins in large 2D electrophoresis gels, a sample was divided in four aliquots which were analyzed in parallel by 1D isoelectric focusing electrophoresis (IEF) – laser ablation inductively coupled plasma mass spectrometry (ICP MS), 1D SDS PAGE – LA ICP MS, and, in duplicate, by 2D IEF-PAGE. On the basis of the 1D electropherograms obtained, areas supposed to contain the largest concentrations of Se were subjected to LA – ICP MS imaging to localize precisely the position of Se-containing proteins.

Figure 2a shows the electropherograms obtained independently by IEF, SDS-PAGE and the final 2D IEF-SDS electropherogram. Most intensive signals in the IEF were in the range of 4.5–6 pI and SDS –PAGE indicated the presence of major peaks in the 45-97

kDa mass range. Based on these electropherograms, areas of interest on 2DE gels were selected for the mass spectrometry imaging.

Selenized proteins identification

Based on LA-ICP-MS imaging, most intense spots in terms of Se signal were chosen for further identification in the parallel gel (Fig. 2b). 10 spots were excised from both gels, destained and digested with trypsin.

The identification procedure schematically illustrated in figure 3 targets the Se-containing peptides which are detected after capillary HPLC separation in parallel by ICP MS and electrospray Orbitrap MS. The ^{778}Se isotope intensity was measured on-line by ICP MS in order to detect selenium-containing peptides.

The results obtained were in agreement with the Orbitrap data; all the peaks present in the chromatogram of each spot showed the identical retention time of the selenopeptides identified by ESI-MS/MS (Fig. 3a). No unexpected Se signals were detected by HPLC-ICPMS, confirming that cysteine residues are the most prone to selenization.

The raw data from mass spectrometry were used for the identification of protein through the Mascot online software, obtaining good results in terms of total protein score and sequence coverage. In table 1 the identified proteins and all the selenopeptides are reported.

Selenocysteines localization

The incorporation of selenium into amino acids was evaluated by analyzing all the methionine and cysteine-containing peptides, searching for characteristic mass shift on scan spectra in the range of 300-1200 m/z. Selenium isotopic pattern was observed for all reported peptides, and it was in good agreement with theoretical prediction; moreover high accuracy (< 2ppm) was achieved thanks to high resolution of 60000 (Fig. 3b).

A more accurate elucidation was achieved by manual interpretation of the fragmented spectra obtained both in automatic and manual mode. For some peptides it was not possible to obtain adequate information from MS/MS spectra because of the presence of interfering ions or due to very low relative abundance of the selenopeptides.

Only selenocysteine-containing peptides were found, while no selenomethionine was detected. Moreover differences in isotopic pattern can be observed in the high resolution MS spectra. As an example figure 3c shows the MS/MS spectrum of the selenocysteine-containing peptide from spot 1. From the interpretation of the MS/MS spectrum it was possible to localize the modification site at level of Cys 151 within the sequence of the phosphoketolase enzyme. The comparison between the retention time of putative selenocysteine-containing peptide from capillary HPLC with parallel detection ICP MS (Fig. 3a) and electrospray LTQ Orbitrap (Fig. 3d) is reported, showing a perfect correspondence of the peaks related to peptides containing selenocysteine. Similar results were obtained for all the putative selenocysteine-containing peptides detected in different protein spots.

Figure 4 reports the shift of retention time of the selenopeptides in comparison to the unmodified (sulphur peptides) one (0.20 - 0.30 min). The same time shift can be observed for all the modified seleno-containing peptides detected. In addition all the selenopeptides detected were found to be one order of magnitude less abundant of the respective non modified.

Moreover the selenization of cysteine into selenocysteine (U) seems to involve specific cysteine residues within protein sequence. An explicative example is represented by

GAPDH (spots 5, 7, 8) and arginine deiminase (spot 3) where only 2 of the 3 cysteine residues were substituted.

Discussion

Experiments on selenium uptake by *L. reuteri* Lb2 BM-DSM 16143 during growth demonstrated the ability of the strain to recover selenium from the medium. Not all the Se added was internalized; moreover it has to be considered that the Se concentration used in this study negatively affected *L. reuteri* growth (5). Thus Se concentration and culture conditions could be optimized in order to reduce selenium-induced stress on bacteria, especially for nutraceutical applications. It was previously demonstrated that exceeding Se is partly released by *L. reuteri* in the form of surface-associated Se(0) particles (5). However in this study no detectable increase in Se concentration was observed in the pellet wash, suggesting that the internalized selenium was chiefly metabolized in a different way from the detoxification mechanism, and inserted into proteins. Moreover, the decrease of Se in the biomass and the corresponding increase in the medium after 6 h growth suggests that internalized selenium is released into the external environment, probably fixed into proteins. Further studies are necessary to determine the presence of SeCys into extracellularly released proteins. This event, if confirmed, could directly provide an organic form of selenium to the human host. Once determined the ability of the strain to internalize selenium, HPLC fractionation of the soluble protein extract followed by ICP MS detection, allowed to determine that about half of internalized Se was covalently incorporated into proteins (data not shown). An in depth investigation on protein selenization mechanism, performed by 2D-LA-ICPMS, demonstrated that in this *L. reuteri* strain all the Se present in the proteins is incorporated as selenocysteine (SeCys), while methionine/selenomethionine substitution, that is typical of other microorganisms such as yeasts (23), did not occur. The results corroborate the data obtained by autoradiography using ^{75}Se and ^{14}C-carboxymethylseleno-cysteine indicating that lactic acid bacteria are able to incorporate selenium into intracellular proteins only as SeCys (24). $SeCys_2$ (seleno-cystine, containing a di-selenide bridge) and MeSeCys (methyl-selenocysteine) were also the predominant organic forms of selenium detected in the Se-enriched yogurt containing *Lactobacillus* species (25,26).

Our data localize the exact position within the primary sequence of proteins in which SeCys is inserted. In this *L. reuteri* strain SeCys was found in two glycolitic enzymes (glyceraldehyde 3-phosphate dehydrogenase, spots 5, 7, 8; pyruvate kinase, spot 2), two pentose phosphate pathway enzymes (phosphoketolase, spot 1; 6-phosphogluconate dehydrogenase, spot 4), two ADI pathway enzymes (arginine deiminase, spot 3; ornithine carbamoyltransferase, spot 6) and a ribonucleoside hydrolase RihC (spots 9, 10). In some of these enzymes (PKP, PK, 6PGD, OTCase and RihC) all the cysteine residues reported in the sequence were modified into selenocysteine. In contrast to that GAPDH and ADI behave in a different way: both possess in their primary sequence three Cys residues but in both enzymes only two of them are replaced by SeCys. In both cases two cysteine residues were present in the same peptide, ^{144}DDIIVSAGS**C**TTS**C**LAPMAK^{163} for GAPDH and ^{398}**C**MS**C**PIVR^{405} for ADI, both belonging to the active site, but only one of the two Cys (the underlined one) is replaced by SeCys (27, 28). Curiously, in both cases it was the catalytic Cys to be replaced (^{153}Cys/^{153}SeCys in GAPDH and ^{398}Cys/^{398}SeCys in ADI). Therefore the catalytic Cys proved to be the most affected by selenization. It is worth noting that the presence of a SeCys residue in these sites could modify the catalytic properties of the enzymes, since the pk_a of SeCys (5.2) is much lower than that of Cys (8.3) (29). Not all the Cys possess the same tendency to be

converted into SeCys. The presence of Se as SeCys in GAPDH was previously reported by Lacourciere et al. which demonstrated that selenium was retained by GAPDH after denaturation, suggesting its role as a selenium delivery protein (10).
Our data demonstrate that in this *L. reuteri* strain Se insertion into proteins exclusively occurs as selenocysteine, although the insertion mechanism still remains to be determined. Since in GAPDH and ADI there is a specific substitution of only two of the three Cys, it can be suggested that the insertion of SeCys can be genetically encoded, according to the mechanism used by other bacteria (4, 16). This hypothesis will be verified in further studies by analyzing gene sequences of the identified proteins searching for UGA codon and putative SECIS elements.
In this paper, it was demonstrated that *L. reuteri* Lb2 BM-DSM 16143 is able to uptake inorganic Se from the medium and to metabolize it into an organic form incorporated into proteins that are crucial for the bacterial energy metabolism. The peculiarity of this strain is its ability to exclusively insert Se into selenocysteine. To the best of our knowledge, this is the first study that describes this event in a probiotic lactic acid bacterium, specifically identifying the sites in which cysteine/selenocysteine substitution occurs. *L. reuteri* Lb2 BM-DSM 16143 can therefore become a viable alternative to Se-rich yeast as food supplement in Se-deficient subjects.

Acknowledgments
This work was supported by Programma Operativo Nazionale “Ricerca e Competitività 2007-2013” PON01_01802” and PON01_00117.

References

1. Burk, R.F. (2002) Selenium, an antioxidant nutrient. *Nutr Clin Care* 5, 75-79.
2. Singhal, N., Austin, J. (2002) A clinical review of micronutrients in HIV infection. *J Int Assoc Physicians AIDS Care* 1, 63-75.
3. Rayman, M.P. (2012) Selenium and human health. *Lancet* 379, 1256–1268.
4. Turner, R.J., Weiner, J.H., Taylor, D.E. (1998) Selenium metabolism in Escherichia coli. *Biometals* 11, 223-227.
5. Lamberti, C., Mangiapane, E., Pessione, A., Mazzoli, R., Giunta, C., Pessione, E. (2011) Proteomic characterization of a selenium-metabolizing probiotic Lactobacillus reuteri Lb2 BM for nutraceutical applications. *Proteomics* 11, 2212-2221.
6. Andreoni, V., Luischi, M.M., Cavalca, M.L., Erba, D., Ciappellano, S. (2000) Selenite tolerance and accumulation in the *Lactobacillus* species. *Ann. Microbiol.* 50, 77–88.
7. Dobias, J., Suvorova, E.I., Bernier-Latmani, R. (2011) Role of proteins in controlling selenium nanoparticle size. *Nanotechnol.* 22, 1-9.
8. Schrauzer, G.N. (2000) Selenomethionine: A Review of Its Nutritional Significance, Metabolism and Toxicity. *J Nutr*, 130, 1653-1656.
9. McSheehy, S., Kelly, J., Tessier, L., Mester, Z. (2005) Identification of selenomethionine in selenized yeast using twodimensional liquid chromatography-mass spectrometry based proteomic analysis. *Analyst* 130, 35–37.
10. Lacourciere, G.M., Levine, R.L., Stadtman, T.C. (2002) Direct detection of potential selenium delivery proteins by using an Escherichia coli strain unable to incorporate selenium from selenite into proteins. *Proc. Natl. Acad. Sci. U. S. A.* 99, 9150-9153.
11. Stolz, J. F., Basu, P., Santini, J. M., Oremland, R. S. (2006) Arsenic and selenium in microbial metabolism. *Annu. Rev. Microbiol.* 60, 107–130.

12. Cone, J.E., Del Rio, R.M, Davis, J.N., Stadtman, T.C. (1976) Chemical characterization of the selenoprotein component of clostridial glycine reductase: identification of selenocysteine as the organoselenium moiety. *Proc. Natl. Acad. Sci. U. S. A.* 73, 2659–2663.
13. Wagner, M., Sonntag, D., Grimm, R., Pich, A., Eckerskorn, C., Söhling, B., Andreesen, J.R. (1999) Substrate-specific selenoprotein B of glycine reductase from Eubacterium acidaminophilum. Biochemical and molecular analysis. *Eur J Biochem.* 260, 38-49.
14 Kabisch, U.C., Gräntzdörffer, A., Schierhorn, A., Rücknagel, K.P., Andreesen, J.R., Pich, A. (1999) Identification of D-proline reductase from Clostridium sticklandii as a selenoenzyme and indications for a catalytically active pyruvoyl group derived from a cysteine residue by cleavage of a proprotein. *J. Biol. Chem.* 274, 8445–8454.
15 Wagner, R., Cammack, R., Andreesen, J.R. (1984) Purification and characterization of xanthine dehydrogenase from Clostridium acidiurici grown in the presence of selenium. *Biochim. Biophys. Acta* 791, 63–74.
16. Stock, T., Rother, M. (2009) Selenoproteins in Archaea and Gram-positive bacteria. *Biochim. Biophys. Acta* 1790, 1520–1532.
17. Zhang, Y., Romero, H., Salinas, G., Gladyshev, V.N. (2006) Dynamic evolution of selenocysteine utilization in bacteria: a balance between selenoprotein loss and evolution of selenocysteine from redox active cysteine residues. *Genome Biology* 7:R94.
18. Talarico, T. L., Casas, I. A., Chung, T. C., Dobrogosz, W. J. (1988) Production and isolation of reuterin, a growth inhibitor produced by *Lactobacillus reuteri*. Antimicrob. *Agents Chemother.* 32, 1854–1858.
19. Whitehead, K., Versalovic, J., Roos, S., Britton, R.A. (2008) Genomic and genetic characterization of the Bile Stress Response of Probiotic *Lactobacillus reuteri* ATCC 55730. *Appl. Environ. Microbiol.* 74, 1812–1819.
20. Lin, Y.P., Thibodeaux, C.H., Pena, J.A., Ferry, G.D., Versalovic, J. (2008) Probiotic *Lactobacillus reuteri* Suppress Proinflammatory Cytokines via c-Jun. *Inflamm Bowel Dis* 14, 1068-1083.
21. Laemmli, U.K. (1970) Cleavage of structural proteins during the assembly of the head of bacteriophage T4. *Nature* 227, 680-685.
22. Schaumlöffel, D., Ruiz Encinar, J., Łobiński, R. (2003) Development of a sheathless interface between reversed-phase capillary HPLC and ICPMS via a microflow total consumption nebulizer for selenopeptide mapping. *Analytical chemistry* 75, 6837-6842.
23. Rayman, M.P. (2004) The use of high-selenium yeast to raise selenium status: how does it measure up? *Brit. J. Nutr.* 92, 557–573.
24. Calomme, M., Hu, J., K. Van Den Branden, K., Vanden Berghe, D.A. (1995) Seleno-Lactobacillus An Organic Selenium Source. *Biological Trace Element Research* 47, 379-383.
25. Alzate, A., Cañas, B., Pérez-Munguía, S., Hernández-Mendoza, H., Pérez-Conde, C., Gutiérrez, A.M., Cámara, C. (2007) Evaluation of the inorganic selenium biotransformation in selenium-enriched yogurt by HPLC-ICP-MS. *J Agric Food Chem.* 55, 9776-9783.
26. Alzate, A., Fernández-Fernández, A., Pérez-Conde, M.C., Gutiérrez, A.M., Cámara, C. (2008) Comparison of biotransformation of inorganic selenium by Lactobacillus and Saccharomyces in lactic fermentation process of yogurt and kefir. *J Agric Food Chem.* 56, 8728-8736.

27. Nakajima, H., Amano, W., Fujita, A., Fukuhara, A., Azuma, Y.T., Hata, F., Inui, T., Takeuchi, T. (2007) The Active Site Cysteine of the Proapoptotic Protein Glyceraldehyde-3-phosphate Dehydrogenase Is Essential in Oxidative Stress-induced Aggregation and Cell Death. *J Biol Chem.* 282, 26562–26574.
28. Lu, X., Galkin, A., Herzberg, O., Dunaway-Mariano, D. (2004) Arginine Deiminase Uses an Active-Site Cysteine in Nucleophilic Catalysis of L-Arginine Hydrolysis. *J Am Chem Soc.* 126, 5374-5375.
29. Wessjohann, L.A., Schneider, A., Abbas, M., Brandt, W. (2007) Selenium in chemistry and biochemistry in comparison to sulfur. *Biological chemistry* 388, 997-1006.

Figure 1: ICP-MS analyses on pellet, supernatant and EDTA wash samples collected at different times of *L. reuteri* Lb2 BM growth during the exponential phase, omitting lag phase. Se concentration is expressed in µg/L.

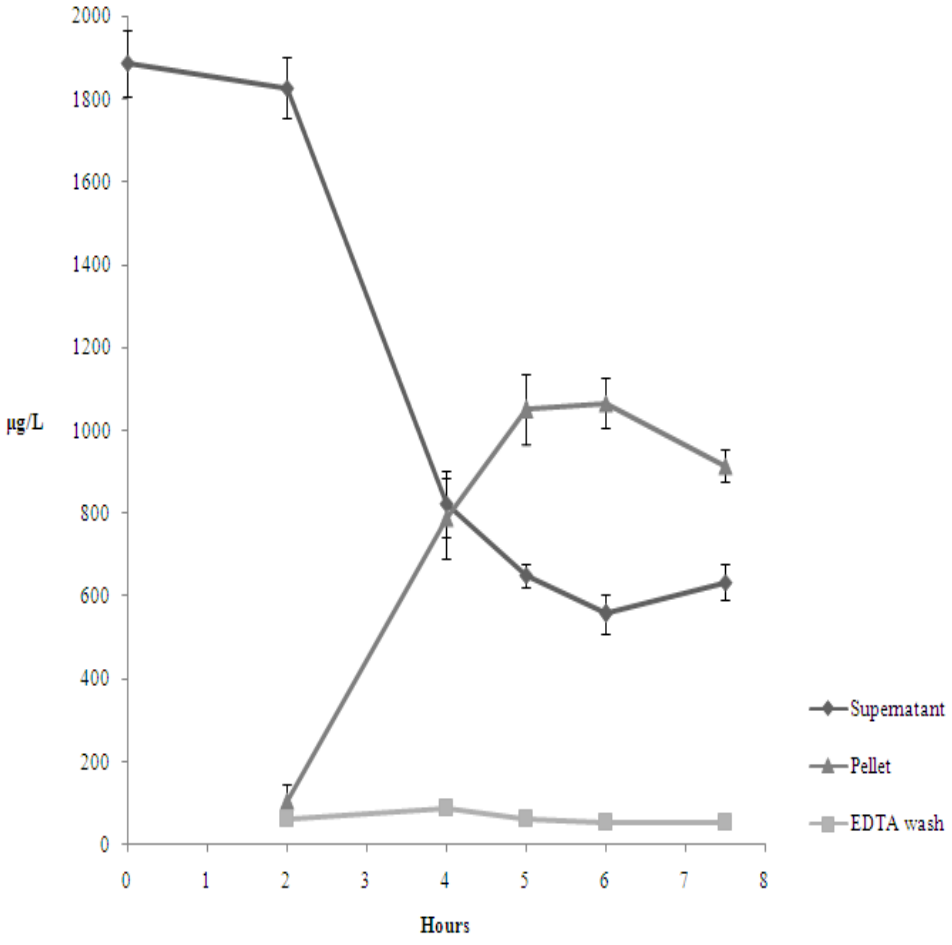

Figure 2: a) Se-containing protein spots after Laser Ablation ICP MS Imaging of 2D SDS-PAGE gel of *L. reuteri* Lb2 BM soluble extract. **b)** Parallel 2D SDS-PAGE of *L. reuteri* Lb2 BM soluble extract for proteomics analysys. Circles and numbers are referred to each spots excised and further analyzed (cfr. Table 1).

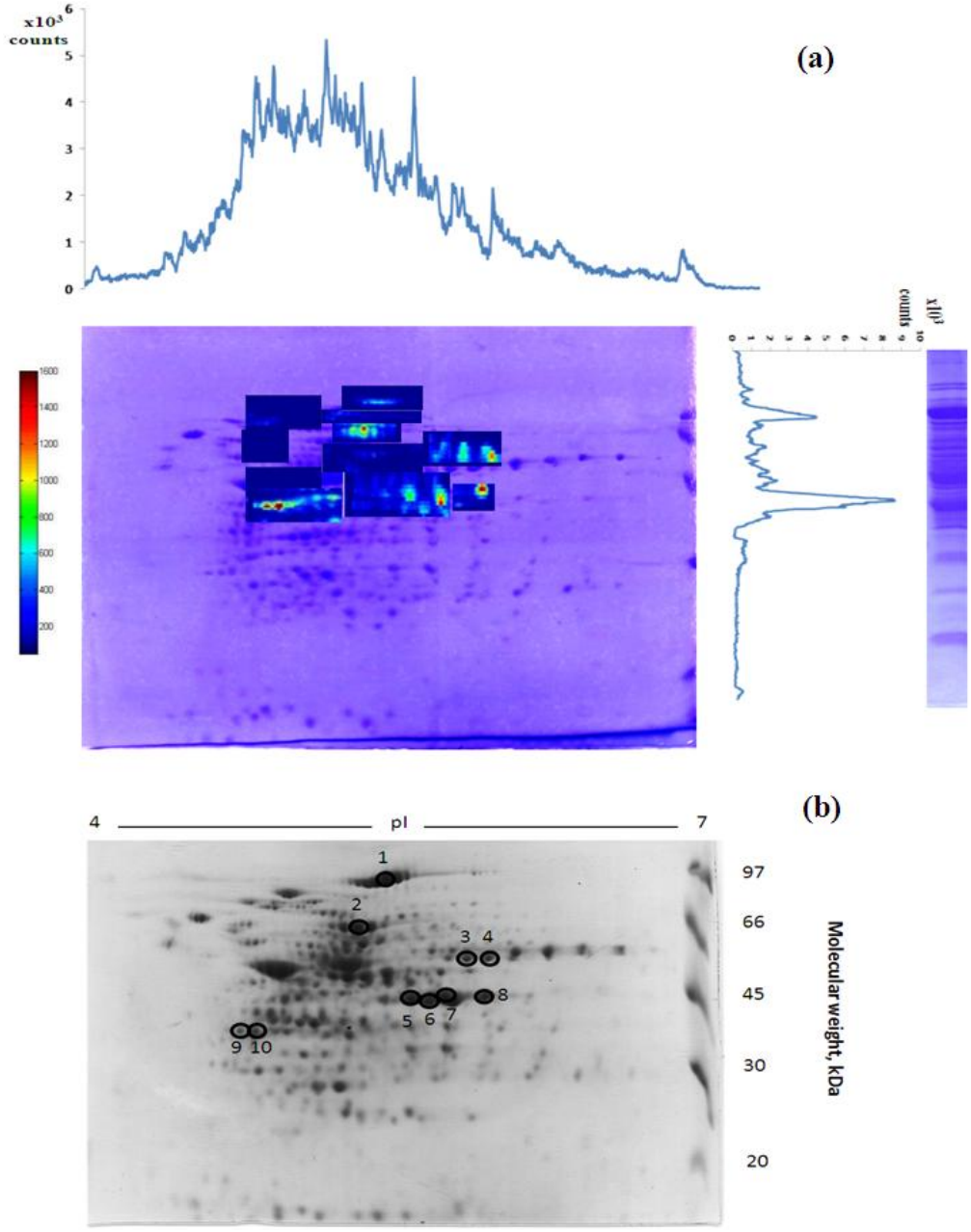

Figure 3: a) Detection of selenocysteine-containing peptide NQEUINLFVTSK from spot 1 by capHPLC-ICPMS; **b)** XIC chromatograms of tryptic peptides of Phosphoketolase. Correspondence of parallel detection ICP MS and electrospray LTQ Orbitrap retention times of selenocysteine-containing peptide NQEUINLFVTSK. The complete fingerprint of identified protein (all peptides from letter A to V) is given in a supplementary material (Table S1); **c)** High accuracy comparison between the observed isotopic pattern and theoretical prediction of selenocysteine-containing peptide NQEUINLFVTSK; **d)** An unambiguously attribution of the Secysteine-containing peptide NQEUINLFVTSK after interpretation of MS/MS spectrum of the double charged ion at m/z 750,8326.

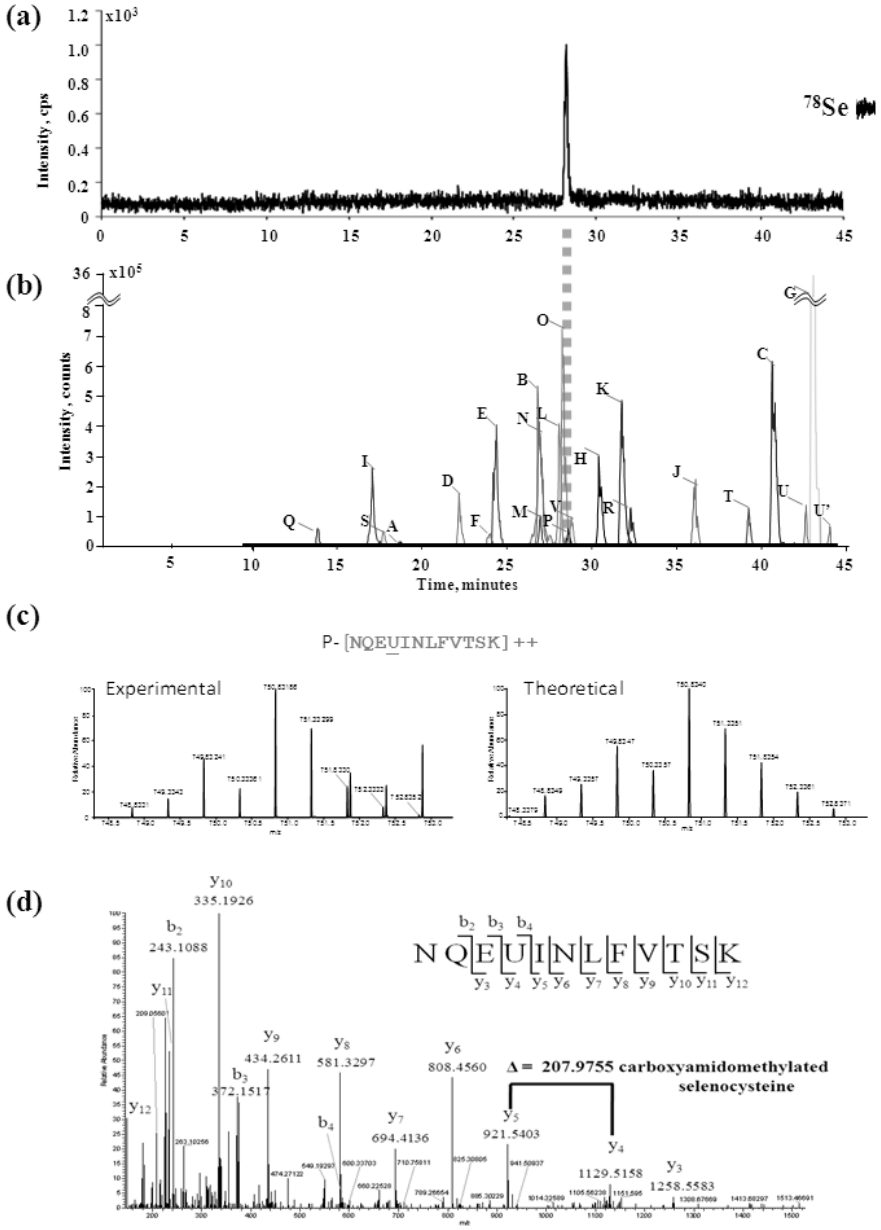

Figure 4: Attribution of the Se-containing peptide from spot 8 at MS level from LTQ Orbitrap spectrum in the range of 300-1200 m/z at a resolution of 60000. A comparison between the isotopic pattern of non-containing selenium peptide (^{144}DDIIVSAGSCTTSCLAPMAK^{163} 1048.9873^{2+}) and selenium-containing peptide (^{144}DDIIVSAGSUTTSCLAPMAK^{163} 1072.9598^{2+}), is given.

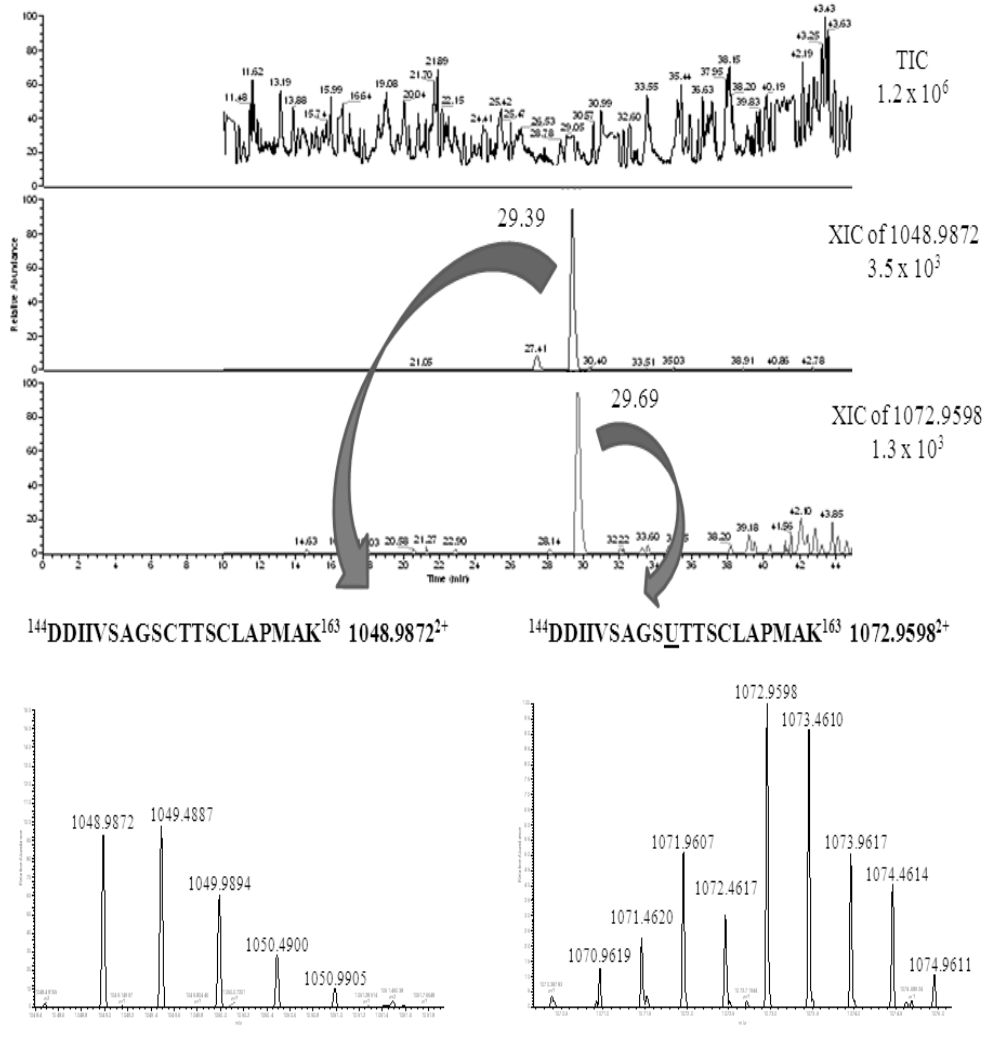

Table 1: List of the identified protein. For GAPDH and RihC in table are reported the results obtained from spot 8 and 10 respectively. Number of peptides, Peptide sequences and Individual ion scores are reported in supplementary material (Table S1).

Spot	Protein	NCBI ID	MW (Da)	pI	Score	Seq. cov. (%)
1	Phosphoketolase	gi|148544892	91346	5.09	2888	39
2	Pyruvate kinase	gi|148543982	51793	5.06	4077	72
3	Arginine deiminase	gi|148543680	46214	5.39	1803	73
4	6-Phosphogluconate dehydrogenase	gi|184154309	53498	5.56	2005	56
5,7,8	Glyceraldehyde 3-phosphate dehydrogenase	gi|184153036	35971	5.41	2913	71
6	Ornithine carbamoyltransferase	gi|148543661	37536	5.21	1791	58
9,10	Ribonucleoside hydrolase RihC	gi|148543341	32552	4.70	1211	60

Spot	Selenocysteine-containing peptide	Obs. mass	Theo. mass	Δm (ppm)
1	NQEUINLFVTSK	750,8326	750,8334	1,0655
2	ELVUHVLNHGVLGS	869,4182	869,4185	0,3451
	UNELGKPVITATQMLDSMQENPRPTR	759,3545	759,3552	0,9218
3	UMoxSCPIVR	543,7015	543,7023	1,4714
	UMSCPIVR	535,7056	535,7049	-1,3067
	DQQAUIGDGITINHMTFK	699,6362	699,6373	1,5722
4	AGUIIR	369,1643	369,1640	-0,8126
	AEEDGKPUVAYIGPNGAGHYVK	794,0203	794,0206	0,3778
5,7,8	DDIIVSAGSUTTSCLAPMAK	1072,9598	1072,9589	-0,8388
	NDGVDFVLEUTGFYTSAEK	1100,4534	1100,4528	-0,5452
6	USFEVGAK	473,1824	473,1826	0,4227
	USFEVGAKDEGAHVTYLGPSGSHIGHK	963,4326	963,4337	1,1417
	ATENPNVLFEHULPAFHNLDTEVGK	725,8341	725,8334	-0,9644
9,10	VULDIDAEYFNK	767,8191	767,8200	1,1721

IV.5 Data not included in the submitted paper

An approach for screening and resolving selenium-containing proteins from *L. reuteri* Lb2 BM-DSM 16143 cellular extracts was employed based on the combination of sample preparation and liquid chromatography "off-line" coupled to ICP-MS detection. Selenium-containing protein screening and fractionation were carried out by SEC-ICP-MS and C4-RP-HPLC-ICP-MS.

IV.5.1 SEC-ICP-MS

Analytical gel filtration experiment was carried out as follows: 5mg of protein extract was loaded on a size exclusion column Superdex G-200 HR 10/30 (10 mm × 300 mm × 13 µm beads size) with the approximate bed volume of 24 mL and a declared linear separation range of 3-600 kDa for globular proteins (GE Healthcare Life Science), previously equilibrated in 0.1 M Tris-HCl, 0.15 M NaCl, pH 7.0, installed on an AKTA^{TM}fplc^{TM} (Amersham Biosciences). Separation was carried out isocratically at a flow rate of 0.3 mL/min using 0.1 M Tris–HCl, 0.15 M NaCl, pH 7.0 as mobile phase. Protein separation was monitored either at 220 and 280 nm. The column had been previously calibrated in the same buffer with the following proteins of know molecular mass: alcohol dehydrogenase (150 kDa), bovine serum albumin (66 kDa), carbonic anhydrase (29 kDa), and cytochrome c (12 kDa). Fractions of 500 µL were collected and stored at 4°C. Aliquots of 100µL for each fraction were diluted 50x in bidistilled water and directly analyzed by ICP-MS. In ICP-MS detection, the most abundant Se isotopes, ^{80}Se (49.7%) suffer from strong interference due to $^{40}Ar^{40}Ar^{+}$ adduct. Thus ^{78}Se (23.6%) was used activating the collision/reaction cell in order to reduce the argon- and solvent- based interferences.

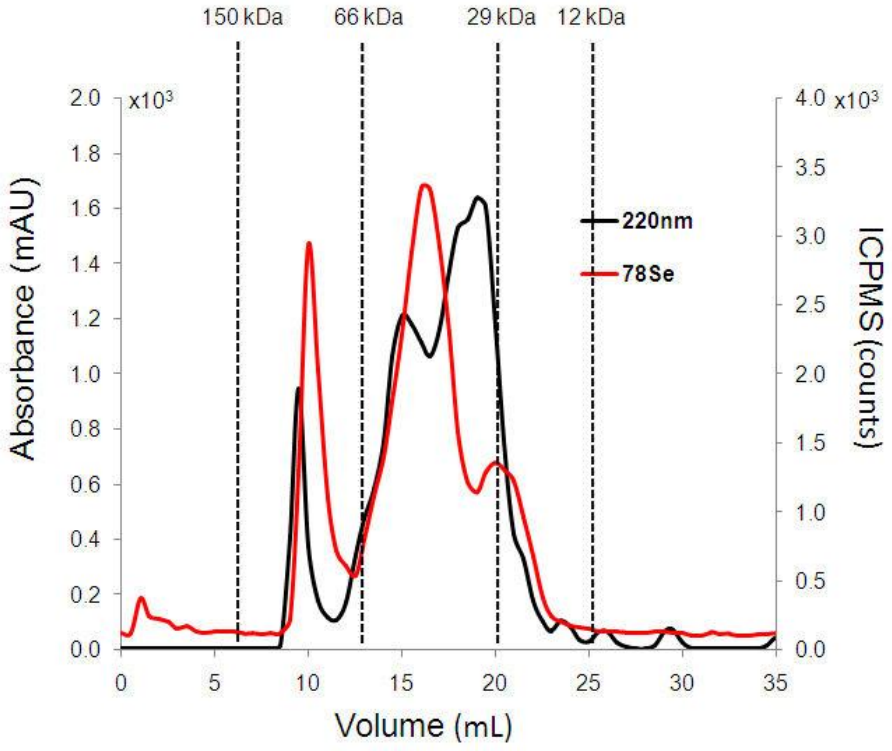

***Figure IV.1**. ^{78}Se SEC-ICP-MS chromatogram of the protein extracts of L. reuteri Lb2 BM-DSM 16143 supplemented with 2 mg/L Na_2SeO_3. Both proteins and selenium showed a coherent elution with UV (black line) and ICP-MS (red line) detection.*

As show in fig. IV.1 the main Se-containing peaks were eluted in a volume range between 8.5-22.5 mL, matching with the major intense peaks observed with the UV detection, whereas no low molecular weight selenium compounds were detected. This may be related to the pre-concentration of the sample by diafiltration, using an Amicon Ultra-0.5 centrifugal filter device (3 kDa MWCO), with consequent lost of low molecular weight compounds, that were apart quantified.
Summing the selenium recovered in each fraction after SEC separation and comparing the obtained value with the total Se quantified in soluble protein extract, the result is that more than 40% of selenium was eluted with protein, most likely fixed into proteins.

IV.5.2 HPLC-ICP-MS

300 µL of protein extract were fractionated by RP-HPLC using an Agilent 1100 HPLC system equipped with a Zorbax C4 column (4,6mm X 150mm) (Palo Alto, California). The optimized gradient elution used was: 0–5 min 15% mobile phase B, 5–35 min 80% mobile phase B, 35–36 min 95% mobile phase B, 36–45 min 95% mobile phase B, where, mobile phase A is 0.1 % TFA, and solvent B is 95% ACN, 5% H_2O and 0.07% TFA, at a flow rate of 1 mL/min. The collected fractions (each 5 min.) were then concentrated by SpeedVac and analysed as well by ICP-MS.

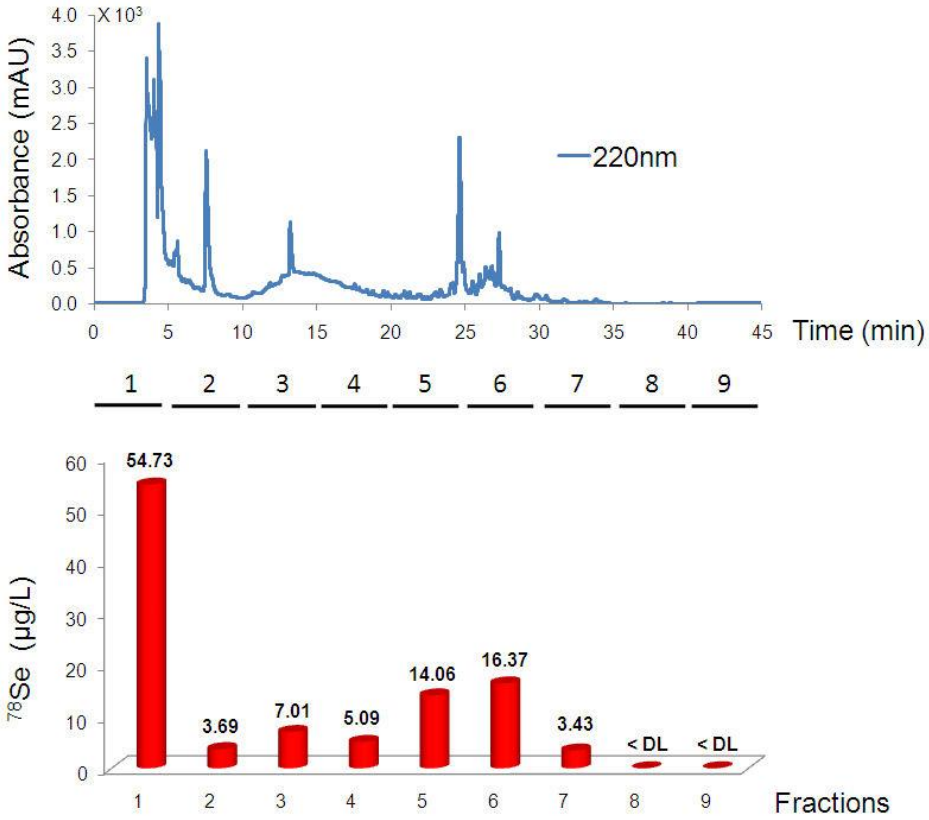

Figure IV.2. *C4-RP-HPLC fractionation (upper panel) of an aliquot of protein extracts of L. reuteri Lb2 BM-DSM 16143 supplemented with 2 mg/L Na_2SeO_3. ICP-MS ^{78}Se quantification (lower panel) of nine fractions recovered from HPLC separation.*

Detection of selenium-containing proteins was performed by fractionation of soluble protein extract with a RP-HPLC separation and offline ICP-MS detection. Protein

extract containing 450 ng of Se was directly loaded on the column. Nine fractions were collected; the first fraction (1-5 min) contained the flowthrough of the chromatographic separation (salts and hydrophilic molecules). The remaining eight fractions were collected each 5 min and they contain proteins eluting from the C4 column. All these fractions were concentrated and analyzed separately by ICP-MS. ICP-MS data revealed that the Se recovered in all fractions was 313 ng, with a column recovery of about 70% of the initial value. 52% of the total Se recovered was found in the flowthrough fraction, thus demonstrating that this amount of Se was not covalently incorporated, as selenium-amino acids, into proteins. The residual 48% of recovered Se was found in the remaining eight fractions, suggesting that it was fixed in the selenium-containing proteins.

IV.5.3 PCR AND RT-PCR

In order to evaluate if the substitution of cysteine with selenocysteine is genetically encoded through the UGA (TGA) codon, PCR and RT-PCR experiments were performed on three genes that codify for three proteins identified with the previous ICP-MS experiments: GAPDH (only two of the three Cys contained in the sequenced were substituted with Sec), phosphoketolase (the only Cys present was converted in Sec) and pyruvate kinase (both Cys residues were substituted by Sec).
PCR experiments followed by sequencing did not reveal the presence of the specific TGA codon instead of the TGT or TGC codon that codify for cysteine.
To verify if the modification/substitution of Cys with Sec happened at mRNA level, RT-PCR experiments were performed on the same three genes.

PCR

Genomic DNA was extracted from *Lactobacillus reuteri* Lb2 BM-DSM 16143 and used for subsequent PCR analyses on three genes: glyceraldehyde 3-phosphate dehydrogenase (A), phosphoketolase (B) and pyruvate kinase (C). The primers used in these experiments are listed in the table.

Gene	Forward	Reverse
A	ATGACTGTAAAAATTGGTATTAACG	TTAAAGAGTAGCAAAGTGAAGTAAAG
B	GGTTACACTCACCAAGATCC	TTACTTAAGACCCTTCCAAGTC
C	CAACTTCTCACACGGTGACC	CCAATCGAACTTTTCAGTACCG

Table IV.1. *List of the primers used for amplification of three genes from Lactobacillus reuteri Lb2 BM-DSM 16143: glyceraldehyde 3-phosphate dehydrogenase (A), phosphoketolase (B) and pyruvate kinase (C)*

RT-PCR

An aliquot of cells was recovered at the moment of maximal Se uptake. Total RNA was extracted and purified using the kit “Total RNA isolation NucleoSpin® RNA II” (Macherey-Nagel). Since usually genomic DNA contamination was observed, the total RNA was also subjected to an additional DNAse treatment with DNAse (Sigma). Reverse transcription of total RNA into cDNA was achieved with random hexamers using “RevertAid Premium Reverse Transcriptase” (Fermentas). Detection of each

transcript was then obtained by PCR using the same specific primers listed in the table IV.1.
During RT-PCR, opportune negative controls were always performed as follows: no template (NTC) and no reverse transcriptase (RT-).
All the PCR products obtained from both the experiments were sequenced to verify the presence of UGA codon, specific for the insertion of SeCys.

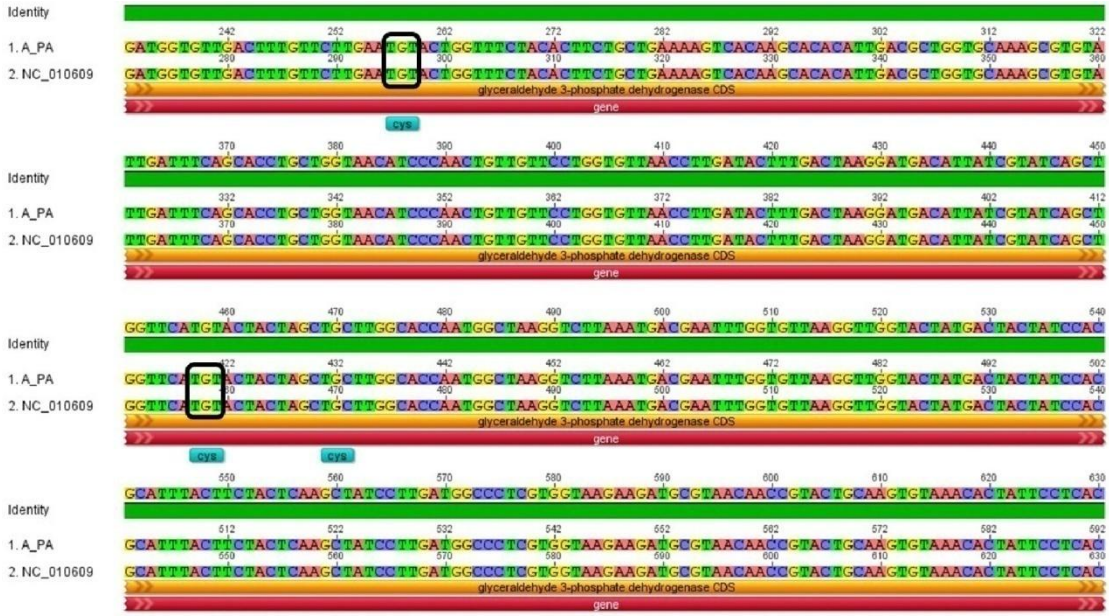

Figure IV.3. *Sequencing results for GAPDH after RT-PCR analysis. The two circled TGT codify for Cys that are substituted with SeCys.*

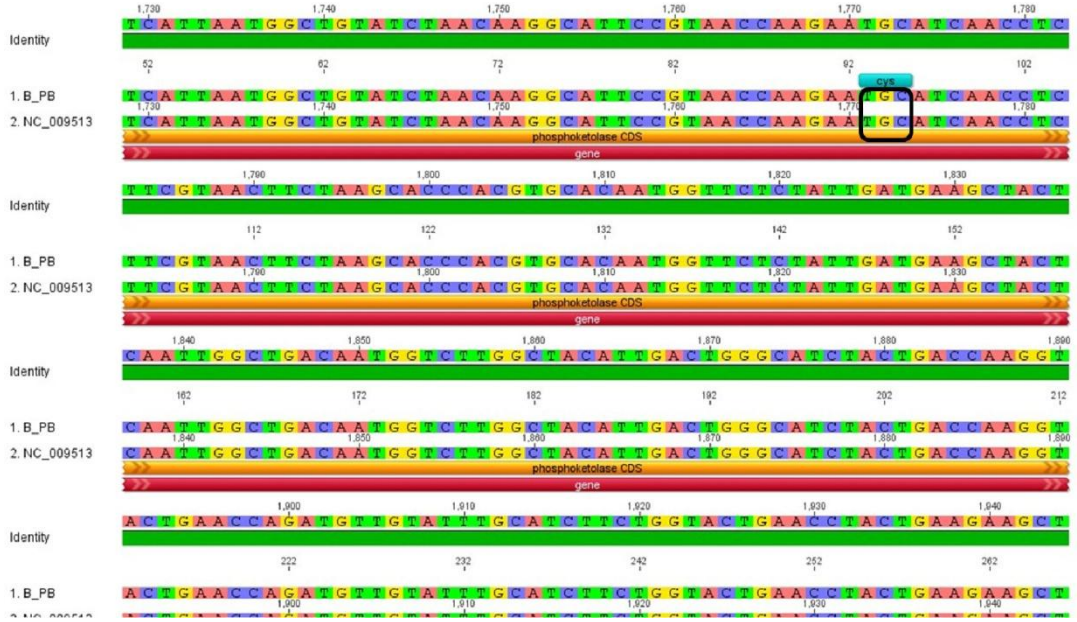

Figure IV.4. *Sequencing results for phosphoketolase after RT-PCR analysis. The circled TGC codify for Cys that is substituted with SeCys.*

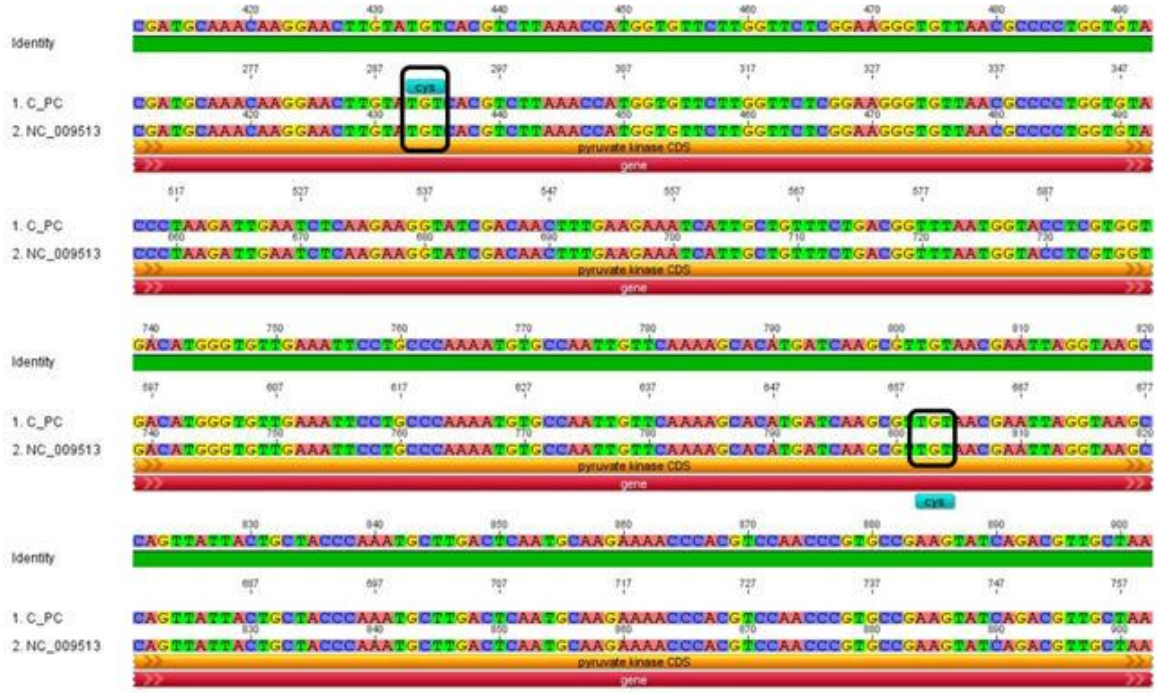

Figure IV.5. *Sequencing results for pyruvate kinase after RT-PCR analysis. The two circled TGT codify for Cys that are substituted with SeCys.*

As all the figures clearly demonstrate there is no evidence upon now that the insertion of SeCys at the place of Cys in genetically encoded. Further studies will be performed on the remaining four genes in order to prove that the results obtained are valid for all the proteins identified and containing SeCys. A new strategy will be developed to clarify the mechanism that controls the insertion of selenocysteine into *L. reuteri* Lb2 BM-DSM 16143 proteins.

IV.6 Acknowledge

Author thank the research groups of prof. E. Pessione from University of Turin and prof. R. Lobinski from Université de Pau et des Pays de l'Adour – CNRS, for their fruitful collaboration.

IV.7 References

[1] Wang, Y.D., Wang, X., Ngai, S.M., Wong, Y.-S., Comparative proteomics analysis of selenium responses in selenium-enriched rice grains. *Journal of proteome research* **2013**, 12, 808-20.

[2] Combs, G. F., Jr. Food system-based approaches to improving micronutrient nutrition: the case for selenium. *Biofactors* **2000**, 12, 39−43.

[3] Suzuki, K.T., Metabolomics of Selenium: Se Metabolites Based on Speciation Studies. *Toxicology* **2005**, 51, 107-114.

[4] Gunzler, W.A., Steffens, G.J., Grossmann, A., Kim, S.M.A., Otting, F., Wendel, A., and Flohe, L. The amino acid sequence of bovine glutathione peroxidase. *Hoppe-Seyler's. Z. Physiol. Chem*. **1984**, 365, 195–212.

[5] Lamberti, C., Mangiapane, E., Pessione, A., Mazzoli, R., Giunta, C., Pessione, E., Proteomic characterization of a selenium-metabolizing probiotic Lactobacillus reuteri Lb2 BM for nutraceutical applications. *Proteomics* **2011**, 11, 2212-2221.

[6] Haft, D.H., Self, W.T., Orphan SelD proteins and selenium-dependent molybdenum hydroxylases. *Biology direct* **2008**, 3, 4.

[7] Veres, Z., Tsai, L., Scholz, T.D., Politino, M., Balaban, R.S., and Stadtman, T.C., Synthesis of 5-methylaminomethyl-2-selenouridine in tRNAs: 31P NMR studies show the labile selenium donor synthesized by the selD gene product contains selenium bonded to phosphorus. *Proc Natl Acad Sci USA* **1992,** 89**,** 2975–2979.

[8] Glass, R.S., Singh, W.P., Jung, W., Veres, Z., Scholz, T.D., and Stadtman, T.C., Monoselenophosphate: synthesis, characterization, and identity with the prokaryotic biological selenium donor, compound SePX. *Biochemistry* **1993,** 32**,** 12555–12559.

[9] Zhang, Y., Turanov, A.A., Hatfield, D.L., and Gladyshev, V.N., *In silico* identification of genes involved in selenium metabolism: evidence for a third selenium utilization trait. *BMC Genomics* **2008**, 9**,** 251.

[10] Mounicou, S., Meija, J., Caruso, J., Preliminary studies on selenium-containing proteins in Brassica juncea by size exclusion chromatography and fast protein liquid chromatography coupled to ICP-MS. *The Analyst* **2004**, 129, 116-23.

[11] EFSA, Selenium-enriched yeast as source for selenium added for nutritional purposes in foods for particular nutritional uses and foods (including food Scientific Opinion of the Panel on Food Additives , Flavourings , Processing Aids and Materials in Contact with Food Adopted on 9 July 2008. *Aids* **2008**, 1-42.

[12] Martinis, E.M., Escudero, L.B., Berton, P., Monasterio, R.P., et al., Determination of inorganic selenium species in water and garlic samples with on-line ionic liquid dispersive microextraction and electrothermal atomic absorption spectrometry. *Talanta* **2011**, 85, 2182-8.

[13] Kápolna, E., Fodor, P., Bioavailability of selenium from selenium-enriched green onions (Allium fistulosum) and chives (Allium schoenoprasum) after 'in vitro' gastrointestinal digestion. *Int J Food Sci Nutr.* **2007**, 58, 282-296.

[14] Kotrebai, M., Birringer, M., Tyson, J.F., Block, E., Selenium speciation in enriched and natural samples by HPLC-ICP-MS and HPLC-ESI-MS with perfluorinated carboxylic acid ion-pairing agents. *Analyst.* **2000**, 125, 71-78.

[15] Ogra, Y., Katayama, A., Ogihara, Y., Yawata, A., Anan, Y., Analysis of animal and plant selenometabolites in roots of a selenium accumulator, Brassicarapa var. peruviridis, by speciation. *Metallomics* **2013,** Epub ahead of print.

[16] Abdulah, R., Faried, A., Kobayashi, K., Yamazaki, C., et al., Selenium enrichment of broccoli sprout extract increases chemosensitivity and apoptosis of LNCaP prostate cancer cells. *BMC cancer* **2009**, 9, 414.

[17] Prins, C.N., Hantzis, L.J., Quinn, C.F., Pilon-Smits, E. a H., Effects of selenium accumulation on reproductive functions in Brassica juncea and Stanleya pinnata. *Journal of experimental botany* **2011**, 62, 5633-40.

Conclusions

This PhD thesis is focused on the investigation of metals involved in relevant biological processes by metallomics and proteomics, in order to obtain a deeper knowledge of how metals and protein are related. The major results obtained in this work are briefly outlined below.

- The investigation of metal-ions tolerance in *E. coli*, looking at the effects on proteome after exposure to cadmium has been reported in the chapter II. By developing an integrated metallomics-proteomics approach, a strong correlation between zinc and cadmium was demonstrated. Moreover a time-course analysis led to the definition of the total amount of cadmium recovered and assimilated into microbial cells and it has established that the entire metals sequestration take place during the lag phase of microbial growth. Finally a proteomic analysis has revealed that cadmium affects several molecular functions, leading to a decrease of proteins involved in biosynthesis processes and energetic metabolism. On the other hand an over-expression of proteins involved in transport mechanism trough membrane was observed.
- The effect of cadmium and lead on the viability of primary renal (HRCE) cells has been described in the chapter III. It was clearly demonstrated, by the activation of caspase-3 and down-regulation of the anti-apoptotic marker Bcl-2, that cell mortality was due to apoptotic death, whereas no apparent activation of caspase-8 was evidenced. The amount of heavy metals in the intracellular compartment was estimated by ICP-MS quantitative analyses. Through a systematic proteomic investigation, 27 proteins particularly affected in their expression levels by metal exposure were identified. The majority of them resulted to be involved in apoptotic pathways, protein folding and energetic metabolism. The emerging scenario reveals that cellular protein patterns are strongly modified in response to metal exposure, leading to massive protein unfolding, ER stress, and cell death. By this integrated workflow, this study represents a contribution to the identification of potential biomarkers of heavy metal environmental pollution.
- In the chapter IV, the incorporation of selenium into selenocysteines in *Lactobacillus reuteri* Lb2 BM-DSM 16143 was reported and achieved by an integrated ICP-MS based approach. The ability of *L. reuteri* Lb2 BM-DSM 16143 to recover selenium from the medium during growth was demonstrated. Moreover was observed by liquid chromatography fractionation and ICP-MS detection, that about half of internalized selenium was covalently incorporated into proteins. Proteomic analysis, performed by 2D-LA-ICPMS, has revealed that all the selenium present in the proteins was incorporated as selenocysteine (SeCys). Obtained results confirm the possibility to use *Lactobacillus reuteri* as a valid alternative to Se-rich yeast, as food supplement in Se-deficient subjects.

Publications

P1: B. Apicella, M. Alfè, A. Amoresano, E. Galano, A. Ciajolo: “Advantages and limitations of laser desorption/ionization mass spectrometric techniques in the chemical characterization of complex carbonaceous materials” *International Journal of Mass Spectrometry,* **2010***,* 295, 98–102.

P2: E. Fregolino,G. Fugazza, E. Galano, V. Gargiulo, P. Landini, R. Lanzetta, B. Lindner, L. Pagani, M. Parrilli, O. Holst, C. De Castro: “Complete Lipooligosaccharide Structure of the Clinical Isolate Acinetobacter baumannii, Strain SMAL” *Eur. J. Org. Chem*., **2010**, 1345–1352.

P3: Galano E., Fidani M., Baia F., Palomba L., Marino G. and Amoresano A.: ”Qualitative screening in doping control by MALDI-TOF/TOF mass spectrometry: a proof-of-evidence**”** *Journal of Pharmaceutical and Biomedical Analysis* **2012,** 71 193-197.

P4: Kaare Lund Rasmussen, Anna Lluveras Tenorio, Ilaria Bonaduce, Maria Perla Colombini, Leila Birolo, Eugenio Galano, Angela Amoresano, Greg Doudna, Andrew Bond, Vincenzo Palleschi, Giulia Lorenzetti, Stefano Legnaioli, Johannes van der Plicht, Jan Gunneweg: “The constituents of a sample of ink from a Qumran inkwell: New prospects for provenancing the ink on the Dead Sea Scrolls” *Journal of Archaeological Science* **2012**, 39, 2956-2968.

P5: Artini M., Papa R., Scoarughi GL., Galano E., Barbato G., Cafiso V., Stefani S., Pucci P., Selan L.: “Comparison of the action of different proteases on *Staphylococcus* virulence properties related to the bacterial surface” *Journal of Applied Microbiology* **2013**, 114, 266-277.

P6: Blanda Di Luccia, Nicola Manzo, Maria Vivo, Eugenio Galano, Angela Amoresano, Federico Infascelli, Alessandra police and Viola Calabrò: "An integrated proteomic and cellular approach to characterize *Aloe Arborescens* biological activities" *Phytotherapy research* **2013**, in press, DOI: 10.1002/ptr.4939

P7: Michela Gambino, Francesca Cappitelli, Cristina Cattò, Aristodemo Carpen, Pamela Principi, Lisa Ghezzi, Ilaria Bonaduce, Eugenio Galano, Pietro Pucci, Leila Birolo, Federica Villa, Fabio Forlani: “A simple and reliable methodology to detect egg white in art samples” *Journal of Biosciences,* **2013**, accepted.

P8: Eugenio Galano, Angela Arciello, Daria Maria Monti, Renata Piccoli and Angela Amoresano “A proteomic approach to investigate the effects of cadmium and lead on human primary renal cells” submitted to *Proteomics* **2013**.

P9: Eugenio Galano, Erika Mangiapane, Juliusz Bianga, Angelo Palmese, Enrica Pessione, Joanna Szpunar, Ryszard Lobinski and Angela Amoresano: “Probiotic *Lactobacillus reuteri* Lb2 BM-DSM 16143 selective incorporation of selenium into selenocysteines proved by inductively coupled plasma mass spectrometry (ICP MS) - assisted proteomics approach” submitted to *Molecular and Cellular Proteomics* **2013**.

Congress communications

Oral communications

C1: E. Galano, E. Mangiapane, E. Pessione, P. Pucci and A. Amoresano: “ICP-MS based strategies to investigate selenium-metabolizing probiotic *Lactobacillus reuteri* Lb2 BM”. MS bio-day, Naples December 2, **2011**.

C2: E. Galano, E. Mangiapane, J. Bianga, A. Palmese, E. Pessione, J. Szpunar, R. Lobinski, A. Amoresano, Metallomic strategies to investigate selenium-metabolizing probiotic Lactobacillus reuteri Lb2 BM, 7th International Franco-Spanish Workshop on Bio-Inorganic Analytical Chemistry, Gijon, Spain, July 1-3, **2012**.

Poster communications

C3: E. Galano, A. Amoresano, G. Scoarughi, A. Cellini, R. Papa, M. Artini, L. Selan P. Pucci: “Proteomic identification of surface proteins involved in *Staphylococcus aureus* USA300 adhesion and invasion impairing by Serratiopeptidase” 5th ItPA National Conference, Firenze June 9-12. **2010**

C4: E. Mangiapane, E. Galano, C. Lamberti, A. Pessione, A. Amoresano, P. Pucci, E. Pessione: “A combined ICP-MS and classical proteomic approach to analyze selenium up-take by a probiotic *Lactobacillus reuteri*”. 6th ItPA National Conference, Turin June 21-24, **2011**.

C5: E. Mangiapane, C. Lamberti, E.Galano, A. Pessione, C. Giunta, A. Amoresano, E.Pessione: “Physiological changes induced by selenium in a probiotic *Lactobacillus reuteri* strain: a proteomic study”. Federation of European Biochemical Societies, Turin June 25-28, **2011**.

C6: Mangiapane E., Galano E., Lamberti C., Pessione A, Korhonen T., Pessione E: “Combined proteomics and ICP-MS to elucidate Selenium uptake and metabolism in a probiotic Lactobacillus reuteri”. 2nd International Symposium “Microbes for health”, Paris, France, December 1-2, **2011**.

C7: Blanda Di Luccia, Nicola Manzo, Maria Vivo, Eugenio Galano, Angela Amoresano, Federico Infascelli, Alessandra police and Viola Calabrò: "Approccio cellulare e proteomico per caratterizzare le attività biologiche dell’Aloe arborescens". Aloe day - Giornata di studio - Tor San Lorenzo, Ardea (RM), 22 settembre **2012**.

C8: C. Giunta Carlo, E. Mangiapane, E. Galano, A. Palmese, A. Pessione, A. Amoresano, E. Pessione: ”Nutraceutical and antioxidant potential of LAB: biochemical and proteomic methods to elucidate the Se-fixing pathway”. 56th National Meeting of the Italian Society of Biochemistry and Molecular Biology, Chieti, September 26-29, Italy, **2012**.

Visiting Appointment

May-August 2012
Prof. Lobinski’s laboratory. Bio-inorganic Analytical and Environmental Chemistry (LCABIE), UMR5254, Université de Pau et des Pays de l'Adour – CNRS, 2, Av. Président Angot FR-64053 Pau, France.

Ringraziamenti

Quando arriva il momento di scrivere questa pagina significa che un passo importante è stato fatto, e il citare qualcuno in queste righe significa che non lo si è fatto da soli.
Il primo ringraziamento però voglio tenerlo tutto per me, perché sono molto orgoglioso di tutto quello che ho fatto in questi ultimi tre anni.
Desidero ringraziare la dott.ssa Angela Amoresano perché per prima ha creduto in me, dandomi completa fiducia e riponendo stima nei miei riguardi.
Ringrazio il prof. Gennaro Marino che mi ha indirizzato, con coinvolgente entusiasmo, verso questo affascinante progetto di dottorato.
Ringrazio il prof. Giovanni Sannia, e non solo in qualità di coordinatore, ma soprattutto perché è sempre stato disponibile e prodigo di consigli.
Ringrazio il prof. Piero Pucci per il supporto tecnico-scientifico che mi ha messo a disposizione.
Ringrazio il gruppo di ricerca della prof.ssa Renata Piccoli, per la preziosa collaborazione.
Ringrazio il prof. Lobinski e tutti i ragazzi del LCABIE di Pau, in modo particolare il dott. Juliusz Bianga, per la fantastica esperienza trascorsa da loro.
Ringrazio il gruppo di ricerca della prof.ssa Pessione, soprattutto i dott. Erika Mangiapane e Alessandro Pessione, che oltre ad essere validi colleghi, sono prima di tutto grandi amici.
A tutti i colleghi e gli studenti passati e presenti va un caloroso ringraziamento, perché da tutti, direttamente o indirettamente, ho appreso qualcosa.
Estendo i ringraziamenti a tutti i ragazzi del gruppo BMA che ho conosciuto in questi anni, per aver reso più piacevole gli anni trascorsi, rendendo più leggero il peso della “cultura”.
Ringrazio la mia famiglia, mio padre, mia madre e i miei fratelli, perché anche se lontani mi hanno sempre fatto sentire la loro vicinanza.
Infine, a testimonianza del detto che “il dottorato ti cambia la vita”, desidero ringraziare mia moglie che da quasi due anni mi supporta e sopporta costantemente!

Grazie di cuore a tutti,
Eugenio.

International Journal of Mass Spectrometry 295 (2010) 98–102

Contents lists available at ScienceDirect

International Journal of Mass Spectrometry

journal homepage: www.elsevier.com/locate/ijms

Short communication

Advantages and limitations of laser desorption/ionization mass spectrometric techniques in the chemical characterization of complex carbonaceous materials

B. Apicella[a,*], M. Alfè[a], A. Amoresano[b], E. Galano[b], A. Ciajolo[a]

[a] Istituto di Ricerche sulla Combustione – C.N.R., Napoli, Italy
[b] Dipartimento di Chimica Organica – Università Federico II, Napoli, Italy

ARTICLE INFO

Article history:
Received 14 April 2010
Received in revised form 21 June 2010
Accepted 21 June 2010
Available online 26 June 2010

Keywords:
Mass spectrometry
Time of flight
Combustion
Carbonaceous samples

ABSTRACT

Laser desorption/ionization techniques coupled with mass spectrometry analyzers have evolved rapidly in the recent years and are currently capable of providing valuable information about the chemical composition and structure of very high molecular weight species, mainly biopolymers or synthetic polymers.

In view of this rapidly increasing interest a thorough understanding of the desorption/ionization process is not only of scientific interest, but also important for a correct spectra interpretation and for further improvements of the technique.

In the present paper, the effect of main experimental parameters on mass range detectable by laser desorption/ionization techniques has been investigated for standard aromatic molecules, like polycyclic aromatic hydrocarbons (PAH), fullerenes, polyacenaphthylene (PACE) and for complex carbonaceous materials like heavy fractions of fuel oils and combustion-formed particulate. In particular, it has been shown that laser power (or more specifically, the surface power density of the laser spot, named laser fluence) as well as the surface concentration of samples are crucial parameters controlling the highest detected molecular weight range. However, neither of these parameters is easily well-controlled and therefore more work is necessary for the standardization of laser/desorption techniques in the analysis of complex samples.

1. Introduction

Laser desorption/ionization (LDI) techniques were firstly developed in the early seventies [1] but only in the late eighties [2,3], with the introduction of matrix-assisted laser desorption/ionization (MALDI), they became an established method for the mass spectrometry of macromolecular compounds. The role of matrix is to absorb UV laser radiation and to give the energy to the analyte, often not absorbing in UV region, for ionizing it in a softer way. However, many polycondensed systems, especially with aromatic moieties and, therefore, strong UV absorption, have the so-called "been self-matrix" property [4,5] that means the capability of the sample (or a part of it) to act as matrix by itself. In this case, their direct photoionization takes place by laser irradiation without the necessity of an external matrix addition.

The physicochemical nature of the desorption/ionization process is still not fully understood as several parameters have a strong influence on it, such as, for example, the laser wavelength and pulse width, the laser fluence and its profile on the sample, the properties of analyte, etc. However, a thorough understanding of desorption/ionization processes is crucial for exploiting the enormous potentiality of the technique in the analysis of high molecular weight and structurally complex samples.

In the present paper, the effect of the main experimental parameters on the mass range detectable by LDI techniques has been investigated for standard aromatic molecules, like polycyclic aromatic hydrocarbons (PAH), polyacenaphthylene, fullerenes and for complex carbonaceous materials like heavy fractions of fuel oils and combustion-formed particulate.

The advantages and limitations of such powerful techniques in the analysis of polydisperse and chemically heterogeneous samples have been critically examined. In particular, the spectra reported in the present study, acquired in different operative conditions, put in evidence the artifacts that can lead to a misleading interpretation of the signals obtained by LDI techniques.

Therefore, a critical evaluation of the LDI data, taking into account for the parameters used, has been suggested based on the analysis of standard molecules and extended to ill-structurally defined complex mixtures.

2. Experimental

2.1. Materials

Standard compounds: PAH mixture is from Supelco (EPA 610). Fullerenes C60 is from Sigma Aldrich. Polyacenaphthylene (Sigma

* Corresponding author.
E-mail address: apicella@irc.cnr.it (B. Apicella).

1387-3806/$ – see front matter © 2010 Elsevier B.V. All rights reserved.
doi:10.1016/j.ijms.2010.06.022

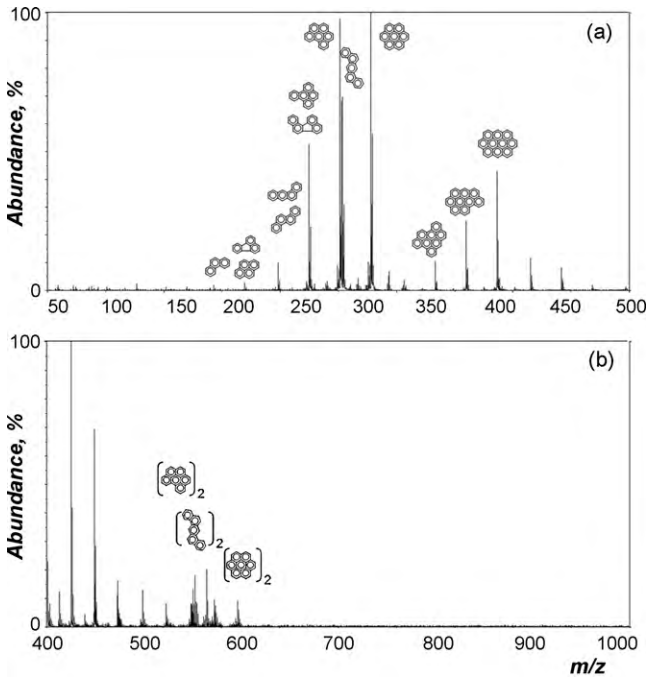

Fig. 1. Linear LDI-MS spectra of a synthetic mixture of PAH in two m/z ranges: (a) 50–500; (b) 400–1000.

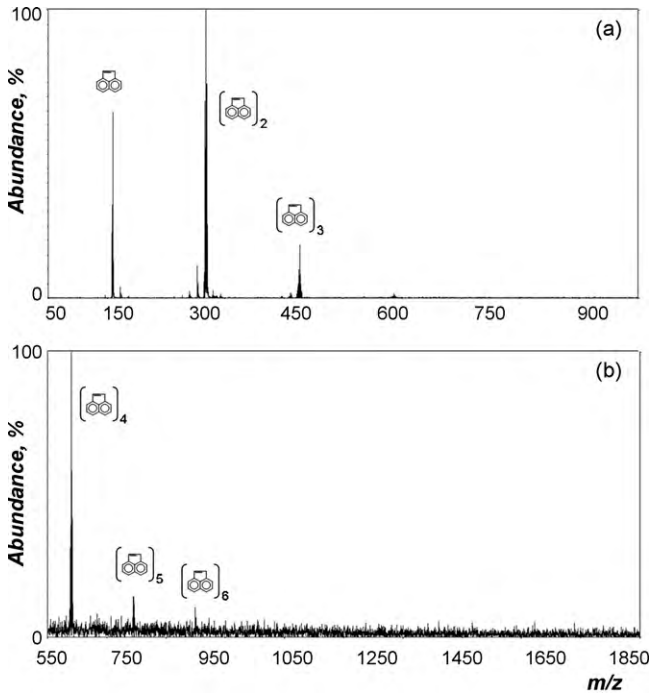

Fig. 2. Linear LDI-MS spectra of PACE in two m/z ranges: (a) 50–1000; (b) 550–1900.

Aldrich), called PACE in this work, is a yellow solid material synthesized by radical polymerization of acenaphthylene (MW 5000–10,000 u) [6].

Samples: Asphaltenes are the alkane insoluble/aromatic soluble fraction of a #6 commercial heavy fuel oil separated by ASTM (D200-75) standard procedure.

The carbonaceous particulate was sampled in a fuel-rich premixed laminar ethylene/oxygen flame (equivalence ratio $\Phi = 3.03$), produced on a commercial McKenna burner. Solid and condensed material collected on the probe walls, on the Teflon filter and in an ice-cooled trap placed in the sampling line was extracted by dichloromethane (DCM) to separate the DCM soluble organic material (named soot extract), from the insoluble solid carbonaceous material (soot). More details are reported in previous works [7,8].

2.2. Techniques

LDI-TOF-MS. Positive linear laser desorption ionization-time-of-flight mass spectrometry spectra were recorded on a Voyager DE STR Pro instrument (Applied Biosystems, Framingham, MA). The target was prepared by depositing a volume variable from 1 and 10 μl of a solution of the sample, dissolved in DCM, on the metallic sample plate. Acceleration and linear voltages set up were: target voltage 25 kV, first grid at 96% of target voltage, delayed extraction at 100–150 ns. More details are given in a previous paper [4].

AP-LDI-MS. The atmospheric pressure laser desorption ionization mass spectra were obtained with an Agilent 1100 Series MSD Trap (Agilent Technologies, Palo Alto, CA, USA). More details are given in a previous paper [9].

3. Results and discussion

The LDI-MS spectra presented in this work are collected in linear mode, in order to get the maximum possible sensitivity in the larger molecular weight range detectable, even though with lower resolution in respect to reflector mode.

The LDI-MS spectrum of a synthetic mixture of PAH from naphthalene to coronene (128–300 u) is reported in Fig. 1. The spectrum was measured using 60% of maximum laser power. In Fig. 1a, the spectrum is reported in the range m/z 50–500, covering the mass range of the mixture, extending up to 300 u, and showing some clusters in the range m/z 300–500. In Fig. 1b the spectrum is reported in a larger range, up to 1000 u, in order to put in evidence the formation of PAH clusters.

It is known that PAH readily aggregate upon desorption under favorable conditions of density and laser power and that the intensity and size of clusters detected increase with the number of fused rings [10]. However, in Fig. 1 it is possible to easily distinguish above 300 u, peaks with gaps among them at 12, 24 and 26 u, ascribable to the growth of PAH for an insertion of a CH_2 bridge followed by hydrogen elimination (12 u gap) and a net sequential addition of C_2 as an ethylene bridge (24 u gap) eventually followed by isomerization (mass increment of 26 units) [4]. The presence of dimer, trimer and bigger homologs of PAH present in the mixture is visible only in the high MW range (552, 556 and 600 u dimers of 276, 278 and 300 u respectively). Therefore, apart from clusterization, growth reactions appear to occur in the laser plume, when high concentration (5 μl of solution on the target spot) and high laser power (60% of the maximum power) are used, as in the case of spectra in Fig. 1. Decreasing the surface concentration and/or the laser power, results in the disappearance of the higher molecular weight (MW) peaks, above 300 u. However, a further increase of concentration and laser power also causes the disappearance of the higher MW peaks, probably because the higher concentration hinders the desorption of the sample, reducing the plume ionic concentration and too high laser power causes a simultaneous cluster fragmentation, globally causing no clusters detection.

On the other hand, the presence in aromatic structures of alkane substituents reduces aggregation largely because of steric effects [10] and also favors fragmentation. To verify this effect a polymer like PACE, with two rings aromatic systems linked among them by aliphatic bridges, presented a strong fragmentation, at the same laser power conditions used for the PAH mixture (60% of the maximum power). Thus, it was not possible to obtain a signal corresponding to its average MW (about 8000 u). In Fig. 2 the LDI spectrum of PACE in linear configuration is reported in two ranges:

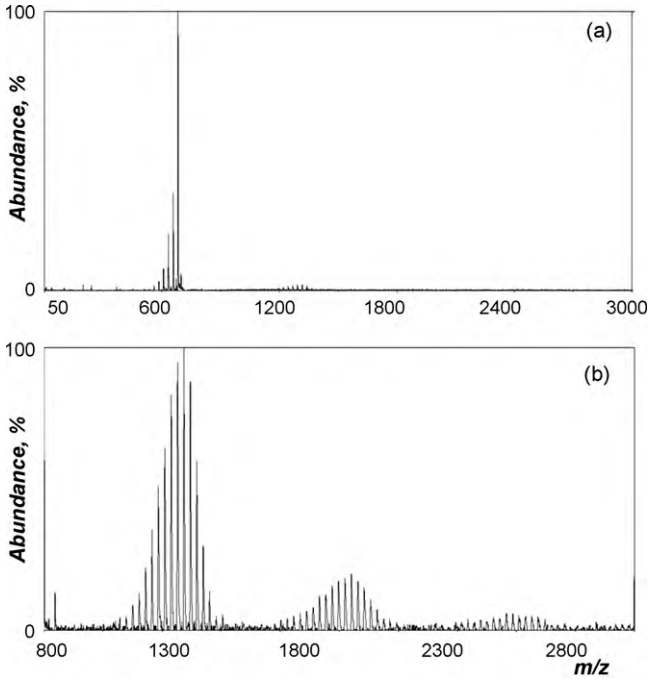

Fig. 3. Linear LDI-MS spectrum of fullerene in the m/z range 50–3000 (a) and its zoom (b).

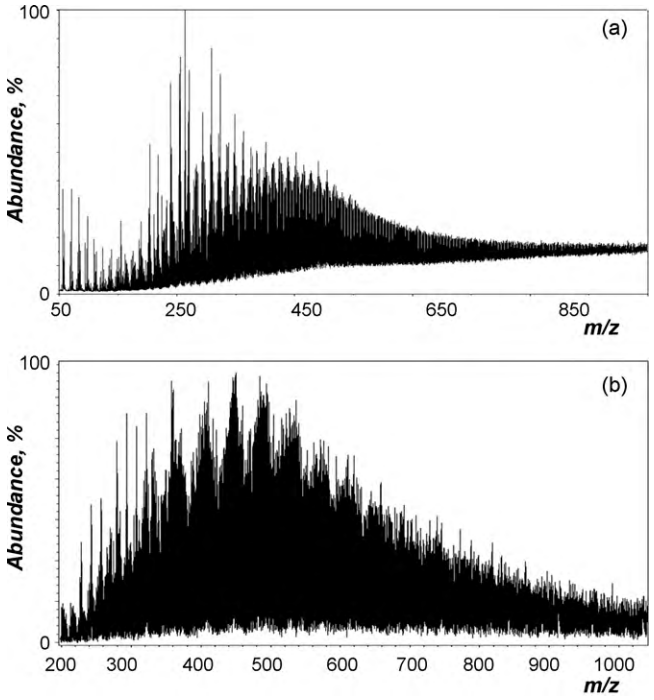

Fig. 4. Spectra of asphaltenes acquired by LDI-MS (a) and AP-LDI-MS (b).

m/z 50–1000 (Fig. 2a) and m/z 550–1900 (Fig. 2b). Peaks between 152 and 911 u with gaps at 152, which is the mass of the monomer (acenaphthylene) can be observed whereas no other signals beyond 2000 u was detected (not reported here).

In the case of fullerene, whose spectrum is reported in Fig. 3, parent peak at 720 u, with the typical isotopic pattern dominates the spectrum (Fig. 3a) whereas no fragmentation is observed with the same laser fluence (60% of maximum laser power) with respect to those used for the previous spectra. Fullerene clusters in the range m/z 1000–3000 are observed in Fig. 3b, with gaps of 600 u, corresponding to C_{50}.

In order to investigate the potentiality of LDI technique, also a much more complex carbonaceous sample, constituted of mixed aromatic/aliphatic moieties, as fuel oil asphaltenes, has been analyzed and the relative spectrum reported in Fig. 4.

The real molecular weight distribution of asphaltenes from fuel oils, coal or petroleum, is a widely debated subject. Briefly, mass spectrometric measurements with electrospray, chemical and field desorption ionization, along with florescence-based diffusion measurements and electron microscopy experiments that relate molecular size to molecular weight, suggest an average MW in the range 100–1000 u [11,12]. On the other hand, fast atom bombardment and plasma desorption mass spectrometry show a pronounced tail extending at times beyond 10,000 u, and size exclusion chromatography (SEC) gives a bimodal distribution containing an intense peak at $>10^6$ u, even though it can be overestimated due to steric effects [13,14]. Also by using LDI-MS, different groups have reported mean MW spanning 2 orders of magnitude for similar LDI setups and asphaltenes samples. However, recently, Pomerantz et al. [15] obtained data by using L^2MS–MS (two colors laser desorption MS) supporting the hypothesis that LDI asphaltene mass spectra peaking at >1000 u result from aggregation in the LDI plasma plume.

The asphaltene spectrum measured in the present work, reported in Fig. 4a, presents a mass distribution extending up to about 1000 u with a maximum around 400 u. This is in agreement with spectra reported by Traldi and co-workers [16], showing no clustering phenomena and MW distribution shifted at lower weight for asphaltenes from young fuel oils with respect to asphaltenes from aged heavy fuel oil, coal and petroleum. The low resolution obtained also in Reflectron conditions in early work [17] is strongly related to the complexity of the sample under examination. It is reasonably due to the high number of ionic components generated by laser irradiation; when present in high density, these ionic species are responsible for space charge phenomena, which lead to an enlargement of the kinetic energy distribution and the consequent peak broadening. The optimization of LDI setups has increased the quality of the spectra, but an apparent noise is still present, largely due to the partial resolution of peaks at every nominal mass in the complex mixture. Moreover, in the present work it is confirmed by using linear configuration what reported in a previous work [17]: asphaltene structure is so labile that can be subjected to fragmentation during ionization desorption, as the same samples, analyzed by atmospheric pressure photoionization mass spectrometry, APPI-MS, presented a MW distribution shifted at higher masses, with a maximum around 600 u. Alternatively, asphaltenes contain species not ionizable by laser in UV range, but easily ionizable by photoionization.

Repeating the LDI analysis by using AP-LDI/MS, a spectrum very similar to that obtained under vacuum is obtained (Fig. 4b).

In the ion source of this system the ions are produced at normal atmospheric pressure differently from the conventional MALDI/LDI ion source where ions are formed inside the vacuum system of the mass spectrometer. The AP-LDI-MS demonstrated large tolerance to the laser fluence variations and minimal fragmentation of molecular ions due to fast thermalization of the ion internal energy at atmospheric conditions. Therefore, the probable fragmentation presented by asphaltenes also in this softer condition, never underlined in the previous works in literature, suggests caution in using LDI techniques in the asphaltene analysis.

The LDI-MS spectrum of a combustion-formed soot extract sample dissolved in DCM is reported, in different m/z ranges, in Fig. 5, by using similar laser power with respect to the previous spectra (60% of the maximum power).

In Fig. 5a it is possible to observe the typical PAH trends with gaps at 12 and 24–26 u [4]. However, in Fig. 5b and its inset it is

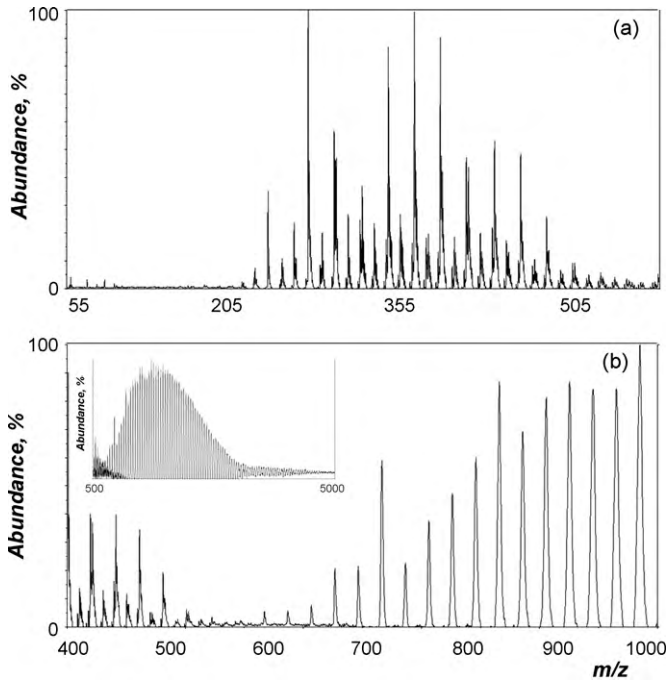

Fig. 5. Linear LDI-MS spectra of soot extract in three different m/z ranges: (a) 50–600; (b) 400–1000; (inset of figure b 500–5000).

observable that after 600 u the gap at 12 u largely decreases up to a complete disappearance, leaving place to only one sequence spaced at 24–26 u, extending up to about 3000 u. The mass difference in the detected peaks of only 24 u gap and their presence only in spectra acquired in linear configuration (for spectra of similar samples in reflectron mode see Refs. [4,17]) could give rise to the suspicion that they do not represent real ionic species, but originate by a clustering into the plume. Indeed, the high laser power used in low vacuum LDI conditions could induce clusterization of large PAH from the samples. However, the 24 u structure does not disappear even in different linear LDI setups. In particular, decreasing the delay time between the ionization and the extraction do not affect the high mass peak intensity.

Moreover, the high mass sequence is much more evident if lower sample concentration is used, in contrast with the clustering occurrence favored in higher concentration conditions.

Similar structures have been found in recent works [5,18] in asphaltene spectra, but only when the parent oil was aged and therefore, when the graphitic structure of asphaltenes was larger. In those papers, the clustering occurrence was ruled out as the spectra were acquired with different instruments with very different setups and 24 μm gaps were always present, but only in samples with extended graphitic moieties.

Soot extract samples have been analyzed also by AP-LDI-MS, after fractionation by SEC for improving sensitivity of ion trap MS, and the spectra were reported in a previous work [9].

The AP-LDI-MS spectra of the heaviest MW fractions separated by SEC (600–2000 u and 600–5000 u fraction) showed a very different pattern with respect to those reported in Fig. 5, appearing as a continuous spectrum of masses typical of polymeric structures, with gaps at 14 and 16 u.

These interesting features can be interpreted with a very intriguing hypothesis.

Two classes of species are present in soot extract and probably constitute soot precursors: the former has mainly aromatic moieties, extending up to about 3500 u (about 2 nm), with structure progressively becoming tridimensional for the insertion of pentagons that are located in the PAH periphery at the beginning (and therefore two PAH sequences are present, one attributable to even PAH and the other to odd-PAH [4]) and afterwards migrate inside the PAH skeleton [19], generating a curvature which brings the net back on itself to form a spheroidal shell which, in turn, can close to form a spherical soot particle; the second class has a polymeric structure with small aromatic moieties linked by aliphatic bridges and probably extends up to nanometric dimensions, but in AP-LDI spectra is observable just up to 1000 u, due to fragmentation occurring at high MW when aliphatic bridges are present.

The softer LDI conditions, due to atmospheric pressure in AP-LDI-MS and very lower laser power, can favour the desorption and therefore the detection of the polymeric structure, whereas the low vacuum and higher laser fluence in LDI-MS conditions hinder the polymeric structure detection for its complete fragmentation (as for PACE, Fig. 2) and allows to detect graphitic moieties, much more difficult to desorb and fragment.

This very fascinating speculation requires deeper investigations that are already in progress.

4. Conclusions

Under appropriate experimental conditions, laser ionization can be a very efficient process, and when combined with the high ion transmission of a time of flight mass spectrometer, excellent sensitivity can be achieved [20].

However, it was noteworthy that the MW distribution can be influenced by operating parameters. In particular, laser energy and sample concentration can lead, if too high, to the production of a high density plume, inside which clustering reaction can occur, with the consequent formation of ions at high m/z values, especially when condensed aromatic structures are present.

On the other hand, if the laser fluence is too high fragmentation can occur, in particular when aliphatic moieties are present and when low vacuum LDI is used.

Therefore, a critical evaluation of the LDI data has to be carried out especially when very complex mixtures are analyzed.

Acknowledgment

The authors want to thank the MSE-CNR project on “Carbone Pulito” for the financial support.

References

[1] F.J. Vastola, R.O. Mumma, A.J. Pirone, Org. Mass Spectrom. 3 (1) (1970) 101.
[2] K. Tanaka, Y. Ido, S. Akita, Y. Yoshida, T. Yoshida, Proceedings of the Second Japan–China Joint Symposium on Mass Spectrometry (1987) 185–188.
[3] M. Karas, F. Hillenkamp, Laser desorption ionization of proteins with molecular masses exceeding 10,000 daltons, Anal. Chem. 60 (1988) 2299–2301.
[4] B. Apicella, A. Carpentieri, M. Alfè, R. Barbella, A. Tregrossi, P. Pucci, A. Ciajolo, Mass spectrometric analysis of large PAH in a fuel-rich ethylene flame, Proc. Comb Inst. 31 (1) (2007) 547–553.
[5] Rizzi, P. Cosmina, C. Flego, L. Montanari, R. Seraglia, P. Traldi, Laser desorption/ionization techniques in the characterization of high molecular weight oil fractions. Part 1. Asphaltenes, J. Mass Spectrom. 41 (2006) 1232–1237.
[6] J. Springer, J. Shmelzer, T. Zeplichal, Analytical and preparative separation of oligoacenaphthylene by gel permeation chromatography, Chromatographia 13 (3) (1980) 164–166.
[7] A. Ciajolo, A. D'Anna, R. Barbella, A. Tregrossi, The formation of aromatic carbon in sooting ethylene flames, Proc. Comb. Inst. 25 (1994) 678–685.
[8] B. Apicella, R. Barbella, A. Ciajolo, A. Tregrossi, Formation of low- and high-molecular-weight hydrocarbon species in sooting ethylene flames, Combust. Sci. Technol. 174 (2002) 309–324.
[9] M. Alfè, B. Apicella, A. Tregrossi, A. Ciajolo, Identification of large polycyclic aromatic hydrocarbons in carbon particulates formed in a fuel-rich premixed ethylene flame, Carbon 46 (2008) 2059–2066.
[10] A.R. Hortal, P. Hurtado, B.M. Martinez-Haya, O.C. Mullins, Molecular-weight distributions of coal and petroleum asphaltenes from laser desorption/ionization experiments, Energy Fuels 21 (2007) 2863–2868.
[11] H. Groenzin, O.C. Mullins, Molecular size and structure of asphaltenes from various sources, Energy Fuels 14 (2000) 677–684.

[12] S. Badre, K. Goncalves, K. Norinaga, G. Gustavson, O.C. Mullins, Molecular size and weight of asphaltene and asphaltene solubility fractions from coals, crude oils and bitumen, Fuel 85 (2005) 1–11.
[13] F. Karaka, C.A. Islas, M. Millan, M. Behrouzi, T.J. Morgan, A.A. Herod, R. Kandiyoti, The calibration of size exclusion chromatography columns: molecular mass distributions of heavy hydrocarbon liquids, Energy Fuels 18 (2004) 778–788.
[14] A.A. Herod, K.D. Bartle, R. Kandiyoti, Comment on a paper by Mullins, Martinez-Haya and Marshall "Contrasting Perspective on Asphaltene Molecular weight. This Comment vs the Overview of Herod, A.A., Bartle, K.D., and Kandiyoti, R.", Energy Fuels 22 (2008) 4312–4317.
[15] A.E. Pomerantz, M.R. Hammond, A.L. Morrow, O.C. Mullins, R.N. Zare, Asphaltene molecular-mass distribution determined by two-step laser mass spectrometry, Energy Fuels 213 (2009) 1162–1168.
[16] A. Smaniotto, C. Flego, L. Montanari, G. Guglielmetti, R. Seraglia, P. Traldi, Laser desorption/ionization mass spectrometric study on asphaltenes from different heavy crude oils and products originating from their thermal treatment, Rapid Commun. Mass Spectrom. 23 (5) (2009) 725–728.
[17] B. Apicella, M. Alfè, R. Barbella, A. Tregrossi, A. Ciajolo, Mass spectrometric advances in the analysis of large aromatic fractions of heavy fuel oils and carbon particulates, Combust. Sci. Technol. 182 (4) (2010) 640–652.
[18] A. Rizzi, P. Cosmina, C. Flego, L. Montanari, A. Smaniotto, R. Seraglia, P. Traldi, Laser desorption/ionization techniques in the characterization of high-molecular-weight oil fractions. Part 2. De-asphalted oils, J. Mass Spectrom. 42 (7) (2007) 874–880.
[19] T. Scott, Fragments of fullerenes: novel syntheses, structures and reactions, Pure Appl. Chem. 68 (2) (1996) 291–300.
[20] R.J. Cotter, Time-of-flight Mass Spectrometry: Instrumentation and Applications in Biological Research, ACS, Washington, DC, 1997.

DOI: 10.1002/ejoc.200901396

Complete Lipooligosaccharide Structure of the Clinical Isolate *Acinetobacter baumannii*, Strain SMAL

Eleonora Fregolino,[a] Giulia Fugazza,[b] Eugenio Galano,[a] Valentina Gargiulo,[a] Paolo Landini,[c] Rosa Lanzetta,[a] Buko Lindner,[d] Laura Pagani,[b] Michelangelo Parrilli,[a] Otto Holst,*[e] and Cristina De Castro*[a]

Keywords: Structure elucidation / Mass spectrometry / Glycolipids / NMR spectroscopy

Acinetobacter baumannii is a pathogenic organism that posesses a serious health threat because of the occurrence of the large number of (multi)drug-resistant strains. It can persist for prolonged periods in the hospital environment, infecting debilitated or immune-compromised patients. In this context, the endotoxin portion of the lipopolysaccharide, the lipid A, plays an important role in the pathogenesis of this bacterium, because it triggers the innate immune response and contributes to the inflammation state of the patient. In this study, the complete structure of the lipooligosaccharide has been determined. The saccharide backbone of the molecule was disclosed through chemical and spectroscopic analysis, whereas the lipid A moiety required detailed MS spectrometry and chemical investigations. The oligosaccharide backbone was found to be similar to that of *A. baumannii* ATCC 19606, although the LOS from the SMAL strain presented an enhanced zwitterionic character. The lipid A moiety comprises a heterogeneous and complex mixture of molecules: it possesses a conserved diphosphorylated disaccharide backbone substituted by three to seven fatty acids. The hexaacylated species appeared as the most abundant, and its chemical features, namely the number and the types of fatty acids, indicates its potential endotoxic activity.

Introduction

Acinetobacter baumannii is a Gram-negative bacterium and is considered an important emerging pathogen in hospital-acquired infections. Its clinical significance is related to its low susceptibility to most antibiotics commonly used such that many strains are now classified as pan-drug resistant.[1]

The growing incidence of nosocomial infections has promoted a significant increase in *Acinetobacter*-related studies. The most common pathogens belong to the so-called *A. calcoaceticus–A. baumannii* complex,[2] and the diseases commonly associated with these bacterial species are urinary tract infections, meningitis and sepsis. The disease outcome depends on the site of infection and on the patient's susceptibility.

The mechanism by which *Acinetobacter* is able to express its pathogenicity has not yet been completely elucidated, but a crucial role is played by components of the cell envelope outer membrane, namely the lipopolysaccharide (LPS) and capsular polysaccharides (CPS). These molecules act in synergy by blocking the access of human complement factors to the bacterial cell wall, which prevents bacterial killing and lysis.[3]

In this context, the establishment of the CPS and LPS structures is of importance for understanding the physical assemblage of the outer membrane and its properties, for example, adhesion to surfaces (i.e., hospital furniture or human skin), permeability to hazardous compounds (e.g., detergents used to clean surfaces) and the endotoxic power resident in the lipid A (LA) moiety of the LPS or lipooligosaccharide (LOS), which is able to activate the innate immune system[4] and may result in septic shock with an often fatal outcome of such bacterial infection.

Lipid A represents the endotoxic centre of the LPS or LOS; however, its endotoxicity is strongly dependent on its structure. It comprises a family of molecules that possess an amino sugar disaccharide as the backbone, which in most cases is β-D-GlcpN-(1→6)-α-D-GlcpN. The first glu-

[a] Department of Organic Chemistry and Biochemistry, University of Napoli Federico II – Complesso Universitario Monte Sant'Angelo,
Via Cinthia 4, 80126 Napoli, Italy
Fax: +39-081-674124
E-mail: decastro@unina.it
[b] Dipartimento di Scienze Morfologiche, Eidologiche e Cliniche, Università di Pavia,
Via Brambilla 74, 27100 Pavia, Italy
[c] Dipartimento di Scienze Biomolecolari e Biotecnologiche, Università di Milano,
Via Caloria 26, 20133 Milano, Italy
[d] Division of Immunochemistry, Research Center Borstel, Leibniz Center for Medicine and Biosciences,
23845 Borstel, Germany
[e] Division of Structural Biochemistry, Research Center Borstel, Leibniz Center for Medicine and Biosciences,
23845 Borstel, Germany
Fax: +49-4537-188-745
E-mail: oholst@fz-borstel.de

Supporting information for this article is available on the WWW under http://dx.doi.org/10.1002/ejoc.200901396.

cosamine is named GlcN-II or the non-reducing unit of the backbone, and the second is the GlcN-I or the reducing moiety. This oligosaccharide is substituted with fatty acids (mostly between 10 and 18 carbon atoms) and further decorated with two phosphate groups, one at O-1 of GlcN-I and the second at O-4 of GlcN-II. Usually, the heterogeneity of the LA is largely due to the fatty acid substituents, the number and length of which may vary, giving rise to penta-, hexa- or heptaacylated species. All these species are present in many LA preparations; however, their relative proportions are characteristic of specific bacterial species and are modulated by environmental stimuli.

The endotoxicity of differently acylated LA molecules depends on the presence of phosphate groups and the number and size of the fatty acids. Thus, a diphosphorylated and hexaacylated species, as is present in, for example, *Escherichia coli* LPS, acts highly agonistically, whereas less acylated species are less efficient or act even as antagonists.[5]

In this work, the complete structure of the lipooligosaccharide from the *A. baumannii* strain SMAL was investigated to gain valuable information that will provide an understanding of the mechanisms of activity adopted by this successful emerging pathogen.

Results and Discussion

LOS Chemical Analysis

Freeze-dried bacterial cells were extracted with phenol/chloroform/light petroleum (PCP).[6] The LOS was found to be composed of D-glucose (Glc), 2-amino-2-deoxy-D-glucosamine (GlcN), 2-amino-2-deoxy-D-galactosamine (GalN), 3-deoxy-*manno*-oct-2-ulosonic acid (Kdo) and 2-amino-2-deoxy-glucuronic acid (GlcNA).

The fatty acids were analysed by GC/MS as the methyl ester derivatives. The combined information concerning the total and *O*-linked composition identified the following ester-linked fatty acids: dodecanoic (12:0), 2-hydroxydodecanoic [12:0(2-OH)] and 3-hydroxydodecanoic [12:0(3-OH)] acid. 3-Hydroxytetradecanoic acid [14:0(3-OH)] is amide-linked. The 3-hydroxy fatty acids are (*R*)-configured and the 2-hydroxy fatty acids are (*S*)-configured.[7]

NMR Analysis of Core Oligosaccharides 2 and 3

The primary structure of the entire core oligosaccharide **1** (Figure 1) was deduced by combining the NMR spectroscopic data of the products isolated by alkaline degradation and acid hydrolysis. The first approach provided the structure of the incomplete core oligosaccharide **2** (Figure 1). Information regarding the unit(s) lost during the alkaline treatment was recovered by analysing the product **3** (Figure 1) obtained by mild acid hydrolysis.

The product isolated after strong alkaline degradation provided the truncated core oligosaccharide (**2**, Figure 1) comprising the lipid A sugar backbone and a 2-amino-2-deoxyuronic acid derivative possessing a double bond conjugated to the carboxy group (ΔHexNA), which results from β-elimination of the 4-substituted GlcNA.

The ^{1}H NMR spectrum of **2** (Figure 2a) contains eight anomeric signals and three sets of diastereotopic methylene signals due to the presence of three Kdo residues. A detailed analysis of both the homo- and heteronuclear NMR spectra (see Table 1 in the Supporting Information) of **2** led to the complete assignment of its proton and carbon chemical shifts, which revealed its structure (**2**, in Figure 1). Because the substituent at O-4 of ΔHexNA was lost during the alkaline treatment of the LPS, the product obtained from mild acid hydrolysis (**3**, Figure 1) was analysed by

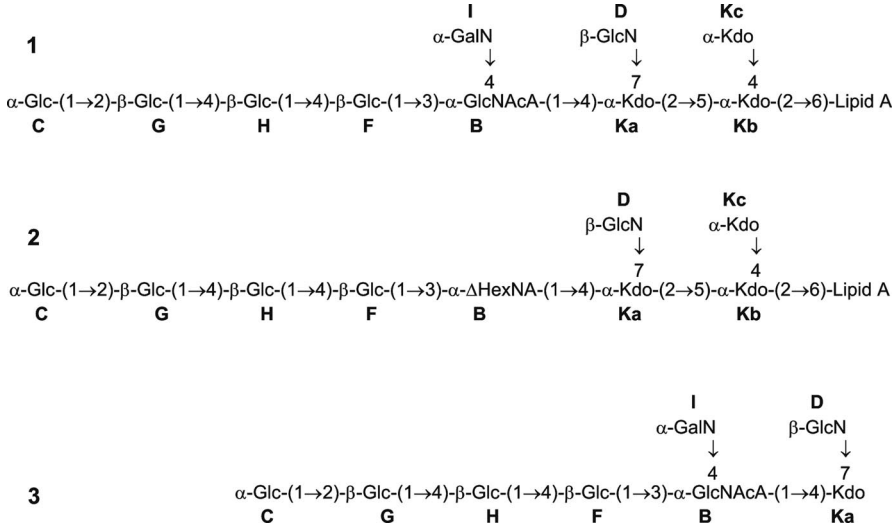

Figure 1. **1**: Complete structure of the oligosaccharide backbone of the LOS from *Acinetobacter baumannii* SMAL. All sugars are D-configured. **2**: Product isolated after complete LOS delipidation. ΔHexNA is a hex-4-en-2-aminuronic residue that results from β-elimination, the two glucosamines of the lipid A backbone are labelled **E** (non-reducing or GlcN-II) and **A** (reducing unit or GlcN-I). **3**: Oligosaccharide structure obtained from LOS after mild acid hydrolysis. The complete lipid A structure is reported in Figure 4.

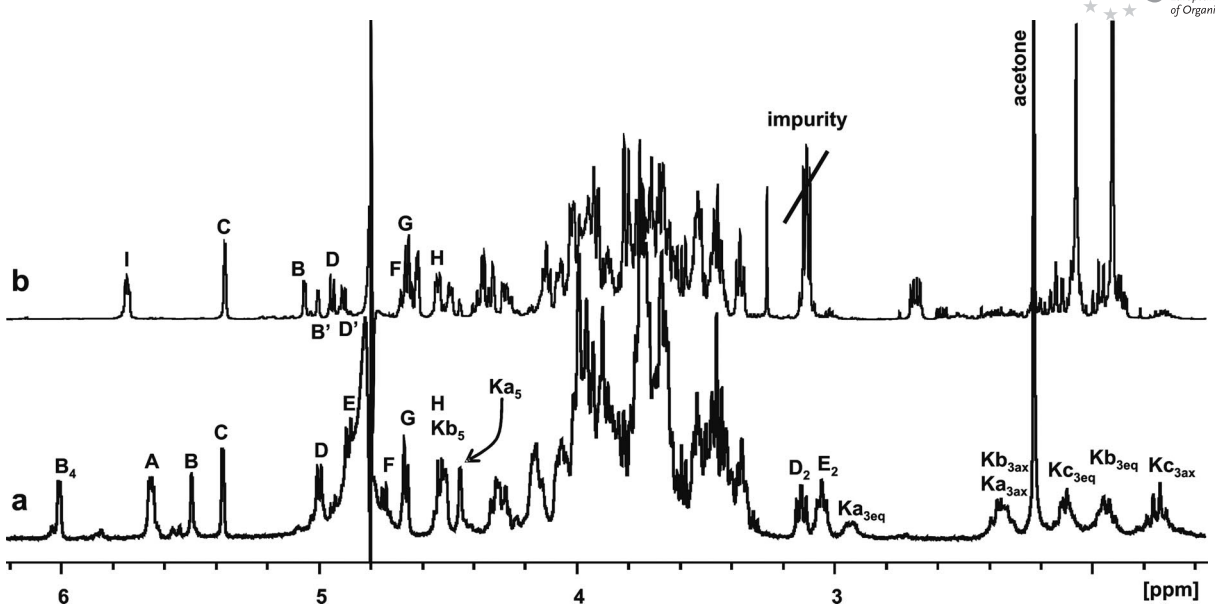

Figure 2. (a) ^{1}H NMR spectrum (500 MHz, 296 K, D_2O) of oligosaccharide **2** derived from the total delipidation of *A. baumannii* LOS. (b) ^{1}H NMR spectrum (600 MHz, 300 K, D_2O) of oligosaccharide **3** derived from LOS after mild acid hydrolysis. Residues **A** and **E** are the nonreducing and reducing glucosamines of lipid A, respectively. The residues close to the free reducing end of the oligosaccharide give rise to different signals in the spectrum, like **B** and **B′**, because their magnetic environment is affected by the different ring forms of the reducing Kdo residue. In both spectra, signals are labelled in accord with Figure 1.

NMR spectroscopy, which revealed an additional monosaccharide residue, unit **I** (Figure 2b, NMR spectroscopic data in Table 2 of the Supporting Information), but lacked the lipid A moiety (residues **A** and **E**) and the two Kdo units (**Kb** and **Kc**) as expected.

Combining the information from both **2** and **3**, the complete structure of the core oligosaccharide was determined as oligosaccharide **1** (Figure 1). Surprisingly, this structure is equivalent to that previously described for *A. baumannii* strain ATCC 19606.[8]

Electrospray Ionization Fourier-Transform Ion Cyclotron Resonance Mass Spectrometry (ESI-FT-ICR MS) Analysis of Intact and Ammonia-Deacylated Lipid A

The charge-deconvoluted mass spectrum obtained in the negative ion mode of the intact LA (Figure 3) comprises five groups of molecular peaks that originate from the intrinsic heterogeneity caused by the type and number of fatty acids linked to the disaccharide backbone. Each set of signals is labelled with a letter and, within each set, the different peaks are distinguished by numbers. Accordingly, group **a** is composed of a heptaacylated species, **b** of a hexaacylated, **c** of a pentaacylated, **d** of a tetraacylated and **e** of a triacylated species (Table 1).

In particular, the composition of the predominant species $\mathbf{b_1}$ (Table 1, Figure 4) is consistent with the occurrence of two 14:0(3-OH), two 12:0(3-OH), one 12:0(2-OH), one 12:0 and two phosphate units, $\mathbf{b_2}$ is related to $\mathbf{b_1}$ but 12:0(2-OH) is replaced by 12:0, $\mathbf{b_3}$ differs from $\mathbf{b_1}$ by the replacement of 14:0(3-OH) with 12:0(3-OH), and $\mathbf{b_4}$ from $\mathbf{b_3}$ by the replacement of 12:0(2-OH) with 12:0.

The presence of one 12:0(2-OH), as identified in the chemical analysis, was confirmed by the difference of 16 u between different couples of molecular peaks, for example, $\mathbf{b_1} - \mathbf{b_2}$ or $\mathbf{b_3} - \mathbf{b_4}$. This difference indicates the replacement of the 12:0(2-OH) unit by one 12:0, a substitution that is only possible for secondary and not primary fatty acids, which are always hydroxylated at C-3.

The species $\mathbf{b_5}$ to $\mathbf{b_7}$ have the same lipid composition as shown for $\mathbf{b_1}$, $\mathbf{b_2}$, $\mathbf{b_4}$, respectively, except that one phosphate group is missing.

A similar pattern was identified for almost all the other peak clusters, although some peaks were missing, probably due to their low abundance. Considering $\mathbf{b_1}$ as a reference, the homologous species in the other clusters were identified as follows (Figure 4): $\mathbf{a_1}$ contains one additional 12:0, $\mathbf{c_1}$ is missing one 12:0(3-OH), $\mathbf{d_1}$ lacks one 12:0(3-OH) and one 12:0, and $\mathbf{e_1}$ has two 14:0(3-OH) and one 12:0(2-OH) fatty acid residues. The occurrence of 12:0(2-OH) in every cluster is indicated by the presence of peaks differing by 16 u, as discussed above. Therefore, considering the composition of $\mathbf{b_1}$, the location of the four primary fatty acids was straightforward: the two amide-linked 14:0(3-OH) units are amide-linked, whereas the other two 3-hydroxy-bearing fatty acids are ester-bound substituents at O-3 of each glucosamine residue (Figure 4). The location of the two secondary fatty acids was inferred by analysis of the infrared multiphoton dissociation MS/MS data recorded in the positive ion mode or the molecular ions complexed with triethylamine.[9]

Under such conditions, $[\mathbf{b_1} + TEA]^+$ at m/z = 1830.4 u produced an abundant oxonium fragment ion at m/z = 1046.8 u (structure shown in Figure 4), representative of the nonreducing glucosamine moiety of LA with its substitu-

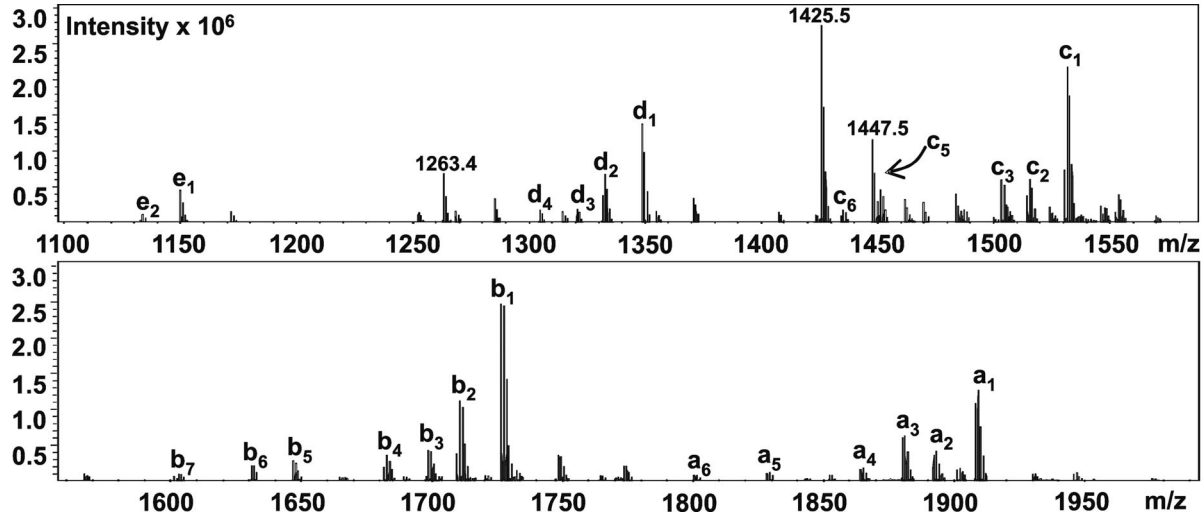

Figure 3. Pseudomolecular peaks of the *Acinetobacter baumannii* strain SMAL lipid A family measured by negative ion ESI-FT-ICR MS (structures are presented in Figure 4). The peaks at *m/z* = 1447.5, 1425.5 and 1263.4 and other minor peaks are impurities not related to lipid A.

Table 1. Lipid A species identified by ESI-FT-ICR MS (spectrum in Figure 3, structures in Figure 4) in *Acinetobacter baumannii* strain SMAL. The two glucosmine units have been omitted.

Mass [Da]	Rel. int. [%]	Species	No. of acyl groups	Proposed composition
1911.3	51.8	$\mathbf{a_1}$	7	2×14:0(3-OH), 2×12:0(3-OH), 12:0(2-OH), 2×12:0, 2×P
1895.3	17.0	$\mathbf{a_2}$	7	2×14:0(3-OH), 2×12:0(3-OH), 3×12:0, 2×P
1883.3	28.0	$\mathbf{a_3}$	7	14:0(3-OH), 3×12:0(3-OH), 12:0(2-OH), 2×12:0, 2×P
1867.3	8.0	$\mathbf{a_4}$	7	14:0(3-OH), 3×12:0(3-OH), 3×12:0, 2×P
1831.3	4.8	$\mathbf{a_5}$	7	2×14:0(3-OH), 2×12:0(3-OH), 12:0(2-OH), 2×12:0, P
1803.3	3.2	$\mathbf{a_6}$	7	14:0(3-OH), 3×12:0(3-OH), 12:0(2-OH), 2×12:0, P
1729.1	100	$\mathbf{b_1}$	6	2×14:0(3-OH), 2×12:0(3-OH), 12:0(2-OH), 12:0, 2×P
1713.1	46.2	$\mathbf{b_2}$	6	2×14:0(3-OH), 2×12:0(3-OH), 2×12:0, 2×P
1700.1	17.5	$\mathbf{b_3}$	6	14:0(3-OH), 3×12:0(3-OH), 12:0(2-OH), 12:0, 2×P
1685.1	14.3	$\mathbf{b_4}$	6	14:0(3-OH), 3×12:0(3-OH), 2×12:0, 2×P
1649.2	11.4	$\mathbf{b_5}$	6	2×14:0(3-OH), 2×12:0(3-OH), 12:0(2-OH), 12:0, P
1633.2	8.5	$\mathbf{b_6}$	6	2×14:0(3-OH), 2×12:0(3-OH), 2×12:0, P
1605.1	3.6	$\mathbf{b_7}$	6	14:0(3-OH), 3×12:0(3-OH), 2×12:0, P
1531.0	86.9	$\mathbf{c_1}$	5	2×14:0(3-OH), 12:0(3-OH), 12:0(2-OH), 12:0, 2×P
1515.0	24.6	$\mathbf{c_2}$	5	2×14:0(3-OH), 12:0(3-OH), 2×12:0, 2×P
1502.9	24.1	$\mathbf{c_3}$	5	14:0(3-OH), 2×12:0(3-OH), 12:0(2-OH), 1×12:0, 2×P
1485.9	7.2	$\mathbf{c_4}$	5	14:0(3-OH), 2×12:0(3-OH), 2×12:0, 2×P
1451.0	18.3	$\mathbf{c_5}$	5	2×14:0(3-OH), 12:0(3-OH), 1×12:0(2-OH), 12:0, P
1435.0	7.0	$\mathbf{c_6}$	5	2×14:0(3-OH), 12:0(3-OH), 2×12:0, P
1347.8	55.8	$\mathbf{d_1}$	4	2×14:0(3-OH), 12:0(3-OH), 12:0(2-OH), 2×P
1332.8	15.5	$\mathbf{d_2}$	4	2×14:0(3-OH), 12:0(3-OH), 12:0, 2×P
1320.8	7.5	$\mathbf{d_3}$	4	14:0(3-OH), 2×12:0(3-OH), 12:0(2-OH), 2×P
1304.8	7.0	$\mathbf{d_4}$	4	14:0(3-OH), 2×12:0(3-OH), 12:0, 2×P
1150.6	18.0	$\mathbf{e_1}$	3	2×14:0(3-OH), 12:0(2-OH), 2×P
1134.6	1.2	$\mathbf{e_2}$	3	2×14:0(3-OH), 12:0, 2×P

ents, one phosphate, one 14:0(3-OH), one 12:0(2-OH), one 12:0(3-OH) and one 12:0. On the basis of this information, the two secondary fatty acids identified in $\mathbf{b_1}$ were located on the nonreducing glucosamine moiety. The same oxonium ion was observed for the $\mathbf{a_1}$ and $\mathbf{c_1}$ species. The exact positions of the ester-linked fatty acids was inferred by analysis of the ammonia-treated LA: this chemical treatment preferentially removes the ester-linked acyloxyacyl esters leaving the amide-linked ones and their acyloxy substituents.[10] Accordingly, analysis of the charge-deconvoluted ESI spectrum (Figure 5) of the ammonia-treated LA allowed the identification of the secondary fatty acids on the corresponding primary residues: it contains three different clusters, named **f**, **g** and **h**, which are consistent with tetra-, tri- and diacylated species, respectively (Table 2). The more informative clusters were **f** and **g**, whereas the diacylated species $\mathbf{h_1}$ to $\mathbf{h_3}$ were identified as side-products of the ammonia-induced removal of the secondary fatty acid located on the amide-linked acyl residue of both the **f** and **g** clusters.

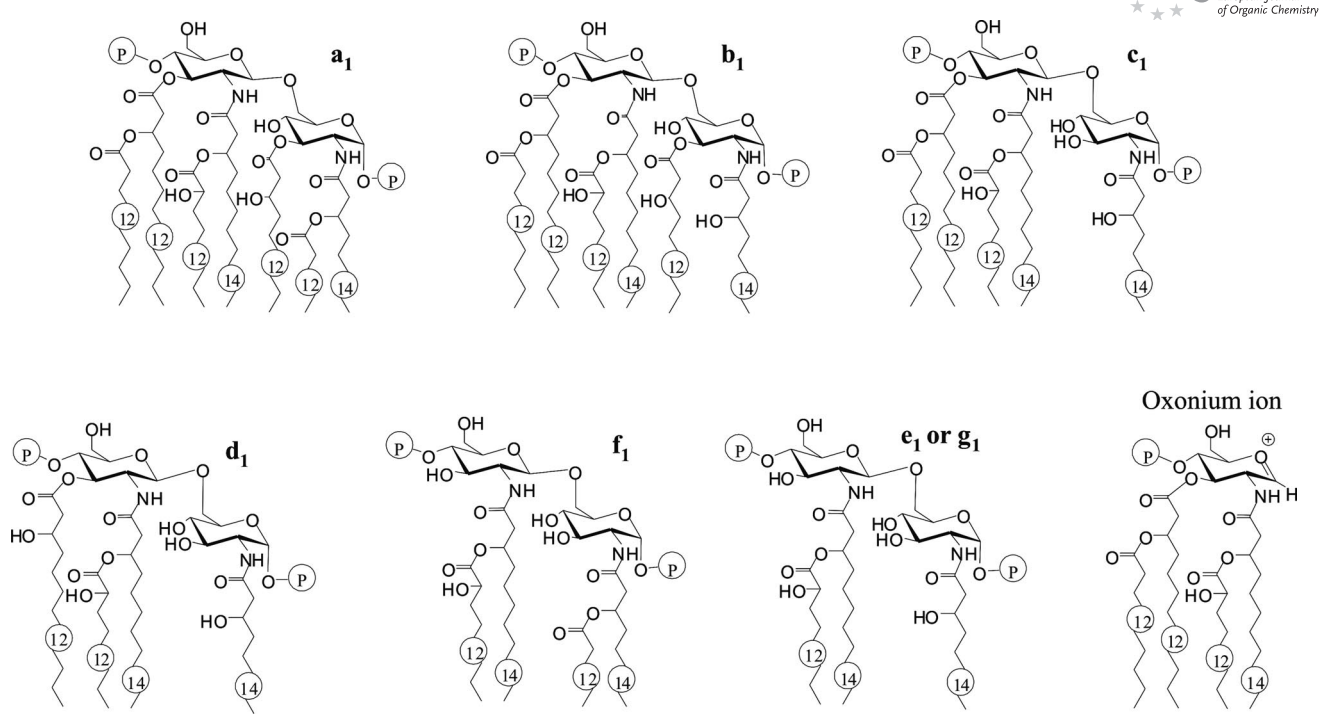

Figure 4. Structures of the lipid A molecules from *Acinetobacter baumannii* strain SMAL. Species from $\mathbf{a_1}$ to $\mathbf{e_1}$ were detected in the intact lipid A and molecules $\mathbf{f_1}$ and $\mathbf{g_1}$ were obtained from ammonia-treated lipid A. $\mathbf{a_1}$, $\mathbf{b_1}$ and $\mathbf{c_1}$ yielded the same oxonium ion.

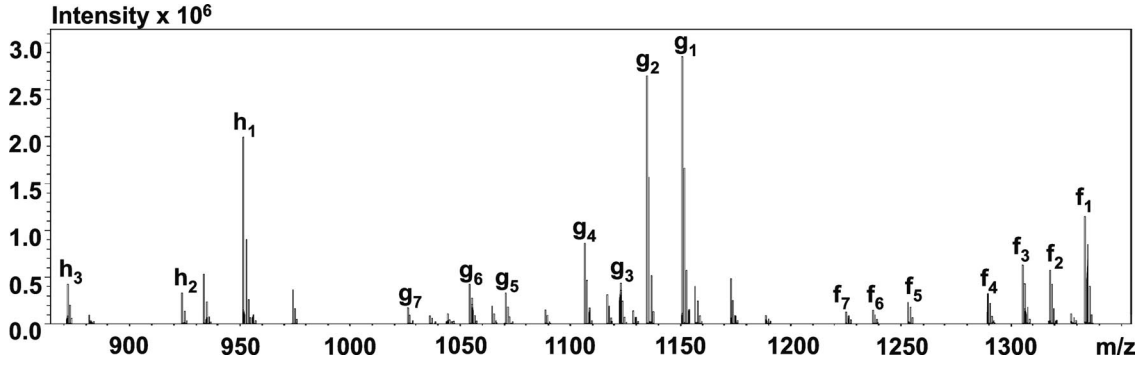

Figure 5. Pseudomolecular peaks identified in negative ion ESI-FT MS (structures shown in Figure 4) of ammonia-treated lipid A from *Acinetobacter baumannii* strain SMAL.

The predominant species, $\mathbf{g_1}$ (Figure 5, Table 2), is composed of two 14:0(3-OH), one 12:0(2-OH) and two phosphates. The distribution pattern within each cluster is similar to that of the intact LA, that is, the substitution of 12:0(2-OH) by 12:0, the replacement of one 14:0(3-OH) by one 12:0(3-OH) and the absence of one phosphate unit.

The information from the ion $\mathbf{g_1}$ was combined with the information provided by the oxonium ion (structure shown in Figure 4) deriving from $\mathbf{b_1}$ of the intact LA. According to the composition of the oxonium ion, hexaacylated species $\mathbf{b_1}$ possesses two secondary fatty acids on the nonreducing glucosamine, one 12:0(2-OH) and one 12:0. The finding that only 12:0(2-OH) was left after ammonia treatment indicates that this fatty acid is linked to the amide-linked 14:0(3-OH), whereas the other, 12:0, which was removed during the chemical treatment, is linked to 12:0(3-OH). Thus, the locations of the secondary fatty acids composing the penta-, tetra- and triacylated species in the intact LA were determined (Figure 4).

The mass distribution in cluster **f** indicates the occurrence of another tetraacylated LA with a fatty acid composition different to that described for the tetraacylated LA in the intact sample (cluster **d**), which reflects the distribution of the ester-bound acyl chains on the primary amide-linked fatty acids of the original heptaacylated LA family (cluster **a**).

From the above information the structure of the heptaacylated species was assigned. Cluster $\mathbf{f_1}$ is composed of two 14:0(3-OH), one 12:0(2-OH), one 12:0 and two phosphates. Therefore, $\mathbf{f_1}$ contains one additional 12:0 compared with $\mathbf{g_1}$: the only position available on the disaccharide backbone for 12:0 is at 14:0(3-OH) on GlcN-I, thus yielding the structures of both $\mathbf{f_1}$ and $\mathbf{a_1}$ as depicted in Figure 4.

Table 2. Molecular species of ammonia-treated lipid A from *Acinetobacter baumannii* strain SMAL identified by ESI-FT-ICR MS (spectrum shown in Figure 5, structures in Figure 4). The two glucosamine units have been omitted.

Mass [Da]	Rel. int. [%]	Species	No. of acyl groups	Proposed composition
1332.8	40.9	$\mathbf{f_1}$	4	2×14:0(3-OH), 12:0(2-OH), 12:0, 2×P
1316.8	20.1	$\mathbf{f_2}$	4	2×14:0(3-OH), 2×12:0, 2×P
1304.8	22.0	$\mathbf{f_3}$	4	14:0(3-OH), 12:0(3-OH), 12:0(2-OH), 12:0, 2×P
1288.8	11.6	$\mathbf{f_4}$	4	14:0(3-OH), 12:0(3-OH), 2×12:0, 2×P
1252.8	11.6	$\mathbf{f_5}$	4	2×14:0(3-OH), 12:0(2-OH), 12:0, P
1236.8	5.1	$\mathbf{f_6}$	4	2×14:0(3-OH), 2×12:0, P
1224.8	4.6	$\mathbf{f_7}$	4	14:0(3-OH), 12:0(3-OH), 12:0(2-OH), 12:0, P
1150.6	100	$\mathbf{g_1}$	3	2×14:0(3-OH), 12:0(2-OH), 2×P
1134.6	95.8	$\mathbf{g_2}$	3	2×14:0(3-OH), 12:0, 2×P
1122.6	15.6	$\mathbf{g_3}$	3	14:0(3-OH), 12:0(3-OH), 12:0(2-OH), 2×P
1106.6	30.1	$\mathbf{g_4}$	3	14:0(3-OH), 12:0(3-OH), 12:0, 2×P
1070.6	11.6	$\mathbf{g_5}$	3	2×14:0(3-OH), 12:0(2-OH), P
1054.7	14.8	$\mathbf{g_6}$	3	2×14:0(3-OH), 12:0, P
1026.6	6.2	$\mathbf{g_7}$	3	14:0(3-OH), 12:0(3-OH), 12:0, P
952.5	69.8	$\mathbf{h_1}$	2	2×14:0(3-OH), 2×P
934.5	18.5	$\mathbf{h_2}$	2	14:0(3-OH), 12:0(3-OH), 2×P
872.5	14.9	$\mathbf{h_3}$	2	2×14:0(3-OH), P

Conclusions

In this report the complete structure of the LOS of *Acinetobacter baumannii* strain SMAL is reported. The sequence of the core oligosaccharide was achieved through the combined use of chemical and spectroscopic procedures. The backbone is formed of 12 sugar residues, which are organized as a highly branched inner core moiety and is equivalent to one of the structures reported for *A. baumannii* ATCC 19606.[8] This region contains a motif that could be present within the *A. baumannii* LPS;[8,11] however, it is also present in the core region of LPS from *A. radioresistens*.[12]

In contrast to the core region of LPS from *A. baumannii* ATCC 19606, the galactosamine linked to GlcNAcA is not *N*-acetylated, and the core oligosaccharide is not truncated. These features might reflect the adaptation of the bacterium to the host environment, in particular, the cationic amino sugars decrease the net negative charge of the core region and thus might shield the bacterial membrane from the effect of host defence agents, like the cationic antimicrobial peptides.

Regarding the endotoxic moiety of the LOS, high-resolution ESI-FT MS revealed that lipid A is formed of a heterogeneous blend of molecules, which contain the conserved diphosphorylated glucosamine disaccharide backbone variously substituted with fatty acid residues, ranging from tri- through to heptaacylated molecules (Figure 4 and Table 1).

Each cluster comprises different species due to the non-stoichiometric replacement of (*S*)-12:0(2-OH) with 12:0, (*R*)-14:0(3-OH) with (*R*)-12:0(3-OH) or from the lack of one phosphate unit. Within *Acinetobacter*, (*S*)-12:0(2-OH) has so far only been reported for the LPS of *A. radioresistant*,[13] in which it is present in only small amounts. The finding of this fatty acid supports the putative function of two genes from *A. baumannii*, deposited in the PubMed database,[14] for which fatty acid 2-*O*-hydroxylase activity was predicted on the basis of sequence homology with other enzymes.

With regard to the fatty acid pattern, the prominent lipid A species is the hexaacylated one, similar to the agonistic endotoxin present in the LPS of *E. coli*, comprising six fatty acids with a chain length of 14 and/or 12 carbon atoms distributed asymmetrically on the glucosamine disaccharide backbone.[15]

Experimental Section

Bacterial Identification and Genotyping: The *Acinetobacter baumannii* SMAL strain was a multidrug-resistant (MDR) clinical isolate representative of a clonal lineage causing nosocomial infections, including sepsis, in different Italian settings and recovered since 2002. The isolate was identified by using the Vitek 2® automated instrument ID system (BioMérieux, Marcy l'Etoile, France) and sequencing of the blaOXA-51-like gene.[16] Species identification was also confirmed by using the *gyrB* PCR method previously described.[17] Genomic relatedness among *A. baumannii* isolates was investigated by pulsed-field gel electrophoresis (PFGE).[18]

Cell Growth and Isolation of LPS: The *Acinetobacter baumannii* strain SMAL was grown in a liquid shake culture in LB medium at 28 °C (20 L). Cells in the early stationary phase, were collected by centrifugation (9800 g, 20 min, 4 °C), washed sequentially with distilled water, ethanol, acetone and diethyl ether and finally freeze-dried. The LOS was isolated on dry cells (yield 0.3 g/L) by aqueous 90% phenol/chloroform/light petroleum (2:8:5, v/v/v) extraction.[6] After removal of the light solvents under vacuum, LOS was precipitated from phenol with water and washed with aqueous 80% phenol and acetone. The pellet was then suspended in water and lyophilized (43 mg, yield 7.2 mg/g_{cells}).

General and Analytical Procedures: The total fatty acid content and monosaccharide composition were determined by treating LPS with methanolic HCl at 80 °C for 18 h. The solution was extracted twice with equal volumes of *n*-hexane, the two top layers (*n*-hexane)

were combined and dried, and the fatty acid methyl esters were analysed directly by GC/MS. The bottom layer (methanol) was dried with a stream of air, and the resulting methyl glycosides were acetylated, as reported elsewhere.[19] The absolute configuration was determined by analysis of the chiral 2-octyl[20] or 2-butyl[21] derivatives. The ester-bound fatty acids were selectively released from LPS by base-catalysed hydrolysis (0.5 M NaOH, 37 °C, 2 h); the solution was acidified to pH = 4.0 by dropwise addition of 1 M HCl and extracted twice with an equal volume of $CHCl_3$. Fatty acids were recovered from the organic layer, esterified with diazomethane and analysed by GC/MS. Each methyl ester derivative was identified by comparison of its retention time with that of the reference compound and by its MS fragmentation. All GC/MS analyses were performed with a Hewlett–Packard 5890 instrument equipped with an SPB-5 capillary column (Supelco, 30 m × 0.25 i.d., flow rate 0.8 mL/min, He as carrier gas) with the following temperature program: 150 °C for 3 min, 150 → 300 °C at 10 °C/min, 300 °C for 18 min. EI MS data were recorded with an ionization energy of 70 eV and an ionizing current of 0.2 mA.

Isolation of Core Oligosaccharides 2 and 3 and Preparation of Intact and Ammonia-Deacylated Lipid A: Total delipidation procedure of the LOS was carried out as reported previously;[22] namely, the sample (20 mg) was deesterified by hydrazinolysis, deamidated by strong alkaline hydrolysis and desalted by size-exclusion chromatography on a Sephadex G10 column. Finally, the oligosaccharide was further purified by HPLC on a TSK-3000 PW_{XL} size exclusion column eluting with water at a flow rate of 0.8 mL/h (product **2**, 3 mg, structure shown in Figure 1). Another LPS portion (15 mg) was hydrolysed in aq. 1% AcOH (100 °C, 2 h), the precipitate (lipid A, 5 mg) was removed by centrifugation, and the supernatant was lyophilized and fractionated by GPC on a TSK HW-40 column. Oligosaccharide **3** (8 mg, Figure 1) was the first compound eluted and was used directly in spectroscopic studies. The selective ester-bound acyloxyacyl deacylation promoted by ammonia treatment was performed directly on lipid A (200 μg) by 1% AcOH LOS hydrolysis as reported previously.[10]

Mass Spectrometry: ESI-FT-ICR MS was performed in negative and positive ion modes with a hybrid Apex Qe FT-ICR mass spectrometer (Bruker Daltonics, Billerica, MA, USA), equipped with a 7 T superconducting magnet and an Apollo dual ion source. The instrument was controlled by Bruker's ApexControl software, version 2.0.0.36, and data was recorded in broadband mode with 512K data sampling rate. The mass scale was calibrated externally by using compounds of known structure. For the negative ion mode samples (ca. 10 ng/μL) were dissolved in a 50:50:0.001 (v/v/v) mixture of 2-propanol/water/triethylamine (pH ≈ 8.5). For the positive ion mode samples, a 50:50:0.03 (v/v/v) mixture of 2-propanol/water/30 mM ammonium acetate adjusted with acetic acid to pH = 4.5 was used. The samples were sprayed at a flow rate of 2 μL/min. The capillary entrance voltage was set to 3.8 kV and the drying gas temperature to 150 °C. The spectra, which showed several charge states for each component, were charge-deconvoluted by using the DataAnalysis Software (Bruker Daltonics), and the mass numbers given refer to monoisotopic molecular masses. For unspecific fragmentation the voltage in the external collision cell was increased from 3 to 30 V. Infrared multiphoton dissociation (IRMPD) of isolated parent ions was performed with a 25 W, 10.6 μm CO_2 laser (Synrad, USA). The unfocused laser beam was directed through the centre of the trap. The duration of the laser irradiation was adapted to generate optimal fragmentation and varied between 10 and 80 ms. Fragment ions were detected after a delay of 0.5 ms.

NMR Spectroscopy: ^1H and ^1H-^{13}C NMR experiments on product **2** were carried out with a Varian Inova 500 spectrometer form Consortium INCA (L488/92, Cluster 11) equipped with a reverse probe operating at 296 K. The spectra of product **3** were recorded at 300 K with a Bruker DRX-600 spectrometer equipped with a cryogenic probe. All spectra were calibrated with respect to internal acetone (δ_H = 2.225 ppm; δ_C = 31.45 ppm). For all homonuclear spectra, experiments were measured with data sets of 2048 × 512 points, 32 scans were acquired, and mixing times of 200 and 120 ms were employed for ROESY and TOCSY experiments, respectively. Each data matrix was zero-filled in both dimensions to give a matrix of 4096 × 2048 points and was resolution-enhanced in both dimensions by a shifted sine-bell function before Fourier transformation. The HSQC experiment was performed by using a data set of 2048 × 512 points, whereas for the HMBC experiment a data set of 2048 × 256 points was used. For each t_1 value, 64 scans were acquired, and the HMBC sequence was optimized for a 6 Hz long-range coupling constant. All NMR spectra were acquired and transformed by using the Topspin 3.0a program and studied with Pronto software.[23]

Supporting Information (see footnote on the first page of this article): ^1H and ^{13}C NMR chemical shifts for oligosaccharides **2** and **3**.

Acknowledgments

The authors thank Regina Engel (Research Center Borstel) for technical assistance.

[1] A. Y. Peleg, H. Seifert, D. L. Paterson, *Clin. Microbiol. Rev.* **2008**, *21*, 538–582.
[2] M. L. Joly-Guillon, *Clin. Microbiol. Infect.* **2005**, *11*, 868–873.
[3] V. K. Goel, A. Kapil, *BCM Microbiol.* **2001**, *1*, 16–24.
[4] R. Medzhitov, *Nat. Rev. Immunol.* **2001**, *1*, 135–145.
[5] S. I. Miller, R. K. Ernst, M. W. Bader, *Nat. Rev. Immunol.* **2005**, *3*, 36–46.
[6] C. Galanos, O. Lüderitz, O. Westphal, *Eur. J. Biochem.* **1969**, *9*, 245–249.
[7] E. T. Rietschel, *Eur. J. Biochem.* **1976**, *64*, 423–428.
[8] E. V. Vinogradov, J. Ø. Duus, H. Brade, O. Holst, *Eur. J. Biochem.* **2002**, *269*, 422–430.
[9] A. Kondakova, A. B. Lindner, *Eur. J. Mass Spectrom.* **2005**, *11*, 535–546.
[10] A. Silipo, R. Lanzetta, A. Amoresano, M. Parrilli, A. Molinaro, *J. Lipid Res.* **2002**, *43*, 2188–2195.
[11] E. V. Vinogradov, B. O. Petersen, J. E. Thomas-Oates, J. Duus, H. Brade, O. Holst, *J. Biol. Chem.* **1998**, *273*, 28122–28131.
[12] S. Leone, A. Molinaro, P. Pessione, R. Mazzoli, C. Giunta, L. Sturiale, D. Garozzo, R. Lanzetta, M. Parrilli, *Carbohydr. Res.* **2006**, *341*, 582–590.
[13] S. Leone, L. Sturiale, P. Pessione, R. Mazzoli, C. Giunta, R. Lanzetta, D. Garozzo, A. Molinaro, M. Parrilli, *J. Lipid Res.* **2007**, *48*, 1045–1051.
[14] GeneIDs 5986103 and 6002532 at www.ncbi.nlm.nih.gov/pubMed.
[15] C. Alexander, E. T. Rietschel, *J. Endotox. Res.* **2001**, *7*, 167–202.
[16] J. F. Turton, N. Woodford, J. Glover, S. Yarde, M. E. Kaufmann, T. L. Pitt, *J. Clin. Microbiol.* **2006**, *44*, 2974–2976.
[17] P. G. Higgins, H. Wisplinghoff, O. Krut, H. Seifert, *Clin. Microbiol. Infect.* **2007**, *13*, 1199–1201.
[18] A. Endimiani, F. Luzzaro, R. Migliavacca, E. Mantengoli, A. M. Hujer, K. M. Hujer, L. Pagani, R. A. Bonomo, G. M. Rossolini, A. Toniolo, *Antimicrob. Agents Chemother.* **2007**, *51*, 2211–2214.

[19] O. Holst in *Methods in Molecular Biology, Bacterial Toxins: Methods and Protocols* (Ed.: O. Holst), Humana Press Inc., Totowa, NJ, **2000**, pp. 345–353.
[20] K. Leontein, J. Lönngren, *Methods Carbohydr. Chem.* **1978**, *62*, 359–362.
[21] G. J. Gerwig, J. P. Kamerling, J. F. G. Vliegenthart, *Carbohydr. Res.* **1978**, *62*, 349–357.
[22] V. Gargiulo, D. Garozzo, R. Lanzetta, A. Molinaro, L. Sturiale, C. De Castro, M. Parrilli, *ChemBioChem* **2008**, *9*, 1830–1835.
[23] M. Kjaer, K. V. Andersen, F. M. Poulsen, *Methods Enzymol.* **1994**, *239*, 288–308.

Received: December 1, 2009
Published Online: January 29, 2010

Journal of Pharmaceutical and Biomedical Analysis 71 (2012) 193–197

Contents lists available at SciVerse ScienceDirect

Journal of Pharmaceutical and Biomedical Analysis

journal homepage: www.elsevier.com/locate/jpba

Short communication

Qualitative screening in doping control by MALDI-TOF/TOF mass spectrometry: A proof-of-evidence

E. Galano[a,*], M. Fidani[c], F. Baia[c], L. Palomba[d], G. Marino[a,b], A. Amoresano[a,b]

[a] Department of Organic Chemistry and Biochemistry, University of Naples "Federico II", Naples, Italy
[b] School of Biotechnology Sciences, University of Naples "Federico II", Naples, Italy
[c] Unirelab s.r.l., Milan and Rome, Italy
[d] Department of Biomolecular Sciences, Urbino University, Urbino, Italy

ARTICLE INFO

Article history:
Received 28 March 2012
Received in revised form 1 August 2012
Accepted 5 August 2012
Available online 27 August 2012

Keywords:
Urine
Cocaine
Drugs
MALDI-TOF/TOF
Nitrocellulose

ABSTRACT

The analysis of doping agents in biological fluids is of top significance in clinical and forensic toxicology. Herein we describe the study of a screening method for the detection of a mixture of drugs of potential abuse including cocaine and its metabolites. By using matrix-assisted laser desorption/ionization MALDI-TOF/TOF mass spectrometry. This screening procedure to detect the presence of different drugs, avoiding time consuming procedures could be useful in different fields of forensic analytical toxicology, including antidoping analysis.

1. Introduction

The analysis of doping agents in biological fluids is of pivotal impact in clinical and forensic toxicology [1].

Traditionally, gas chromatography coupled to mass spectrometry (GC/MS) was the standard technique used for the analysis of anabolic steroids or drugs of abuse [2]. More recently, liquid chromatography coupled with tandem mass spectrometry (LC/MS/MS) is becoming an key tool in doping control, even if lengthy separation times and the preceding step up of chromatographic separation procedures are usually required [3].

Thus, several research groups are working on developing new fast methods for doping analysis. Therefore, matrix-assisted laser desorption/ionization time-of flight mass spectrometry (MALDI-TOF/MS) is acquiring new inputs due to the ever increasing need for an analytical technique allowing simplicity, speed and high throughput for the screening of the massive number of drugs currently available [4,5]. As previously discussed for other drugs, GC/MS and LC/MS are the most commonly analytical techniques employed for cocaine and its metabolites detection in biological samples, i.e. urine and hair [2,6]. Recently, Vogliardi and coworkers, proposed a method for the MALDI detection of cocaine and its metabolites from human hair samples [7,8].

Our work has focused on the study of a screening method for the detection of mixtures of drugs of potential abuse, including sedative drugs and drug metabolites in serum and urine equine samples using MALDI-TOF/TOF mass spectrometry technique. To the best of our knowledge, this is the first report of an application of collisionally induced fragmentation of drugs of abuse by MALDI-TOF/TOF tandem mass spectrometry. As proof-of-concept, serum and urine horse samples spiked with sedative drugs, as well as real samples, human cocaine "positive" urines, were analyzed.

2. Materials and methods

Standard solutions of Xylazine, Acepromazine, Nordazepam, Diazepam and Detomidine were purchased from Sigma Aldrich (St. Louis, MO, USA). Standard methanolic solutions of cocaine, benzylecgonine and ecgonine methyl ester at a concentration of 100 μg/mL were purchased from Sigma Aldrich (St. Louis, MO, USA). Working solutions of the three analytes were prepared in methanol at different concentration (from 10 μg/mL to 10 ng/mL) for each analyte. Chloroform was acquired from Pestanal Fluka (Milan, Italy). MALDI matrix 2,5-dihydroxybenzoic acid (DHB) was obtained from Sigma (Milan, Italy).

* Corresponding author at: Department of Organic Chemistry and Biochemistry, Federico II University of Naples, Monte S. Angelo, via Cynthia 4, 80126 Naples, Italy. Tel.: +39 081679950; fax: +39 081674313.
E-mail address: eugenio.galano@unina.it (E. Galano).

0731-7085/$ – see front matter © 2012 Elsevier B.V. All rights reserved.
http://dx.doi.org/10.1016/j.jpba.2012.08.003

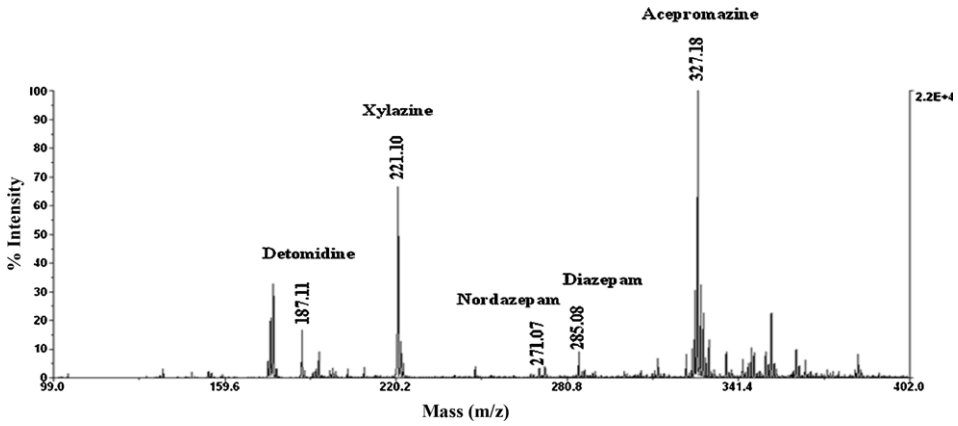

Fig. 1. MALDI-TOF spectrum of six standard analytes at concentration of 10 μg/mL.

The equine and human urine used in this study were originally collected and analysed for clinical and forensic toxicology by Unirelab s.r.l. (Settimo Milanese, Milan, Italy).

2.1. Sample preparation

The method uses a single-step extraction in chloroform; for urine samples pH was adjusted at a value of 9. Aliquots of 1 mL of horse serum and urine was extracted with an equal volume of chloroform. Extraction was performed for 30 min in shaking wheel, to exchange sample and extractant, and then the mixture was centrifuged for 30 min at 4 °C. The organic phase containing the analytes was briefly recovered by removing the aqueous phase and the lipidic interface between the two phases. Aliquots of 0.5 μL of organic phase were directly analyzed by MALDI-MS and MS/MS.

2.2. Nitrocellulose layer/DHB matrix

The nitrocellulose (NC) layer was obtained by dissolving pure Transblot-NC membrane (BioRad, Milan, Italy); the concentration of NC was 5 mg/mL in acetonitrile/methanol 7:3 (v/v). DHB was prepared at a concentration of 10 mg/mL in 35% acetonitrile and 65% formic acid 0.1%. Spotting of samples (0.5 μL) on OptiTOF plate (AB Sciex) were executed with the "multilayer" method, NC-DHB-samples 1:1:1 according to Picariello et al. [9].

2.3. MALDI-TOF analysis

MALDI-TOF/MS and MS/MS experiments were carried out on a 4800 *Plus* MALDI TOF/TOF™ Analyzer AB Sciex; mass spectra were acquired in the reflector mode in the *m/z* 100–400 mass range.

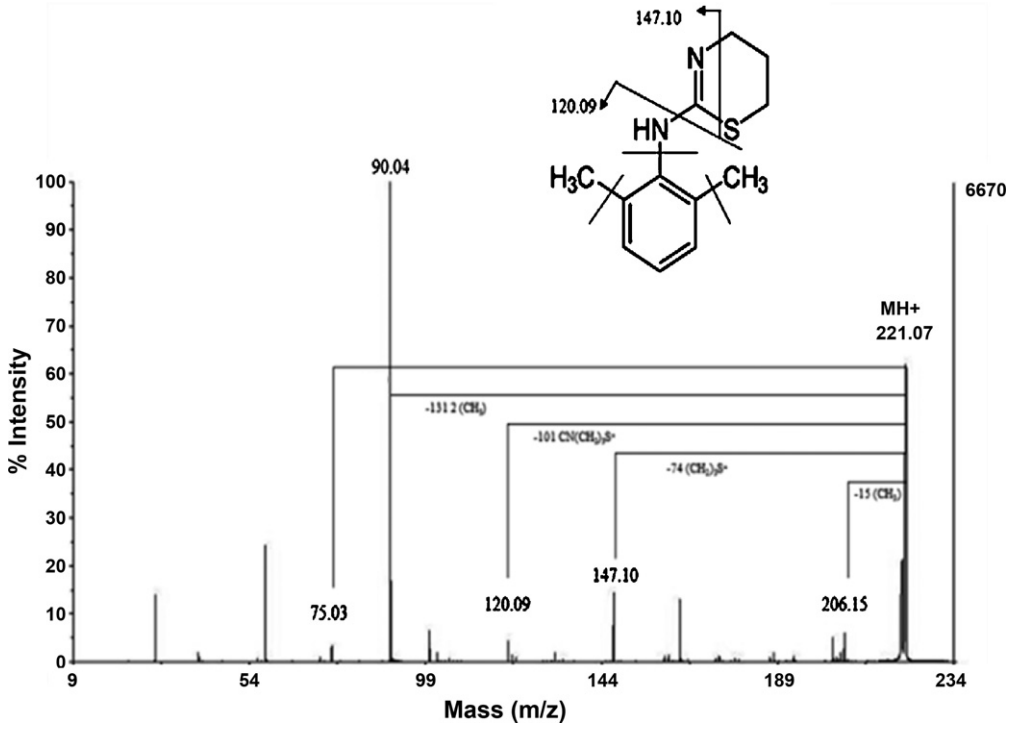

Fig. 2. MALDI-TOF/TOF spectrum of xylazine.

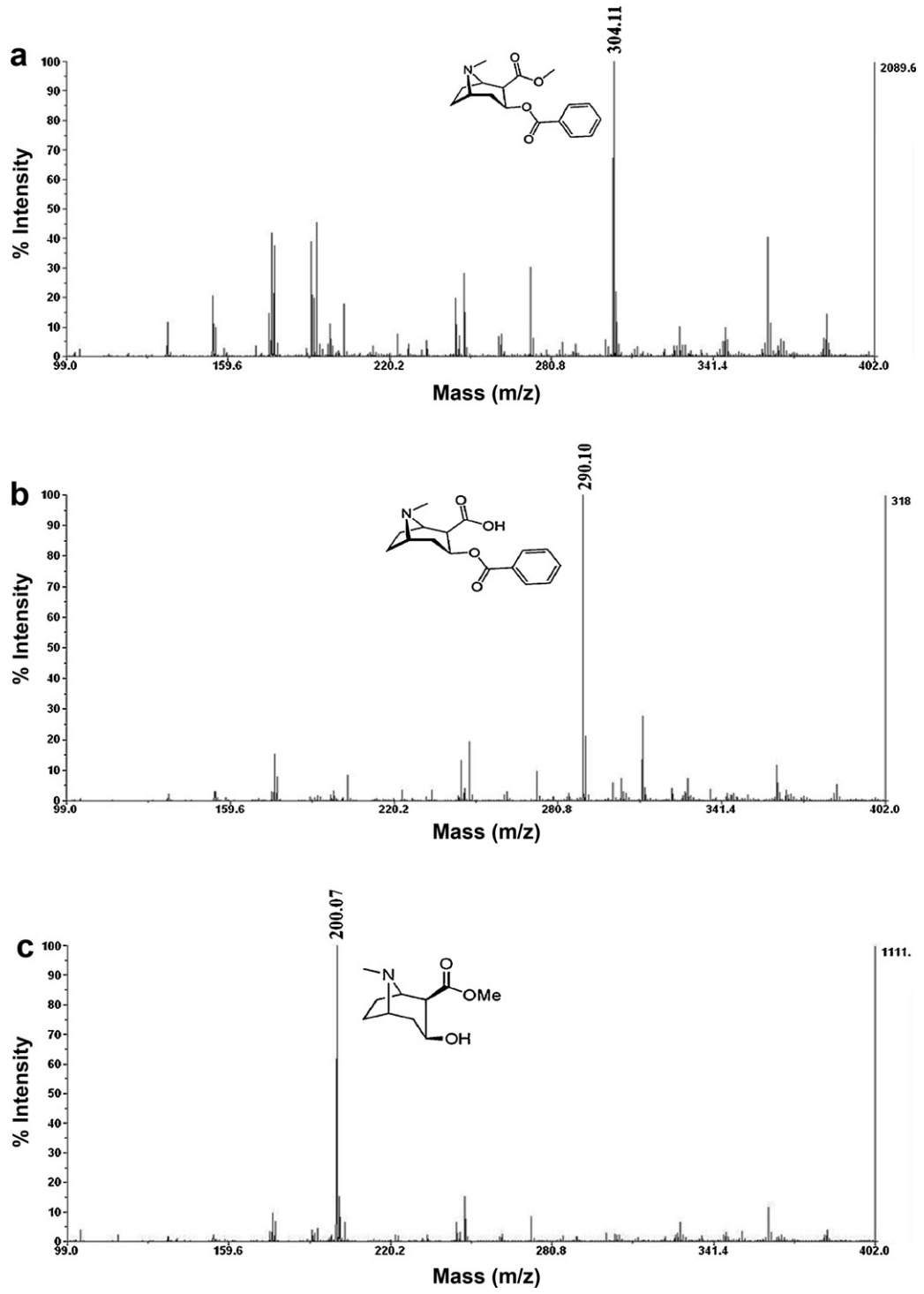

Fig. 3. MALDI-MS of (A) cocaine, (B) benzoylecgonine and (C) ecgonine methyl ester standards, extracted at concentration of 10 μg/mL.

Acquisition laser power was optimized at 3500 for MS spectra and 4500 for MSMS spectra. All acquisitions were generated automatically in the instrument software and based on averaging 5000 shots per spectrum.

3. Results and discussion

This paper demonstrates the feasibility of MALDI TOF/TOF analysis as a fast screening test in antidoping field, in order to identify putative candidates to be further investigated by well established anti-doping procedures. The paper reports on the analysis of a set of 5 common sedative drugs used in horse doping and cocaine and its metabolites, in humans.

3.1. Drugs analysis

The first step in the development of a screening method for the detection of drugs in biological fluids was the choice of best MALDI matrix. To this purpose different matrices were tested. DHB and α-ciano-4-hydroxycinnamic acid, in different matrix composition

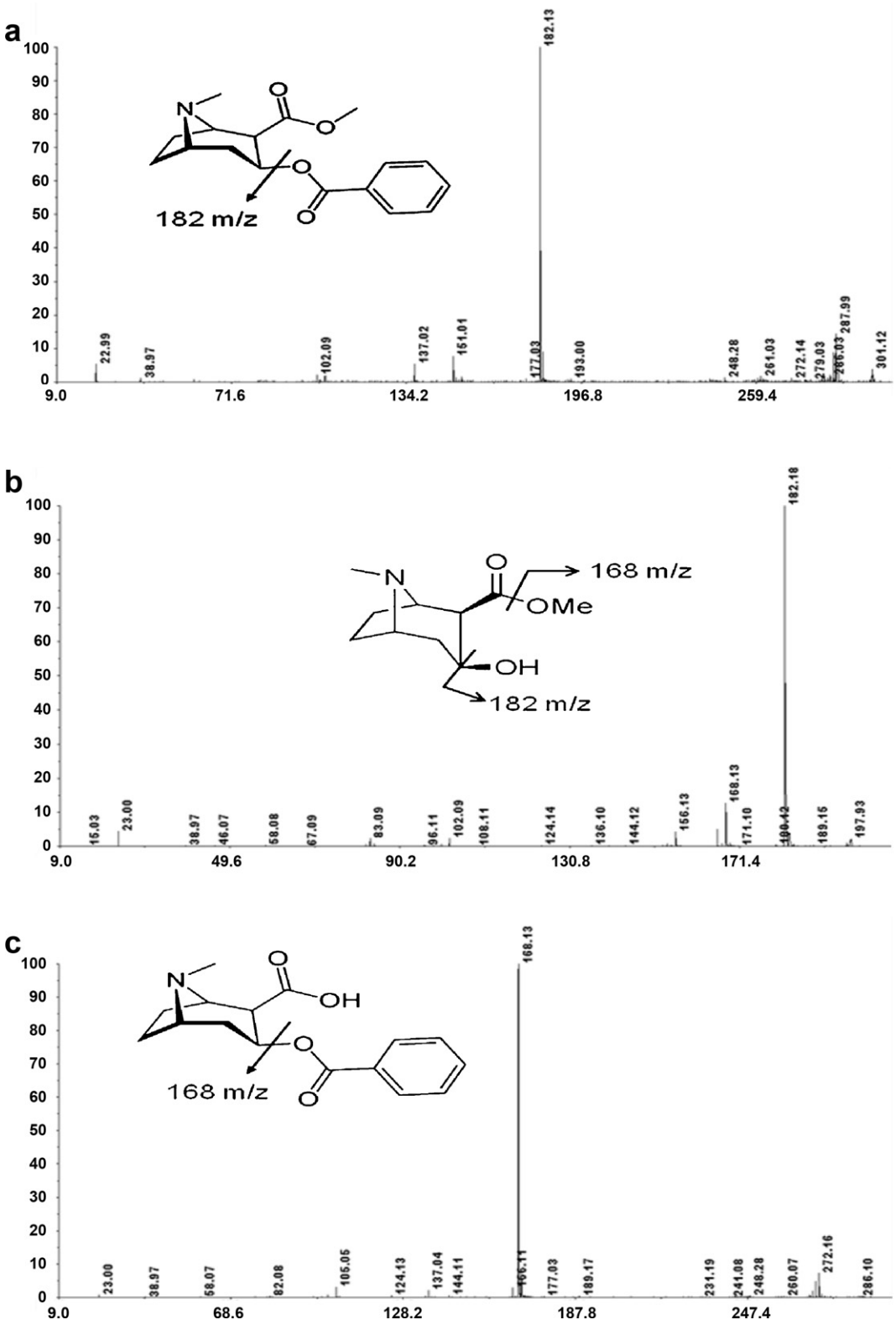

Fig. 4. MALDI-TOF/TOF spectra from human "positive" urine sample of precursor ions at *m*/*z* 304.11, 290.10 and 200.07, panels a, b, c respectively.

were used. In particular, DHB matrix in 50% acetonitrile/water with or without 0.1% formic acid, a ionic liquid matrix prepared dissolving DHB in equimolar mixtures of an organic bases represented by pyridine, and a nitrocellulose layer dissolved in DHB were evaluated. As first attempt, the matrix preparation method was initially tested on five drugs used in veterinary medicine in order to evaluate the best matrix conditions. Xylazine, Acepromazine, Nordazepam, Diazepam and Detomidine were used. Thus, standard solutions were prepared as described in Section 2 and analyzed by MALDI-TOF/TOF mass spectrometer using different matrices previously described. Analyses were performed using different drugs concentration (10 μg/mL, 1 μg/mL, 100 ng/mL and 10 ng/mL). The most

reliable results in terms of reproducibility were achieved using a NC layer dissolved in DHB. Once formed the layer of nitrocellulose on the plate, no influence of organic solvents was observed, most likely due to the high volatility of chloroform.

For the choice of the matrix, reproducibility parameter was preferred to others for the homogenous layer and the possibility to work in full automatic acquisition mode with the MALDI-TOF/TOF. Moreover using an organic extraction no influence of salts were detected. The resulting urine spectra were completely different if compared with urine samples directly loaded on the plate. Fig. 1 reports the MALDI/MS spectrum detected when the mix of the different analytes was analyzed. As a whole, the LoD observed resulted to be 100 ng/mL. In order to test the possibility to use MALDI-MS/MS technique for the detection of drugs in complex matrices, standard solution of five analytes were spiked in horse blank urine and serum. MALDI-MS data showed that the LoD observed was the same of the standard analysis. The validation of the identity of each molecule was obtained by the analysis of the MSMS spectra of each standard drug to confirm the correct assignments for the peaks detected in the MALDI spectrum. Our analyses in tandem MS (TOF/TOF) mode took advantage from the possibility to have in a single instrument high sensitivity, mass accuracy, and resolution. Thus, the ions detected occurring at m/z 327.18 for Acepromazine, m/z 221.10 for Xylazine, m/z 187.11 for Detomidine, m/z 271.07 and m/z 285.08 for Norazepam and Diazepam, respectively, were fragmented in the collision chamber. The interpretation of collision induced dissociation spectra led to the unique identification of analytes. As an example Fig. 2 shows the MS/MS spectrum of the precursor ion occurring at m/z 221.10 and identified as Xylazine on the basis of the fragment ions. Similar attributions were achieved for the other signals occurring in the spectrum. However, the data here reported merely represent preliminary study, method validation in terms of reproducibility, robustness and selectivity, are currently in progress (manuscript in preparation). Once set up, in a proof of experience, the procedure was tested on real samples of horse urine and serum resulted to be positive for the presence of some analyzed drugs, after conventional LC–MS/MS analysis carried out by anti-doping laboratories at Unirelab. The method let us to positively identify 2 serum samples and 1 urine sample for the presence of Diazepam and Nordazepam respectively. As for the other serum and urine samples analysed, the detection limits of the other searched analytes resulted much lower than the detection limit our study. In fact, traditionally in doping control, sedative drugs are identify in horse urine at a concentration ranging from 1 to 100 ng/mL. Values below 100 ng/mL can be detected only by using LCMS or for more sensible analysis (below 1 ng/mL) LCMSMS in MRM or PIS modes.

3.2. Drugs of abuse analysis

In order to provide an efficient and reliable method for drugs of abuse screening in complex biological fluids such as urine, the MALDI-MS/MS technique was proposed. As described before, the best MALDI matrix was evaluated. Thus MALDI-MS/MS spectrum was acquired by using standard solution of cocaine and its metabolite at different concentrations (10 μg/mL, 1 μg/mL, 100 ng/mL, 50 ng/mL and 10 ng/mL). NC layer loading procedure resulted in the best signal to noise ratio as reported in Fig. 3. As for urine samples, the same procedure already described was applied for the extraction of the three analytes. On the basis of the MALDI-MS analysis, the LoD of each molecule resulted to be 50 ng/mL. To verify the interference of the biological medium, equine urine was spiked with the same standard concentrations. An aliquot of urine was directly loaded on the MALDI plate and analyzed thus avoiding long lasting procedures. Each experiment was performed in triplicate as sum of 5000 laser shots per spectrum. The molecular ion of cocaine (304.11m/z) and one or both principal urinary metabolites were detected in the MALDI-MS spectrum. Finally, five samples of human cocaine "positive" urines were analyzed by MALDI-MS/MS. In four cases the positivity for the presence of drug of abuse was confirmed. In fact, the molecular ion of cocaine (304.11 m/z) and one or both principal urinary metabolites were detected in the MALDIMS spectrum. As an example, Fig. 4 shows the MALDI-MS spectrum of a human urine sample in which there are the presence of the diagnostic signals at m/z 304.11, 290.10 and 200.07. In order to confirm the attribution, MALDI-MS/MS spectra, showed in Fig. 4, were performed on the precursor ions at m/z 304.11, 290.10 and 200.07, leading to the identification of cocaine, benzylecgonine and ecgonine methyl ester, respectively.

4. Conclusions

We have described a simple and rapid screening method based on MALDI-TOF/TOF mass spectrometry for the qualitative determination of doping agent as well as drugs of potential abuse, as a promising confirmatory test using MS/Ms with a TOF/TOF instrument. Target doping compounds in horse samples were detected by MALDI-TOF/TOF with a LoD of 100 ng/mL. For the analysis of cocaine and its metabolite in human urine samples the LoD was 50 ng/mL. This study based on a screening procedure to detect the presence of cocaine and its metabolites could be useful in different fields of forensic analytical toxicology, including antidoping analysis. The simultaneous analysis by MALDI-TOF/TOF of a considerable number of samples can be achieved thus resulting in an effective qualitative screening to identify the positive samples which can be selected to further LC-MS/MS quantitative analysis. Even if recent applications in UPLC-MS/MS allow to reach comparable (if not better) LOD by direct injection of human urine for quantitative detection of cocaine in short chromatographic run time [10], it must be underlined that a fully automation could be achieved with recent MALDI-TOF/TOF instrumentation. Automation of MALDI-MS for the acquisition of mass spectra is nowadays feasible and relatively simple, leading to a multiple sample simultaneously analysis through the use of automated MALDIMS procedure.

References

[1] K. Henne, WADA, the promises of law and the landscapes of antidoping regulation, PoLAR 33 (2010) 306–325.
[2] S. Strano-Rossi, F. Molaioni, F. Rossi, F. Botre, Rapid screening of drugs of abuse and their metabolites by gas chromatography/mass spectrometry: application to urinalysis, Rapid Commun. Mass Spectrom. 19 (2005) 1529–1535.
[3] H. Umezawa, X.P. Lee, Y. Arima, C. Hasegawa, A. Marumo, T. Kumazawa, K. Sato, Determination of diazepam and its metabolites in human urine by liquid chromatography/tandem mass spectrometry using a hydrophilic polymer column, Rapid Commun. Mass Spectrom. 22 (2008) 2333–2341.
[4] D.L. Dehn, D.J. Claffey, M.W. Duncan, J.A. Ruth Nicotine, Cotinine adducts of a melanin intermediate demonstrated by matrix-assisted laser desorption/ionization time-of-flight mass spectrometry, Chem. Res. Toxicol. 14 (2001) 275–279.
[5] M. Galesio, R. Rial-Otero, J.-L. Capelo-Martinez., Comparative study of matrices for their use in the rapid screening of anabolic steroids by matrix-assisted laser desorption/ionisation time-of-flight mass spectrometry, Rapid Commun. Mass Spectrom. 23 (2009) 1783–1791.
[6] M. Barroso, M. Dias, D.N. Vieira, J.A. Queiroz, M. Lopez-Rivadulla., Development and validation of an analytical method for the simultaneous determination of cocaine and its main metabolite, benzoylecgonine, in human hair by gas chromatography/mass spectrometry, Rapid Commun. Mass Spectrom. 22 (2008) 3320–3326.
[7] S. Vogliardi, D. Favretto, G. Frison, S.D. Ferrara, R. Seraglia, P. Traldi, A fast screening MALDI method for the detection of cocaine and its metabolites in hair, J. Mass. Spectrom. 44 (2009) 18–24.
[8] S. Vogliardi, D. Favretto, G. Frison, S. Maietti, G. Viel, R. Seraglia, P. Traldi, S.D. Ferrara, Validation of a fast screening method for the detection of cocaine in hair by MALDI-MS, Anal. Bioanal. Chem. 396 (2010) 2435–2440.
[9] G. Picariello, R. Romano, F. Addeo, Nitrocellulose film substrate minimizes fragmentation in matrix-assisted laser desorption ionization time-of-flight mass spectrometry analysis of triacylglycerols, Anal. Chem. 82 (2010) 5783–5791.
[10] C.L. Snozek, M.W. Bjergum, L.J. Langman Cocaine, Metabolites by LC–MS/MS, J. Methods Mol. Biol. 902 (2012) 91–103.

Journal of Archaeological Science 39 (2012) 2956–2968

Contents lists available at SciVerse ScienceDirect

Journal of Archaeological Science

journal homepage: http://www.elsevier.com/locate/jas

The constituents of the ink from a Qumran inkwell: new prospects for provenancing the ink on the Dead Sea Scrolls

Kaare Lund Rasmussen [a,*], Anna Lluveras Tenorio [b], Ilaria Bonaduce [b], Maria Perla Colombini [b], Leila Birolo [c], Eugenio Galano [c], Angela Amoresano [c], Greg Doudna [d], Andrew D. Bond [a], Vincenzo Palleschi [e,f], Giulia Lorenzetti [e,g], Stefano Legnaioli [e], Johannes van der Plicht [h,i], Jan Gunneweg [j]

[a] Institute of Physics, Chemistry and Pharmacy, University of Southern Denmark, Campusvej 55, DK-5230 Odense M, Denmark
[b] Dipartimento di Chimica e Chimica Industriale, Via Risorgimento 35, 56126 Pisa, Italy
[c] Dipartimento di Chimica Organica e Biochimica, Università degli Studi di Napoli Federico II, Napoli, Via Cinthia, I-80127, Italy
[d] Columbia College, 13910 45th Avenue NE #802, Marysville, WA 98271, USA
[e] Institute of Chemistry of Organometallic Compounds of CNR, Applied Laser Spectroscopy Laboratory (ALS-ICCOM), Area della Ricerca del CNR, Via G. Moruzzi 1, I-56124 Pisa, Italy
[f] University of Pisa, Department of Archaeology, Via Galvani 1, Pisa, Italy
[g] University of Florence, Department of Chemistry, Via della Lastruccia 1, Sesto Fiorentino, Italy
[h] Center for Isotope Research, Nijenborgh 4, 9747 AG Groningen, The Netherlands
[i] Faculty of Archaeology, Leiden University, P.O. Box 9515, 2300 RA Leiden, The Netherlands
[j] Institute of Archaeology, Hebrew University of Jerusalem, Mount Scopus, 91905 Jerusalem, Israel

ARTICLE INFO

Article history:
Received 4 December 2011
Received in revised form
13 March 2012
Accepted 11 April 2012

Keywords:
Ink
Qumran
GC–MS
Raman
FT-IR
PXRD
LIBS
ICP-MS
Proteomic analyses
Radiocarbon dating

ABSTRACT

A unique sample of ink from an inkwell in the Schøyen Collection allegedly found at Qumran has been subjected to analyses by several analytical techniques: GC–MS, proteomic analysis, PXRD, Raman, (ATR) FT-IR, LIBS, ICP-MS and MS. The results reveal to an unexpected level of detail how the ink was manufactured, which gives insight into the industrial processes and craftsmanship that were practiced at the Qumran settlement during the Second Temple period (100 BCE–CE 70). The identified minerals and other organic and inorganic materials are sufficiently multiple and diverse that it is probable that this specific ink can be recognized if analyses of inks are performed on manuscripts from Qumran and other locations in Israel and the Middle East. The present work exposes a distinct and unique possibility to shed light on early Jewish manuscript controversies, including their provenance.

1. Introduction

In 1947–1955 a large quantity of fragmentary scrolls from approximately two thousand years ago was found in caves around Qumran near to the Dead Sea east of Jerusalem, amounting to over nine hundred ancient Jewish, biblical and sectarian texts. Three-quarters of the texts were found in one cave, Cave 4, which can be accessed only from the site of Khirbet Qumran, thereby raising the question of whether the scrolls were actually written at the site. Due to the variety of kinds of scrolls and scribal hands, it has long been accepted that many of the scrolls must have been imported. However, following the interpretation of the excavator, Roland de Vaux (*e.g.* de Vaux, 1973), most scholars working on the texts today believe that at least some were written by the Qumran residents. While this seems plausible, it has so far remained unproven.

No scraps of parchment were found at the site—a fact commonly attributed to destruction by fire and/or water over time—but de Vaux reported finding three inkwells, two made of

* Corresponding author. Tel.: +45 28713709.
E-mail addresses: klr@sdu.dk (K.L. Rasmussen), anna.lluveras@for.unipi.it (A.L. Tenorio), ilariab@dcci.unipi.it (I. Bonaduce), perla@dcci.unipi.it (M.P. Colombini), birolo@unina.it (L. Birolo), eugenio.galano@unina.it (E. Galano), angela.amoresano@unina.it (A. Amoresano), gdoudna@msn.com (G. Doudna), adb@sdu.dk (A.D. Bond), vincenzo.palleschi@cnr.it (V. Palleschi), a_lorenzetti@hotmail.com (G. Lorenzetti), stefano.legnaioli@pi.iccom.cnr.it (S. Legnaioli), J.van.der.Plicht@rug.nl (J. van der Plicht), jan.gunneweg@huji.ac.il (J. Gunneweg).

0305-4403/$ – see front matter © 2012 Elsevier Ltd. All rights reserved.
doi:10.1016/j.jas.2012.04.041

clay and one made of bronze. Two of the inkwells were found in locus 30, commonly referred to as the "scriptorium" (Fig. 1), and one was found in an immediately adjacent room (Nir-El and Broshi, 1996). One further inkwell was found by another excavator of Qumran, Solomon Steckoll, in 1966–1967 (Steckoll, 1968, 1969; Goranson, 1993), and a fifth inkwell said to be from Qumran was bought by a private person in 1967 from Kando (Khalil Eskander Shahin), the antiquities dealer who also bought many of the Dead Sea Scrolls from the Bedouin (Goranson, 1992: 39). In 1994, Stephen Goranson published a sixth inkwell identified as coming from Qumran in the private antiquities collection of Martin Schøyen of Oslo (Goranson, 1994). This last inkwell (Fig. 2), referred to here as the Schøyen inkwell, is the subject of our present study.

Goranson reported that the Schøyen inkwell is "made of bronze and has two handles on top that turn in opposite directions. It is a little over three inches (ca 8 cm) high and the same in diameter. Its shape, however, differs from the other known Qumran inkwells" (1994: 39). According to Schøyen, "this inkwell was discovered in the Qumran ruins by Bedouin of the Ta'amireh tribe in about 1950, after the Qumran Cave 1 scrolls had come to light, but before Roland de Vaux began excavating the ruins in 1951". According to Goranson Kando confirmed this account in 1993. Goranson noted that the number of inkwells found at Qumran is unusually high compared to reported results from other excavations, and concluded that the writing or copying done at Qumran "most likely produced some—though surely not all—of the Qumran manuscripts" (Goranson, 1994: 39).

According to Elgvin and Pfann (2002) the Schøyen inkwell was found together with a bronze incense altar. The antiques dealer Kando said that these two items were found together by the Bedouin at Khirbet Qumran "sometime before R. de Vaux and L. Harding started their preliminary excavations in November 1951". Kando sold them to J. Allegro in 1953. John Allegro sold the two items to an anonymous private collector in 1963. Subsequent proprietors were Fayez Barakat, Los Angeles, 1975; Mathias Komor, New York, 1975; an anonymous collector until 1992; David Goldstein, Los Angeles, 1992; and finally Martin Schøyen, 1994. According to Elgvin and Pfann, Kando confirmed in 1993 that the inkwell and the altar indeed were the same as those found by the Bedouin at Qumran around 1950.

In 2002, tests carried out at the Norwegian Technical University of Trondheim showed that the bronze of the Schøyen inkwell comprised of 55–68 wt% Cu, 23–39 wt% Pb, and 5–8 wt% Sn. Traces of ink in the inkwell were also tested, but the stated results were only that the ink "was black, based on lamp-soot, as was the ink used at Qumran" (Elgvin and Pfann, 2002, no mention of the analytical techniques used). Previous analyses of inks from the Dead Sea Scrolls, for example that of Nir-El and Broshi in 1996, encountered difficulties in distinguishing the inorganic composition of the ink from that of the parchment, and the only conclusion drawn was that the ink was made of a "carbonaceous material". Metals such as Cu and Pb were detected (Nir-El and Broshi, 1996), but it was concluded that these were contaminants from the walls of the inkwells. Further analyses by Rabin et al. (2009) and Mantouvalou et al. (2011), based on infrared spectroscopy and X-ray fluorescence (XRF) techniques, did not provide satisfactory identification of any binder in the ink, and significant uncertainty exists in the quantitative interpretation of their IR results. The proposal that Br from Dead Sea brine was used deliberately in the ink and that elevated Br-concentrations allow unique provenancing of ink to Qumran, as stated by Rabin et al. (2009) and Mantouvalou et al. (2011), seems somewhat speculative. There were large and multiple freshwater reservoirs available at Qumran, and it seems equally plausible that ink manufactured at Qumran would have used freshwater without elevated amounts of Br. The stated uncertainties and the relatively large inter-sample variations in the Br-data of Mantouvalou et al. (2011, Fig. 9) also do not provide statistically significant differences between the analyzed samples. As an alternative, it can be suggested that the Br found by Rabin et al. (2009) and Mantouvalou et al. (2011) could have come to the scrolls via sea spray, provided the manuscripts were stored near to the Dead Sea for a prolonged time. Until more comparative data are obtained concerning Br-levels on ink from other places than Qumran, *e.g.* Jericho and Jerusalem, we are not convinced that Br level provides an adequate provenancing tool.

In the present study we have analyzed the ink from the Schøyen inkwell using a wide variety of contemporary analytical techniques that can provide a detailed profile of both the organic and inorganic content. We pinpoint ten distinct characteristics which may provide a sufficient basis to match the ink from the Qumran inkwell to specific inks on the Dead Sea Scrolls or other manuscripts from the region.

Fig. 1. Photo of locus 30 – the scriptorium – in the Qumran settlement (Photo: from Wikipedia). The Qumran settlement is situated on the western bank near the northern end of the Dead Sea (KML-link to Google Maps).

Fig. 2. The Schøyen inkwell, inventory number MS 1655/2 (Photo: From the Schøyen Collection home page).

2. Methods

2.1. Sampling

A solid sample was scraped out of the Qumran inkwell in the Schøyen Collection, MS 1655/2, by one of us (J. Gunneweg) using a scalpel and kept in a pre-cleaned plastic vial. Part of the sample was handed over to University of Southern Denmark, from where sub-samples were distributed to the other partners in pre-cleaned glass vials, or in some case in pre-cleaned plastic vials, taking care that the samples were not exposed to contamination. After a sample was exposed to a non-destructive analysis it was returned to University of Southern Denmark and from there send out for the next analysis. At each instance the content of the vials were inspected and found in accordance with the description of the sample when it was sent out, in this way making sure that samples were not interchanged. A bulk sample of a few milligrams was photographed (Fig. 3) and subsequently used for Gas Chromatography–Mass Spectrometry analysis (GC–MS). Four morphologically distinct grain types can be identified in the sample. Characterized by their colour the four grain types are: white, black, green, and brown/black (see Fig. 3). The last type can also be described as black with rusty spots. Single grains of each of these four types ranging in size from 50 to a few hundred μm were subjected separately to non-destructive powder X-ray diffraction (PXRD), Raman and Fourier Transform Infrared (FT-IR) spectroscopy, and finally analyzed destructively by Laser-Induced Breakdown Spectroscopy (LIBS) analysis. A further set of 4 grains were analyzed by Induced Coupled Plasma Mass Spectroscopy (ICP-MS) and a single black grain was analyzed for protein identification. Finally two bulk samples of 8 and 22 mg of the remainder of the bulk ink sample were measured for stable carbon isotopes and subjected to attempts of radiocarbon dating by Accelerator Mass Spectrometry (AMS). A summary of the analyses performed is given in Table 1.

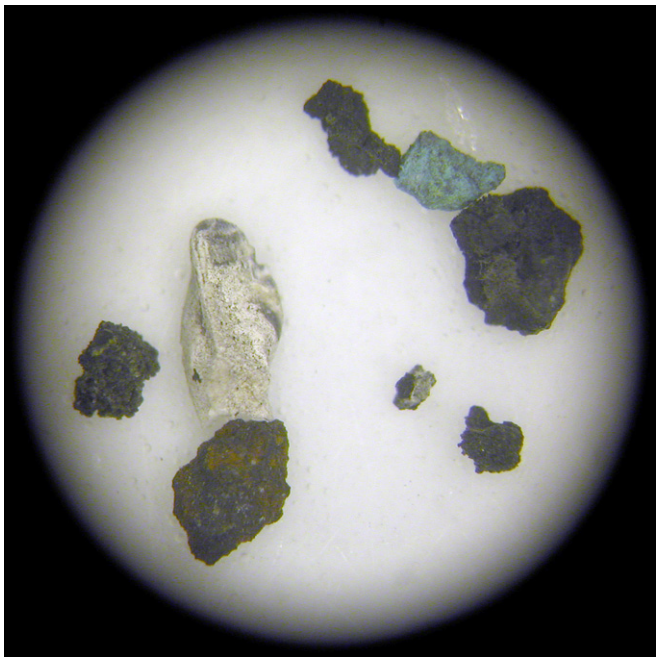

Fig. 3. Optical micrograph of the bulk ink sample prior to GC–MS analysis. The four distinctly different types of grain can be seen in this photo: the white, the black (5 pieces), the green, the black with brown spots. Field of view ca 4 mm. (For interpretation of the references to colour in this figure legend, the reader is referred to the web version of this article.)

Table 1
Sample numbers, description and analyses applied. KLR-8007 is a bulk sample taken from sample number QUM-435 in the records of Jan Gunneweg. The others (KLR-8223 through KLR-8227) are sub-samples from KLR-8007. KLR-8007 is a bulk sample, *i.e.* consisting of a mixture of all four grains types. Concerning the description of the grain types refer to Fig. 3.

Sample no.	Description	Analytical techniques applied
KLR-8007	Bulk	GC–MS, Radiocarbon
KLR-8223	White	Raman (Ar), FT-IR, LIBS, XRD, ICP-MS
KLR-8224	Black	Raman (Ar), FT-IR, LIBS, ICP-MS
KLR-8225	Green	Raman (Ar), ICP-MS
KLR-8226	Brown/black	Raman (Ar), Raman (diode), FT-IR, LIBS, ICP-MS
KLR-8227	Black	Proteins

2.2. GC–MS

GC–MS was carried out on a bulk sample of a few milligrams consisting of all four grain types to analyse the organic materials present. The system used was a 6890N GC System Gas Chromatograph from Agilent Technologies coupled with a 5975 Mass Selective Detector (also Agilent Technologies) with a single quadrupole mass spectrometer equipped with a PTV injector. The mass spectrometer was operating in the electron impact (EI) positive mode (70 eV). The MS transfer line temperature was 280 °C; the MS ion source temperature was kept at 230 °C; and the MS quadrupole temperature was 180 °C. The detailed analytical procedure is described in Lluveras et al. (2010). The sample was digested in a microwave oven model MLS-1200 MEGA Milestone. The acidic hydrolysis of proteins was performed using a power of 250 W for 10 min and 500 W for 30 min with 30 mL of 6 N HCl at 160 °C for 40 min. The acidic hydrolysis of polysaccharides was performed using a power of 500 W for 20 min, at 120 °C, with 500 μl of TFA 2M. Saponification was performed using a power of 200 W for 60 min at 80 °C, with 300 μL of KOH in ETOH 10% wt. The detection limit (LOD) and the quantization limit (LOQ) of amino acids, aldoses, uronic acids and fatty and dicarboxylic acids were calculated. At a statistical significance level of 0.05, the LOD and LOQ of the proteinaceous, glycerolipids and saccharide materials were as follows:

- Proteinaceous materials: LOD: 0.2 μg; LOQ: 0.4 μg
- Glycerolipids: LOD: 1.2 μg; LOQ: 2.5 μg
- Saccharide materials: LOD: 0.3 μg; LOQ: 0.6 μg.

2.3. PXRD

Powder X-ray diffraction data were measured at room temperature using a PANalytical X'Pert PRO diffractometer, equipped with CuKα radiation (λ = 1.5418 Å) and a solid-state PIXcel detector (PANalytical B.V., The Netherlands). The samples were mounted between two Kapton foils and measured in transmission geometry over the range 5–70° 2θ.

2.4. LIBS

Laser-Induced Breakdown Spectroscopy analysis (Miziolek et al., 2006) was performed using the double pulse MODI' LIBS Instrument (Bertolini et al., 2006). The instrument uses two Nd:YAG lasers at the fundamental wavelength (1064 nm). One laser pulse was delayed by 1 μs relative to the other. The energy delivered in each laser pulse was around 60 mJ in 10 ns. The analyzed spectra correspond to a single measurement. The plasma signal was collected by an AVANTES spectrometer, with an acquisition gate of 2.48 ms and a delay after the second laser pulse of 2 μs.

2.5. (ATR) FT-IR

The samples were subjected to Attenuated Total Reflection Fourier Transform Infrared spectroscopy (ATR) FT-IR. All FT-IR spectra were recorded with a Spectrum-100 from Perkin Elmer equipped with an ATRU diamond. 64 scans were recorded from each sample with a resolution of 4 cm^{-1}. Acquisition ranged from 600 cm^{-1} to 4000 cm^{-1}.

2.6. Micro-Raman

Micro-Raman measurements were carried out using a Renishaw RM 2000 instrument, coupled with an optical Leica DLML microscope, equipped with a NPLAN objective 50×. The laser source was an argon ion laser (Ar^+) with a wavelength of $\lambda = 514.5$ nm and a laser power output at the objective of around 2 mW. The spectrometer consists of a single grating monochromator (1200 lines mm^{-1}), coupled with a CCD detector, a RenCam 578 × 400 pixels (22 μm × 22 μm) cooled by a Peltier-element. The spectral calibration of the instrument was performed on the 520.5 cm^{-1} band of a silicon wafer.

2.7. ICP-MS

Minute sub-samples of the ink were analyzed by ICP-MS. Each sample (white, green, black, and brown/black grains) was re-suspended in 1 mL of Milli-Q water and digested in acid in a microwave oven (Milestone Ethos 900-Mega II), in a Teflon vessel by adding a mixture of 4 mL of 67–69% HNO_3, 2 mL of 40% HF and 1 mL of 37% HCl. HNO_3 and HCl were SpS™ grade Super Purity Solvent from Romil, Cambridge, UK. Mineralization was achieved with the following microwave oven program: 20 min to reach 220 °C at 1400 W; 15 min at 220 °C and 1400 W; ventilation for 30 min. The solution was then quantitatively transferred into polystyrene liners and stored at +4 °C until the ICP-MS analysis was performed.

The analyses were carried out in triplicate on an Agilent 7700 ICP-MS, equipped with a frequency-matching RF generator and 3rd generation Octopole Reaction System (ORS^3), operating with helium as cell gas on diluted samples (1:10 v/v Milli-Q water). The parameters were set as follows: radiofrequency power 1550 W, plasma gas flow 14 L min^{-1}; carrier gas flow 0.99 L min^{-1}; He gas flow 4.3 mL min^{-1}. The Octopole Reaction System was activated to improve the metal quantification because of the interferences by polyatomic species produced by a combination of isotopes coming from plasma, reagents and matrix. ^{103}Rh was used as an internal standard (50 μg mL^{-1} final concentration). Multi-element calibration standards were prepared in 5% HNO_3 at 4 different concentrations (1, 10, 50, and 100 μg L^{-1}). The standard addition approach for calibration on 4 concentration levels was used in order to keep the matrix-induced variations to a minimum. At least three replicates of each calibration standard were run. Moreover, in order to correct possible instrumental drifts, ^{103}Rh was added as internal standard to all the samples and calibration standards. It should be noted that the samples were analyzed by two different analytical techniques, LIBS and ICP-MS, in order to monitor possible sample inhomogeneity.

2.8. Proteomic analyses

The identification of the proteinaceous material in the ink sample was carried out following the same proteomic analytical procedure described previously (Leo et al., 2009), except for a preliminary incubation of the sample in strongly protein denaturing conditions (6M urea) that was introduced in order to favour the exposure of the proteinaceous material to the action of proteases.

A black sub-sample, KLR-8227, of ca 500 μg was digested in an enzymatic reaction by proteomics-grade trypsin. A pre-treatment of the solid sample with 6M urea was carried out by incubation for 1 h in 20 μL followed by sonication for 30 min at room temperature. The sample was then 6-fold diluted with ammonium bicarbonate 10 mM pH 7.5 and enzymatic digestion carried out by addition of 1 μg of trypsin at 37 °C for 16 h. The supernatant was then recovered by centrifugation and the peptide mixture was concentrated and purified using a reverse-phase C18 Zip Tip pipette tip (Millipore). The peptides were eluted with 20 μL of a solution made of 50% acetonitrile, 0.1% formic acid in Milli-Q water and analyzed by LC–MS/MS.

The peptide mixtures were analyzed using a CHIP MS 6520 QTOF mass spectrometer equipped with a capillary 1200 HPLC system and a chip cube (Agilent Technologies, Palo Alto, CA). After loading, the peptide mixture (8 μL in 0.1% formic acid) was first concentrated and washed at 4 μL min^{-1} in 40 nL enrichment column (Agilent Technologies chip), with 0.2% formic acid in 2% acetonitrile as eluent. The sample was then fractionated on a C18 reverse-phase capillary column (75 μm × 43 mm in the Agilent Technologies chip) at flow rate of 400 nL min^{-1} with a linear gradient of eluent B (0.2% formic acid in 95% acetonitrile) in A (0.2% formic acid in 2% acetonitrile) from 7 to 60% in 50 min.

2.9. Carbon isotopes and attempts at radiocarbon dating

Radiocarbon dating was attempted on two samples at the Groningen AMS facility in The Netherlands, as described in detail in van der Plicht et al. (2000). The first sample was not pre-treated in any way, *i.e.* without the usual AAA pre-treatment procedure (acid–alkaline–acid). The second was treated with 4% HCl at room temperature in order to remove carbonates. The samples were combusted to CO_2 and transformed into graphite for AMS measurement (Aerts-Bijma et al., 2001). The stable isotope ratios $\delta^{13}C$ were measured on an elemental analyser/isotope ratio mass spectrometer (Fisons Instruments EA/IRMS) (Aerts-Bijma et al., 2001).

3. Results

3.1. GC–MS

The combined GC–MS analytical procedure allows identification of glycerolipids (linseed oil, walnut oil, poppy seed oil, and egg), natural waxes (beeswax and Carbauba wax), proteinaceous materials (animal glue, milk or casein, egg, and garlic), plant resins (such as Pinaceae resin, mastic, dammar, and sandarac) and animal resins (shellac), and polysaccharide materials (such as starch, tragacanth gum, arabic gum, fruit tree gum, guar gum, or karaya gum) in the same micro sample (Lluveras et al., 2010). The procedure is based on a multi-step chemical pre-treatment entailing solvent extractions and microwave-assisted chemolysis of the sample, in order to separate three fractions: an amino acidic, a lipid-resinous, and a saccharide fraction. The amino acids in KLR-8007 were at the quantization limit, and the relative content of the sample analyzed is shown in Table 2.

The absence of hydroxyproline indicates the absence of animal glue in the sample. To determine the source of the proteinaceous

Table 2
Amino acid relative percentage content of the bulk sample KLR-8007.

Sample	Ala	Gly	Val	Leu	Ile	Ser	Pro	Phe	Asp	Glu	Hyp
KLR-8007	9.2	14.7	8.8	16.0	8.9	6.6	4.9	6.2	10.1	14.7	0.0

material in the sample, the amino acid percentage content was subjected to a multivariate statistical analysis together with a data set of 121 reference samples of animal glue, casein, and egg (whole egg, albumen and yolk) (Bonaduce et al., 2009) using principal component analysis (PCA) (Brereton, 2004). The resulting score plot, presented in Fig. 4, clearly reveals that the sample is located in the egg cluster.

The lipid-resinous fraction of the sample (chromatogram not reported) revealed the presence of small amounts of fatty acids, and some hydroxylated fatty acids (above the detection limit), indicating the presence of traces of a lipid material partially oxidized. The profile cannot be ascribed to either a drying oil or egg lipids (Colombini et al., 2010), and must thus be related to the material used to prepare the black pigment and not to the binder.

The saccharide fraction showed the presence of sugars at the quantization limit. The chromatogram of the saccharide fraction is presented in Fig. 5 and the relative sugar percentage content is listed in Table 3. The presence of arabinose and galactose, together with the absence of xylose and mannose points to the presence of *Gum Arabica* (Lluveras et al., 2010).

3.2. PXRD

The single grain of sample KLR-8223 produced a diffraction pattern that could be matched completely to that of monohydrocalcite, $CaCO_3 \cdot H_2O$ (Fig. 6, Effenberger, 1981). The remaining samples, KLR-8224, KLR-8225 and KLR-8226, did not yield any measurable diffraction pattern. This does not necessarily exclude that the samples are crystalline, since the amount of each sample was significantly smaller than for KLR-8223 and smaller than would usually be examined using this equipment.

3.3. FT-IR, Raman, and LIBS

3.3.1. Sub-sample KLR-8223 (white)

The presence of monohydrocalcite ($CaCO_3 \cdot H_2O$), which was detected as the only crystalline phase by PXRD, is confirmed by both Raman and FT-IR (Fig. 7). The main monohydrocalcite bands cited in the literature are easily identifiable in the FT-IR spectra:

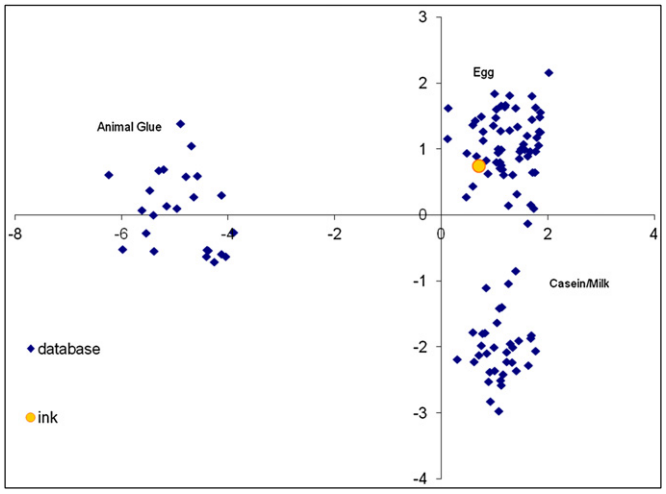

Fig. 4. Results of the GC–MS analyses. The graph shows the principal component analysis score plot of the amino acid relative percentage content of the bulk sample KLR-8007. The PCA analysis was performed using XLstat 6.0 software (Addinsoft, France) on the correlation matrix of the data. The first two components accounted for 82% of the variance in the data. The blue points are database entries for animal glue, egg, and casein. The yellow circle is KLR-8007. (For interpretation of the references to colour in this figure legend, the reader is referred to the web version of this article.)

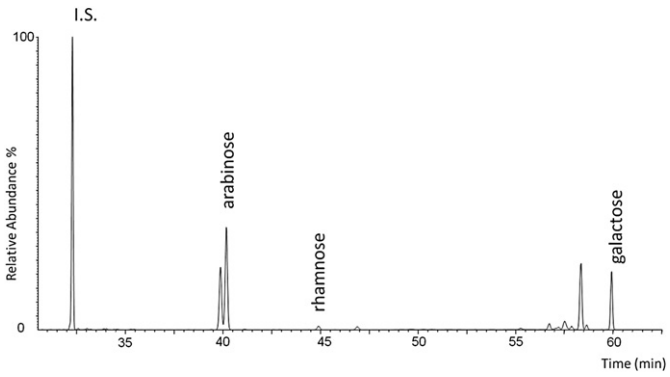

Fig. 5. SIM chromatogram of the saccharide fraction of the bulk sample KLR-8007. The sugars over the detection limit are indicated. I.S. is the internal standard (mannitol).

a strong doublet corresponding to the asymmetric C–O vibrations at 1408 and 1487 cm^{-1} and the bands at 700, 871 and 1067 cm^{-1} corresponding to the carbonate stretching modes. Moreover, the O–H stretching bands at 3225 cm^{-1} and the H_2O deformation band at 1700 cm^{-1} are also observed (Coleyshaw et al., 2003; Neumann and Epple, 2007; Senorale-Pose et al., 2008; Jones and Jackson, 1993). Calcium is also abundant in the LIBS spectrum (Fig. 8).

3.3.2. Sub-sample KLR-8224 (black)

The Raman spectrum of the black sub-sample KLR-8224 shows the presence of calcium carbonate ($CaCO_3$) as the main component: the peak at 1087 cm^{-1} is characteristic of calcite (Burgio and Clark, 2001). Calcite is also confirmed by the bands at 1400, 870 and 710 cm^{-1} in the FT-IR spectra (Fig. 9, right), which are characteristic of calcite. The band around 1000 cm^{-1} in the FT-IR spectra has been attributed to the presence of small amounts of silicates in the sample (Pretti and Singh, 2007; Madejova, 2003). However, the presence of a non-intense broad band at around 1550 cm^{-1} in the Raman spectrum of KLR-8224, can be interpreted as the result of the presence of carbon black. When reported in the literature, FT-IR spectrum of the black pigment *vine black* shows an intense band at around 1000 cm^{-1} (Vila et al., 2007). The LIBS spectrum (Fig. 10) shows the organic nature of the sample with a major C peak and a C–N peak. The fact that silicates were not detected by LIBS is attributed to sample inhomogeneity.

3.3.3. Sub-sample KLR-8225 (green)

Sample KLR-8225 was too small to allow analysis by LIBS and FT-IR, therefore only Raman analysis was performed. The Raman spectrum taken from the green grains (Fig. 11) suggests that it is a copper-based green pigment that has suffered degradation. This degradation could be due to the laser light, even though very low laser energy was used for acquisition of the spectrum. A similar degradation phenomenon was seen by Mattei et al. (2008) in the degradation of azurite to tenorite under laser irradiation. The green grain could, however, also has been degraded before the analysis.

3.3.4. Sub-sample KLR-8226 (brown/black)

Both Raman and FT-IR results for sub-sample KLR-8226 show the presence of carbon black. The Raman spectrum (Fig. 12)

Table 3
Glycoside profile of the bulk sample KLR-8007.

Sample	Sugars (% relative)								
	Xyl	Arab	Rham	Fuc	Gal ac	Gluc ac	Gluc	Mann	Galact
KLR-8007	0.0	38.9	5.4	0.0	0.0	0.0	0.0	0.0	55.7

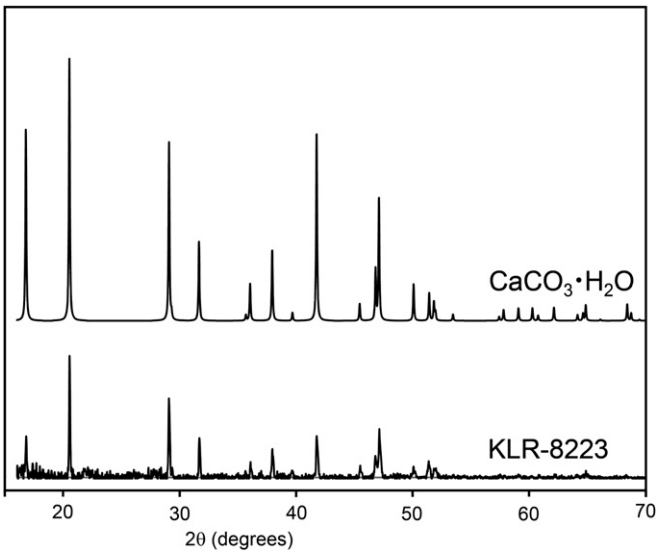

Fig. 6. Powder X-ray diffraction pattern for KLR-8223 in the range 15–70° 2θ, and simulated pattern for monohydrocalcite ($CaCO_3 \cdot H_2O$) (Effenberger, 1981). There are no diffraction peaks at lower angles. The broad features associated with the background in the region 15–30° 2θ are produced by the Kapton foils.

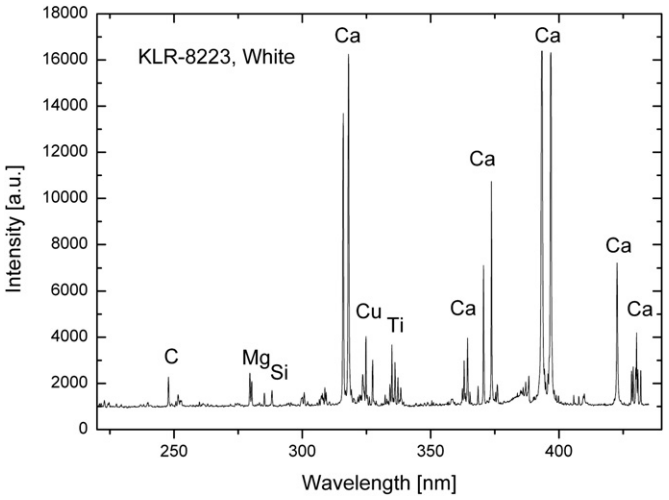

Fig. 8. LIBS spectrum of sub-sample KLR-8223 white.

resembles that of the black pigment reference materials reported by Bell et al. (1997), which lists two broad bands at ca 1325 cm^{-1} and ca 1580 cm^{-1}. It is interesting to note the absence of any band at around 950 cm^{-1}, which would correspond to phosphates. The absence of this band suggests that the sample consists of a lamp black or vine black, as both black pigments are devoid of calcium

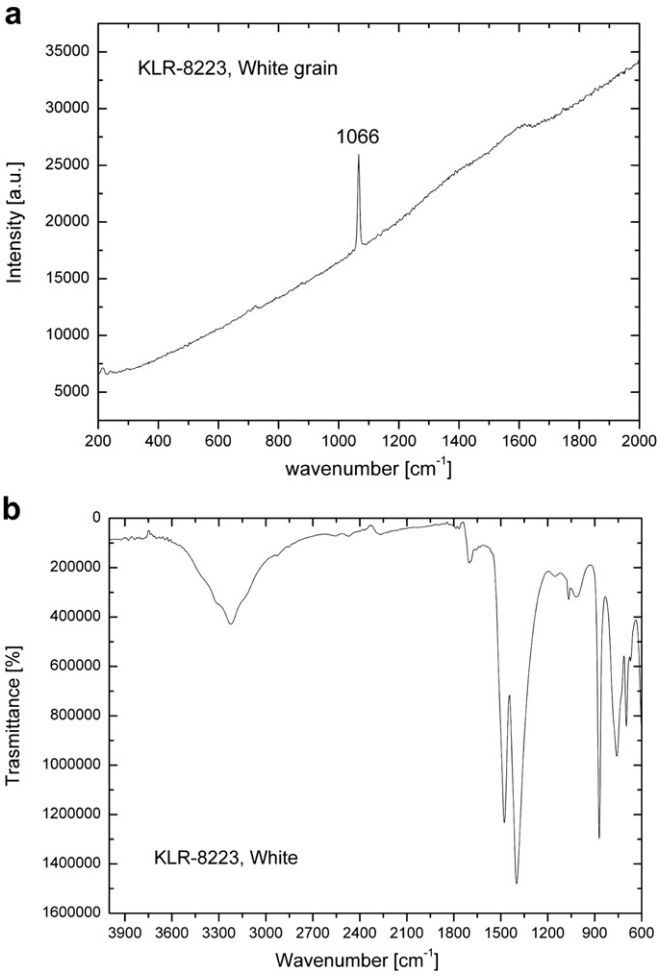

Fig. 7. (a) Raman and (b) FT-IR spectra of sub-sample KLR-8223 white.

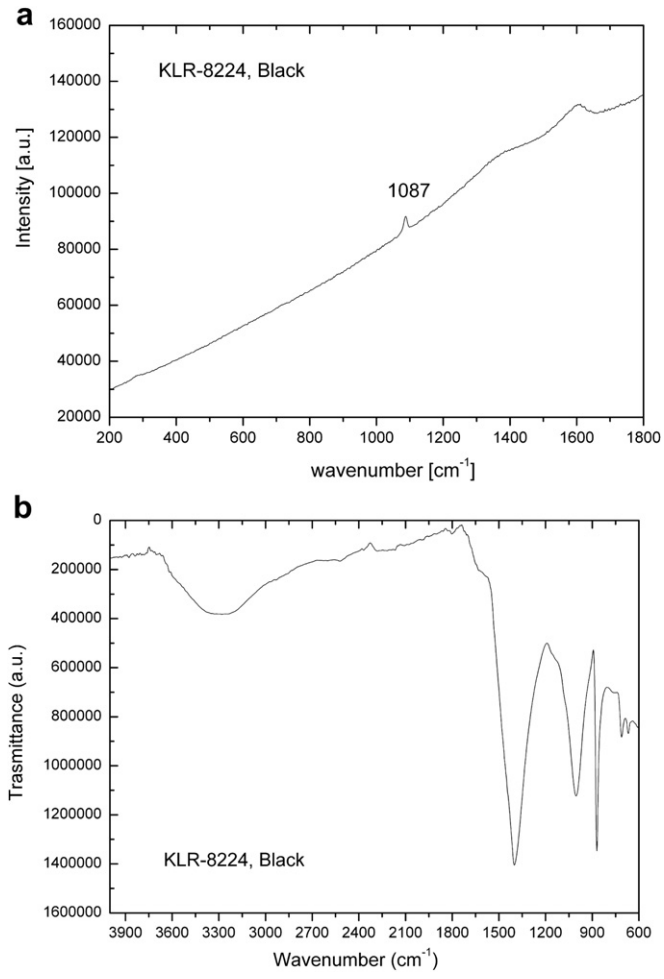

Fig. 9. (a) Raman and (b) FT-IR spectra of sub-sample KLR-8224 black.

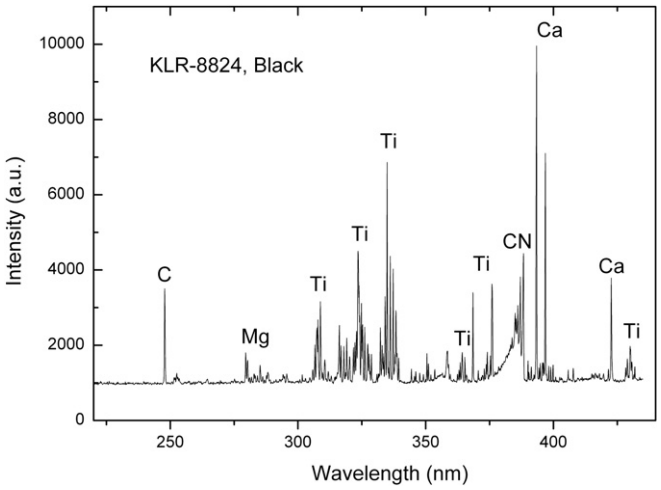

Fig. 10. LIBS spectrum of sub-sample KLR-8224 black.

phosphate (Bell et al., 1997). Moreover, the FT-IR spectrum, showing mainly a band at around 1000 cm^{-1}, resembles closely that of vine black shown in the literature (Vila et al., 2007). Lamp black, containing only amorphous charcoal, does not exhibit any relevant FT-IR signal (Vila et al., 2007). Therefore, the evidence points to vine black as the black pigment in the ink sample, supporting the same identification made for sub-sample KLR-8224, and it definitely excludes the presence of ivory or bone black as these are characterized by the presence of phosphates. Moreover, from the spectra obtained with the diode laser, it is evident that the brown/black grains contain iron-based compounds, which is substantiated by the LIBS spectrum showing a complex mixture of elements: among others Fe, Si, Mg, and Cu (Fig. 13).

3.4. ICP-MS

Intra-day reproducibility was checked by measurements of the sample 3 times on the same day. Inter-day reproducibility was checked by analysis of a similar digested solution on 3 separate days over a period of 1 week. The performance of the ICP-MS analysis is listed in Table 4, and the results of the ink analyses are shown in Table 5.

The Ca-concentration in KLR-8223 corresponds stoichiometrically to a composition of ca 37 wt% monohydrocalcite, which is consistent

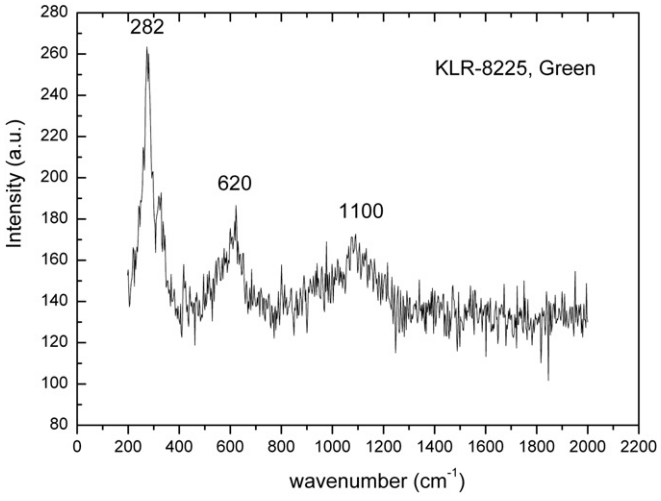

Fig. 11. Raman spectrum for sub-sample KLR-8225 green.

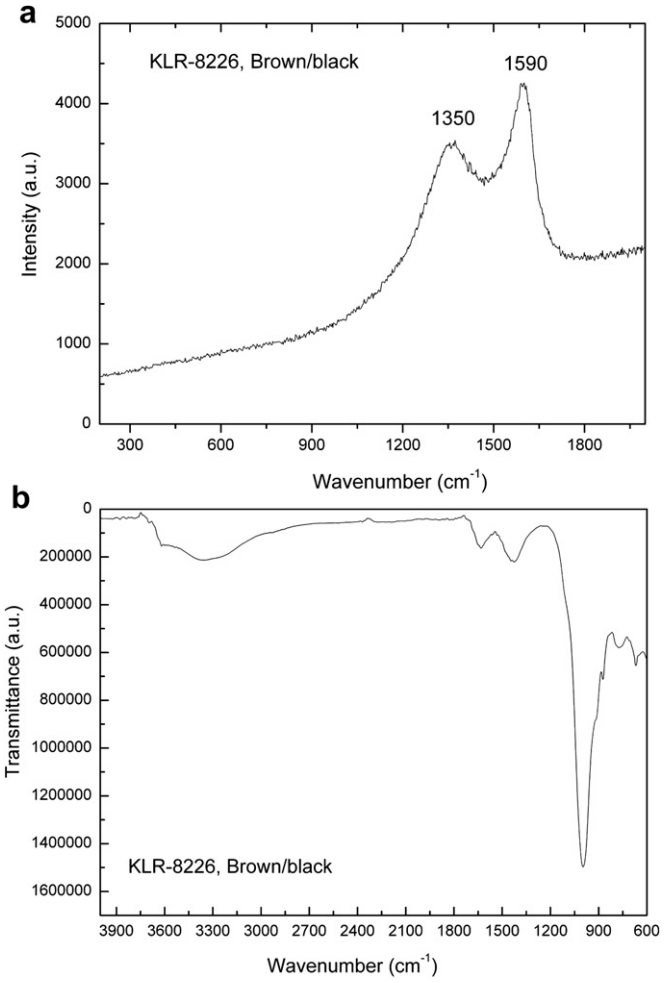

Fig. 12. FT-IR spectra of sub-sample KLR-8226 brown/black obtained with Argon laser (a) and the Raman spectrum (b).

with the LIBS data. Carbon is not analyzed by ICP-MS, but the other elements in the black grain KLR-8224 exhibit more or less even concentrations. The green sample, KLR-8225, has a Ca-concentration corresponding stoichiometrically to ca 25 wt% monohydrocalcite and ca 9 wt% Cu, both of which are consistent with the LIBS data. Besides Ca, the brown/black grain KLR-8226 is high in Al and Fe, indicating the possible presence of clay minerals, which is also in accordance with the other measurements in this study.

3.5. Proteomic analyses

Peptide analysis was performed using data-dependent acquisition of one MS scan (mass range from 400 to 2000 m/z) followed by MS/MS scans of the three most abundant ions in each MS scan. Raw data from nano-LC–MS/MS analyses were used to query non-redundant protein databases (UniprotSprot, either on all entries or with the taxonomy restriction to Chordata) using the MASCOT software (Matrix Science, Boston, USA), without the insertion of any fixed chemical modification but the possible oxidation of methionine and the formation of pyroglutammic acid from glutamine residues at the N-terminal position of peptides. The identification of 4 peptides from chicken ovalbumin allowed confident identification of egg in the sample (Table 6).

As further confirmation of the identification, a residual aliquot (1/5 of the initial sample) was analyzed on LC–MS/MS with a Selected Ion Monitoring program, in order to fragment selectively

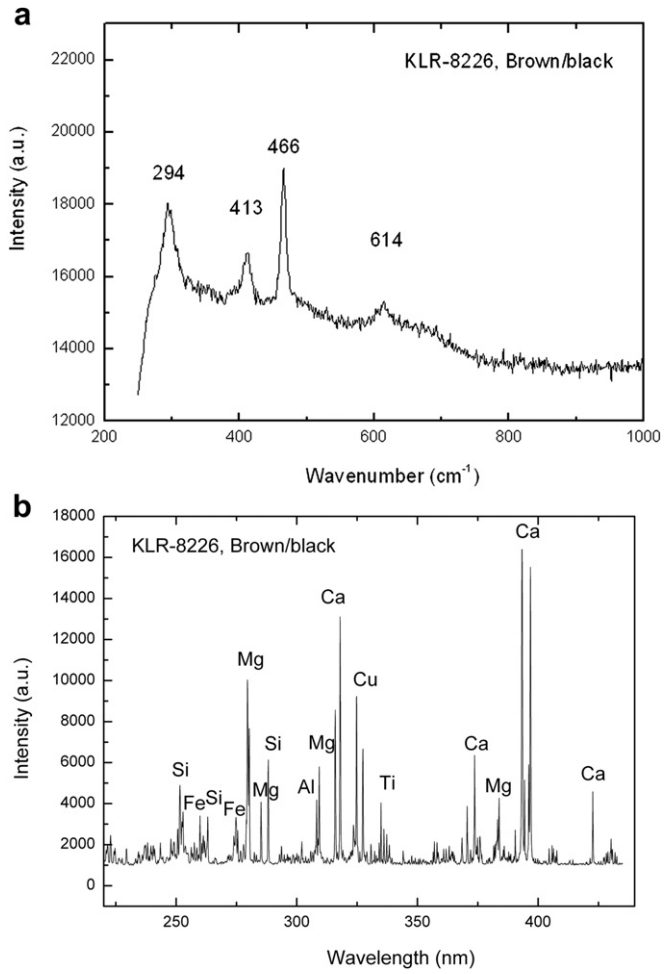

Fig. 13. The FT-IR spectrum obtained with a diode laser (a) and LIBS spectrum (b) of sub-sample KLR-8226 brown/black.

the target ions that had been identified in the previous run. This strategy allowed improvement of the quality of the fragmentation spectra which could all be manually inspected and unambiguously interpreted, and which confirmed the assignment to the peptides inferred above. As an example, in Fig. 14 is shown the fragmentation spectra of the doubly charged ion at 844.42 *m*/*z* that can be interpreted as the peptide GGLEPINFQTAADQAR spanning from residue G128 to residue R143 of ovalbumin from *Gallus gallus* (P01012).

3.6. Carbon isotopes and attempts at radiocarbon dating

The $\delta^{13}C$-values expressed in ‰ deviation from the standard and the carbon content (wt% C) are listed in Table 7. The ^{14}C-age is conventional, *i.e.* reported in BP (Mook and van der Plicht, 1999). The ^{14}C date is rounded off to the nearest 5, and the error is 1-sigma. The $\delta^{13}C$ and C% are normally intended as quality parameters for the dated material (van Strydonck et al., 1999).

Table 5
Quantitative analysis by ICP-MS of a set of the four optically discernable grain types. The concentrations are given in wt%.

	KLR-8223 white	KLR-8224 black	KLR-8225 green	KLR-8226 brown/black
Sample weight (mg)	0.025	0.660	0.030	0.220
Mg	1.71	0.31	2.10	0.17
Al	1.96	0.04	4.82	1.19
K	1.33	0.17	0.82	0.14
Ca	14.76	0.54	8.85	1.12
Ti	1.12	0.03	0.15	0.02
Cr	0.44	0.02	0.35	0.03
Mn	0.07	0.01	0.28	0.01
Fe	2.44	0.50	1.28	0.64
Cu	1.55	1.52	6.62	0.47
Sr	0.26	0.01	0.11	0.02
Pb	0.19	0.19	1.51	0.06
Total wt%	25.82	3.33	26.89	3.87

For reasons explained below we do not believe that the dates reflect the true age of the ink, but rather the combined date of the ink and some contaminants.

4. Discussion

In 2002, Torleif Elgvin and Stephen Pfann noted a further detail that had not previously been reported: according to Kando, the Schøyen inkwell had been found together with a bronze incense altar. Based on comparative parallels of the items, their luxurious nature, and the plausibility that a surface find by the Bedouin would be from an upper layer, Elgvin and Pfann tentatively concluded that the Schøyen inkwell should be attributed to Qumran Period III (although they noted Period II was also possible). Period III is the period of habitation at Qumran defined by the original excavator, Roland de Vaux, to be after the First Jewish Revolt of 66–70 CE. According to de Vaux, Qumran was at this time inhabited by Roman soldiers, after the sectarians believed to be associated with the scrolls had been forced to flee and the site was destroyed by fire (de Vaux, 1973). Virtually all Qumran scholars hold that none of the texts in the caves were produced after the First Revolt. Elgvin and Pfann suggested that Period III was a Jewish habitation, although also unconnected to the scrolls. The notion that Period III Qumran may have been Jewish, not Roman, appears to have first been suggested by Doudna (2001: 744, building from 1999: 39–42). One of the three inkwells found by de Vaux (the one found in locus 36) also was from a Period III context, *i.e.* also unrelated to the scrolls by the traditional archaeological understanding.

Doudna's argument was as follows: as was noted by Konik (1998), there is no evidence that the inhabitants at Qumran following the Jewish Revolt of 66–70 CE were Romans. No ostracon naming a Roman military commander, no Roman military supplies, or any other sign of Roman occupation have been found at Qumran. The premise of de Vaux's argument for a Jewish/Roman distinction between pre-68 and post-68 Qumran was a distinction between Jewish First Revolt coins and Roman city coins. As de Vaux put it: "these two groups of coins are distributed precisely between two successive levels, the Jewish coins certainly belonging to the lower

Table 4
ICP-MS performances in terms of limit of detection (LoD), limit of quantification (LoQ), and intra- and inter-day reproducibility. Limits of detection and quantification are expressed as ng/g, while intra- and inter-day reproducibility values are reported as percentage (%).

Parameter	Al	Cr	Cu	Fe	Mn	Pb	Mg	K	Ca	Ti	Sr
LoD (ng/g)	1.58	0.06	0.46	0.06	0.09	0.08	1.08	1.75	15.9	0.20	0.04
LoQ (ng/g)	1.47	0.16	0.30	78.2	0.10	0.10	3.07	59.7	19.1	0.22	0.16
Intra-day reprod (%)	1.96	3.64	1.44	6.50	4.69	1.39	1.96	3.36	12.8	5.90	3.63
Inter-day reprod (%)	2.15	4.01	1.58	7.15	5.16	1.53	2.16	3.69	14.2	6.49	3.99

Table 6
Identification of the proteins in the ink sample after trypsin digestion and LC–MS/MS analysis. Proteins were identified by searching the UniprotSprot database, with no taxonomy restriction, with MSMS Ion search Mascot software (Matrix Science, http://www.matrixscience.com/help/interpretation_help.html). Ions score is $-10*\mathrm{Log}(P)$, where P is the probability that the observed match is a random event. In this analysis, individual ion scores >35 indicate identity or extensive homology. Protein scores are derived from ion scores as a non-probabilistic basis for ranking protein hits. Only identification of proteins with at least two peptides was considered significant.

Protein (accession number)	Matched sequence (peptide score) (oxidation of methionine, and pyro-Glu formation at Gln at the N-terminus of peptides were inserted as variable modifications in the MS/MS Ion Search Program)	Sequence coverage %	MW
Ovalbumin (P01012)	^{128}GGLEPINFQTAADQAR^{143} (23) ^{201}VTEQESKPVQMMYQIGLFR^{219} (39) ^{160}NVLQPSSVDSQTAMVLVNAIVFK^{182} (39) ^{230}ILELPFASGTMSMLVLLPDEVSGLEQLESIINFEK^{264} (22)	24	42,854

level, that of the destruction [Period II], and the Roman coins certainly belonging to the level above this [Period III]..." (1973: 41). This distinction claimed by de Vaux, which was widely repeated in secondary literature, was contradicted by the report of Humbert and Chambon (1994): 306, concerning Qumran locus 40, in which hidden inside the same lamp were found coins now identified as from both the First Revolt and Caesarea of 67/68 CE. Likewise, Roman city coins were found in the same level with Agrippa I coins at loci 8A and 32. It seems that de Vaux's basis for his Period III argument arose from these early coin identifications which in certain cases were later discovered to be erroneous. Leonard commented correctly that de Vaux's Period III scheme unravelled almost completely in light of updated published coin identifications (1997: 230). These factors raised the question whether there was a Period III at all.

But in favour of de Vaux's suggestion that Romans destroyed the site when they arrived in Jericho in 68 CE are arguments from analogy concerning Roman procedures as told by Josephus in *War*: destroying by fire villages in the neighbourhood of a site taken (*War* 4.437–438, 443, 446); the strategy of leaving no outpost of rebels in the rear in preparation for a focused siege on Jerusalem (*War* 4.413, 450); control of roads and passages (*War* 4.445, 486); and resettling of destroyed sites with deserters to the Romans and assigning them to rebuild the destroyed or burnt sites (*War* 4.438, 444, 448). Therefore it is very plausible that the fire at Qumran in 68 CE was caused by the Romans, as de Vaux thought, but the people to whom Qumran was given after the fire need not be the garrison of Roman soldiers of de Vaux's portrayal. They may have been Jews who previously had deserted to the Roman side (Doudna, 2001: 744).

The suggestion of a Jewish character of Qumran's Period III was taken up by Elgvin and Pfann (2002) and argued in detail by Taylor (2006). Magen and Peleg (2007: 62) also noted that it seemed "highly unlikely that a Roman garrison would have been stationed at a burned, abandoned site, whose water supply system was no longer operative". Magness, however, appears to continue to maintain that Qumran Period III was occupied by a garrison of Roman soldiers (Magness, 2002: 62, 2004: 134). A study of Roman inkwells of Khairy (1980) concluded that "the bronze inkwell from Qumran was known elsewhere from about the turn of the Christian era to the second century A.D." (p. 161).

It should also be noted that Magen Broshi, former curator of the Shrine of the Book, has expressed doubt about the reliability of the antiquities dealer Kando's information concerning the Schøyen inkwell: "He [Broshi] thinks the items are too beautiful in style to have come from Qumran, and that they more likely derive from a larger Hellenistic site on the East Bank such as Jerash" (Elgvin and

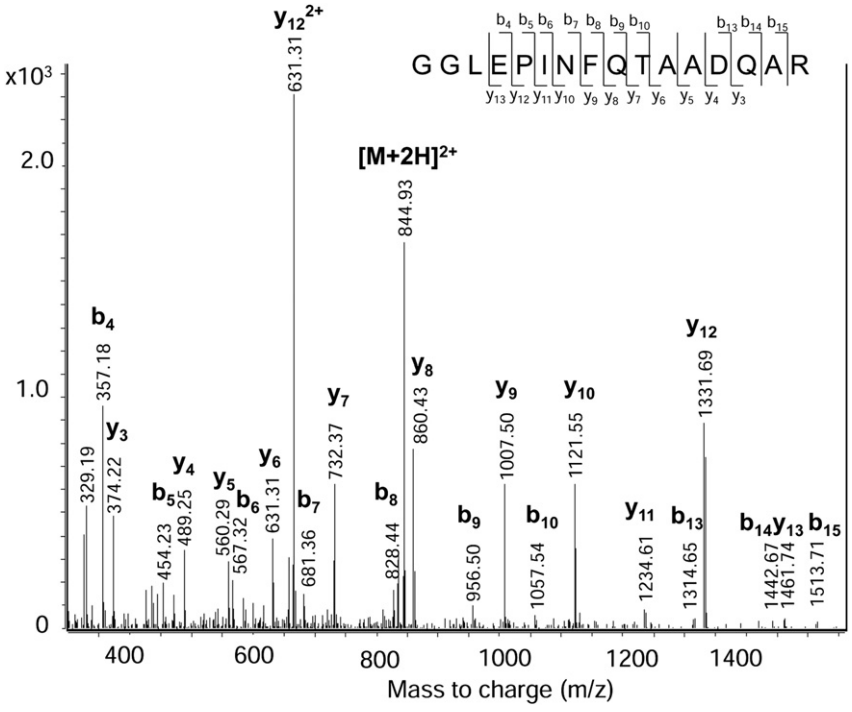

Fig. 14. LC–MS/MS spectrum of the black grain KLR-8227.

Table 7
Results of the stable carbon isotope measurements and the attempts to radiocarbon date the ink.

GrA	Mass used (mg)	Pre-treatment	Age (BP)	1-sigma	$^{13}\delta$ (‰ VPDB)	C (wt%)
49,448	7.8	None	2780	50	−19.97	6.0
50,219	21.5	4% HCl at RT	2425	40	−24.04	2.4

Pfann, 2002: 26, citing oral communication with Broshi). But Elgvin and Pfann note that another bronze inkwell which is so similar to the Schøyen inkwell that it "suggests the same manufacturer" was found on the West bank (p. 21). Elgvin and Pfann also note a range of luxury items found at Qumran which appear to be associated with Period III, such that the luxurious Schøyen inkwell would not be out of place. The reported objection of Broshi to the claim of Qumran provenance for the Schøyen inkwell therefore seems insubstantial, and we accept that the Schøyen inkwell originated from Qumran.

What then, about the ink inside the inkwell? None of the analyses in the present work have proven that the ink in the Schøyen inkwell was manufactured at Qumran. Any ink, parchments or other commodity utilized in the Qumran settlement could have been imported. It is possible that the constituents of the ink were imported separately and used together with local Qumran products to produce the ink. However, it is also possible that the ink was manufactured at Qumran with all its components.

It was a priority during this study to radiocarbon date the ink to see if it agreed with the period of habitation at Qumran. However, this goal was not achieved. We suspect that in both dating attempts there remained some contamination in the samples. The $\delta^{13}C$ of sample GrA-49448 was −19.97‰ VPDB, which is far from the expected value. It is likely that the major part of the carbon in the sample is in the black colour pigment, which is soot produced by burning an organic material under restricted oxygen supply. As has been shown above, the most likely candidate for the soot is vine black. The soot is therefore probably derived from a material which prior to burning is expected to have a $\delta^{13}C$-value of −25‰ VPDB. The process of making vine black is likely to produce an isotopic fractionation towards more negative values in the soot, but we have no way of knowing precisely how much more negative than −25‰ VPDB. However, it is clear that the date of the first sample (analyzed before we identified monohydrocalcite by PXRD), was affected by the presence of monohydrocalcite, which is most likely derived from a geological formation of considerable age. We therefore attempted a second radiocarbon date, this time on a pre-treated sample. Experiments on a minute part of the sample showed that a full AAA would dissolve the sample completely, so it was decided to expose the second sample to one acid treatment only (the first A in the AAA). This treatment undoubtedly removed the monohydrocalcite, but even so the $\delta^{13}C$ was measured to −24.04‰ VPDB, which is more positive than −25 and still more positive than the isotope fractionated soot. We therefore suspect that even after the sample was pre-treated in acid there remained a contaminant with a $\delta^{13}C$-value significantly more positive than −25‰ VPDB. We have not been able to identify this contamination. However, one possibility is that it could be tar. Josephus wrote that there were pieces of tar floating in the Dead Sea the size and shape of "headless bulls" (*War* 4.479 (4.8.3)).

Although our attempts to radiocarbon date the ink have failed, it remains likely—judging from the progression in $\delta^{13}C$-values from the untreated sample to the A-treated sample—that the majority of the carbon in the sample is derived from C3 plant material, which would be consistent with the identification of vine black by Raman and FT-IR spectroscopy. Besides the plant-derived carbon, there is a small amount (maybe 5–15 wt%) of organic material with a more positive $\delta^{13}C$-value than −25‰; a possible candidate for this minor component is tar. We are thus only able to state that the true date of the ink is younger by an unknown number of years than 750–400 BCE, which is the 2 sigma calibrated date interval of our last dating attempt, but besides this, the dating issue remains unsolved.

The information about the composition of the ink, on the other hand, was unexpectedly rich. The inventory of organic compounds revealed by the GC–MS analysis identified as many as three different compounds: 1) a polysaccharide, *Gum Arabica*; 2) proteins, which were then by proteomic analyses identified as albumen from the eggs of the species *Gallus gallus*; and 3) traces of lipids in the form of fatty and hydroxylated fatty acids, which could have been part of the black colour pigment. A mixture of egg white and arabic gum was thus the binder of the black pigment. Polysaccharide materials, primarily gum arabic, have been used in works of art since antiquity (Laurie, 1911; Doerner, 1934; Mills and White, 1994; Vallance, 1997). Ancient texts on painting techniques cite polysaccharide materials for different purposes (Bonaduce, 2005; Doerner, 1998; Merrifield, 2004; Cennini, 2003). Particularly during the middle ages, polysaccharide materials were used for gilding and in illuminated manuscripts (Bonaduce and Boon, 2008; Bleton et al., 1996). In the Strasburg Manuscript (15th century), the preparation of gum solutions for illuminated manuscripts is described extensively (Doerner, 1998) and they have already been identified in inks (Bleton et al., 1996). The use of albumen is also described as a binder (Mills and White, 1994). The traces of oxidised lipid found are ascribed, most likely, to the residues of the pyrolysis of vine leaves used to prepare the pigment, more than to any binder.

According to Pfann (no date): "Early results of the flotation of materials from an oven in the southern enclosure [of Qumran], excavated in 2002 and sampled again in 2004, includes a fragment of a chicken egg (the author [Pfann] is grateful to Egon Lass for this information)". In light of this report it is interesting to note that albumen from chicken egg has been identified in the ink from the Schøyen inkwell, as this resource apparently was available at Qumran. While the inventory of organic phases may not be surprising taking each component into consideration individually, the number of them leaves open the very distinct possibility of exact matching of inks with that of the Schøyen inkwell, should analyses of ink samples from the Dead Sea Scrolls or other parchments from the region become available in the future.

The analyses of the four optically distinguishable grain types encompassed microscopic and diffraction examination, the molecular techniques Raman and FT-IR, and elemental analysis by LIBS and ICP-MS. The investigations show that the ink consists of four physically very distinct phases, which can be described as: 1) a white phase consisting mainly of monohydrocalcite; 2) a black organic phase with carbon black, probably vine black, as the black colour pigment and some traces of monohydrocalcite; 3) a green phase consisting of a calcium carbonate matrix discoloured by Cu; and finally 4) a brown/black phase, consisting of carbon black colour pigment and a complex mixture of silicates. The composition of the green phase is consistent with previous analyses from the Norwegian Technical University of the inkwell bronze to 55–68 wt % Cu, 23–39 wt% Pb, and 5–8 wt% Sn; it seems likely that the high Cu values, and possibly also the smaller amounts of Pb, could be due to some chemical reaction taking place over the millennia between the bronze of the inkwell and the monohydrocalcite of the ink allowing Cu from the inkwell walls to diffuse into decomposed monohydrocalcite.

Monohydrocalcite is a rare mineral found in exotic geological settings, *e.g.* in connection with the decay of ikaite in the arctic waters of Greenland (Dahl and Buchardt, 2006), in the Shiowakka cold saline spring in Japan, where ikaite is deposited in the cold winter months but monohydrocalcite during the summer (Coleyshaw et al., 2003), in Solar Lake on the Sinai coast (Krumbein,

1975), and in South Australian beach rocks (Swainson, 2009). It has also been associated with environments in which evaporation exceeds precipitation such as salt lakes, tropical lagoons, and sabkhas (Fischbeck and Müller, 1971). Monohydrocalcite has been identified as a biomineral (Neumann and Epple, 2007), and in a variety of exotic species, such as woodlice *Porcellio scaber* (Becker et al., 2003), *Porcellio pachydermatina*, from lobster carapacethe and from plant cystoliths (Levi-Kalisman et al., 2002), in the bacteria *Halobacillus trueperi* (Rivadeneyra et al., 2004), and in bladder stones of guinea pigs (Catherine et al., 1977). Even though monohydrocalcite is found in many and very different environments all authorities agree that it is a very rare mineral.

There are no known occurrences of monohydrocalcite near Qumran, in the Judean hills or on the banks of the Dead Sea today, which leaves three possibilities open. The first is that the monohydrocalcite in the ink was imported from elsewhere (*e.g.* from Solar Lake on the Sinai shoreline). The second is that monohydrocalcite did exist near Qumran at that time but does not today. Hypothetically it is possible that a small epiphemeral lake detached from the Dead Sea in a geologic setting analogous with that of Solar Lake could have existed. The third is that a source of monohydrocalcite does exist in the vicinity of Qumran today but has not yet been discovered or identified. In any event, monohydrocalcite is not a common rock forming mineral and it must have been a very scarce resource also at the time of the main habitation in Qumran. It seems likely that the monohydrocalcite was added as filler, ensuring that the ink obtained the desired opacity.

The black colour pigment in the ink is most likely vine black, situated in the brown/black phase and in the black phase. Vine black is produced as soot made by burning grape vines. Due to the lack of phosphates in the samples, the presence of ivory black or bone black, *i.e.* soot made from burning bones or antlers can be excluded. It is interesting that fat, bones, and antlers from goats can be eliminated as a source for the black colour pigment, as hides of goats most likely were prepared in a rather complicated industrial process for the production of the parchment on which the Dead Sea Scrolls were written (Bar-Gal et al., 2001, 2010). It would have been straightforward if the bones and antlers of the goats which were available from the production of parchment had been used for the production of ivory black, provided both parchment and ink were made at the site. This was, however, not the case with the ink in the Schøyen inkwell.

It is possible that the black grains are in fact monohydrocalcite grains coated with or saturated with vine black. However, since the black grains contain monohydrocalcite and an organic phase but only minute amounts of silicates and the brown/black grains contain no monohydrocalcite, it is likely that the origin of the two types of grains are distinctly different, *i.e.* two different phases that were brought together and physically mixed.

The green phase was found to be a calcium carbonate matrix with traces of Cu. We speculate that the green phase could be degradation products of monohydrocalcite that has somehow reacted with the metal inkwell which has Cu as its main constituent. However, it has not been confirmed that the green grains are decomposed monohydrocalcite grains. The green phase could alternatively be yet another independent exotic compound. Even so, a future identification of Cu-discoloured calcium carbonate grains may act as a provenancing tool linking the ink with a metal inkwell such as the present one. As Cu occurs most abundantly in the green phase, and less abundantly in the black and brown/black phases, it seems unlikely that the Cu originated from the production of the black pigment, for instance by scraping the soot off a metallic lamp made of a Cu alloy.

Besides the carbon black, the brown/black phase contains silicates, which, judging from the high Al content could well be clay minerals. The mineralogical composition has not been established due to the small sample size, but the main element and trace element composition have been documented by the ICP-MS analysis. The pattern of variation between the elements may be used as a fingerprint to match inks from texts written with a similar ink. When looking at the abundances (Fig. 15) it is clear that the elemental fingerprint is quite similar for the black and the brown/black phases with the Al concentration as the only large difference, Al being higher in the brown/black phase. The white and the green phases resemble each other and are distinct from the black and the brown/black phases, but there are several distinct differences between the abundances of the white phase and the green phase, notably in the elements Al, Ti, Mn, and Pb.

The results of our investigation can be compiled into a list of parameters suitable for provenancing or matching the ink if similar analyses of ink on parchments from Qumran or the region become available. Ten compounds or observations listed in Table 8 have been identified that singly or in combination can act as tools for provenancing the ink. This possibility of provenancing the ink of the Dead Sea Scrolls may prove to be a very potent tool capable of solving issues of interest to scholars working on the history of Jewish texts, *e.g.* the question of whether or not some of the Dead Sea Scrolls were in fact written at Qumran, or were brought there from elsewhere, *e.g.* Jerusalem, Jericho, or Damascus.

In terms of industrial processes, handicrafts, or other information pertinent to the people inhabiting Qumran (which would be relevant under the hypothesis that the ink was manufactured at Qumran), the following items have been identified:

1) The raising of chickens (*Gallus gallus*).
2) The procurement of *Gum Arabica*.
3) The production or procurement of the black colour pigment vine black.
4) The procurement of the rare mineral monohydrocalcite.

The presence of—or agreement with—the ten parameters mentioned above in another ink, such as *e.g.* on a Dead Sea Scroll, cannot in itself provenance the ink to Qumran. What the ten parameters can do is match ink from a specific text to the producer of the ink in the Schøyen inkwell, whether the place of production of that ink was Qumran or some other site. The methodology may, however, provide unique information pertinent to assignment of scribal hands.

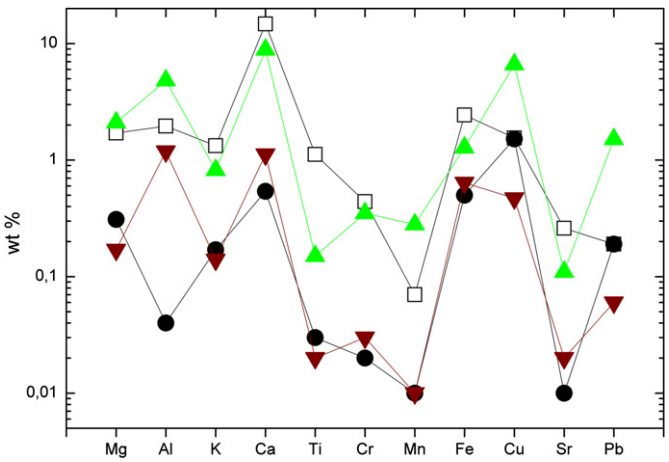

Fig. 15. Fingerprint of elemental abundances measured by ICP-MS. Squares: white grain KLR-8223; circles: black grain KLR-8224; pyramids: green grain KLR-8225; triangle on the tip: brown/black grain KLR-8226. (For interpretation of the references to colour in this figure legend, the reader is referred to the web version of this article.)

Table 8
Ten diagnostic components in or observations about the ink which can be used to diagnose provenance in the ink of parchments.

	Diagnostic component	Techniques used
1	4 optically distinct grain types: white, black, green, and brown/black	Microscope
2	Monohydrocalcite in the white grains	PXRD, Raman, FT-IR
3	Proteins, albumen of *Gallus gallus*	GC–MS, Proteins
4	Polysaccharides, *Gum Arabica*	GC–MS
5	Fatty acids and hydroxylated fatty acids	GC–MS
6	Black colour pigment with no phosphates, probably vine black	Raman, FT-IR
7	C3 plant material present in the non-carbonate carbon	MS
8	Copper in a carbonate matrix in the green grains	Raman, LIBS
9	Aluminium in the brown/black grains	LIBS, ICP-MS
10	Distinct trace element compositional fingerprint of the 4 grain types	ICP-MS

5. Conclusions

An entirely new insight has been obtained concerning the composition of the ink from the Schøyen inkwell, which could have been used in the *scriptorium* at Qumran. Ten distinct, recognizable and diagnostic parameters of the ink have been identified: (1) the ink contains four different and easily recognizable grain types: white, green, black, and brown/black; (2) the white grains are identified as the rare mineral monohydrocalcite, which is not found naturally near the Dead Sea, and therefore provides a highly specific link to Qumran; (3) the green phase consists of a degraded carbonate matrix discoloured by copper; (4) the colour pigment in the black phase can probably be identified as vine black; (5) the brown/black grains contain aluminium, probably from clay minerals; (6) protein analysis shows that albumen of *Gallus gallus* (chicken) is present in the ink as a binder; (7) *Gum Arabica*, a polysaccharide binder, is also present; (8) fatty acids and hydroxylated fatty acids are present, hypothetically as part of the black colour pigment; (9) the bulk of the organic carbon most likely originated from C3 plant material with a δ^{13}C-value of $-25‰$ VPDB; (10) the ink shows a characteristic elemental concentration pattern that can be used as a fingerprint for each of the four grain types.

These ten parameters constitute a new and potent tool for matching parchments which were inscribed with the same unique ink. This study therefore opens, for the first time, an opportunity to establish the provenance of ink on Dead Sea Scrolls and other manuscripts from Israel and the Levant at the time of main habitation at Khirbet Qumran.

Acknowledgements

Martin Schøyen is thanked for granting access to sample the inkwell. The Carlsberg Foundation and Møllerens Fond are thanked for support. The Chemistry Department of Florence University, Italy, is thanked for facilitating the Micro-Raman spectroscopy. Two anonymous referees are thanked for constructive reviews.

Appendix A. Supplementary material

Supplementary material related to this article can be found online at doi:10.1016/j.jas.2012.04.041.

References

Aerts-Bijma, A.T., van der Plicht, J., Meijer, H.A.J., 2001. Automatic AMS sample combustion and CO_2 collection. Radiocarbon 43, 293–298.
Bar-Gal, G.K., Rosenberg, T., Greenblatt, C., 2010. Animal remains from Khirbet Qumran: a case study of two bones (QUM 392 and 393) from two bone burials. In: Gunneweg, Jan, Adriaens, Annemie, Dik, Joris (Eds.), Holistic Qumran: Trans-disciplinary Research of Qumran and the Dead Sea Scrolls. Studies on the Texts of the Desert of Judah, vol. 87. Brill, Leiden, pp. 67–76.
Bar-Gal, G.K., Greenblatt, C., Woodward, S.R., Broshi, M., Smith, P., 2001. The genetic signature of the Dead Sea Scrolls. In: Goodblatt, David, Pinnick, Avital, Schwartz, Daniel R. (Eds.), Historical Perspectives: From the Hasmoneans to Bar Kokhba in Light of the Dead Sea Scrolls. Proceedings of the Fourth International Symposium of the Orion Center for the Study of the Dead Sea Scrolls and Associated Literature, 27–31 January 1999. Studies on the Texts of the Desert of Judah, vol. 37. Brill, Leiden, pp. 165–171.
Becker, A., Bismayer, U., Epple, M., Fabritius, H., Hasse, B., Shi, J., Ziegler, A., 2003. Structural characterisation of X-ray amorphous calcium carbonate (ACC) in sternal deposits of the crustacea *Porcellio scaber*. Dalton Transactions, 551–555.
Bell, I.M., Clark, R.J.H., Gibbs, P.J., 1997. Raman spectroscopic library of natural and synthetic pigments. Spectrochimica Acta Part A 53 (12), 2159–2179.
Bertolini, A., Carelli, G., Francesconi, F., Francesconi, M., Marchesini, L., Marsili, P., Sorrentino, F., Cristoforetti, G., Legnaioli, S., Palleschi, V., Pardini, L., Salvetti, A., 2006. Modi: a new mobile instrument for in situ double-pulse LIBS analysis. Analytical and Bioanalytical Chemistry 385, 240–247.
Bleton, J., Coupry, C., Sansouet, J., 1996. Approche d'etude des encres anciens. Studies in Conservation 41 (2), 95–108.
Bonaduce, I., 2005. A multiy-analytical approach for the investigation of materials and techniques in the art of gilding, Unpublished PhD thesis, Universita di Pisa.
Bonaduce, I., Boon, J.J., 2008. An integrated mass spectrometric and molecular imaging analytical approach to identify and localise constituents in paintings applied to gilded multilayer structures from the 14th to 16th C works of art. In: Colombini, M.P., Tassi, L. (Eds.), New Trends in Analytical, Environmental and Cultural Heritage Chemistry. Transworld Research Network, pp. 345–388.
Bonaduce, I., Cito, M., Colombini, M.P., 2009. The development of a gas chromatographic–mass spectrometric analytical procedure for the determination of lipids, proteins and resins in the same paint micro-sample avoiding interferences from inorganic media. Journal of Chromatography A 1216, 5931–5940.
Brereton, R.G., 2004. Chemometrics Data Analysis for the Laboratory and Chemical Plant. J. Wiley & Sons Ltd, West Sussex, England.
Burgio, L., Clark, R.J.H., 2001. Library of FT-Raman spectra of pigments, minerals, pigment media and varnishes, and supplement to existing library of Raman spectra of pigments with visible excitation. Spectrochimica Acta Part A 57, 2231–2239.
Catherine, H., Skinner, W., Osbaldiston, G.W., Wilner, A.N., 1977. Monohydrocalcite in a guinea pig bladder stone, a novel occurrence. American Mineralogist 62 (3–4), 273–277.
Cennini, C., 2003. In: Frezzato, F. (Ed.), Il libro dell'Arte, first ed. Neri Pozza Editore, Vicenza.
Coleyshaw, E.E., Crump, G., Griffith, W.P., 2003. Vibrational spectra of the hydrated carbonate minerals ikaite, monohydrocalcite, lansfordite and nesquehonite. Spectrochimica Acta Part A 59, 2231–2239.
Colombini, M.P., Andreotti, A., Bonaduce, I., Modugno, F., Ribechini, E., 2010. Analytical strategies for characterizing organic paint media using gas chromatography/mass spectrometry. Accounts of Chemical Research 43, 715–727.
Dahl, K., Buchardt, B., 2006. Monohydrocalcite in the Arctic Ikka Fjord, SW Greenland: first reported marine occurrence. Journal of Sedimentary Research 76, 460–471.
Doerner, M., 1934. The Materials of the Artist and Their Use in Painting. Harcourt, Brace, New York. 223–224.
Doerner, M., 1998. Los materiales de pintura y su empleo en el arte, 18ª edición. Editorial Reverté, Barcelona.
Doudna, G., 1999. Redating the Dead Sea Scrolls Found at Qumran. Qumran Chronicle 8 [special issue, Dec. 1999]. Enigma Press, Cracow.
Doudna, G., 2001. 4Q Pesher Nahum. A Critical Edition. JSPS 35. Sheffield Academic Press, Sheffield.
Effenberger, H., 1981. Kristallstruktur und Infrarot- Absorptionsspektrum von synthetischem Monohydrocalcite, $CaCO_3 \cdot H_2O$. Monatshefte für Chemie 112, 899–909.
Elgvin, T., in collaboration with S. Pfann, 2002. An incense altar from Qumran? Dead Sea Discoveries 9 (1), 20–33.
Fischbeck, R., Müller, G., 1971. Monohydrocalcite, hydromagnesite, nesquehonite, dolomite, aragonite, and calcite in speleothems of the Fränkische Schweiz, Western Germany. Contributions to Mineralogy and Petrology 33 (2), 87–92.
Goranson, S., 1992. An inkwell from Qumran. Michmanim 6, 37–40.
Goranson, S., 1993. Qumran: the evidence of the inkwells. Biblical Archaeology Review 19 (6), 67.
Goranson, S., 1994. A hub of scribal activity? Biblical Archaeology Review 20 (5), 37–39.
Humbert, J.-B., Chambon, A. (Eds.), 1994. Fouilles de Khirbet Qumrân et de 'Ain Feskha. Album de photographies. Répertoire du fonds photographiques. Synthèse des notes de chantier du Père Roland de Vaux, NTOA.SA 1, vol. 1. Editions Universitaires-Vandenhoeck & Ruprecht, Fribourg-Göttingen.
Jones, G.C., Jackson, B., 1993. Infrared Transmission Spectra of Carbonate Minerals. Chapman & Hall, Glasgow, UK.
Khairy, N.I., 1980. Inkwells of the Roman Period From Jordan. Levant. 155–162.
Konik, J., 1998. Qumran – the analysis of the chronology and the attempt to define the character of the building. Qumran Chronicle 8, 105–107.

Krumbein, W.E., 1975. Biogenic monohydrocalcite spherules in lake sediments of Lake Kivu (Africa) and the Solar Lake (Sinai). Sedimentology 22, 631–634.
Laurie, A.P., 1911. The Materials of the Painters' Craft. J.B. Lippincott, Philadelphia. 164 p.
Leo, G., Cartechini, L., Pucci, P., Sgamellotti, A., Marino, G., Birolo, L., 2009. Proteomic strategies for the identification of proteinaceous binders in paintings. Analytical and Bioanalytical Chemistry 395, 2269–2280.
Leonard, R.D., 1997. Numismatic evidence for the dating of Qumran (review article). Qumran Chronicle 7, 225–234.
Levi-Kalisman, Y., Raz, S., Weiner, S., Addadi, L., Sagi, I., 2002. Structural differences between biogenic amorphous calcium carbonate phases using X-ray absorption spectroscopy. Advanced Functional Materials 12 (1), 43–48.
Lluveras, A., Bonaduce, I., Andreotti, A., Colombini, M.P., 2010. A GC/MS analytical procedure for the characterization of glycerolipids, natural waxes, terpenoid resins, proteinaceous and polysaccharide materials in the same paint micro sample avoiding interferences from inorganic media. Analytical Chemistry 82, 376–386.
Madejova, J., 2003. FT-IR techniques in clay mineral studies. Vibrational Spectroscopy 31, 1–10.
Magen, Y., Peleg, Y., 2007. The Qumran Excavations 1993–2004: Preliminary Report. IAA, Jerusalem.
Magness, J., 2002. The Archaeology of Qumran and the Dead Sea Scrolls. Eerdmans, Grand Rapids, Michigan.
Magness, J., 2004. Debating Qumran. Collected Essays on its Archaeology. Peeters, Leuven.
Mantouvalou, I., Wolff, T., Hahn, O., Rabin, I., Lühl, L., Pagels, M., Malzer, W., Kanngiesser, B., 2011. 3D micro-XRF for cultural heritage objects: new analysis strategies for the investigation of the Dead Sea Scrolls. Analytical Chemistry 83, 6308–6315.
Mattei, E., de Vivo, G., De Santis, A., Gaetani, C., Pelosi, C., Santamaria, U., 2008. Raman spectroscopic analysis of azurite blackening. Journal of Raman Spectroscopy 39, 302–306.
Merrifield, M.P., 2004. The Art of Fresco Painting in the Middle Ages and the Renaissance. Courier Dover Publications, ISBN 0486432939.
Mills, J., White, R., 1994. The Organic Chemistry of Museum Objects, second ed. Butterworth Heineman, London.
Miziolek, A.W., Palleschi, V., Schechter, I., 2006. In: Laser Induced Breakdown Spectroscopy. Cambridge University Press.
Mook, W.G., van der Plicht, J., 1999. Reporting ^{14}C activities and concentrations. Radiocarbon 41, 227–239.
Neumann, M., Epple, M., 2007. Monohydrocalcite and its relationship to hydrated amorphous calcium carbonate in biominerals. European Journal of Inorganic Chemistry, 1953–1957.
Nir-El, Y., Broshi, M., 1996. Black ink of the Qumran Scrolls. Dead Sea Discoveries 3 (2), 157–167.
Pfann, S., no date. A Table Prepared in Wilderness: Pantries and Tables, Pure Food and Sacred Space at Qumran. http://www.uhl.ac/articles/TableInWilderness.pdf.
van der Plicht, J., Wijma, S., Aerts, A.T., Pertuisot, M.H., Meijcr, H.A.J., 2000. Status report: the Groningen AMS facility. Nuclear Instruments and Methods in Physics Research B172, 58–65.
Pretti, S.N., Singh, B.K., 2007. Instrumental characterization of clay by XRF, XRD and FT-IR. Bulletin of Material Science 30 (3), 235–238.
Rabin, I., Hahn, O., Wolff, T., Masic, A., Weinberg, G., 2009. On the origin of the ink of the thanksgiving scroll (1QHodayota). Dead Sea Discoveries 16, 97–106.
Rivadeneyra, M.A., Parraga, J., Delgado, R., Ramos-Cormenzana, A., Delgado, G., 2004. Biomineralization of carbonates by *Halobacillus trueperi* in solid and liquid media with different salinities. FEMS Microbiology Ecology 48, 39–46.
Senorale-Pose, M., Chalar, C., Dauphin, Y., Massard, P., Pradel, P., Marıin, M., 2008. Monohydrocalcite in calcareous corpuscles of *Mesocestoides corti*. Experimental Parasitology 118, 54–58.
Steckoll, S., 1968. Investigation of the inks used in writing the Dead Sea Scrolls. Nature 220, 91–92.
Steckoll, S., 1969. An inkwell from Qumran. Mada 13, 260–261 [in Hebrew].
van Strydonck, M., Nelson, D.E., Combre, P., Bronk Ramsey, C., Scott, E.M., van der Plicht, J., Hedges, R.E.M., 1999. What's in a ^{14}C date. In: Actes du 3ème Congrès International ^{14}C et Archéologie, Lyon, 6–10 avril 1998, 433–448. Mémoires de la Société Préhistorique Française, vol. 26.
Swainson, I.P., 2009. The structure of monohydrocalcite and the phase composition of the beachrock deposits of Lake Butler and Lake Fellmongery, South Australia. American Mineralogist 93 (7), 1014–1018.
Taylor, J., 2006. Khirbet Qumran in period III. In: Galor, Katharina, Humbert, Jean-Baptiste, Zangenberg, Jürgen (Eds.), Archaeological Interpretations and Debates. Proceedings of a Conference Held at Brown University, November 17–19 2002. Brill, Leiden, pp. 133–146.
Vallance, S.L., 1997. Applications of chromatography in art conservation: techniques used for the analysis and identification of proteinaceous and gum binding media. Analyst 122, 75R–81R.
de Vaux, R., 1973. Archaeology and the Dead Sea Scrolls: the Schweich Lectures of the British Academy 1959. Oxford University Press, Oxford.
Vila, A., Ferrer, N., Garcia, J.F., 2007. Chemical composition of contemporary black printing inks based on infrared spectroscopy: basic information for the characterization and discrimination of artistic prints. Analytica Chimica Acta 591, 97–105.

Journal of Applied Microbiology

Journal of Applied Microbiology ISSN 1364-5072

ORIGINAL ARTICLE

Comparison of the action of different proteases on virulence properties related to the staphylococcal surface

M. Artini[1]*, R. Papa[1]*, G.L. Scoarughi[1], E. Galano[2], G. Barbato[3], P. Pucci[2] and L. Selan[1]

1 Department of Public Health and Infectious Diseases, Sapienza University, Rome, Italy
2 Department of Organic Chemistry and Biochemistry,Federico II University, Complesso Universitario Monte Sant'Angelo, Naples, Italy
3 Department of Science and Chemical Technologies, University of Rome Tor Vergata, Rome, Italy

Keywords
biofilm, cellular invasion, metalloprotease, serine protease, virulence inhibition.

Correspondence
Laura Selan, Public Health and Infectious Diseases, Sapienza University, Piazzale Aldo Moro 5, 00185 Rome, Italy. E-mail: laura.selan@uniroma1.it

*These authors equally contributed to this work.

2012/1377: received 1 August 2012, revised 19 September 2012 and accepted 4 October 2012

doi:10.1111/jam.12038

Abstract

Aims: The purpose of this study was to evaluate the antimicrobial efficacy of five different proteases belonging to two different families on *Staphylococcus aureus* and *Staphylococcus epidermidis* strains.

Methods and Results: We used three serine proteases and two metalloproteases in single species biofilm formation assays and in human cell invasion processes. Following each protease incubation with bacterial cells, surface protein patterns were analysed by SDS-PAGE and zymography. Some differently expressed proteins were identified by mass spectrometry.

Conclusions: The effect of tested proteases on biofilm formation was not related to the protease category but was strain-dependent and was related to the biofilm formation capacity of each staphylococcal strain. Some proteases showed a nonspecific and indiscriminate effect on surface proteins, while others induced a discrete and reproducible action on protein profiles.

Significance and Impact of the Study: The inhibition of the surface-related virulence factors is a promising avenue to overcome persistent infections caused by bacterial biofilms. To this end, we show here that proteases, in particular the metalloprotease serratiopeptidase, can interfere with adhesion and invasion of eukaryotic cells and biofilm formation in staphylococci and their use could represent a viable treatment for the development of novel combination therapies.

Introduction

Staphylococcus epidermidis and *Staphylococcus aureus*, the most relevant species of their genus, inhabit the skin and mucous membranes of animals and humans. Surface-mediated infectious disease transmission is a major concern in various settings, including schools, hospitals and food-processing facilities. Several surface proteins expressed by these bacteria interact with solid surfaces and are essential in bacterial adhesion and promote, together with exopolysaccharides (EPS), biofilm formation and maturation. In *Staph. aureus*, these proteins also take part in the invasion process of different mammalian cell types. Both species produce various microbial surface proteins recognizing adhesive matrix molecules of eukaryotic cells (MSCRAMMS), as well as other adhesive proteins, which enable bacteria to bind different surfaces moieties. Among them, fibrinogen, collagen and elastin adhesins (*fnbA-B*, *clfA-B*, *cna* and *ebpS*), sialoprotein-binding proteins (*bbp*, *sdrC* and *sdrE*), extracellular matrix-binding proteins (*map*, *eap* and *sasG*), biofilm-associated proteins (*bap*) and adhesins/autolysins (*atl*) were identified (Cucarella *et al.* 2002; Rohde *et al.* 2007). Although biofilm formation in staphylococci typically relies on the production of extracellular polysaccharide adhesin (PIA/PNAG), strains that are able to produce a protein-dependent biofilm were also identified (Götz 2002; O'Gara 2007; Rohde *et al.* 2007; Vergara-Irigaray *et al.* 2009; Christner *et al.* 2010).

Considering the impact of bacterial biofilms on human health, industrial and food-processing activities, the interest in the development of approaches for the prevention

and treatment of staphylococcal adhesion and biofilm formation capabilities has increased. A viable approach should target staphylococcal adhesive properties without affecting bacterial vitality to avoid the rapid appearance of escape mutants. Molecules implicated in active biofilm dispersal include glycosidases, deoxyribonucleases and proteases (Kaplan 2010). Furthermore, the production of extracellular enzymes that degrade adhesive components in the biofilm matrix is a basic mechanism used in the biological competition between phylogenetically different bacteria (Brook 1999; Wang *et al.* 2007, 2010). An inhibitory effect of D-amino acids on *Staph. aureus* biofilm has been recently demonstrated (Hochbaum *et al.* 2011). With the aim of targeting some surface-related virulence features of staphylococci, our first choice was to use proteases. An interesting report by Iwase *et al.* (2010) showed an interesting example of a bacterial exoprotease acting as an antibiofilm and anticolonization agent. In this work, the authors demonstrate that the protease *Esp* secreted by *Staph. epidermidis in vivo* hinders colonization and biofilm formation of *Staph. aureus* cells living in the same ecological niche. Moreover, in the work of Hochbaum *et al.* (2011), it is shown that the action on staphylococcal surface-associated proteins of some D-amino acids resulted in impaired biofilm maturation, while the same amino acids had no effect on EPS. This evidence, together with previous work, gave a significant clue on the importance of surface-associated proteins in the entire process of biofilm development (Hochbaum *et al.* 2011) and not only in initial attachment to the substrate.

In our work, we examined the effect of two families of proteases on *Staph. aureus* and *Staph. epidermidis* strains. We established the following selection criteria: (i) with a relatively small number of proteases, we should explore a large variety of different substrate specificity (i.e. recognition of aromatic, charged, small/large residues, etc.); (ii) the proteases should belong to at least two different enzymatic classes; (iii) they should explore a broad range of molecular weight (to allow for different steric hindrance impact); (iv) they should be monomeric, soluble and function without the need of activating factors and (v) last but still important practically, the proteases should be commercially available. In particular, we used three serine proteases (proteinase K, PK; trypsin, TRY; and chymotrypsin, CHY) and two metalloproteases (serratiopeptidase, SPEP; carboxypeptidase A, CpA) in biofilm formation assays and in human cell invasion processes (invasion only for *Staph. aureus*). Some of these proteases are already utilized in human therapy for different purposes (Martin *et al.* 2002; Hao *et al.* 2006). SPEP is widely used as an anti-inflammatory agent (Kee *et al.* 1989; Mazzone *et al.* 1990), and it has been shown to modulate adhesin expression in some bacterial species and to enhance antibiotic efficacy towards biofilm-forming bacteria (Selan *et al.* 1993; Maheshwari *et al.* 2006; Longhi *et al.* 2008). Our present results show that proteases could represent a viable treatment that could lead to the development of novel combination therapies to prevent staphylococcal colonization and infection.

Materials and methods

Bacterial strains and culture conditions

Bacterial strains used in this work were the following: *Staph. aureus* ATCC 6538P (DSMZ 346), reference strain for antimicrobial testing; *Staph. aureus* ATCC 25923 (DSMZ 1104), clinical isolate; *Staph. aureus* ATCC 12598 (DSMZ 20372), clinical isolate from septic arthritis; *Staph. epidermidis* ATCC 35984 (DSMZ RP62A), reference strain isolated from infected catheter; *Staph. epidermidis* XX-17, clinical isolate; and *Staph. epidermidis* O-47, clinical isolate from septic arthritis kindly provided by Prof. Gotz.

Brain heart infusion broth (BHI; Oxoid, Basingstoke, UK) was used for biofilm formation and planktonic cultures for *Staph. aureus* strains; for *Staph. epidermidis* strains, tryptic soy broth (TSB; Oxoid) was used instead. For all strains, biofilm formation was assessed in static chamber system where planktonic cultures were grown under vigorous agitation both at 37°C.

Cells

HeLa cells were cultured in minimal essential medium with Earle's salts (MEM/EBSS), supplemented with 10% foetal calf serum, 1% glutamine and 1% penicillin–streptomycin in an atmosphere of 95% air and 5% CO_2 at 37°C. All media were from Euroclone. Monolayers were used 48 h after seeding.

Chemicals

SPEP (2540 U mg^{-1}; Takeda Italia Farmaceutici, Rome, Italy), PK (949 U mg^{-1}; Euroclone, Pero, Italy), TRY from bovine pancreas (10 000 U mg^{-1}; Sigma-Aldrich, St Louis, MO) and CHY type I-S from bovine pancreas (58·3 U mg^{-1}; Sigma-Aldrich) were dissolved in PBS and stored at −20°C. Aqueous suspension of CpA from bovine pancreas (1704 U ml^{-1}; Sigma-Aldrich) was stored at 4°C.

Detection of *Staphylococcus aureus* and *Staphylococcus epidermidis* virulence-associated genes

DNA preparation and PCR were performed as follows. Thirty microlitres of each bacterial culture in planktonic

conditions was harvested by centrifugation at 3542 ***g***. The bacterial pellet was washed twice in TE buffer (Tris–HCl 10 mmol l^{-1} pH 8, EDTA 10 mmol l^{-1} pH 8) and resuspended in 100 μl of TE buffer, boiled for 10 min and then centrifuged at 16 627 ***g*** at 4°C to eliminate bacterial debris. Ten microlitres of supernatant containing bacterial DNA partially purified was used for PCR amplifications. Primers and PCR conditions used are summarized in Table 1.

Quantification of biofilm formation in the presence of a protease

Biofilm formation of staphylococcal species was evaluated in the presence of the aforementioned proteases, each at a concentration of 50 U ml^{-1}. Preliminary experiments were carried out to assess the effect of selected proteases on the growth rate of previously described bacterial strains. Cultures were treated with serial dilutions of

Table 1 Primers used for the PCR-based detection of staphylococcal factors involved in the pathogenesis of foreign-body-associated infections

Putative function of encoded protein	Gene	Sequence	References
Staphylococcus epidermidis			
N-acetylglucosaminyltransferase involved in PIA synthesis	*icaR*	5′-TACTGTCCTCAATAATCCCGAA 5′-GGTACGATGGTACTACACTTGATG	Cafiso *et al.* 2004
	icaA	5′-TCTCCCCCTTATTCAATTTTCT 5′-CGATACAATACATCCAAAATACTC	
	icaD	5′-CAGACAGAGGCAATATCCAAC 5′-ACAAACAAACTCATCCATCCG	
	icaB	5′-ATGGCTTAAAGCACACGACGC 5′-TATCGGCATCTGGTGTGACAG	
	icaC	5′-ATCATCGTGACACACTTACTAACG 5′-CTCTCTTAACATCATTCCGACGCC	
Fibronectin adhesin	*embp*	5′-AGCGGTACAAATGTCAAT 5′-AGAAGTGCTCTAGCATCATCC	Rohde *et al.* 2007
Housekeeping gene	*pta*	5′-TTAAAATCGTATTACCTGAAGG 5′-GACCCTTTTGTTGAAAAGCTTAA	Enright *et al.* 2000
Intercellular adhesin	*aap*	5′-AAACGGTGGTATCTTACGTGAA 5′-CAATGTTGCACCATCTAAATCAGCT	Rohde *et al.* 2007
Promotes binding to polystyrol; vitronectin adhesin	*atlE*	5′-CAACTGCTCAACCGAGAACA 5′-TTTGTAGATGTTGTGCCCCA	Rohde *et al.* 2007
Staphylococcus aureus			
N-acetylglucosaminyltransferase involved in PIA synthesis	*icaR*	5′-AGTAGCGAATACACTTCATCTTTGA 5′-GTTGTACCGTCATACCCCTTCTCTG	Cafiso *et al.* 2007
	icaA	5′-CATTGAACAAGAAGCCTGACA 5′-ATATGATTATGTAATGTGCTTGGATG	Cafiso *et al.* 2007
	icaD	5′-ATGGTCAAGCCCAGACAGAG 5′-CGTGTTTTCAACATTTAATGCAA	Arciola *et al.* 2001
	icaB	5′-AGAATCGTGAAGTATAGAAAATT 5′-AGAATCGTGAAGTATAGAAAATT	Kiem *et al.* 2004
	icaC	5′-ACACAGCGTTTCACGATACCG 5′-CCAATAGTCTCCATTTGCTAACGC	Valle *et al.* 2003
Putative adhesin with unknown ligands	*sdrC*	5′-AGCGGTACAAATGTCAAT 5′-GTACTTGAAATAAGCGGTTG	Rohde *et al.* 2007
Fibrinogen adhesin	*clfA*	5′-GTAGGTACGTTAAATCGGTT 5′-CTCATCAGGTTGTTCAGG	Rohde *et al.* 2007
Fibronectin adhesin	*fnbA*	5′-CACAACCAGCAAATATAG 5′-CTGTGTGGTAATCAATGTC	Rohde *et al.* 2007
Housekeeping gene	*gyr*	5′-TTATGGTGCTGGGCAAATACA 5′-CACCATGTAAACCACCAGATA	Wolz *et al.* 2002
Biofilm formation in *Staph. aureus* bovine mastitis isolates	*bap*	5′-CCCTATATCGAAGGTGTAGAATTGCAC 5′-GCTGTTGAAGTTAATACTGTACCTGC	Rohde *et al.* 2007
Adherence to desquamated nasal epithelial cells	*sasG*	5′-CGCGGATTCGCAGCTGAAAACAATATT 5′-CCAAGCTTTAATTCTGTTATTGTTTTTGG	Rohde *et al.* 2007
Autolysin involved in initial adhesion	*atl*	5′-CAGTTAGCAAGATTGCTCAAG 5′-CCGTTACCTGTTTCTAATAGG	Wootton *et al.* 2005

SPEP, PK, TRY, CHY and CpA, respectively (1 : 2 dilutions starting from 200 U ml^{-1}), and bacterial growth was monitored over 24 h. Bacterial growth curves were nearly superimposable both in the presence and in the absence of each protease. Quantification of *in vitro* biofilm production in the presence and in the absence of each protease was based on method previously reported (Artini *et al.* 2011). Briefly, the wells of a sterile 24-well flat-bottomed polystyrene plate were filled with 900 μl of the appropriate medium (BHI for *Staph. aureus* and TSB for *Staph. epidermidis*, respectively). A volume of 100 μl of overnight bacterial cultures was added into each well. The first row contained the untreated bacteria, while each of the remaining rows contained 50 U ml^{-1} of a different single protease per row. The plates were incubated aerobically for 24 h at 37°C. After rinsing with PBS, adhered cells were stained with 0·1% crystal violet, rinsed twice with double-distilled water and thoroughly dried as previously described (Christensen *et al.* 1994). The dye bound to adherent cells was resolubilized with 20% (v/v) glacial acetic acid and 80% (v/v) ethanol per well. The OD of each well was measured at 590 nm. Each data point is composed of three independent samples. Based on the OD per ml obtained from crystal violet coloration, each strain was classified as strong, medium and weak biofilm producer, with appropriate rescaling of the OD range accounting for the different multiwell format utilized in this study (according to the literature, Cafiso *et al.* 2004, 2007).

Adhesion–invasion assays (antibiotic protection assays)

Staphylococcus aureus 6538P from 18-h cultures in BHI broth, grown in the absence of proteases, were further subcultured up to OD_{600} = 0·5 at 37°C in BHI with or without 50 U ml^{-1} SPEP and 50 U ml^{-1} CpA, respectively. HeLa cells were cultured in 24-well plates (BD Falcon, Franklin Lakes, NJ) to obtain semi-confluent monolayers (1×10^5 cells/well) and then were inoculated with 0·05 ml of logarithmic-growing bacterial suspensions at a MOI (multiplicity of infection) of about 10 bacteria per cell. The adhesion–invasion assays were carried out by infecting cells for 1 h at 37°C. Adhesion and invasion were conducted in parallel on twin cellular monolayers. Loosely bound bacteria were removed from the cell monolayers by two washes with PBS. The cells were then lysed with 0·025% Triton X-100 and plated on tryptic soy agar (TSA; Oxoid) to determine viable bacteria (A: cellular adhesion plus invasion). After incubation, to evaluate the infection rates, the monolayers were washed with PBS and 0·5 ml of fresh medium containing 200 μg ml^{-1} of gentamicin was added to each well and maintained for 1 h at 37°C to kill noninternalized bacteria. Cells were then lysed by the addition of 0·025% Triton X-100 and plated on TSA to count viable intracellular bacteria (B: cellular invasion). We further calculated adhesion efficiency by subtraction of B-cfu to A-cfu. Adhesion and invasion efficiency were expressed as percentage of the inoculated bacteria that adhered or invaded HeLa cells, respectively.

Data represent the mean of three independent experiments.

Surface protein extraction and processing

Surface proteins were extracted as follows. Briefly, after centrifugation of 50 ml of each bacterial culture grown in the presence and in the absence of 50 U ml^{-1} of each protease (OD_{600} = 0·6), pellets were washed twice in PBS and then suspended in 500 μl of PBS containing 1% SDS. Samples were incubated at 37°C for 15 min, and after centrifugation, the supernatants were collected and used for further analyses. The protein content was determined by the Bradford procedure (Sambrook and Russell 2001).

SDS-PAGE and zymogram

Equivalent amounts of protein samples were used for each condition (5 μg). SDS-PAGE was carried out by standard methods (Sambrook and Russell 2001) with SDS-polyacrylamide separating gel (10% acrylamide, pH 8·8). Following electrophoresis, proteins were stained with Coomassie Brilliant Blue (Bio-Rad, Hercules, CA). The renaturation of SDS-PAGE was performed as previously reported (Artini *et al.* 2011). Briefly, SDS-PAGE was prepared adding 0·2% (w/v) lyophilized *Micrococcus luteus* cells provided by Sigma, to detect the lytic activities. After electrophoresis, the gels were soaked and then transferred into the renaturing buffer (50 mmol l^{-1} Tris–HCl, pH 8·0, containing 1% Triton X-100) and shaken for 2 h at 37°C. The renatured autolysins appeared as clear translucent bands on opaque background. For each experiment, two gels were simultaneously prepared and electrophoresed. No difference was noted in the migration of the standards because of the presence of *M. luteus* cells in the gel.

In situ digestion and protein identification

Protein identification following *in situ* digestion was performed as previously reported (Artini *et al.* 2011). Briefly, protein bands were excised from the gel and washed; protein samples were reduced, and free cysteines were alkylated by incubation with 10 mmol l^{-1} DTT and 55 mmol l^{-1} iodoacetamide, respectively. After wash, gel particles were digested with trypsin. Peptides were

extracted and then analysed by LC-MS/MS using a CHIP-QTOF 6520 equipped with a capillary 1200 HPLC system and a chip cube (Agilent Technologies, Palo Alto, CA, USA). After loading, each peptide mixture was first concentrated, washed and then fractionated on a C18 reverse-phase capillary column (75 μm × 43 mm in the Agilent Technologies chip). Peptide analysis was performed using data-dependent acquisition of one MS scan (mass range from 300 to 2000 *m*/*z*) followed by MS/MS of the three most abundant ions using in-house MASCOT software (Matrix Science, Boston, MA, USA).

Results

Identification of genes involved in adhesion and correlation with biofilm production

In staphylococci, bacterial adhesion and biofilm formation depend on a complex interplay of adhesins comprising fibrinogen-binding proteins (FnBP-A/B, Embp and ClfA), sialoprotein-binding proteins (SdrC), extracellular matrix-binding proteins (SasG), biofilm-associated protein (Aap and Bap), proteins involved in PIA synthesis (IcaADBC), autolysins (Alt and AtlE), etc. (Rohde *et al.* 2007). The six staphylococcal strains here considered (see Material and Methods section) were investigated by PCR to assess the presence of genes coding for various proteins involved in adhesion and biofilm formation. Results are summarized in Table 2. Two of three *Staph. epidermidis* strains were positive for genes involved in PIA synthesis (XX-17 strain is negative for the presence of entire *ica* locus). Furthermore, all strains were positive for *atlE*, *aap* and *embp* genes coding for adhesins. Determination of biofilm formation showed a strong production for the O-47 strain (2·08 ± 0·11), medium/strong production for the reference strain ATCC35984 (0·74 ± 0·07) and a medium/weak biofilm formation for the XX-17 strain (0·35 ± 0·02).

From a genetic point of view, the three *Staph. aureus* strains are identical for the presence of *ica* operon and adhesion genes. The biofilm-forming ability of *Staph. aureus* strains was tested by quantitative assay. They showed different capabilities to form biofilm that can be schematized as reported: ATCC 6538P is a strong biofilm producer (1·65 ± 0·15), ATCC 25923 is a medium/strong biofilm producer (0·79 ± 0·21), and ATCC 12598 is a medium/weak biofilm producer (0·22 ± 0·03).

Effect of two different classes of protease on staphylococcal biofilm formation

The effect of each protease was related to the biofilm formation capacity of the staphylococcal strains here considered. Results are summarized in Fig. 1 and Table 3.

The inhibition of biofilm formation ranges from almost total (approx. 5% of residual biofilm formation) to just slight inhibition (approx. 90%). Taking into account wide fluctuation in biofilm formation among three replicates of the same experimental set, in the range of 90–110% biofilm formation, the process was considered essentially not affected, being this value the same as the control. When the value was >110%, the action of the protease was considered as favouring biofilm formation. The statistical significance of effect obtained from each protease treatment was calculated with unpaired *t*-Student test.

TRY and CpA hampered biofilm formation, in some cases slightly, of three bacterial strains, PK of 4, CHY of 5 and only SPEP showed inhibiting activity of all the tested strains (see Fig. 1 and Table 3).

The inhibition of biofilm formation among strains was compared. Inhibition in *Staph. aureus* strains was slightly more pronounced than that in *Staph. epidermidis*, as shown in Fig. 1, with a stronger inhibition exerted on the best biofilm former *Staph. aureus* 6538P. In *Staph. aureus*, CHY and SPEP exhibited the stronger inhibition capability (36 and 59% biofilm formation on average, respectively), while PK had a weak inhibition effect (69% biofilm formation), TRY did not show any effect (107% biofilm formation on average), and CpA displayed an average favouring effect (approx. 140% biofilm formation). In *Staph. epidermidis*, SPEP, PK and CHY showed an almost equivalent inhibitory action with values ranging 70–80% biofilm formation, TRY had no effect, while CpA again exhibited a favouring effect (approx. 240%).

SPEP action seemed to be proportional to the ability to form biofilm of each tested strain. The esometalloprotease CpA showed a good effect on stronger biofilm producers (*Staph. aureus* ATCC 6538P, ATCC 25923 and *Staph. epidermidis* O-47) but, conversely, seemed to favour biofilm formation in the case of medium and weak biofilm producers (*Staph. aureus* ATCC 1298, *Staph. epidermidis* ATCC 35984 and XX-17). The three serine proteases showed different behaviour on each bacterial strain, inhibiting and/or facilitating biofilm formation (Fig. 1).

Analysis of surface protein pattern following the treatment with proteases

Cell surface protein samples from treated and untreated cultures of all the strains were simultaneously analysed by SDS-PAGE and zymogram assays. *Staph. aureus* ATCC 6538P was chosen as representative strain because it is a strong biofilm producer and it showed a better response to treatment with proteases. Fig. 2 shows the SDS

Table 2 Genotype characterization of staphylococcal strains

	Staphylococcus aureus			*Staphylococcus epidermidis*		
Putative function of encoded protein	ATCC 6538P (DSMZ 346)	ATCC 25923 (DSMZ 1104)	ATCC 12598 (DSMZ 20372)	O-47	ATCC 35984 (DSMZ RP62A)	XX-17
Biofilm production	Strong	Medium	Weak	Strong	Medium	Weak
N-acetylglucosaminyltransferase involved in PIA synthesis (*ica locus*)	+	+	+	+	+	−
Autolysin gene involved in initial adhesion (*atl*)	+	+	+	+	+	+
Fibronectin adhesin (*fnbA*)	+	+	+			
Putative adhesin with unknown ligands (*sdrC*)	+	+	+			
Fibrinogen adhesin (*clfA*)	+	+	+			
Intercellular adhesin (*aap*)				+	+	+
Fibronectin adhesin (*embp*)				+	+	+
Involved in biofilm formation in *Staph. aureus* bovine mastitis isolates (*bap*)	−	−	−			
Adherence to desquamated nasal epithelial cells (*sasG*)	−	−	−			

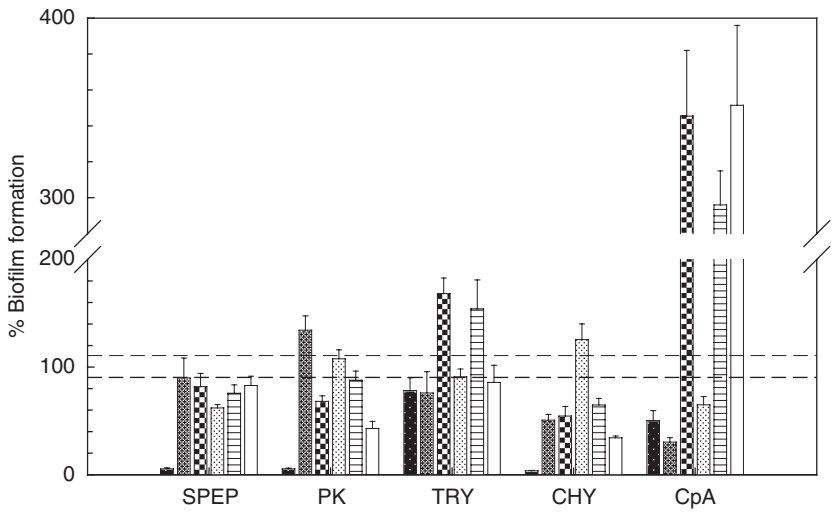

Figure 1 Effect of protease treatment on biofilm formation for each staphylococcal strain. Data are reported as percentage of residual biofilm formation in the presence of each protease in comparison with the untreated one (100%). Biofilm formation was considered unaffected in the range 90–110%. Each data point represents the mean ± SD of three independent experiments. SPEP, serratiopeptidase; PK, proteinase K; TRY, trypsin; CHY, chymotrypsin; CpA, carboxypeptidase A; *Staphylococcus aureus* ATCC 6538P; *Staph. aureus* ATCC 25923; *Staph. aureus* ATCC 12598; *Staph. epidermidis* ATCC 35984; *Staph. epidermidis* XX-17; *Staph. epidermidis* O-47. (▩) 6538P; (▩) 25923; (▩) 12598; (▩) O-47; (▤) 35984 and (□) XX-17.

electrophoretic profiles of the protein mixtures obtained from surface protein extracts of *Staph. aureus* ATCC 6538P following colloidal Coomassie blue staining (left panel) and after the autolytic pattern analysis (right panel).

Several discrete protein bands corresponding to the surface proteins extracted from untreated *Staph. aureus* 6538P cells were present in the control lane 1. This profile was compared with the protein patterns obtained after protease treatment (lanes 2–6).

Metalloprotease treatments (lanes 2 and 6) induced a light modification of surface protein patterns and CpA seemed to remain anchored to the bacterial surface producing the most intense band at about 28 kDa in lane 6. A number of protein bands visible in the untreated *Staph. aureus* 6538P protein profiles either disappeared or

Table 3 Effect of protease treatment on staphylococcal biofilm formation

	NT	SPEP	PK	TRY	CHY	CpA
Staphylococcus aureus						
ATCC 6538P	1·647 ± 0·150	0·086 ± 0·015	0·090 ± 0·012	1·287 ± 0·196	0·059 ± 0·006	0·825 ± 0·152
ATCC 25923	0·793 ± 0·206	0·711 ± 0·146	1·061 ± 0·105	0·604 ± 0·157	0·397 ± 0·043	0·240 ± 0·032
ATCC 12598	0·227 ± 0·032	0·179 ± 0·027	0·146 ± 0·011	0·372 ± 0·032	0·122 ± 0·020	0·756 ± 0·080
Staphylococcus epidermidis						
O-47	2·088 ± 0·108	1·295 ± 0·067	2·241 ± 0·174	1·885 ± 0·151	2·611 ± 0·304	1·352 ± 0·161
ATCC 35984	0·744 ± 0·076	0·563 ± 0·058	0·652 ± 0·063	1·140 ± 0·199	0·476 ± 0·044	2·189 ± 0·141
XX-17	0·354 ± 0·022	0·290 ± 0·030	0·148 ± 0·023	0·300 ± 0·056	0·121 ± 0·006	1·277 ± 0·163
P-value		<0·05	<0·05	<0·001	<0·001	<0·05

NT, nontreated samples; SPEP, serratiopeptidase; PK, proteinase K; TRY, trypsin; CHY, chymotrypsin; CpA, carboxypeptidase A.
Based on OD absorbance at 590 nm. Data represent the mean ± SD of three independent experiments.
Statistical significance is calculated with unpaired *t*-Student test.

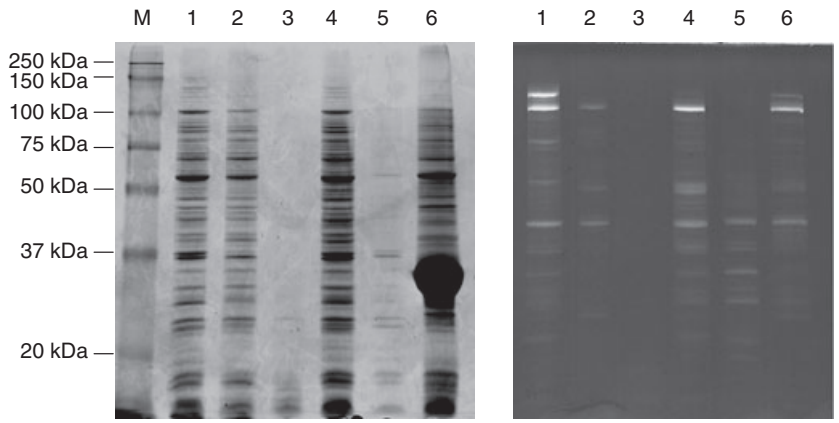

Figure 2 SDS-PAGE and zymogram analyses of *Staphylococcus aureus* 6538P surface proteins. Crude cell envelope SDS extracts from treated and untreated (control) cells were analysed by SDS-PAGE (left panel) and zymogram assay (right panel). The apparent molecular masses of standard indicated are in kDa. Autolysins formed translucent areas in the zymogram. *M*, Molecular weight marker (Bio-Rad); 1, untreated sample; 2, serratiopeptidase-treated sample; 3, proteinase K-treated sample; 4, trypsin-treated sample; 5, chymotrypsin-treated sample; 6, carboxypeptidase A-treated sample.

were drastically reduced in intensity after incubation with the proteases. The protein bands present in the untreated *Staph. aureus* protein profile and disappearing upon SPEP and CpA treatments were selected for further analyses (see below).

PK and CHY treatments (lanes 3 and 5) induced a nearly complete digestion of most of the surface proteins, suggesting a nonspecific and indiscriminate effect of these proteases. These data could confirm the strong effect of the two serine proteases as biofilm inhibitors. TRY did not exhibit any major influence on the surface protein pattern of *Staph. aureus* ATCC 6538P, thus in agreement with its neutral effect on biofilm formation (lane 4).

The autolytic profiles of treated and untreated surface proteins extracted from *Staph. aureus* 6538P were in accordance with the results observed from SDS-PAGE analysis. Treatment with SPEP and CpA led to the disappearance of a discrete number of autolysin bands. On the contrary, treatment with PK led to a complete digestion of surface autolysins while, following treatment with CHY, a shift from high molecular weight to low molecular weight of specific autolytic bands was observed. This latter was in accordance with the results obtained from SDS-PAGE analysis.

Effect of proteases on *Staphylococcus aureus* adhesion to and invasion of HeLa cells

The adhesion efficiency of untreated *Staph. aureus* 6538P was about 2·75% ± 0·45, while $0{\cdot}7 \times 10^{-2}\% \pm 0{\cdot}1 \times 10^{-2}$ of these bacteria invaded HeLa cell line.

The ability of each protease to interfere with *Staph. aureus* capacity to adhere and invade human cells was tested by antibiotic protection assay on HeLa cell

line. Preliminary experiments were addressed to assess the cytotoxicity of each protease on HeLa cells using the same protease concentrations adopted in the previous assays. Cell morphology, viability and proliferation remained unaffected by SPEP and CpA treatments. In contrast, incubation with PK, TRY and CHY strongly affected morphology, viability and proliferation of HeLa cells, which detached from the solid support. According to these data, the effect of the proteases on *Staph. aureus* adhesion to and invasion of eukaryotic cells was analysed only in the presence of SPEP and CpA. *Staph. aureus* ATCC 6538P was chosen as reference strain because in previous work, it showed proper invasion capability (Artini *et al.* 2011).

Figure 3 shows the adhesion and invasion efficiency of SPEP-treated and CpA-treated bacteria compared with untreated control cells. Our results showed that the adhesion efficiency of *Staph. aureus* 6538P was only slightly affected by enzymatic incubation with SPEP (reduction approx. 20%), while it was strongly influenced by treatment with CpA (reduction > 85%) (Fig. 3a). On the contrary, the invasion efficiency was drastically reduced (about 200-fold) following SPEP treatment, while it was reduced by incubation with CpA of approx. 52%.

Identification of surface proteins affected by SPEP and CpA treatment

The duration of the electrophoretic run was extended to achieve a better separation of high molecular weight protein bands. The protein bands occurring in the untreated *Staph. aureus* SDS-PAGE protein profile and disappearing upon SPEP and CpA treatments (numbered from one to eight in Fig. 4) were excised from the gel and submitted to identification by mass spectrometric methodologies. The corresponding gel slices from SPEP-treated sample and CpA-treated sample lanes were also excised and submitted to the identification procedure as control. Proteins identified by mass spectrometric analyses are listed in Table 4.

Discussion

Recently, experimental evidences suggest that in *Staph. epidermidis*, the proteinaceous intercellular adhesin Embp is sufficient and necessary for biofilm formation (Christner *et al.* 2010). Embp is a 1-MDa giant surface protein that mediates attachment to host extracellular matrix, biofilm accumulation and escape from phagocytosis and appears to be well suited for promoting implant-associated infections. Another example of proteinaceous adhesin is the accumulation-associated protein Aap, identified as a polysaccharide-independent intercellular adhesin mediating *Staph. epidermidis* biofilm formation (Rohde *et al.* 2007).

In the light of these considerations, we sought for a proof of concept about the use of proteases for the inhibition of staphylococcal virulence related to the bacterial surface. To this end, we examined the effect of two classes of proteases on different *Staph. aureus* and *Staph. epidermidis* strains. It has been shown by us and others that SPEP is effective in preventing experimental infections caused by biofilm-forming bacteria and enhances antibiotic efficacy (Selan *et al.* 1993; Maheshwari *et al.* 2006; Longhi *et al.* 2008). None of the tested proteases showed an effect on the planktonic growth rate of the staphylococcal strains analysed. This result was in accordance with previous work (Selan *et al.* 1993).

We compared the biofilm formation with the genetic background of the strains here analysed. In *Staph. aureus*, *ica* operon alone is not sufficient to account for high

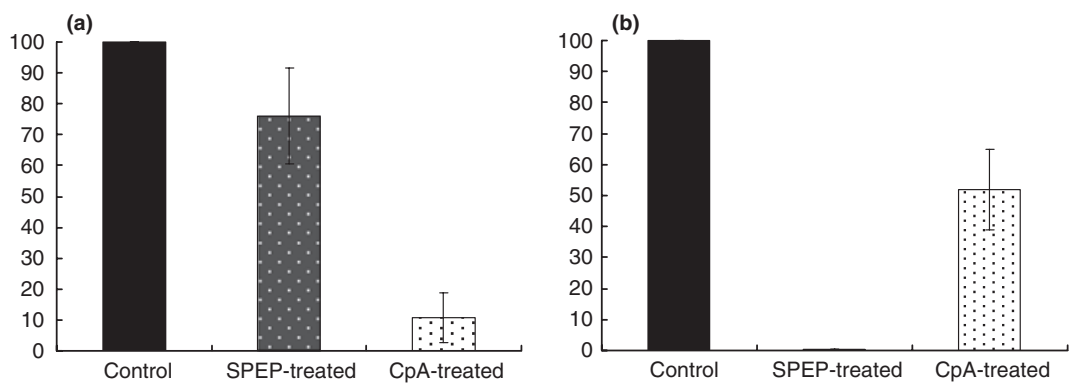

Figure 3 Adhesion and invasion capabilities of serratiopeptidase- and carboxypeptidase A-treated *Staphylococcus aureus* 6538P bacteria in comparison with untreated bacteria. (a) shows the percentage of adhered bacteria compared with the control (untreated sample). (b) reports the percentage of internalized bacteria in HeLa cells compared with the control (untreated sample).

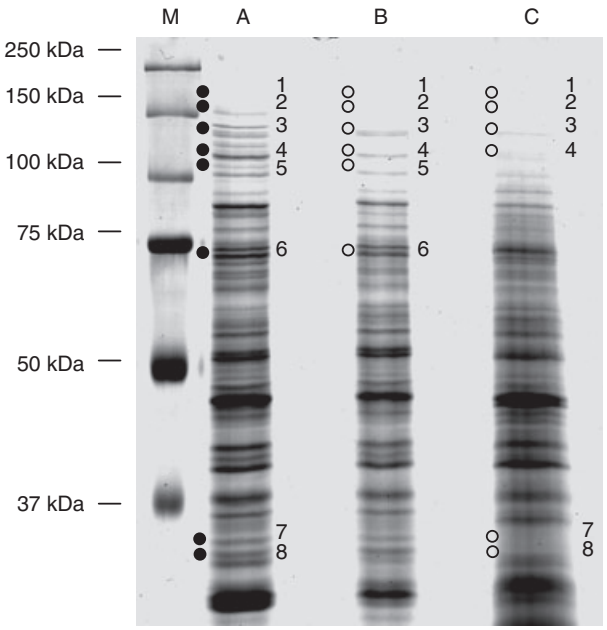

Figure 4 Crude cell envelope SDS extracts from (a) untreated, (b) serratiopeptidase- and (c) carboxypeptidase A-treated *Staphylococcus aureus* 6538P cells analysed by SDS-PAGE. Protein bands indicated with black dots and numbered from one to eight, which were present in the untreated samples and completely disappeared following enzymatic treatment, were identified by mass spectrometric analysis. Gel slices from treated sample lanes corresponding to the selected one to eight bands (empty dots) were also submitted to the identification procedure as control.

biofilm production, whereas in *Staph. epidermidis*, its absence seems to correspond to a lower biofilm production (Table 2). There is no evident correlation between the genetic background of the staphylococcal strains here tested and protease effectiveness. Considering a single strain, the best antibiofilm performance was obtained using CHY. All tested serine proteases showed different behaviour on each bacterial strain. In *Staph. aureus*, PK and CHY displayed a strong *in vitro* effect as biofilm inhibitors. However, their action induced a nearly complete digestion of most of surface proteins, suggesting a nonspecific and indiscriminate effect of these proteases. On the contrary, CpA treatment enhanced biofilm formation in three of six tested strains (one *Staph. aureus* strain and two *Staph. epidermidis* strains). This closely recalls the effect found for GelE, a metalloprotease produced by *Enterococcus faecalis*, which belongs to the thermolysin M4 family (Hancock and Perego 2004; Thomas and Hancock 2009). CpA enzymatic function shows mechanistic similarities with thermolysins (Adekoya and Sylte 2009). Interestingly, GelE is required for the formation of *Ent. faecalis* biofilm and increases biofilm accumulation by a sophisticated fratricide mechanism (Waters *et al.* 2003). Cell death and lysis have been ascribed to play important biological roles in bacterial developmental processes, including biofilm development, by means of a rapid release of adhesive moieties, among them proteins anchored to the cytoplasmic side of the membrane. This mechanism was found to regulate the biofilm phenotype

Table 4 Proteins identified by mass spectrometry analysis in untreated, SPEP- and CpA-treated surface protein samples from *Staphylococcus aureus* 6538P

Band	MW		Untreated protein	SPEP-treated protein	CpA-treated protein	Accession number
1	133 504	DNA-directed RNA polymerase subunit beta	+	–	–	Q932F8
2	137 339	Autolysin, N-acetylmuramyl-L-alanine amidase	+	–	–	Q931U5
3	117 554	Carbamoyl phosphate synthase large subunit	+	–	–	P63739
3	99 213	DNA gyrase, A subunit	–	–	+	Q932M0
4	89 113	Phenylalanyl-tRNA synthetase beta chain	+	–	na	P67040
4	96 114	SecA1 translocase	+	–	+	Q99VM2
5	63 876	Prolyl-tRNA synthetase	+	–	na	Q99UK9
5	66 728	Aspartyl-tRNA synthetase	+	–	na	P67014
5	39 890	Cell division protein ftsA	+	–	na	P63764
6	38 850	Uncharacterized protein SAV1921	+	na	–	Q99SW6
6	33 465	Aspartate carbamoyltransferase catalytic subunit	+	na	–	P65617
7	36 266	Branched chain alpha ketoacid DH E1	+	na		Q99tx7
8	33 021	Fructose-1,6-bisphosphate aldolase	–	na	+	P67472
8	34 047	Ferric hydroxamate receptor 1	–	na	+	Q99RY8
8	52 899	Staphylocoagulase	–	na	+	Q99WZ3

SPEP, serratiopeptidase; CpA, carboxypeptidase A; +, protein present in the sample analysed; –, protein not present in the sample analysed; na, the sample was not analysed.

also in *Pseudomonas aeruginosa* and *Staph. aureus* (Thomas and Hancock 2009).

SPEP treatment resulted in an effective and broad-spectrum reduction in biofilm formation. Moreover, its action appears to be more selective, sequence specific (Miyata *et al.* 1970a,b) and proportional to biofilm production (this study).

The use of PK, TRY and CHY in antibiotic protection assay strongly affected morphology, viability and proliferation of HeLa cells, while SPEP and CpA did not. For these reasons, only SPEP and CpA were considered for further investigations. SPEP treatment strongly impaired *Staph. aureus* invasion efficiency of HeLa cells. This is similar to what found for *Listeria monocytogenes* (Longhi *et al.* 2008), thus confirming the broad spectrum of this protease also against other virulence properties different from biofilm formation. CpA displayed a strong inhibitory effect only on the adhesion efficiency, and this could be related to the CpA ability to bind bacterial surface as shown by SDS-PAGE analysis. The presence of CpA may exert a steric effect masking bacterial proteins involved in the adhesion to the host cells. The remaining CpA-treated bacteria that retain the capability to adhere to host cells might still be able to invade them.

Comparative proteomic investigations on SPEP-treated, CpA-treated and untreated *Staph. aureus* 6538P cells revealed a number of proteins affected by the enzymatic treatment (Table 3). SPEP and CpA treatment showed a specific and reproducible action on bacterial cells, leading to the disappearance of discrete protein bands in the SDS-extracted protein pattern. Among the negatively regulated proteins, some surface proteins like the adhesin/autolysin N-acetylmuramyl-L-alanine amidase, SecA1 translocase that has a role in the transfer of proteins into and across the cell membrane and the cell division protein FtsA were identified (Table 3). The biofilm production, the adhesion and the invasion capabilities (mainly in *Staph. aureus*) are essential virulence factors of staphylococci that directly or indirectly are related to proteins located on the bacterial surface. Extensive functional roles are played by adhesins that show high affinity for eukaryotic epithelial structures and are also involved in numerous cellular processes including anchoring to a substrate and biofilm formation (Cucarella *et al.* 2001; Foster 2005; Clarke and Foster 2006). Surface proteins are then critically important in determining the success of bacterial strains in their competition for survival (Navarre and Schneewind 1999; Roche *et al.* 2003; Pinheiro and Ellar 2006; Tjalsma *et al.* 2008).

The other proteins affected by the protease treatment are strictly cytoplasmic proteins, like the nucleic acid-binding proteins, DNA-directed RNA polymerase subunit beta and the DNA gyrase A subunit, or the t-RNA synthetases (phenylalanil, aspartyl and prolyl), or the aspartate carbamoyl transferase and carbamoyl phosphate synthetase subunits. A number of hypotheses can be drawn from these results. For example, the protease action could induce bacterial lysis or could imply its internalization within the bacteria. However, these two hypotheses can be ruled out because we did not evidence an effect on the bacterial growth rate.

A third and to our opinion most likely hypothesis assumes that protease action on cytoplasmic proteins can occur only on a subpopulation of cells deputed to suicidal behaviour. The altruistic suicide mechanism was found to be responsible for the lysis of a bacterial subfraction by *Staph. aureus* biofilm (Rice *et al.* 2007). SPEP and CpA are able to act both on surface adhesins and on the lysed cellular debris derived from the suicidal subpopulation. While the action of CpA, analogously to that of GelE, results in an increase in biofilm accumulation, the action of SPEP is impairing both surface adhesins/autolysins and the adhesive moieties of the altruistic suicidal cells. It is important to underline that SPEP neither influences bacterial viability when used at the concentrations adopted in this work and at higher concentrations nor displays a cytotoxic effect on eukaryotic cell lines (this study, Longhi *et al.* 2008).

The present study was intended at obtaining a broader knowledge regarding the possible use of proteases as anti-adhesive molecules whose use could be proposed in combination therapy with antibiotics. In this respect, among the tested proteases, SPEP seems the most promising molecule to be developed as a novel antivirulence tool. Its action selectively affects a discrete number of proteins clearly involved in fundamental mechanisms associated with bacterial virulence, such as adhesion, invasion and biofilm formation and would thus hinder staphylococcal virulence properties.

Acknowledgements

The Authors thank Dr A. Cellini for his precious technical support.

References

Adekoya, O.A. and Sylte, I. (2009) The thermolysin family (M4) of enzymes: therapeutic and biotechnological potential. *Chem Biol Drug Des* **73**, 7–16.

Arciola, C.R., Collimati, S., Donati, E. and Montanaro, L. (2001) A Rapid PCR Method for the Detection of Slime-producing Strains of *Staphylococcus epidermidis* and *S. aureus* in Periprosthesis Infections. *Diagn Mol Pathol* **10**, 130–137.

Artini, M., Scoarughi, G.L., Papa, R., Cellini, A., Carpentieri, A., Pucci, P., Amoresano, A., Gazzola, S. *et al.* (2011) A new anti-infective strategy to reduce adhesion-mediated virulence in *Staphylococcus aureus* affecting surface proteins. *Int J Immunopathol Pharmacol* **24**, 661–672.

Brook, I. (1999) Bacterial interference. *Crit Rev Microbiol* **25**, 155–172.

Cafiso, V., Bertuccio, T., Santagati, M., Campanile, F., Amicosante, G., Perilli, M.G., Selan, L., Artini, M. *et al.* (2004) Presence of the ica operon in clinical isolates of *Staphylococcus epidermidis* and its role in biofilm production. *Clin Microbiol Infect* **10**, 1081–1088.

Cafiso, V., Bertuccio, T., Santagati, M., Demelio, V., Spina, D., Nicoletti, G. and Stefani, S. (2007) agr-Genotyping and transcriptional analysis of biofilm-producing *Staphylococcus aureus*. *FEMS Immunol Med Microbiol* **51**, 220–227.

Christner, M., Franke, G.C., Schommer, N.N., Wendt, U., Wegert, K., Pehle, P., Kroll, G., Schulze, C. *et al.* (2010) The giant extracellular matrix-binding protein of *Staphylococcus epidermidis* mediates biofilm accumulation and attachment to fibronectin. *Mol Microbiol* **75**, 187–207.

Christensen, G.D., Baldassarri, L. and Simpson, W.A. (1994) *Colonization of Medical Devices by Coagulation-Negative Staphylococci.* Washington, DC: ASM Press.

Clarke, S.R. and Foster, S.J. (2006) Surface adhesins of *Staphylococcus aureus*. *Adv Microb Physiol* **51**, 187–224.

Cucarella, C., Solano, C., Valle, J., Amorena, B., Lasa, I. and Penades, J.R. (2001) Bap a S*taphylococcus aureus* surface protein involved in biofilm formation. *J Bacteriol* **183**, 2888–2896.

Cucarella, C., Tormo, M.A., Knecht, E., Amorena, B., Lasa, I., Foster, T.J. and Penadés, J.R. (2002) Expression of the biofilm-associated protein interferes with host protein receptors of *Staphylococcus aureus* and alters the infective process. *Infect Immun* **70**, 3180–3186.

Enright, M.C., Day, N.P., Davies, C.E., Peacock, S.J. and Spratt, B.G. (2000) Multilocus sequence typing for characterization of methicillin-resistant and methicillin-susceptible clones of *Staphylococcus aureus*. *J Clin Microbiol* **38**, 1008–1015.

Foster, T.J. (2005) Immune evasion by staphylococci. *Nat Rev Microbiol* **3**, 948–958.

Götz, F. (2002) *Staphylococcus* and biofilms. *Mol Microbiol* **43**, 1367–1378.

Hancock, L.E. and Perego, M. (2004) The *Enterococcus faecalis* fsr two-component system controls biofilm development through production of gelatinase. *J Bacteriol* **186**, 5629–5639.

Hao, X.K., Liu, J.Y., Yue, Q.H., Wu, G.J., Bai, Y.J. and Yin, Y. (2006) *In vitro* and *in vivo* prodrug therapy of prostate cancer using anti-gamma-Sm-scFv/hCPA fusion protein. *Prostate* **66**, 858–866.

Hochbaum, A.I., Kolodkin-Gal, I., Foulston, L., Kolter, R., Aizenberg, J. and Losick, R. (2011) Inhibitory effects of D-amino acids on *Staphylococcus aureus* biofilm development. *J Bacteriol* **193**, 5616–5622.

Iwase, T., Uehara, Y., Shinji, H., Tajima, A., Seo, H., Takada, K., Agata, T. and Mizunoe, Y. (2010) *Staphylococcus epidermidis* Esp inhibits *Staphylococcus aureus* biofilm formation and nasal colonization. *Nature* **465**, 346–349.

Kaplan, J.B. (2010) Biofilm dispersal: mechanisms, clinical implications, and potential therapeutic uses. *J Dent Res* **89**, 205–218.

Kee, W.H., Tan, S.L., Lee, V. and Salmon, Y.M. (1989) The treatment of breast engorgement with Serrapeptase (Danzen): a randomised double-blind controlled trial. *Singapore Med J* **30**, 48–54.

Kiem, S., Oh, W.S., Peck, K.R., Lee, N.Y., Lee, J.Y., Song, J.H., Hwang, E.S., Kim, E.C. *et al.* (2004) Phase variation of biofilm formation in *Staphylococcus aureus* by IS 256 insertion and its impact on the capacity adhering to polyurethane surface. *Korean Med Sci* **19**, 779–782.

Longhi, C., Scoarughi, G.L., Poggiali, F., Cellini, A., Carpentieri, A., Seganti, L., Pucci, P., Amoresano, A. *et al.* (2008) Protease treatment affects both invasion ability and biofilm formation in *Listeria monocytogenes*. *Microb Pathog* **45**, 45–52.

Maheshwari, M., Miglani, G., Mali, A., Paradkar, A., Yamamura, S. and Kadam, S. (2006) Development of tetracycline SPEP-containing periodontal gel: formulation and preliminary clinical study. *AAPS Pharm Sci Tech* **7**, 76.

Martin, T., Uhder, K., Kurek, R., Roeddiger, S., Schneider, L., Vogt, H.G., Heyd, R. and Zamboglou, N. (2002) Does prophylactic treatment with proteolytic enzymes reduce acute toxicity of adjuvant pelvic irradiation? Results of a double-blind randomized trial. *Radiother Oncol* **65**, 17–22.

Mazzone, A., Catalani, M., Costanzo, M., Drusian, A., Mandoli, A., Russo, S., Guarini, E. and Vesperini, G. (1990) Evaluation of Serratia peptidase in acute or chronic inflammation of otorhinolaryngology pathology: a multicentre, double-blind, randomized trial versus placebo. *J Int Med Res* **18**, 379–388.

Miyata, K., Maejima, K., Tomoda, K. and Isono, M. (1970a) Serratia protease: Part I. Purification and general properties of the enzyme. *Agric Biol Chem* **34**, 310–318.

Miyata, K., Tomoda, K. and Isono, M. (1970b) Serratia protease: Part II. Substrate Specificity of the Enzyme. *Agric Biol Chem* **34**, 1457–1462.

Navarre, W.W. and Schneewind, O. (1999) Surface proteins of Gram-positive bacteria and mechanisms of their targeting to the cell wall envelope. *Microbiol Mol Biol Rev* **63**, 174–229.

O'Gara, J.P. (2007) ica and beyond: biofilm mechanisms and regulation in *Staphylococcus epidermidis* and *Staphylococcus aureus*. *FEMS Microbiol Lett* **270**, 179–188.

Pinheiro, V.B. and Ellar, D.J. (2006) How to kill a mocking bug? *Cell Microbiol* **8**, 545–557.

Rice, K.C., Mann, E.E., Endres, J.L., Weiss, E.C., Cassat, J.E., Smeltzer, M.S. and Bayles, K.W. (2007) The cidA murein hydrolase regulator contributes to DNA release and biofilm development in *Staphylococcus aureus*. *Proc Natl Acad Sci (USA)* **104**, 8113–8118.

Roche, F.M., Meehan, M. and Foster, T.J. (2003) The *Staphylococcus aureus* surface protein SasG and its homologues promote bacterial adherence to human desquamated nasal epithelial cells. *Microbiology* **149**, 2759–2767.

Rohde, H., Burandt, E.C., Siemssen, N., Frommelt, L., Burdelski, C., Wurster, S., Scherpe, S., Davies, A.P. *et al.* (2007) Polysaccharide intercellular adhesin or protein factors in biofilm accumulation of *Staphylococcus epidermidis* and *Staphylococcus aureus* isolated from prosthetic hip and knee joint infections. *Biomaterials* **28**, 1711–1720.

Sambrook, J. and Russell, D.W. (2001) *Molecular Cloning: A Laboratory Manual*, 3rd edn. Cold Spring Harbor, NY: Cold Spring Harbor Laboratory Press.

Selan, L., Berlutti, F., Passariello, C., Comodi-Ballanti, M.R. and Thaller, M.C. (1993) Proteolytic enzymes: a new treatment strategy for prosthetic infections? *Antimicrob Agents Chemother* **37**, 2618–2621.

Thomas, V.C. and Hancock, L.E. (2009) Suicide and fratricide in bacterial biofilms. *Int J Art Organs* **32**, 537–544.

Tjalsma, H., Lambooy, L., Hermans, P.W. and Swinkels, D. W. (2008) Shedding & shaving: disclosure of proteomic expressions on a bacterial face. *Proteomics* **8**, 1415–1428.

Valle, J., Toledo-Arana, A., Berasain, C., Ghigo, J.M., Amorena, B., Penadés, J.R. and Lasa, I. (2003) SarA and not sigmaB is essential for biofilm development by *Staphylococcus aureus*. *Mol Microbiol* **48**, 1075–1087.

Vergara-Irigaray, M., Valle, J., Merino, N., Latasa, C., García, B., de Los, Ruiz, Mozos, I., Solano, C. *et al.* (2009) Relevant role of fibronectin-binding proteins in *Staphylococcus aureus* biofilm-associated foreign-body infections. *Infect Immun* **77**, 3978–3991.

Wang, C., Li, M., Dong, D., Wang, J., Ren, J., Otto, M. and Gao, Q. (2007) Role of ClpP in biofilm formation and virulence of *Staphylococcus epidermidis*. *Microbes Infect* **9**, 1376–1383.

Wang, C., Fan, J., Niu, C., Wang, C., Villaruz, A.E., Otto, M. and Gao, Q. (2010) Role of spx in biofilm formation of *Staphylococcus epidermidis*. *FEMS Immunol Med Microbiol* **59**, 152–160.

Waters, C.M., Antiporta, M.H., Murray, B.E. and Dunny, G. M. (2003) Role of the *Enterococcus faecalis* GelE protease in determination of cellular chain length, supernatant pheromone levels, and degradation of fibrin and misfolded surface proteins. *J Bacteriol* **185**, 3613–3623.

Wolz, C., Goerke, C., Landmann, R., Zimmerli, W. and Fluckiger, U. (2002) Transcription of clumping factor A in attached and unattached *Staphylococcus aureus in vitro* and during device-related infection. *Infect Immun* **70**, 2758–2762.

Wootton, M., Bennett, P.M., MacGowan, A.P. and Walsh, T. R. (2005) Reduced expression of the atl autolysin gene and susceptibility to autolysis in clinical heterogeneous glycopeptide-intermediate *Staphylococcus aureus* (hGISA) and GISA strains. *J Antimicrob Chemother* **56**, 944–947.

PHYTOTHERAPY RESEARCH
Phytother. Res. (2013)
Published online in Wiley Online Library
(wileyonlinelibrary.com) **DOI**: 10.1002/ptr.4939

A Biochemical and Cellular Approach to Explore the Antiproliferative and Prodifferentiative Activity of Aloe Arborescens Leaf Extract

Blanda Di Luccia,[1] Nicola Manzo,[1] Maria Vivo,[1] Eugenio Galano,[2] Angela Amoresano,[2] Elvira Crescenzi,[4] Alessandra Pollice,[1]* Raffaella Tudisco,[3] Federico Infascelli[3] and Viola Calabrò[1]

[1]Dipartimento di Biologia Strutturale e Funzionale, Università di Napoli 'Federico II', Naples, Italy
[2]Dipartimento di Chimica Organica e Biochimica, Università di Napoli 'Federico II', Naples, Italy
[3]Dipartimento di Scienze Zootecniche e Ispezione degli Alimenti, Università di Napoli 'Federico II', Naples, Italy
[4]Istituto di Endocrinologia ed Oncologia Sperimentale, CNR, via S. Pansini, 580131, Naples, Italy

***Aloe arborescens Miller*, belonging to the Aloe genus (Liliaceae family), is one of the main varieties of Aloe used worldwide. Although less characterized than the commonest *Aloe vera*, *Aloe arborescens* is known to be richer in beneficial phytotherapeutic, anticancer, and radio-protective properties. It is commonly used as a pharmaceutical ingredient for its effect in burn treatment and ability to increase skin wound healing properties. However, very few studies have addressed the biological effects of *Aloe* at molecular level. The aim of the research is to provide evidences for the antiproliferative properties of *Aloe arborescens* crude leaf extract using an integrated proteomic and cellular biological approach. We analysed the composition of an *Aloe arborescens* leaf extract by gas chromatography-mass spectrometry analysis. We found it rich in Aloe-emodin, a hydroxylanthraquinone with known antitumoral activity and in several compounds with anti-oxidant properties. Accordingly, we show that the *Aloe* extract has antiproliferative effects on several human transformed cell lines and exhibits prodifferentiative effects on both primary and immortalized human keratinocyte. Proteomic analysis of whole cell extracts revealed the presence of proteins with a strong antiproliferative and antimicrobial activity specifically induced in human keratinocytes by *Aloe* treatment supporting its application as a therapeutical agent. Copyright © 2013 John Wiley & Sons, Ltd.**

Keywords: Aloe arborescence; differentiation; proliferation.

Supporting information may be found in the online version of this article (Supplementary Material)

INTRODUCTION

Plants and their extracts are appreciated for their specific aroma, nutraceutical, and therapeutical properties, such as antimicrobial, antiproliferative, anti-inflammatory, immunostimulant, and antioxidative (Greathead, 2003). *Aloe arborescens Miller*, belonging to the Aloe genus (Liliaceae family), is one of the main varieties of Aloe used worldwide. It is commercially grown in South America (Brazil and Uruguay), South Africa and some Asian countries. The concentrated active extract from *Aloe arborescens* shares some therapeutical properties with the well-known and studied *Aloe vera* and is commonly used in medicinal applications to treat burn wounds and help accelerating the healing process of the skin. Recent studies have demonstrated that *Aloe arborescens* has immunostimulating activity in animal trials (Infascelli *et al.*, 2010), and it was found to have beneficial phytotherapeutic and anticancer properties (Lissoni *et al.*, 2009). It is known that the anticancer properties of *Aloe arborescens* depend not only on its immuno-modulatory effect, but also on a direct inhibition of cancer cell proliferation (Bedini *et al.*, 2009). Immunostimulatory effects are due to acemannan, while antiproliferative effects have been ascribed to anthracenic, antraquinonic, and aloenin-like compounds (Lissoni *et al.*, 2009). *Aloe arborescens* is also known for its effective burn treatment and ability to increase skin wound healing properties. Furthermore, it has been shown to be useful in reducing microbial growth and to kill a broad range of viruses and fungi, thereby providing extraordinary support for the gastrointestinal tract, mucous membranes, and connective tissue (Falcetti A., personal communications).

To determine the therapeutic effects of *Aloe arborescens*, a considerable number of clinical investigations have been done; however, very few studies have addressed the biological effects of *Aloe* at molecular level. The aim of the present study is to analyse the cellular response to treatment with *Aloe arborescens* crude leaf extract through a biochemical and cellular approach in order to support its application as a therapeutical agent.

MATERIALS AND METHODS

Preparation of the whole-leaf extract. Plants from Italian farms (Marsala, Sicily) certified for organic systems were cultivated in natural habitat and

* Correspondence to: Dr Alessandra Pollice, PhD. Dipartimento di Biologia Strutturale e Funzionale, Università di Napoli, 'Federico II', Via Cinzia, Monte S Angelo, 80126 Napoli, Italy.
E-mail: apollice@unina.it

Received 05 August 2012
Revised 26 November 2012
Accepted 09 January 2013

harvested when they were older than 4 years. The leaves were washed in tanks, laid in plastic bags, successively washed at 25°C and brushed in order to eliminate external impurity. After air drying, the leaves were submitted to a 'cold method' provided by HDR sas (Caserta, Italy) which allows to extract the active principles either from the inner part or from the cuticle. Commercial preparation of *Aloe* extract was stabilized by potassium sorbate and citric acid. Successively, the extract was stored in stainless still containers which were sealed to avoid air contact.

Cell culture and Aloe arborescens treatment. NHEK primary cells, derived from neonatal foreskin, were from Clonetics (San Diego, California).The HaCaT (human spontaneously immortalized keratinocyte) and MDA-MB231 (human breast adenocarcinoma) cell lines were maintained in Dulbecco's Modified Eagle's Medium (DMEM) supplemented with 10% fetal bovine serum and 1% penicillin-streptomycin. The keratinocyte-derived squamous carcinoma cell lines (SCC011 and SCC012) were previously described (Lefort *et al.*, 2007). The A431 (human epidermoid carcinoma) cell line was maintained in RPMI 1640 supplemented with 10% fetal bovine serum and 1% penicillin-streptomycin. All cell lines were cultured at 37°C in humidified atmosphere of 5% CO_2. Aliquots of *Aloe arborescens* fresh leaf extract were centrifuged at 10000 rpm for 10 min and sterilized using disposable Millex syringe filter units, pore size 0.22 μm (Millipore). Sterile extract was employed for the treatment at 10, 20, and 50% v/v, as indicated, in cell culture medium. Equal amounts of Aloe preservation medium were added to control samples. *Aloe*-treated and untreated cells were photographed and harvested for Western-blot analysis as described below.

Cell growth analysis. HaCaT spontaneously immortalized human keratinocytes, MDA-MB231 metastatic breast adenocarcinoma, A431 human epidermoid carcinoma, CaCo2 human epithelial colorectal adenocarcinoma cells, SCC011, and SCC022 squamous cell carcinoma (SCC) were plated in 35 mm dishes, at a cell density of 1×10^5 cells/plate. Cells were cultured in complete growth media supplemented or not with aliquots of fresh *Aloe arborescence* extract (10% v/v) for 6, 24, 30, 48, and 54 h collected, and counted in a Burker chamber. Cell extracts from treated and untreated cells were prepared and subjected to SDS-PAGE and immunoblot for gene-expression analysis.

Flow cytometry analysis. After treatments, cells were washed twice with phosphate-buffered saline (PBS) and harvested with 0.05% trypsin in 0.15% Na_2EDTA. Cells were then centrifuged, washed in PBS, fixed with ice-cold 70% ethanol, and stored overnight at 4°C. Fixed cells were washed in PBS and then incubated with propidium iodide (50 μg/ml) and RNAse A (10 μg/ml) for 30 min at room temperature. Data acquisition was performed using a CyAn ADP Flow Cytometer (Beckman Coulter, Inc., Milano, Italy) and Summit Software.

Keratinocyte differentiation. Non tumorigenic HaCaT cells were chosen because they retain the ability to differentiate upon Ca2+ treatment thus representing an intermediary between normal and cancerous keratinocytes. HaCaT cells were grown to confluence in complete growth medium and switched into differentiation medium (serum-free DMEM) with 1.2 mM $CaCl_2$ with or without *Aloe extract* (10% v/v) for 6 days according to (Vivo *et al.*, 2009), with the exception that the medium was changed every 48 h. Differentiated cells treated or not with *Aloe* were photographed and harvested for SDS-PAGE and immunoblot analysis as described below. NHEK cells were propagated in serum-free keratinocyte growth medium containing 0.05 mM calcium. NHEK cells with 70%–80% cell confluency were switched to high-calcium medium (1.2 mM) to induce differentiation. Extracts from *Aloe*-treated or untreated NHEK cells were then subjected to SDS-PAGE and immunoblot analysis as described below.

SDS-PAGE and immunoblot analysis. *Aloe arborescens* treated and untreated cells were harvested in lysis buffer (50 mM Tris–HCl pH 7.5, 5 mM EDTA, 150 mM NaCl, 1% NP-40, 1 mM phenylmethylsulfonyl fluoride, 0.5% sodium deoxycholate, and protease inhibitors). Cell lysates were incubated on ice for 40 min, and the extracts were centrifuged at 13200 rpm for 15 min to remove cell debris. Protein concentrations were determined by the Bio-Rad protein assay (Bio-Rad). After the addition of 2× Laemmli buffer (SIGMA), the samples were boiled at 100°C for 5 min and resolved by SDS-polyacrylamide gel electrophoresis. Proteins were transferred to a polyvinylidene difluoride membrane (Millipore). The PVDF membrane was blocked in 5% w/v milk buffer (5% w/v non-fat dried milk, 50 mM Tris, 200 mM NaCl, 0,2% Tween 20) and incubated with primary antibodies diluted in 5% w/v milk or bovine serum albumine buffer for 2 h at room temperature or overnight at 4°C. Primary antibodies were anti-mouse p63-4A4 (Calbiochem), anti-mouse involucrin (Abcam antibody), anti-mouse cytokeratin 1 (Santa-Cruz biotechnology), anti-rabbit transglutaminase type 2 (Abcam antibody), anti-rabbit pErks 42/44 (Cell signalling), anti-rabbit p21 (Santa-Cruz biotechnology), anti-rabbit cyclin D1 (Cell Signalling), anti-rabbit PARP-1 (Cell Signalling), and anti-goat β-actin (Santa-Cruz biotechnology). Data were visualized by enhanced chemiluminescence method (GE-Healthcare) using HRP-conjugated secondary antibodies (Santa-Cruz biotechnology) incubated for 1 h at room temperature and analysed by Quantity One ®software of ChemiDoc ™XRS system (Bio-Rad).

Cell fluorescent staining. SCC011 and SCC022 cells were seeded on sterile coverslips and treated or not with Aloe arborescens extract (10% v/v) for 48 h. After the treatment, three washes with PBS were performed, and cells were fixed with 4% paraformaldehyde at RT for 15 min. Then, cells were incubated with Wheat Germ Agglutinin (WGA) membrane fluorescent stain (1:200) for 1 h at 37°C. After three washes with PBS, cells were permeabilized with 0.5% Triton-X100 (Sigma-Aldrich, Selze/Germany) at room temperature for 5 min. Following permeabilization, cells were incubated with DAPI (1:10000) for 3 min at RT. After three washes with 0.05% PBS-Tween, slides were mounted and analysed.

Metabolite analysis. Aliquots of commercial preparation of aloe extract were submitted to liquid–liquid extraction procedure by using equal amount of chloroform (1:1 v/v). The extraction step was performed three times, and the

organic extracts were collected and dried. Analyte mixtures were finally trimethylsilylated in 200 µl of N, O-bis(trimethylsilyl) acetamide at 80°C for 45 min. The sample was dried down under nitrogen, dissolved in 50 µl of hexane, and centrifuged to remove the excess of solid reagents. The hexane supernatant (1/50) was used for the gas chromatography-mass spectrometry (GC-MS) analysis.

GC-MS analysis. GC-MS analyses were performed on a 5390 MSD quadrupole mass spectrometer (Agilent technologies) equipped with a gas chromatograph by using a DB-5MS fused silica capillary column (30 m, 0.5 mm ID, 0.25 µm ft) from G&W. The injection temperature was 250°C. For lipid analyses, the oven temperature was increased from 25°C to 90°C in 1 min and held at 90°C for 1 min before increasing to 140°C at 25°C/min, to 200°C at 5°C/min and finally to 300°C at 10°C/min. Electron Ionization mass spectra were recorded by continuous quadrupole scanning at 70eV ionization energy. Each species was interpreted on the basis of electron impact spectra (NIST library and Analyst Software).

Two-dimensional electrophoresis (2DE). The first dimensional electrophoresis (isoelectric focusing, IEF) was carried out on non-linear wide-range immobilized pH gradients (pH 4–7; 7 cm long IPG strips; GE Healthcare, Uppsala, Sweden) and achieved using the Ettan IPGphor system (GE Healthcare, Uppsala, Sweden). 200 µg of protein extracts was precipitated with methanol/chloroform according to (Wessel and Flugge, 1984) and solubilized in 125 µl of rehydratation buffer and 0.2% (v/v) carrier ampholyte for 12 h, at 50 mA, at 20°C. The strips were then focused according to the following electrical conditions at 20°C: 500 V for 30 min, 1000 V for 30 min, 5000 V for 10h, until a total of 15000 Vt was reached. After focusing, analytical and preparative IPG strips were equilibrated for 15 min in 6 M urea, 30% (V/V) glycerol, 2% (w/V) SDS, 0.05 M Tris–HCl, pH 6.8, 1% (w/V) dithiothreitol (DTT), and subsequently for 15 min in the same urea/SDS/Tris buffer solution but substituting the 1% (w/V) DTT with 2.5% (w/V) iodoacetamide. The second dimension was carried out on 12.5% (w/w) polyacrylamide gels (10 cm × 8 cm × 0.75 mm) at 25 mA/gel constant current and 10°C until the dye front reached the bottom of the gel, according to (Laemmli, 1970; Hochstrasser *et al.*, 1988). MS-preparative gels were stained overnight with colloidal Coomassie Brilliant Blue and destained with MilliQ grade water.

Image analysis. Gels images were acquired with an Epson expression 1680 PRO scanner. Computer-aided 2-D image analysis was carried out using the ImageMasterTM 2D Platinum software. Relative spot volumes (%V) (V = integration of OD over the spot area; %V = V single spot/V total spot) were used for quantitative analysis in order to decrease experimental errors.

In situ digestion. Trypsin, DTT, iodoacetamide, and R-cyano-4-hydroxycinnamic acid were purchased from Sigma. NH4HCO3 was from Fluka. Trifluoroacetic acid-high-performance liquid chromatography (HPLC) grade was from Carlo Erba. All other reagents and solvents were of the highest purity available from Baker. Analysis was performed on the Coomassie blue-stained spots excised from the gels. The spots were excised from the gel and destained by repetitive washes with 0.1 M NH4HCO3, pH 7.5, and acetonitrile. Samples were reduced by incubation with 50 µl of 10 mM DTT in 0.1 M NH4HCO3 buffer, pH 7.5 and carboxyamidomethylated with 50 µl of 55 mM iodoacetamide in the same buffer. Enzymatic digestion was carried out with trypsin (12.5 ng/µl) in 10 mM ammonium bicarbonate buffer, pH 7.8. Gel pieces were incubated at 4°C for 2 h. Trypsin solution was then removed, and a new aliquot of the same solution was added; samples were incubated for 16 h at 37°C. A minimum reaction volume was used as to obtain the complete rehydration of the gel. Peptides were then extracted by washing the gel particles with 10 mM ammonium bicarbonate and 1% formic acid in 50% acetonitrile at room temperature. The resulting peptide mixtures were filtrated using 0.22 PDVF filter from Millipore, following the recommended procedure.

NanoHPLC-chip MS/MS analysis. The peptide mixtures were analysed using a CHIP MS 6520 QTOF equipped with a capillary 1200 HPLC system and a chip cube (Agilent Technologies, Palo Alto, Ca). After loading, the peptide mixture (8 µl in 0.1% formic acid) was first concentrated and washed at 4 µl min^{-1} in 40 nl enrichment column (Agilent Technologies chip), with 0.1% formic acid in 2% acetonitrile as eluent. The sample was then fractionated on a C18 reverse-phase capillary column (75 µm × 43 mm in the Agilent Technologies chip) at flow rate of 400 nl min^{-1} with a linear gradient of eluent B (0.1% formic acid in 95% acetonitrile) in A (0.1% formic acid in 2% acetonitrile) from 7 to 60% in 50 min.

Peptide analysis was performed using data-dependent acquisition of one MS scan (mass range from 400 to 2000 m/z) followed by MS/MS scans of the three most abundant ions in each MS scan. The acquired MS/MS spectra were transformed in Mascot generic file format and used for peptides identification with a licensed version of MASCOT 2.1, in a local database (Swiss Pro).

Protein identification. Raw data from nano-LC–MS/MS were analysed using Qualitative Analysis software, and MSMS spectra were searched against non-redundant protein databases (NCBInr 20090924, 9760158 sequences) and UniprotSwissprot (2011, 167910 sequences), with the taxonomy restriction to Homo sapiens, using in-house MASCOT 2.1 software (Matrix Science, Boston, USA).

The Mascot search parameters were: 'trypsin' as enzyme allowing up to three missed cleavages, carbamidomethyl on as fixed modification, oxidation of M, pyroGlu N-term Q, as variable modifications, 20 ppm MSMS tolerance, and 0.6 Da peptide tolerance. The score used to evaluate quality of matches for MSMS data was higher than 32.

Phase-contrast microscopy. HaCaT and A431 cells were grown and (HaCaT) induced to differentiate on glass coverslips in six-well plates, washed with PBS and fixed with cold methanol for 10 min. Treated and not-treated cells were photographed (40×) with Olympus BX51 microscope.

Bacterial strains and growth conditions. Bacterial strains used in this study were *Bacillus cereus* (*6A2*) (Naclerio *et al.*, 1993), *Staphylococcus aureus* (ATCC 6538), *Listeria monocitogenes* (ATCC 7644), *Salmonella typhimurium*

(ATCC 14028), *Shigella sonnei* (ATCC25931), *Escherichia coli* (DH5α), *Bacillus subtilis* (PY79) (Youngman *et al*., 1984), *Lactobacillus mucosae* (SF1031), and *Lactobacillus gasseri* (SF1109) (Fakhry *et al*., 2009). Lactobacilli cultures were cultured in MRS broth (Difco) at 37°C in microaerophilic conditions, while for all other strains, LB medium (8 g/l NaCl, 10 g/l tryptone, 5 g/l yeast extract) and aerobic conditions at 37°C were used. *Aloe*-containing liquid media, obtained by adding 2 ml of an aqueous *Aloe* leaf extract to 8 ml of LB or MRS media, were inoculated with 0.1 ml of an overnight culture and growth at 37°C followed for 8-12 h by spectrophotometer (OD_{600}) analysis.

Plate antibacterial assays. For each indicator strain utilized, 100 µl aliquots of exponential growth cultures was mixed with 10 ml of LB or MRS soft agar (0.7%). Plates were then spotted with 10 µl of *Aloe arborescens* extract, incubated at 37°C and the inhibition halo measured as previously reported (Baccigalupi *et al*., 2005). The effects of *Aloe arborescens* extracts on bacterial growth were also measured on LB and MRS agar plates prepared by adding various dilutions of *Aloe* extract (1:1, 1:5, 1:10) to the media and then spotting on the solidified plates aliquots (10 µl) of each bacterial culture in stationary growth phase. *Aloe*-containing plates were then incubated 37°C and checked for bacterial growth after 24 and 48 h.

RESULTS AND DISCUSSION

GC-MS analysis

The composition of the *Aloe arborescens* preparation was determined by GC-MS analyses following liquid–liquid extraction of different analytes from the extract. The extracted mixture of species was derivatized to TMS derivatives and directly analysed by GC-MS by monitoring the total ion current as a function of time. Each species was univocally identified on the basis of the electron impact fragmentation spectra. All the analyses were performed as triplicates. The chromatograms of organic phase extracted in chloroform essentially revealed the presence of hesenoic (C6H12O2), sorbic (C6H8O2), and benzoic acid (C6H8O7). In the aqueous phase, 22 predominant species were identified and are listed in Table 1. Aloin, one of the main component of Aloe species with known pharmacological activities, was not detected, while a significant amount of Aloe-emodin, a hydroxylanthraquinone having specific antineuroectodermal tumor activity (Pecere *et al*., 2000), was present (14%).

Aloe arborescens affects cancer cell proliferation

It is already known that *Aloe arborescens* has antiproliferative and anticancer effects (Lissoni *et al*., 2009; Bedini *et al*., 2009); however, the molecular mechanisms underlying the cellular response to *Aloe* treatment remains to be defined. This prompted us to analyse the effect of an *Aloe arborescens* leaf extract on cell proliferation at cellular and molecular level, by comparing the rate of cell proliferation, the cell-cycle distribution, and the expression of cell-cycle-related molecular markers in *Aloe*-treated and untreated human cells. These analyses were performed in A431 (epidermoid skin carcinoma), MDA-MB231 (metastatic breast cancer), CaCo-2 (epithelial colorectal adenocarcinoma), and HaCaT spontaneously immortalized keratinocytes. As shown in Fig. 1, we reproducibly

Table 1. List of species identified by GC-MS in the *Aloe arborescens* commercial preparation. The relative abundance is expressed as percentage of total volume injected. Preservatives are indicated in bold.

Peak N°	Retention time (min)	Compound	Molecular formula	% of total
1	**4.28**	**Sorbic acid**	**$C_6H_8O_2$**	**3.88**
2	5.00	Benzoic acid	$C_7H_6O_2$	10.95
3	5.16	Phosphoric acid	H_3PO_4	9.27
4	5.76	Succinic acid	$C_4H_6O_4$	11.67
5	6.17	Itaconic acid	$C_5H_6O_4$	0.27
6	7.54	Octanoic acid	$C_8H_{16}O_2$	0.10
7	8.68	Malic acid	$C_4H_6O_5$	0.06
8	9.19	4-hydroxycyclohexylcarboxylic acid	$C_7H_{12}O_3$	1.76
9	10.08	Rythronic acid	$C_{16}H_{40}O_5Si_4$	0.08
10	10.58	α-hydroxycinnamic acid	$C_9H_{10}O_3$	0.11
11	12.01	Pimelic acid	$C_7H_{12}O_4$	0.35
12	13.17	Isocitric acid lactone	$C_6H_6O_6$	0.39
13	13.50	Cyclooctene-1,2-diol	$C_8H_{14}O_2$	0.21
14	13.71	Tricarballylic acid	C_6H_8O6	0.96
15	14.21	para-Coumaric acid	$C_9H_8O_3$	0.38
16	14.72	Terephtalic acid	$C_8H_6O_4$	0.08
17	**15.27**	**Citric acid**	**$C_6H_8O_7$**	**44.74**
18	16.37	Ferulic acid	$C_{10}H_{10}O_4$	0.15
19	17.11	2,4,6-tri-tert-butylphenol	$C_{18}H_{30}O$	0.24
20	18.34	Palmitic acid	$C_{16}H_{32}O_2$	0.10
21	19.92	1H-Indole-2,3-dione-6-ethoxy	$C_{22}H_{22}N_2O_5$	0.08
22	22.26	1,8-Dihydroxy-3-(hydroxymethyl)-9,10-anthracenedione (Aloe-emodin)	$C_{15}H_{10}O_5$	14.01

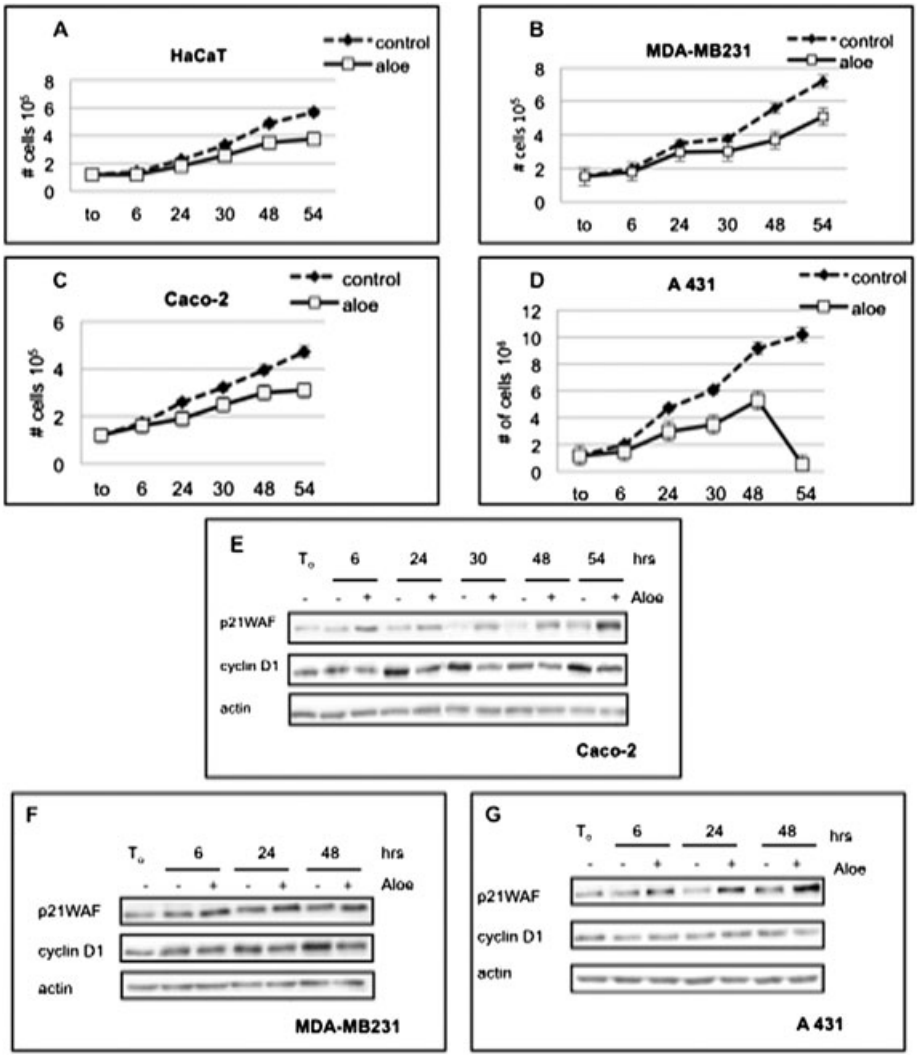

Figure 1. (A) Proliferating HaCaT, (B) MDA-MB231, (C) CaCo-2, (D) A431 cells were incubated in complete cell culture medium supplemented or not with *Aloe* extract (1:10 v/v). Control and *Aloe*-treated cells were collected at 6, 24, 30, 48, and 54 h and counted in a Burker chamber. (E) 'Proliferating CaCo-2, (F) MDA-231, (G) A431 cells were incubated in complete cell culture medium supplemented or not with *Aloe* extract (1:10 v/v). Control and *Aloe*-treated cells were harvested at indicated different times (h). Equal amount of cell lysates was subjected to immunoblot analysis with antibodies against cyclin D1 and p21WAF. Actin was used as a loading control.

found that *Aloe* extract reduces the cell proliferation rate in all cell lines tested. At 54 h of exposure to *Aloe*, a 30 to 40% reduction in the number of cells was observed in MDA-MB231, CaCo2, and HaCaT cells, while A431 cells stopped to proliferate and underwent a drastic massive cell death (Fig. 1D). The cell-cycle distribution of control and *Aloe*-treated cells by flow cytometry shows that HaCaT cells display only a slight increase (3%) in the percentage of G2/M cells after 48 h of *Aloe* treatment (Fig. 2), while the other cell lines tested display an increase of cells in S and/or G2/M phase with a compensatory decrease of G0/G1 phase population indicating that cells were unable to resume the cell cycle at normal phase transit rate. Moreover, except for HaCaT keratinocytes, *Aloe* treatment also caused a significant increase in sub-G1 cell population.

Expression of the cell-cycle markers p21WAF and Cyclin D1 was also investigated to explore *Aloe* effect at the molecular level. Immunoblots with the appropriate antibodies show that *Aloe* treatment significantly induced p21WAF in all tumor cells tested, while Cyclin D1 expression was inhibited in CaCo-2 and MDA-MB231 cells (Fig. 1E and F). Cyclin D1 is a labile factor required at high level for progression through the G1 phase of the cell cycle. Mitogenic pathways directly up-regulate the expression of Cyclin D1; therefore, impaired induction of Cyclin D1 with the concomitant increase of p21WAF is perfectly in line with the ineffectiveness of *Aloe*-treated cells to efficiently resume the cell cycle. Unexpectedly, A431 cells seemed to be unable to regulate Cyclin D1 expression (Fig. 1G). We can speculate that the delay or failure of Cyclin D1 induction with the concomitant increase of p21WAF might be responsible, at least in part, for the massive A431 cell detachment at 54 h of Aloe treatment. Importantly, although we observed an increase of sub-G1 cells upon *Aloe* treatment (Fig. 2), we were unable to observe PARP-1 cleavage by western blot analyses (see Supplementary Fig. 1a) thereby indicating that *Aloe* treatment was not inducing apoptosis. Annexin V assay confirmed the result (see Supplementary Fig.1b).

Aloe arborescens induces keratinocyte differentiation

The concentrated leaf extract from *Aloe arborescens* plants has been used for hundreds of years in medicinal applications to help accelerating the healing process of

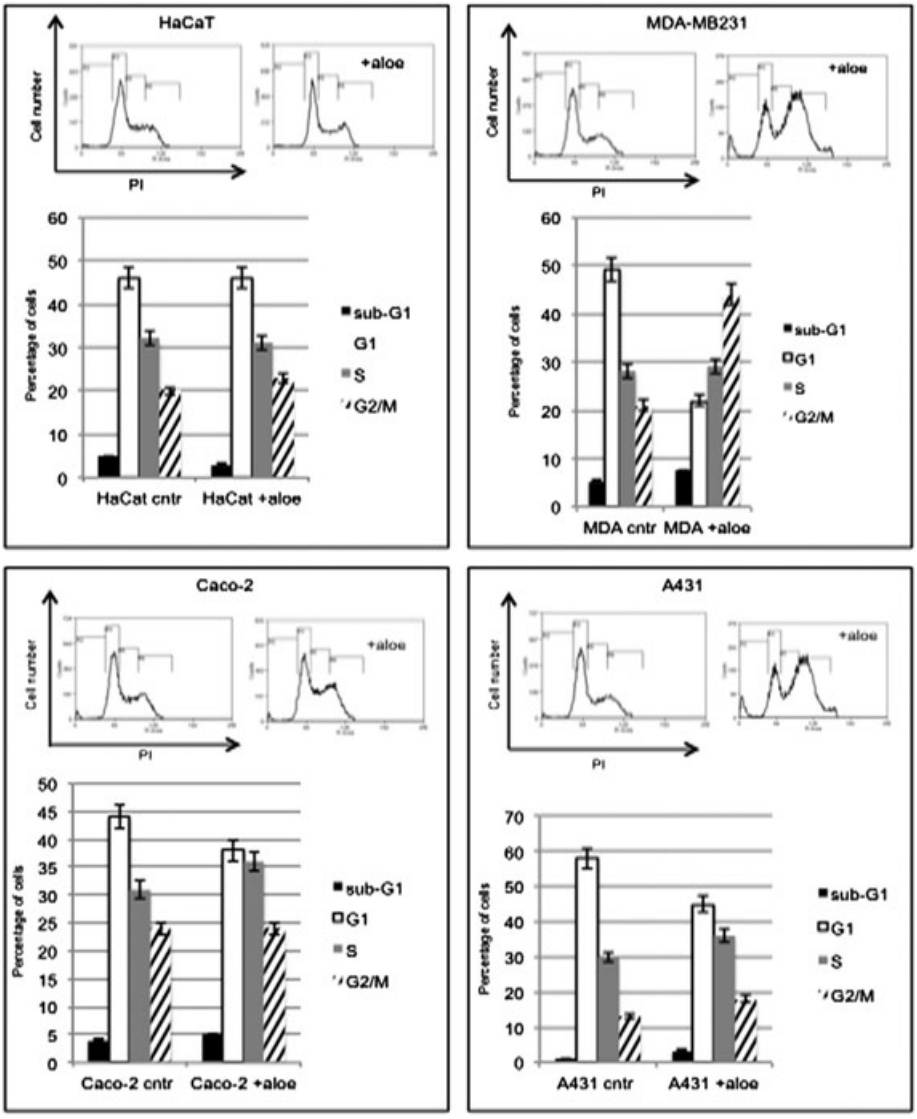

Figure 2. Representative data obtained from flow-cytometric analysis of cell cycle of HaCat, MDA-MB231, CaCo-2, and A-431cells incubated with or without *Aloe* for 48 h.

the skin. Therefore, we decided to analyse the effect of *Aloe arborescens* on differentiation of human keratinocytes. We decided to compare the behavior of HaCaT cells (spontaneously immortalized human keratinocytes) that retain the ability to differentiate upon Ca^{2+} treatment with that of human primary keratinocytes. Addition of calcium to keratinocyte cultures is the most physiological stimulus to elicit a rather complete differentiation program, inducing not only biochemical markers but also many of the structural changes occurring *in vivo* (Dotto, 1999). To check whether the differentiation profile is altered by *Aloe* treatment, HaCaT cells were induced to terminally differentiate by adding 1.2 mM calcium in a serum-free medium, supplemented or not with *Aloe* extract. After 6 days of culture, *Aloe*-treated cells became shrunken and pluristratified (Fig. 3A). To provide molecular evidence that differentiation was anticipated by *Aloe* treatment, we performed immunoblot analyses on extracts derived from treated and untreated cells. In particular, we observed that Involucrin and Transglutaminase, two well-characterized differentiation markers (Paramio and Jorcano, 1997), were expressed at higher levels in *Aloe*-treated cells. Conversely, ΔNp63α that is associated with the proliferative potential of epithelial cells and disappears in terminally differentiated keratinocytes (Di Costanzo *et al.*, 2009) was down-regulated earlier upon *Aloe* treatment (Fig. 3B).

In human primary keratinocytes (NHEK), *Aloe* treatment caused a dramatic increase of Involucrin gene expression that was already evident after 1 day of treatment. Similar to what we have observed in HaCaT cells, ΔNp63α level decreased faster in *Aloe*-treated keratinocytes compared with control cells (Fig. 3C).

We then looked more deeply into the effect of *Aloe* treatment during the early phases of HaCaT cell differentiation. To this purpose, HaCaT cells were seeded at medium density (2.5×10^5) in complete medium supplemented or not with *Aloe* extract (1:10 v/v) and collected before *Aloe* addition (t0) or after 6, 24, 30, 48, and 54 h after *Aloe* treatment (Fig. 3D). Equal amounts of cell lysates were subjected to immunoblot analysis to detect endogenous p21WAF and Cyclin D1. ΔNp63α and Cytokeratin 1 (CK1) were also monitored as early differentiation markers. As shown in Fig. 3D, we initially observed an increase of Cyclin D1 protein levels both in *Aloe*-treated and untreated keratinocytes. However,

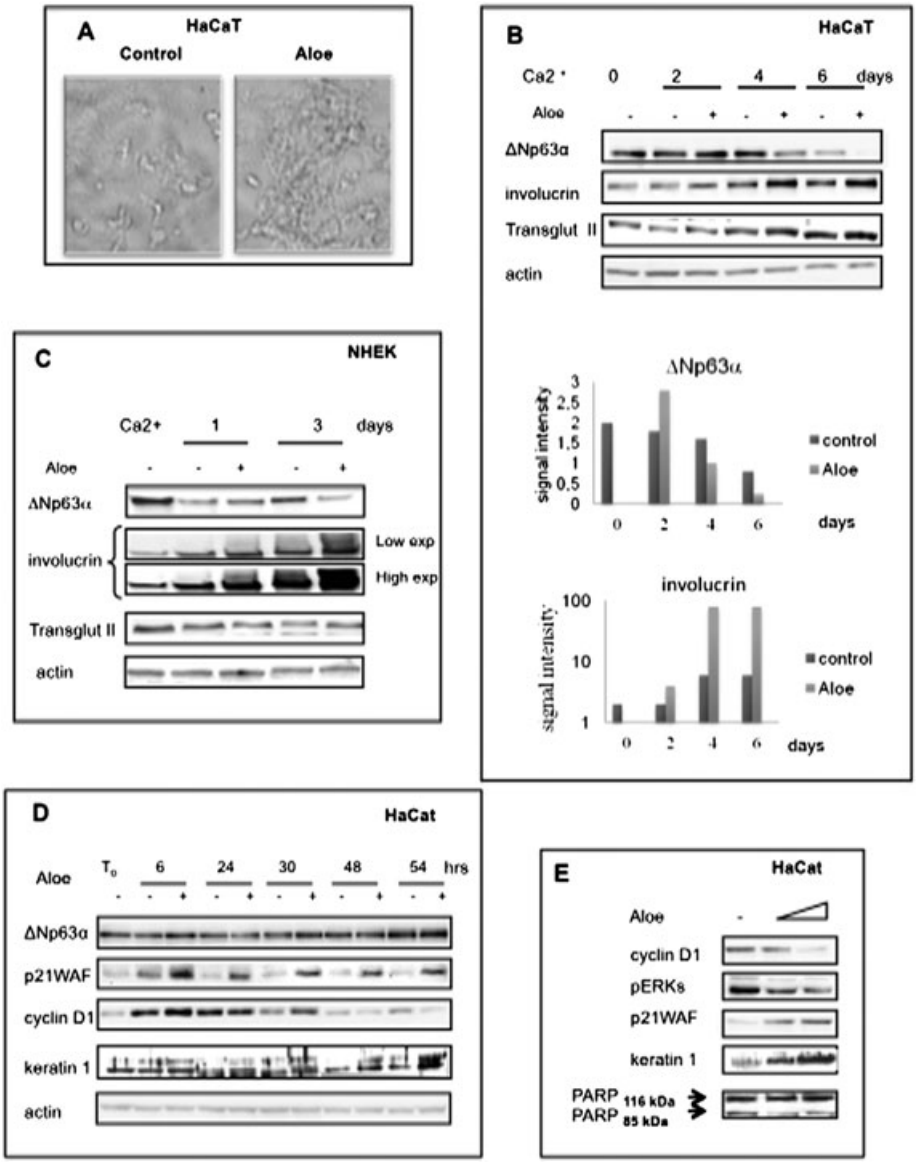

Figure 3. (A) Confluent HaCaT cells were induced to terminally differentiate by serum withdrawal and calcium addition (1,2 mM) in DMEM cell culture media supplemented or not with Aloe extract (1:10 v/v). After 6 days of culture, treated and non-treated cells were fixed with cold methanol and analysed by phase-contrast microscopy. (B) Differentiated HaCaT and (C) NHEK cells in presence or absence of *Aloe* extract (1:10 v/v) were collected at different indicated times. Equal amount of cell lysates was subjected to immunoblot analysis with antibodies against ΔNp63α, involucrin, and transglutaminase type II. Actin was used as a loading control. (D) Proliferating HaCaT cells were incubated in DMEM or DMEM *Aloe* extract containing medium (1:10 v/v). Control and *Aloe*-treated cells were collected at 6, 24, 30, 48, and 54 h. Equal amount of cell lysates was subjected to immunoblot analysis with antibodies against ΔNp63α, cyclin D1, p21WAF, and Keratin 1, an early differentiation marker. Actin was used as a loading control. (E) Proliferating HaCaT cells were incubated in DMEM or DMEM *Aloe* extract containing medium (20% or 50% v/v). Control and Aloe-treated cells were collected at 24 h. Equal amount of cell lysates were subjected to immunoblot analysis with antibodies against cyclin D1, p21WAF, Keratin 1, an early differentiation marker, and PARP-1. Actin was used as a loading control.

according to what observed in tumor cells, Cyclin D1 tended to be down-regulated faster in *Aloe*-treated HaCaT cells while the p21WAF protein was up-regulated only in *Aloe*-treated cells. At 54 h of *Aloe* treatment, the remarkable decrease of Cyclin D1 along with sustained expression of p21WAF indicates that keratinocytes were anticipating cell-cycle withdrawal. p21WAF-depleted keratinocytes exhibit an increased proliferative potential and a drastic down-modulation of keratinocyte differentiation markers (Di Cunto *et al.*, 1998) pointing to an essential involvement of p21WAF in the control of keratinocyte terminal differentiation. In line with these observations, compared to control cells, *Aloe*-treated keratinocytes exhibited higher levels of p21WAF and CK1, in agreement with the induction of a differentiation program. However, the persistence of ΔNp63α protein expression indicates that both treated and untreated keratinocytes were not fully differentiated (Fig. 3D).

Cyclin D1 protein is known to increase under mitogenic signals, through activation of the ERK's pathway. Remarkably, immunoblot analysis of lysates from proliferating HaCaT keratinocytes treated for 24 h with increasing amounts of *Aloe arborescens* extract (20% or 50% v/v) show that the reduction of Cyclin D1 and phosphorylated ERKs, as well as the induction of p21WAF and CK1, was dose dependent. Moreover, the signal corresponding to the cleavage of PARP1 was not enhanced, thus indicating that cells were not undergoing apoptosis (Fig. 3E).

We then decided to look at the effect of *Aloe* treatment on squamous carcinoma cell lines (SCC011 and SCC022). SCC is an uncontrolled growth of abnormal cells arising in the squamous layer, which composes most of the skin's upper layers. SCC cells retain high levels of ΔNp63α that is absolutely required for the survival of early stages of the squamous carcinoma. We first determined the rate of cell proliferation in control and *Aloe*-treated SCC011 and SCC022 cells. As shown in Fig. 4A and B, in *Aloe* containing medium, both SCC011 and SCC022 cells stop growing. The cell-cycle profile of *Aloe*-treated SCC022 cells reveals a dramatic increase in percentage of sub-G1 cells at the expenses of G1 and G2/M cells (Fig. 4C). In SCC011, the increase of subG1 cells was less dramatic although the S phase arrest was evident (Fig. 4D). Growth arrest was associated with a characteristic enlarged and flattened cell morphology as shown by fluorescence microscopy in SCC011 cells (Fig. 4E). Interestingly, compared to SCC022, SCC011 cells display a stronger activation of the Akt survival marker (data not shown) suggesting that Akt may, indeed, counteract *Aloe*-induced cell death. Western blot analysis of control and *Aloe*-treated SCC011 shows a dramatic decrease of ΔNp63α and a concomitant increase of p21WAF and CK1 polymers (Fig. 4F). Importantly, since it has been shown that SCC011 and SCC022 proliferation is strictly dependent on ΔNp63α (Rocco *et al*., 2006), the dramatic reduction of ΔNp63α induced by *Aloe* in these tumor cells may account for the cell death observed

Antibacterial tests

Inner leaf extract from *Aloe vera* was shown to inhibit growth of Streptococcus and Shigella species in vitro (Arunkumar and Muthuselvam, 2009). Aloe-emodin has been proposed to have direct antimicrobial activity. To assess whether the *Aloe* aqueous extract had antibacterial effects, two different plate antibacterial assays were performed with a panel of nine bacterial strains. As a first assay, LB or MRS plates were disseminated with each of the bacterial strain and spotted with the aliquots of *Aloe* extract. As a second assay, LB or MRS solid media containing various amounts of *Aloe* extract were spotted with aliquots of bacterial cells previously grown in liquid media. With both assays, no inhibition of bacterial growth was observed for any of the nine bacterial strains analysed (data not shown).

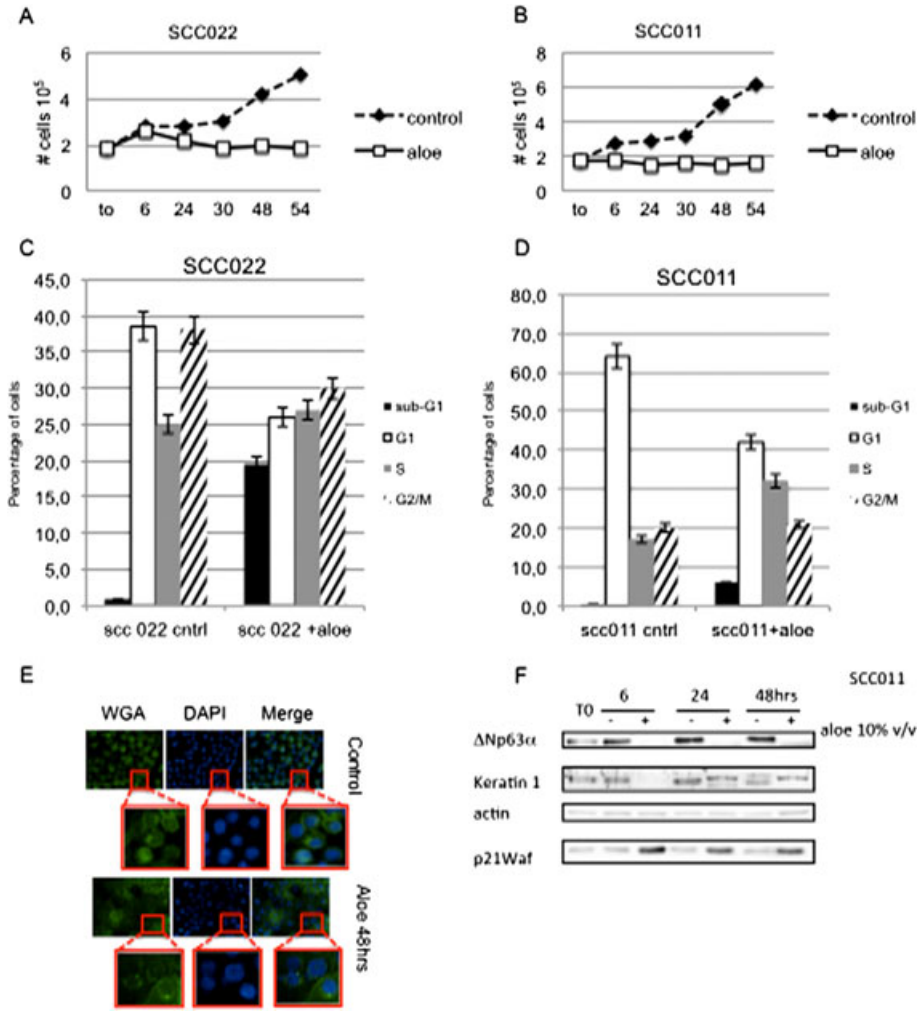

Figure 4. (A) Proliferating SCC022 and (B) SCC011 cells were incubated in complete cell culture medium supplemented or not with *Aloe* extract (1:10 v/v). Control and *Aloe*-treated cells were collected at 6, 24, 30, 48, and 54 h and counted in a Burker chamber. (C) and (D) Representative data obtained from flow-cytometric analysis of cell cycle of SCC022 and SCC011 cells incubated with or without *Aloe* for 48 h. (E) Representative images of SCC011 cells fluorescently stained with WGA (labeling membrane glycoproteins) or DAPI. (F) Equal amount of cell lysates was subjected to immunoblot analysis with indicated antibodies. Actin was used as a loading control. This figure is available in colour online at wileyonlinelibrary.com/journal/ptr.

Table 2. List of proteins differentially represented in *Aloe*-treated or control HaCaT cells identified by mass spectrometry.

Aloe-treated Spot	MW	Score	Protein	Swissprot code	Peptides	Sequence coverage
1	72402	186	**78 kDa glucose-regulated protein**	P11021	8	20%
2	50095	325	**Tubulin beta chain**	P07437	11	34%
3	11391	37	**Dermcidin**	P81605	3	30%
4	29843	60	**Prohibitin**	P35232	6	25%
5	22826	175	**Heat shock protein beta-1**	P04792	4	33%
6	22436	53	**UMP-CMP kinase**	P30085	4	42%
7	23569	47	**Glutathione S-transferase P**	P09211	6	42%
8	17292	60	**Stathmin**	P16949	2	18%
Control						
Spot	**MW**	**Score**	**Protein**	**Swissprot Code**	**Peptides**	**Sequence coverage**
9	62255	83	**Keratin, type I cytoskeletal 9**	P35527	5	10%
10	71082	224	**Heat shock cognate 71 kDa protein**	P11142	13	23%
11	73920	49	**Stress-70 protein, mitochondrial**	P38646	7	12%
12	70294	68	**Heat shock 70 kDa protein 1A/1B**	P08107	4	8%
13	61187	492	**60 kDa heat shock protein, mitochondrial**	P10809	24	50%
14	42052	156	**Actin, cytoplasmic 1**	P60709	9	34%
15	32726	267	**Nucleophosmin**	P06748	10	26%
16	27871	189	**14-3-3 protein sigma**	P31947	9	37%
17	16827	101	**Calmodulin**	P62158	2	29%

Proteomic analysis

Although *Aloe arborescens* extract has been largely used for its immunostimulating and anticancer properties, little is known of its impact at the proteome level. We thus decided to look at cell proteome changes of HaCaT keratinocytes induced by *Aloe* treatment. Protein extracts from untreated (Control) or *Aloe*-treated (Sample) HaCaT cells were fractionated by 2D-GE and stained with colloidal Blue Coomassie. The gels were run in triplicate and compared using the ImageMaster 2D Platinum 6.0 software. A few initial reference points (landmarks) were affixed for gels alignment in the first step of the images analysis. The spots were detected on the gels and the software 'matched' the gels and the corresponding spots. The spots representing the same protein in different gels were paired. Pairs were automatically determined using ImageMaster powerful gel matching algorithm. The different 2DE images were compared by synchronized 3-D spots view. Among the spots corresponding to *Aloe*-sensitive proteins clearly detected in repeated trials, 17 were selected for proteomic analysis. The image analysis enabled the identification of eight spots that were present either in higher amount or exclusively in the *Aloe*-treated sample, thereby indicating that they were induced by *Aloe* treatment. In the control sample, instead, nine spots that were undetectable or whose signal decreased after *Aloe* treatment were detected. These spots were selected for mass spectral identification by the merging of images analyses. Proteins excised from the gel were reduced, alkylated, and, in situ, digested with trypsin. The resulting peptide mixtures were analysed by nanoLC/MS/MS experiments. The peptide mixtures were fractionated by nanoHPLC and sequenced by MS/MS, generating sequence information on individual peptides. MSMS spectra were used to search for a non-redundant sequence using the in-house MASCOT software, thus taking advantage of the specificity of trypsin and of the taxonomic category of the samples. The number of measured masses that matched within the given mass accuracy was recorded, and the proteins that had the highest number of peptide matches were examined leading to the identification of the protein components. As further selection criteria, only the proteins, identified by MASCOT search with at least two peptides and found exclusively in the replicates, were selected. The list of proteins identified by this approach is illustrated in Table 2.

Among the identified proteins, a signal corresponding to **Tubulin** showed an increment in the treated sample as well as that of a powerful antimicrobial peptide known as **Dermcidin** (DCD). This observation was particularly intriguing as we failed to detect a direct antimicrobial activity of *Aloe arborescens* against several bacterial strains (see above). DCD is constitutively expressed in eccrine sweat glands and is part of the constitutive innate defence of human skin and stimulates keratinocytes to produce cytokines and chemokines (Niyonsaba *et al.*, 2009). So far, no DCD expression was found, neither at RNA nor at protein level, in primary keratinocytes, fibroblasts, and melanocytes both in normal conditions, or in cells stimulated by LPS, TNFα, or TPA. Although the *Aloe* ability to stimulate DCD production by keratinocytes needs further investigations, our observation provides a novel insight for the *Aloe* implication in microbicidal ability and skin immunity. *Aloe* treatment also induced the expression of molecules involved in several aspects of keratinocyte proliferation and differentiation such as **GRP78**, **Prohibitin**, and **Stathmin**. Prohibitin is a potential tumor suppressor protein that exhibits growth suppressor ability by repressing E2F-mediated gene transcription (Joshi *et al.*, 2003). Stathmin is a microtubule-destabilizing protein and, in association with Tubulin and HSP70, was reported to be functionally relevant in the control of numerous regulatory pathways that require a reorganization of the entire cytoskeleton. GRP78 (also known as HSRPA5) was found to be increased in the suprabasal layers of

normal epidermis and can work as a molecular chaperone in cooperation with other Heat Shock Proteins being part of the unfolded protein response activated in differentiating epidermal keratinocytes (Sugiura *et al*., 2009). In *Aloe*-treated HaCaT cells, heat shock proteins, essential for the survival of malignant cells, were under-represented. However, heat-shock proteins also occur under non-stressful conditions, simply 'monitoring' the cell's recycling or folding. Further experiments are needed to clarify this phenomenon.

Remarkably, Calmodulin and Keratin 1 signals were detected only in the control sample and disappeared following the *Aloe* treatment. The remaining proteins exhibited a sensitive decrement in the *Aloe*-treated sample.

CONCLUSIONS

The results presented in this study indicate a clear antiproliferative effect of an Aloe extract on several tumor cells and a prodifferentiative effect both on primary and immortalized human keratinocytes.

For a medicinal application perspective, our study supports the use of *Aloe arborescens* extract for topic treatment of hyperproliferative skin diseases or skin SCC. *In vivo* animal experimentation will be necessary to further confirm the proposed health benefit of the extract.

Acknowledgements

This work was funded by MIUR (PRIN 2009KFS94X_003) to V. Calabrò. This work was also supported by Aloe-Beta-HDR sas Capriati a Volturno - ITALY.

Conflict of Interest

The authors declare no conflict of interest.

REFERENCES

Arunkumar S, Muthuselvam M. 2009. Analysis of phytochemical constituents and antimicrobial activities of Aloe vera L. against Clinical Pathogens. *World J Agric Sci* **5**(5): 572–576.

Baccigalupi L, Di Donato A, Parlato M, *et al*. 2005. Small surface-associated factors mediate adhesion of a food-isolated strain of Lactobacillus fermentum to Caco-2 cells. *Res Microbiol* **156**: 830–8365

Bedini C, Caccia R, Triggiani D, Mazzucato A, Soressi GP, Tiezzi A. 2009. Micropropagation of Aloe arborescens Mill: A step towards efficient production of its valuable leaf extracts showing antiproliferative activity on murine myeloma cells. *Plant Biosystems-an Int J Deal Aspects Plant Biol* **143**(2): 233–240.

Di Costanzo A, Festa L, Duverger O, *et al*. 2009. Homeodomain protein Dlx3 induces phosphorylation-dependent p63 degradation. *Cell Cycle* **8**(8): 1185–95.

Di Cunto F, Topley G, Calautti E, *et al*. 1998. Inhibitory function of p21Cip/Waf1 in differentiation of primary mouse keratinocytes independent of cell cycle control. *Science* **280**: 1069–72.

Dotto P. 1999. Signal Transduction Pathway controlling the switch between keratinocyte growth and differentiation. *Crit Rev Oral Biol Med* **10**: 442–457

Fakhry S, Manzo N, D'Apuzzo E, *et al*. 2009. Characterization of intestinal bacteria tightly bound to the human ileal epithelium. *Res Microbiol* **160**(10): 817–823.

Greathead H. 2003. Plants and plants extracts for improving animal productivity. *Proc Nutr Soc* **62**: 279–290

Hochstrasser DF, Patchornik A, Merril CR. 1988. Development of polyacrylamide gels that improve the separation of proteins and their detection by silver staining. *Anal Biochem* **173**(2): 412–23.

Infascelli F, Tudisco R, Mastellone V, *et al*. 2010. Diet Aloe supplementation in pregnant buffalo cows improves colostrum immunoglobulin content. *Revista Veterinaria* **21**(Suppl. 1): 151–153.

Joshi B, Ko D, Ordonez-Ercan D, Chellappan SP. 2003. A putative coiled-coil domain of prohibitin is sufficient to repress E2F1-mediated transcription and induce apoptosis. *Biochem Biophys Res Commun* **312**(2): 459–6.

Laemmli UK. 1970. Cleavage of structural proteins during the assembly of the head of bacteriophage T4. *Nature* **227**: 680–685.

Lefort K, Mandinova A, Ostano P, *et al*. 2007. Notch1 is a p53 target gene involved in human keratinocyte tumor suppression through negative regulation of ROCK1/2 and MRCKα kinases. *Genes Dev* **21**: 562–577.

Lissoni P, Rovelli F, Brivio F, *et al*. 2009 A randomized study of chemotherapy versus biochemotherapy with chemotherapy plus Aloe arborescens in patients with metastatic cancer. *In Vivo* **23**(1): 171–5.

Naclerio G, Ricca E, Sacco M, De Felice M. 1993. Antimicrobial activity of a newly identified bacteriocin of B. cereus. *Appl Environ Microbiol* **59**: 4313–4316.

Niyonsaba F, Suzuki A, Ushio H, Nagaoka I, Ogawa H, Okumura K. 2009. The human antimicrobial peptide dermicin activates normal human keratinocytes. *Br J Dermatol* **160**(2): 243–249.

Paramio JM, Jorcano JL. 1997. Role of protein kinases in the in vitro differentiation of human epidermal HaCaT cells. *Br J Dermatol* **137**(1): 44–50.

Pecere T, Gazzola V, Mucignat C, *et al*. 2000. Aloe-emodin is a new type of anticancer agent with selective activity against neuroectodermal tumors. *Cancer Res* **60**: 2800–2804.

Rocco JW, Leong CO, Kuperwasser N, DeYoung MP, Ellisen LW. 2006. p63 mediates survival in squamous cell carcinoma by suppression of p73-dependent apoptosis. *Cancer Cell* **9**(1): 45–56.

Sugiura K, Muro Y, Futamura K, *et al*. 2009. The unfolded protein response is activated in differentiating epidermal keratinocytes. *J Invest Dermatol* **129**(9): 2126–35.

Vivo M, Di Costanzo A, Fortugno P, Pollice A, Calabrò V, La Mantia G. 2009. Downregulation of ΔNp63α in keratinocytes by p14ARF-mediated SUMO-conjugation and degradation. *Cell Cycle* **31**: 8(21): 3537–3543.

Wessel D, Flugge UI. 1984. A method for the quantitative recovery of protein in dilute solution in the presence of detergents and lipids. *Anal Biochem* **138**(1): 141–143.

Youngman P, Perkins JB, Sandman K. 1984. New genetic methods, molecular cloning strategies and gene fusion techniques for /Bacillus subtilis/ which take advantage of Tn/917/ insertional mutagenesis. In Hoch JA, Ganesan AT (eds.). Genetics and Biotechnology of Bacilli. Academic Press: NY; 103–111.

Journal of Biosciences

A simple and reliable methodology to detect egg white in art samples

--Manuscript Draft--

Manuscript Number:	
Full Title:	A simple and reliable methodology to detect egg white in art samples
Article Type:	Research article
Keywords:	dot-blot immunoassay; egg paint binder; cultural heritage; ovalbumin; proteomics; pigments
Corresponding Author:	Fabio Forlani, Ph.D. Università degli Studi di Milano Milano, ITALY
Corresponding Author Secondary Information:	
Corresponding Author's Institution:	Università degli Studi di Milano
Corresponding Author's Secondary Institution:	
First Author:	Michela Gambino
First Author Secondary Information:	
Order of Authors:	Michela Gambino
	Francesca Cappitelli
	Cristina Cattò
	Aristodemo Carpen
	Pamela Principi
	Lisa Ghezzi
	Ilaria Bonaduce
	Eugenio Galano
	Pietro Pucci
	Leila Birolo
	Federica Villa
	Fabio Forlani, Ph.D.
Order of Authors Secondary Information:	
Abstract:	A protocol for a simple and reliable dot-blot immunoassay was developed and optimized to test work of art samples for the presence of specific proteinaceus material (i.e. ovalbumin-based). The analytical protocol has been extensively set up with respect, among the other, to protein extraction conditions, to densitometric analysis and to the colorimetric reaction conditions. Feasibility evaluation demonstrated that a commercial scanner and a free image analysis software can be used for the data acquisition and elaboration thus facilitating the application of the proposed protocol to commonly-equipped laboratories and to laboratories of museums and conservation centres. The introduction of method of standard additions in the analysis of fresh and artificially-aged laboratory-prepared samples, containing egg white and various pigments, allowed us to evaluate the matrix effect and the effect of sample aging and to generate threshold density values useful for the detection of ovalbumin in samples from ancient works of art. The efficacy of the developed dot-blot immunoassay was proved testing microsamples from 13th-16th century mural paintings of Saint Francesco Church in Lodi (Italy). Despite the aging, the altered conditions of conservation, the complex matrix, and the micro-size of samples, the presence of

	ovalbumin was detected in all those mural painting samples where mass-spectrometry-based proteomic analysis unambiguously detected ovalbumin peptides.

Dear Sir,

please find enclosed a manuscript entitled “A simple and reliable methodology to detect egg white in art samples.”, by Michela Gambino, Francesca Cappitelli, Cristina Cattò, Aristodemo Carpen, Pamela Principi, Lisa Ghezzi, Ilaria Bonaduce, Eugenio Galano, Pietro Pucci, Leila Birolo, Federica Villa and myself that we would like to have considered for publication as “Research Article”.

This work deals with the challenge to detect specific proteinaceus material in works of art. Starting from the need to use severe conditions for the efficient extraction of the proteinaceous material from the ancient art samples, considering the typical micro-size (e.g. 0.4-1.1 mg) of this kind of samples, and taking into account the aim to address the assay to the simply-equipped laboratories of museums and conservation centres, we describe the development of a simple and reliable dot-blot immunoassay for ovalbumin detection in samples from works of art of the 14^{th}-16^{th} century. The developed method uses easily available reagents and materials, and assessed the presence of ovalbumin in all the samples in which also a mass-spectrometry-based proteomic approach unambiguously detected ovalbumin peptides. To our knowledge immunochemical assay was never compared with a proteomic approach in the analysis of cultural heritage samples, and the effect of pigments and sample aging has never been explored in the development of dot-blot immunoassay as an analytical tool for the analysis of samples from works of art.

We hope to have fulfilled all the editorial and scientific requirements of this Journal, and look forward to hearing from you.

Yours sincerely,

Fabio Forlani,
Dipartimento di Scienze per gli Alimenti, la Nutrizione e l'Ambiente,
Sezione di Chimica e Scienze Biomolecolari,
Università degli Studi di Milano,
Via Celoria, 2
20133 Milano,
Italy
Phone: 00390250316839
Fax: 00390250316801
Email: fabio.forlani@unimi.it

A simple and reliable methodology to detect egg white in art samples.

Michela Gambino[#], *Francesca Cappitelli*[#], *Cristina Cattò*[#], *Aristodemo Carpen*[#], *Pamela Principi*[#§], *Lisa Ghezzi*[†], *Ilaria Bonaduce*[†], *Eugenio Galano*[‡], *Pietro Pucci*[‡], *Leila Birolo*[‡], *Federica Villa*[#], *Fabio Forlani*[#]*

[#] Dipartimento di Scienze per gli Alimenti, la Nutrizione e l'Ambiente, Università degli Studi di Milano, Milano, Italy.

[†] Dipartimento di Chimica e Chimica Industriale, Università di Pisa, Pisa, Italy.

[‡] Dipartimento di Scienze Chimiche, Università di Napoli "Federico II", Napoli, Italy

* **Corresponding Author:** Fabio Forlani, Dipartimento di Scienze per gli Alimenti, la Nutrizione e l'Ambiente (DeFENS), Università degli Studi di Milano, via Celoria 2, 20133 Milano, Italy. Phone: +390250316839. Fax: +390250316801. E-mail: fabio.forlani@unimi.it

[§] **Present Address:** Bio & Environmental Technologies, Institute CIM for Sustainable Innovation, Department of Innovative Technologies, University of Applied Sciences of Southern Switzerland, Manno, Switzerland

Supporting Information: Additional information as noted in text.

Keywords: dot-blot immunoassay, egg paint binder, cultural heritage, ovalbumin, proteomics, pigments

Running title: Dot-blot immunoassay for protein detection in art samples

Abstract.

A protocol for a simple and reliable dot-blot immunoassay was developed and optimized to test work of art samples for the presence of specific proteinaceus material (i.e. ovalbumin-based). The analytical protocol has been extensively set up with respect, among the other, to protein extraction conditions, to densitometric analysis and to the colorimetric reaction conditions. Feasibility evaluation demonstrated that a commercial scanner and a free image analysis software can be used for the data acquisition and elaboration thus facilitating the application of the proposed protocol to commonly-equipped laboratories and to laboratories of museums and conservation centres. The introduction of method of standard additions in the analysis of fresh and artificially-aged laboratory-prepared samples, containing egg white and various pigments, allowed us to evaluate the matrix effect and the effect of sample aging and to generate threshold density values useful for the detection of ovalbumin in samples from ancient works of art. The efficacy of the developed dot-blot immunoassay was proved testing microsamples from 13^{th}-16^{th} century mural paintings of Saint Francesco Church in Lodi (Italy). Despite the aging, the altered conditions of conservation, the complex matrix, and the micro-size of samples, the presence of ovalbumin was detected in all those mural painting samples where mass-spectrometry-based proteomic analysis unambiguously detected ovalbumin peptides.

1. INTRODUCTION.

The correct identification of materials used by artists is of paramount importance for conservators in revealing working practices, authenticating and dating the artworks (Leo et al. 2011). Different substances, including oils, gums, and proteins (mainly hen's egg, milk or casein, and animal glue) have been used as paint binders in mural and easel paintings. In particular, protein identification is a challenging problem to solve (Cartechini et al. 2010), given the low protein content of paint samples (Colombini et al. 2010), and the degradation undergone by these materials in the course of aging (Bonaduce et al. 2012; Duce et al. 2012).

Protein identification in art objects is often performed through Fourier transform infrared (FTIR) spectroscopy that, in imaging mode, allow the stratigraphic localization of proteinaceous material in paintings (Van Der Weerd et al. 2002; Bonaduce and Boon 2008; Cotte et al. 2008; Cotte et al. 2009). Unfortunately often FTIR spectroscopy techniques lack the required specificity and the presence of different proteins may return arduous signals to interpret (Colombini and Modugno 2004; Dolci et al. 2008; Vagnini et al. 2008), often masked in ancient paint samples by the massive simultaneous presence of other organic and inorganic components (Arslanoglu et al. 2010). Other techniques used in this field are gas chromatography coupled to mass-spectrometric analysis detection (GC-MS) and to flame ionization detection (GC-FID), and high performance liquid chromatography (HPLC) coupled to mass-spectrometric or spectroscopic detection (UV-Vis absorption or fluorescence)(Gimeno-Adelantado et al. 2002; Rampazzi et al. 2004; Bonaduce et al. 2009; Lluveras et al. 2010; Sciutto et al. 2011). Nevertheless, several doubts were advanced because of the susceptibility to matrix interference and degradation process of the relative abundance of quantified amino acids (Colombini et al. 2004). Recently, since the first report on the use of proteomic strategies by Tokarski et al.

(2006), to identify egg proteins in samples from a Renaissance painting, several papers reported the successful application of advanced mass spectrometric analyses of enzymatically hydrolysed samples of different origin, to identify proteinaceous material (milk, animal glue, egg) in artworks (Leo et al. 2009; Fremout et al. 2010; Dallongeville et al. 2011; Leo et al. 2011; Rasmussen et al. 2012; Toniolo et al. 2012). The approach was revealed extremely successful in unambiguously determining the protein nature in artworks, as also demonstrated by the development of a library specifically dedicated to various sources of proteins in works of art (Fremout et al. 2012). However, the amino acid approach suffers complex sample pre-treatment by using multistep procedures (i.e. protein extraction, hydrolysis, sample clean-up, derivatization) which increase the risk of analyte loss and contamination. In lucky cases, this pre-treatment can be avoided in the proteomic approach (Leo et al. 2009), since an enzymatic hydrolysis in heterogeneous phase can be carried out directly on the sample. In addition, although these methods have proven to be highly successful and reliable, they are not usual in conservation laboratories because of the expensive equipments and the dedicated skills needed (Arslanoglu et al. 2010).

Immunochemical methods are widely used in clinical and bioanalytical chemistry, in various branches of medicine, pharmaceutical and food industries, and in environmental monitoring (Morozova et al. 2005; Schubert-Ullrich et al. 2009). Based on the high specificity and sensitivity of the antigen antibody interaction, immunochemical methods are very precise in protein identification, distinguishing among different proteins (Tijssen 1985; Dolci et al. 2008). The identification of proteins is possible due to the high specificity of antibody-antigen binding (Vagnini et al. 2008), detecting protein presence at very low quantities, like often happens in mural samples (Colombini and Modugno 2004). Furthermore immunochemical methods are

rapid, applicable to routine analysis, simple in the sample preparation and do not require expensive instrumentation (Tijssen 1985; Morozova et al. 2005). Despite that, in the last twenty years relatively few works have exploited immunochemical methods in the field of conservation science for the identification of proteins in artworks, mostly based on immunochemical imaging methodology (Kockaert et al. 1989; Ramirez-Barat and De La Vina 2001; Heginbotham et al. 2006; Dolci et al. 2008; Vagnini et al. 2008; Cartechini et al. 2010; Sciutto et al. 2011). Other studies have been based on the enzyme-linked immunosorbent assay (ELISA) methodology (Heginbotham et al. 2006; Zevgiti et al. 2007; Scott et al. 2009; Cartechimi et al. 2010; Arslanoglu et al. 2010; Palmieri et al. 2011).

Dot-blot immunoassay was developed in 1982 as a screening method for protein markers in bacteriological, epidemiological and immunological studies (Hawkes et al. 1982). This technique summarizes principal advantages both from ELISA, more commonly used for protein quantification, and from Western Blot where the immunodetection is usually achieved on protein samples subjected to electrophoresis under denaturing conditions. Respect to ELISA, dot-blot immunoassay methodology better fits with the need to detect analytes in samples treated with denaturing agents to ease protein solubilisation (Gil et al. 2003; Yamada et al. 2004; Guillemin et al. 2009). Moreover dot-blot immunoassay is very simple and affordable, and its principle is similar to that of other immunochemical assay formats amenable also for a not-specialized laboratory known as strip-based immunoassays (Matsumoto et al. 1997; Blazkova et al. 2009). A revised procedure for a dot-blot immunoassay able to detect ovalbumin in wall paintings was recently reported (Potenza et al. 2012), but to our knowledge the effect of pigments and sample aging has never been explored in the development of dot-blot immunoassay as an analytical tool for the analysis of samples from works of art.

In this work, we present the development of an analytical method based on the use of non-competitive dot-blot immunoassay to detect ovalbumin in paint samples from works of art, and to be addressed to museum and conservation centre laboratories. Ovalbumin is the most abundant protein present in the egg albumen (Phenix 1997), and its detection allows the identification of egg white or whole egg in a paint sample. The study was performed on laboratory-prepared samples of egg white paint layers, with and without various pigments, using denaturing sample-extraction conditions. Fresh and artificially-aged pigmented laboratory-prepared samples were analysed to yield threshold response values that were defined by the evaluation of matrix and sample aging effects. The developed analytical methodology has been then applied to the analysis of gilding samples collected from 13^{th}-16^{th} century mural paintings, and results were compared with the unambiguous identification of the protein component in the sample obtained by MS-based proteomic analyses.

2. MATERIALS AND METHODS.

2.1 Reagents.

Ovalbumin (chicken egg albumin; A5378), fish gelatine (G7765), anti-ovalbumin antibody (rabbit anti-chicken egg albumin whole antiserum; C6534), secondary antibody (goat anti-rabbit IgG conjugated with alkaline phosphatase; A3687), 5-bromo-4-chloro-3-indolyl phosphate/nitro blue tetrazolium (SigmaFast BCIP/NBT; B5655), and bovine serum albumin (A2153) were purchased from Sigma-Aldrich (St. Louis, MO, USA). Egg white powder, casein, rabbit glue were purchased from Bresciani S.r.l. (Milano, Italy).

2.2 Paint laboratory samples.

The laboratory samples were prepared by applying to glass slides a mixture of a water solution of dry egg white and the following pigments: azurite ($Cu_3(CO_3)2(OH)_2$), red ochre (Fe_2O_3), minium (Pb_3O_4), cinnabar (HgS) and calcite ($CaCO_3$). Binder and pigments were mixed until a fluid paintable consistence was reached. Painted glass slides were left to dry at room temperature. One set was then analysed by dot-blot immunoassay, and another one set was artificially-aged in an aging chamber Solarbox 1500e RH (Erichsen, Germany). Samples were exposed for 720 h at 25 °C and 40% relative humidity with a Soda-lime glass UV filter, in order to simulate indoor exposure, according to the normative UNI 10925:2001 (UNI 2001). For protein extraction, the painted layer was scraped from the paint laboratory samples by a scalpel to obtain a powder.

2.3 Gilding samples from works of art.

The choice of the samples from works of art was driven by the fact that egg was often used as binder in mural paintings (Cennini 1954), but it is also a proteinaceous material that it's possible to find in mordants for gilding (Bonaduce et al. 2006). Gilding samples (0.399 – 1.021 mg) from mural paintings from Saint Francesco Church in Lodi (Italy) were thus selected to be tested, after a short-timed pre-treatment, for the presence of ovalbumin with dot-blot immunoassay. The sample description is reported in **Table S-1**.

2.4 Sample pre-treatment.

Sample powder (5 mg; i.e. scraped paint layer of laboratory samples) was homogenised by pestle and mortar in 1 ml of 6 M urea for 2 min. Gilding samples were shortly crushed against the Eppi tube walls by a spatula and suspended to 1 mg/ml in 6 M urea. The suspension was mixed 15

min by vortex, and centrifuged for 15 min, 11000 *g*, room temperature. Where it is stated, the vortex step was replaced by a 15 min ultrasound treatment in water bath (Elma Transsonic T700, Singen, Germany), or homogenisation step was not carried out. For the laboratory samples, the supernatant was diluted to 0.05 mg ml^{-1} with 6 M urea prior the dot-blot immunoassay.

2.5 Dot-blot immunoassay analysis.

The MiniFold 1 System dot-blotting apparatus (Whatman) was assembled according to the manufacturer instructions with 3MM (Whatman) blotting paper (2 sheets) and 0.45 µm nitrocellulose membrane (N9763-5EA, Sigma-Aldrich, St. Louis, MO, USA) pre-wetted in 0.1 M Tris-HCl pH 7.4, 0.5 M NaCl (TBS). One-hundred and forty µl of sample (laboratory samples: 0.21 - 3500 ng; gilding samples: 0.002 - 100 µg), ovalbumin (0.21 - 3500 ng), or sample spiked with known amount of ovalbumin (see "Results" section), in 6 M urea was pipetted in each well of the mounted dot-blotting apparatus, let stand for 20 minutes and then adsorbed by gentle vacuum application. Wells were washed four times with TBS (200 µl/well). The first two times, the excess buffer solution was pipetted up, and twice it was removed by gentle vacuum application. The dot-blotting apparatus was dismounted and the membrane was washed once with 0.05% Tween 20 in TBS (TBS-T), and blocked with 2% fish gelatine in TBS by a two-hour incubation at room temperature under constant agitation. Blocking solution was well drained away and the membrane was incubated with anti-ovalbumin antibody diluted 1:2000 in TBS containing 1% fish gelatine (TBS-G) for 3 h at room temperature under constant agitation. After 4 washes with TBS-T (5 min each), membrane was incubated with secondary antibody at a concentration of 1:3000 in TBS and 1% fish gelatine for 2 h at room temperature. Both incubations and washes were carried out under constant agitation. Secondary-antibody excess was removed by 4 washes with TBS-T and a final one with TBS (5 min each). The

membrane was incubated in 12 ml of the 5-bromo-4-chloro-3-indolyl phosphate/nitro blue tetrazolium chromogenic substrate (1 tablet) in deionised water without agitation. The reaction was stopped by water dilution after 4 min and the membrane was dried on filter paper. The image of the developed membrane was digitized using Expression 1680PRO scanner (Epson) or, where it is stated, using a consumer use scanner (SX115, Epson). All scanner automatisms were removed and the scanner cover was used as white reference for the white point correction. Densitometric analyses were performed using ImageMaster 1D Elite software (Nonlinear Dynamics Ltd/Amersham Pharmacia Biotech, Cologno Monzese, Italy) or, where it is stated, using the freely-downloadable software ImageJ (Abramoff et al. 2004) equipped with the Dot Blot Analyzer tool (Gilles Carpentier, Faculté des Sciences et Technologies, Université Paris, France). In the densitometric analyses, to minimize the effect of variability in the definition of well area, density values were obtained subtracting the ratio between volume (sum of intensities of every pixel within the defined area) and the defined area (pixel number) with the density of the background (6 M urea in the absence of sample or ovalbumin). A non-linear regression function (logistic, 4 parameters) was fitted to the data of the density values (Motulsky et al. 2006) in order to generate dose-response curve.

The method of standard additions (MSA) (Howey et al. 1987) was applied to the dot-blot immunoassay (MSA-DBA) in order to assess the presence and quantify ovalbumin in samples in the presence of matrix interference (**see Supporting Information S-2**).

Considering the average values and variability of both density at the lower limit of detection, and matrix effect obtained by MSA-DBAs of paint laboratory samples (fresh and artificially-aged), threshold density values were calculated to decide about the presence of ovalbumin in work of art samples. In every membrane, a set of ovalbumin amounts in 6 M urea

(0.21 – 3500 ng) was always included and the highest response density value was used as normalizator. The same normalization procedure was applied in the calculation of threshold density values. According to the normalized values of the response densities, work of art samples were considered for ovalbumin presence as: negative when the normalized value was < 9%; suspect positive, or false positive due to the matrix interference contribute, when the normalized value was comprised between 9% and 29%; positive when the normalized value was > 29%.

2.6 Proteomic analyses.

The identification of the proteinaceous material was carried out following the same proteomic analytical procedure described previously (Leo et al. 2009), except for a preliminary incubation of the sample in strongly protein denaturing conditions (6 M urea) that was introduced in order to favour the exposure of the proteinaceous material to the action of proteases.

Microsamples (~100-500 μg) were digested in an enzymatic reaction by proteomics-grade trypsin. A pre-treatment of the solid samples with 6 M urea was carried out by incubation for 1 h in 20 μL followed by sonication for 30 min at room temperature. The samples were then 6-fold diluted with 10 mM ammonium bicarbonate pH 7.5 and enzymatic digestion carried out by addition of 1 μg of trypsin at 37°C for 16 hours. The supernatants were then recovered by centrifugation and the peptide mixtures concentrated and purified using reverse phase C18 Zip Tip pipette tips (Millipore). Peptides were eluted with 20 μL of a solution made of 50% acetonitrile, 0.1% formic acid in Milli-Q water and analysed by LC-MS/MS.

The peptide mixtures were analysed using a CHIP MS 6520 QTOF mass spectrometer equipped with a capillary 1200 HPLC system and a chip cube (Agilent Technologies, Palo Alto, Ca). After loading, the peptide mixture (8 μL in 0.1% formic acid) was first concentrated and

washed at 4 µL min^{-1} in 40 nL enrichment column (Agilent Technologies chip), with 0.2% formic acid in 2% acetonitrile as eluent. The sample was then fractionated on a C18 reverse-phase capillary column (75 µm x 43 mm in the Agilent Technologies chip) at flow rate of 400 nL min^{-1} with a linear gradient of eluent B (0.2% formic acid in 95% acetonitrile) in A (0.2% formic acid in 2% acetonitrile) from 7 to 60% in 50 min.

2.7 Other analyses.

2.7.1 Thermogravimetry (TG). The protein content of the laboratory samples was determined on an aliquot of the paint layer analysed by thermogravimetric analysis (TGA) (**see Supporting Information S-2**). Since cinnabar has no residual mass at 800 °C, we could not determine the protein content in the laboratory samples with this pigment.

2.7.2 Colorimetric method for protein quantification. Protein concentration in 6 M urea extracted samples was determined by the Bradford assay (Bradford 1976) using bovine serum albumin in 6 M urea as standard.

2.7.3 Denaturing gel electrophoresis. Denaturing gel electrophoresis (SDS-PAGE) was run under reducing conditions (0.175 M 2-mercaptoethanol) according to Laemmli (1970) by using 6 M urea samples (0.3-3 µg protein) properly diluted in Laemmli sample buffer. Western blot analyses were carried out by a standard protocol using anti-ovalbumin antibody.

2.8 Statistical analysis.

Statistically significant differences in pairwise comparisons were determined by Student's *t*-test analysis ($p < 0.05$).

Analysis of variance (ANOVA) via a software run in MATLAB environment (Version 7.0, The MathWorks Inc, Natick, USA) was applied to statistically evaluate any significant differences among more than two samples. Tukey's honestly significant different test (HSD) was used for pairwise comparison to determine the significance of the data. Statistically significant results were depicted by p-values < 0.05.

3. RESULTS AND DISCUSSION.

3.1 Development of dot-blot immunoassay for ovalbumin detection.

Considering altogether both the denaturing conditions needed for the sample preparation and the conditions optimized for immunochemical reactions, a dot-blot based immunoassay procedure was developed using a commercially available anti-ovalbumin antibody. Shortly the immunochemical assay consisted of i) coating the sample protein material to a solid-membrane support in a 96-spot format, ii) saturating the solid-membrane support with an antibody-unrecognized protein, iii) immunorecognition of the analyte (i.e. ovalbumin) by incubation with the primary antibody, iv) immunorecognition of bound primary antibody by incubation with an enzyme-conjugated secondary antibody, v) colorimetric reaction driven by the enzyme conjugated to the secondary antibody, and finally, vi) densitometric analysis of the digitized image of the developed solid-membrane support. Some basic parameters were optimized preliminarily, facing the problems of sample leakage, background evaluation and cross-contamination. During the coating step, sample-leakage from the spot was avoided by inserting two sheets of blotting paper to increase the tightness of the system. Nitrocellulose was chosen as solid-membrane support because it generated a lighter background than polyvinylidene

difluoride. Taking into account that proteins of samples from works of art are aged for years in complex matrices, the coating solution was chosen accordingly to the need of efficiently extracting such degraded materials, and keeping it solubilised during the whole coating process. As coating solution, 6 M urea in the presence of 1% SDS (Heginbotham et al. 2006) and 6 M urea alone were compared. The 6 M urea coating solution was preferred because SDS caused foaming during the coating step, leading to cross-contaminated spots, and because it gave rise to signals of a lower intensity after the colorimetric reaction. Using the established coating solution, 6 M urea, the incubation times (coating, blocking, primary antibody, and secondary antibody steps), and the concentrations of the saturating agent (i.e. fish gelatin), primary antibody, and secondary antibody were defined by using different ovalbumin concentrations in 6 M urea, and choosing the conditions (described in the "Experimental Section") that allowed to obtain highest signal above background responses (data not shown).

The conditions for the colorimetric step and the densitometric analysis were also evaluated. Different times of incubation (1-6 min) of the colorimetric reaction were carried out and the background incidence was measured as the percent ratio between the response of 6 M urea in the absence of ovalbumin (negative control) and the response in the presence of 3500 ng ovalbumin in 6 M urea. Beyond background incidence, the ovalbumin detectability (ED_{50}) was measured as the concentration that yielded half of the maximum response. The background incidence (± SD) ranged from 22.3 (± 9.2) to 31.1 (± 0.5) % in the time window of 3 to 5 min incubation of the colorimetric reaction, and was lower than that observed at 2 and 6 min (40.3 (± 10.0) and 38.9 (± 9.8) %, respectively). Although the lowest background incidence (16 (± 5 %)) was reported at 1 min of incubation time, the ED_{50} value was 2.3 times higher than the lowest ED_{50} value that was observed at 4 min incubation. Therefore the 4-min incubation time was chosen for the

colorimetric reaction in the optimized immunochemical assay. Probably because of the choice of different extracting solutions, the background incidence in dot-blot immunoassay is higher than that reported for the ELISA assay for ovalbumin detection in paintings (Palmieri et al. 2011). However, since samples from artworks are complex, 6 M urea, which ensures an efficient extraction of the proteins, was preferred to the phosphate buffer saline solution used for ELISA, despite the higher background observed.

To verify the contribute of the densitometric analysis to the response variability, 4 independent densitometric analyses were carried out on the same membrane containing 3 replicates of each set of different ovalbumin amounts (0.1 – 7000 ng) in 6 M urea. The precision profile of the response (**Figure 1**) shows that intra-assay response variability (RSD%) was above 30 % only at ovalbumin amounts below 10 ng, and that response variability is thus not linked to the digitization step and data elaboration protocol. This indicates that densitometric analysis contributes very little to the response variability, which must mainly be ascribed to one or more steps taking place before the colorimetric reaction. As immunochemical reaction steps are by now highly standardized leading to minimization of the response variability (Tijssen 1985) we can suppose that the sample coating was an important source of the response variability observed at the low ovalbumin amounts.

Different tools for the densitometric analysis of dot-blot immunoassay of ovalbumin in 6 M urea were employed. In particular, densitometric analysis performed by a purchased scientific software (ImageMaster 1D Elite) on images digitized by a professional scanner (Expression 1680PRO) was compared with that carried out by a freely downloadable scientific software (ImageJ) on images digitized by a consumer-use scanner (Epson Stylus SX115). The elaborated results showed no difference by Student's *t*-test analysis ($p < 0.05$; data not shown)

indicating that the densitometric analysis does not require dedicated professional equipment thus being feasible also to commonly-equipped labs.

A typical dose-response plot generated by the optimized dot-blot immunoassay (DBA) of 15 different ovalbumin amounts (0.2 – 3500 ng) in 6 M urea is shown in **Figure S-1**. The lower limit of detectability (LOD), i.e. the analyte amount giving a response 2-times the standard deviation calculated on background noise, and the upper limit of detectability (UOD), i.e. the analyte amount giving a response equal to density of maximum value minus 2-times its standard deviation, were calculated on the fitted non linear regression. The LOD and UOD values were used to delimitate the response linearity range showing that it encompassed over at least 1 order of magnitude of the ovalbumin amounts (i.e. 4.9 – 228.8 ng) with an ED_{50} (± SD) value of 41.2 ± 2.9 ng.

Immunospecificity of the anti-ovalbumin antibody was investigated by carrying out DBA of different amounts of other proteinaceous binders and conservation materials: egg white, casein and rabbit glue, as well as bovine serum albumin and fish gelatine. Only egg white showed a response different from the background over all the tested amounts (**Figure 2**), and similar to the response yielded by ovalbumin, showing that the developed DBA should discriminate ovalbumin-derived proteinaceus material from the other kinds of proteinaceus materials commonly present in samples from works of art.

3.2 Detection of ovalbumin in the laboratory samples.

Painting laboratory samples were prepared by painting microscope glass slides with a mixture of egg white and various pigments. Pigments were chosen among the most used in all the art history (i.e. azurite, red ochre, minium, cinnabar and calcite) (Matteini and Moles 2003). Our

preliminary investigations by DBA indicated that a lower concentration of immunodetected protein was present in calcite painting laboratory samples respect to the painting laboratory samples with the other pigments. Therefore different procedures for sample preparation from calcite painting laboratory samples were considered and compared for the response to the DBA of different amounts of extracted material. When homogenization, combined with a vortexing step, was included in the 6 M urea extraction of the powder scraped from calcite painting laboratory samples, the ED_{50} value was 7.0-fold lower than that obtained by the omission of the homogenization step or 4.0-fold lower than that obtained by replacing vortexing step with an ultrasound treatment. This means that homogenisation improves 6 M urea extraction of immunodetectable material especially when it is combined with a vortexing step. The entire optimized extraction procedure take only ~ 35 min.

DBAs of egg white painting laboratory samples containing as pigments azurite, red ochre, minium, cinnabar and calcite were performed. The amounts of ovalbumin specifically-immunodetected in these samples are reported in **Table 1** and are compared with the amounts of total protein detected by both a colorimetric method and a thermogravimetric method. Immunodetected ovalbumin was at least 2.4-fold overestimated respect to the protein amount. The azurite painting laboratory samples gave the highest overestimation (4.0-fold) of the immunodetected ovalbumin. Western blot analyses of ovalbumin and egg white were carried out using the anti-ovalbumin antibody to assess its specificity toward the protein components of egg white. The immunodetected profile of egg white was similar to that of ovalbumin (data not shown), indicating that the bias in the ovalbumin detection must be due to matrix effects and not to different immunoreactivity properties of ovalbumin and egg white. It is recognized that the analysis of proteinaceous material can be affected by the presence of mineral pigments

(Bonaduce et al. 2009), and this aspect was till now poorly explored in the immunoassay protocols proposed for cultural heritage analyses.

The method of standard additions (MSA) (Howey et al. 1987) was used to solve the matrix effect problem. The pigmented painting laboratory samples were spiked with known amounts of ovalbumin. The amount of sample to be spiked was defined analyzing detectability in dose-response curves generated by preliminary DBAs of different amounts of unspiked samples. This value was 6.8 ng for all samples with the exception of calcite painting laboratory samples (13.7 ng). The amounts of immunodetected ovalbumin by applying the method of standard addition to the dot-blot immunoassay (MSA-DBA) of the pigmented egg white painting laboratory samples were significantly not different from the protein amount determined by the thermogravimetric method (TGA; **Figure 3**). The protein amount detected in the same samples by the colorimetric method resulted to be lower than that determined by TGA method in azurite and minium painting laboratory samples (Student's *t*-test; $p < 0.05$). This can be explained hypothesising that the dye used has a lower reactivity towards ovalbumin than to the protein used for calibration (bovine serum albumin)(Read and Northcote 1981).

Artificially-aged laboratory samples were also analysed. The amounts of ovalbumin quantified by MSA-DBA in the aged samples were statistically similar to those revealed in the fresh samples (**Table 2**). This result is extremely important as it indicates that the set up method for the MSA-DBA quantification of ovalbumin is not affected by the tested aging conditions.

Once the quantification of ovalbumin by the developed MSA-DBA was showed to be unaffected by the presence of pigments and the sample-aging, the results of many MSA-DBAs of ovalbumin in fresh and artificially-aged pigmented laboratory samples were analyzed using a

normalization routine in order to face the challenge of the typical micro-size and low-number features of samples from works of art. The variability and the matrix effect components of density values were evaluated and threshold density values were defined (see "Experimental Section") as a decisional tool for detection of ovalbumin by DBA of samples from works of art.

3.3 Detection of ovalbumin in gilding samples from works of art.

The developed DBA was used to detect ovalbumin in gilding samples collected from 13^{th}-16^{th} century mural paintings. The obtained response densities were compared with the threshold density values defined by MSA-DBAs of laboratory samples (see above) in order to decide about positivity of the ancient gilding samples for the presence of ovalbumin. These samples have been categorized as reported in **Table 3** according to the results of DBA of 100 µg sample amount per assay. Among these samples, differences in the detection of ovalbumin with DBA could be noticed and were underlined with a semi-quantitative scale based on the recurrence in the threshold density category. Samples 13, 19, 22 and 25 resulted positive for ovalbumin presence. Sample 18 was classified as negative, while samples 20 and 28 were classified as maybe positive because their response densities were not lower than the threshold density for negativity in all the DBA assays. Sample 19 was suspected to be positive also when the amount of sample tested by DBA was lowered to 30 µg. Considering both the amounts of tested samples and the LOD for ovalbumin, detected ovalbumin could be estimated to be at least 5 ng in 100 µg of the work of art samples classified as positive.

In order to evaluate the performances of the developed DBA method, the results described above on the analysis of gilding samples were compared to the results obtained by

MS-based proteomics on the same samples. Briefly, the proteomic approach relies on matching experimental mass spectra of digested proteins to the virtual ones calculated for the proteins that are present in sequence databases. Following trypsin digestion of the gilding samples that had been previously treated with 6 M urea, peptide analysis was performed using data-dependent acquisition of one MS scan (mass range from 400 to 2000 m/z) followed by MS/MS scans of the three most abundant ions in each MS scan. Raw data from nano-LC–MS/MS analyses were used to query non-redundant protein databases (NCBI, on all entries or with the taxonomy restriction to Chordata) using in-house MASCOT software (Matrix Science, Boston, USA), without the insertion of any fixed chemical modification but the possible oxidation of methionine and the formation of pyroglutamic acid from glutamine residues at the N-terminal position of peptides. In four samples proteins from chicken egg were identified with reasonable confidence. **Table 4** reports the identification of the proteins in the samples after trypsin digestion and LC-MS/MS analysis, with the sequences of the peptides that allowed protein identification. Interestingly, in all the samples the identification of chicken egg as the proteinaceous binder present in the painting gilding samples was allowed by the detection of ovalbumin (only in the case of sample 25, vitellogenin-2 was also identified); even more worth noting, in all the cases the peptide 128-143 (GGLEPINFQTAADQAR) has been detected and its fragmentation spectrum scored very high, thus providing the identification with high confidence.

All samples were collected from gildings on mural paintings from the 13^{th}-16^{th} centuries, and their protein content had thus undergone severe aging conditions, compared to the artificial aging performed in this study on the laboratory samples. Despite the scarcity of sample together with the very low amount of ovalbumin, the proposed DBA has been able to detect ovalbumin in such complex samples, and the results are highly reliable given the comparison with the

unambiguous identifications performed by MS-based proteomics. Moreover the tested laboratory samples were valuable for estimating the threshold density values useful in the interpretation of the results of DBAs of the gilding samples. The presence of ovalbumin in these gilding samples is in agreement with the fact that proteinaceous materials were commonly used to apply metallic leaves ensuring the cohesion between the mordant and the preparatory layers (Bonaduce et al. 2006; Bonaduce and Boon 2008).

4. CONCLUSIONS.

The need to use harsh conditions (e.g. 6 M urea) to efficiently extract proteinaceous material from a complex and aged matrix, led us to develop a fast and reliable dot-blot immunoassay (DBA) for ovalbumin detection in paint laboratory samples and in work of art samples (i.e. gildings on mural paintings) of 13^{th}-16^{th} century. The inclusion of the method of standard additions in the dot-blot immunoassay procedure (MSA-DBA) allowed the quantification of ovalbumin in fresh and artificially-aged paint laboratory samples composed of egg white binder and different pigments. Moreover the extensive analysis of differently-pigmented paint laboratory samples by MSA-DBA allowed the evaluation of the matrix effect to define threshold density values that were used as decisional parameters in the detection of ovalbumin by dot-blot immunoassay of the work of art samples.

To our knowledge, for the first time results of an immunochemical assay (i.e. dot-blot immunoassay) of work of art samples were compared with those obtained by a MS-based proteomic approach. Despite the aging, the altered conditions of conservation and the complex matrix, it was possible to detect by DBA the presence of ovalbumin in all the work of art samples

in which ovalbumin peptides were unambiguously identified by the proteomic approach, thus validating the DBA for the detection of ovalbumin in works of art. Considering the specificity of the anti-ovalbumin antibody, the DBA developed in this work can be used to assess the presence of albumen within the sample. This is an important information when deepen knowledge of the artistic techniques used in a work of art is requested, and is an advantage of DBA over the other techniques (e.g. GC-MS) that cannot discriminate between egg albumen and egg yolk.

Feasibility evaluation demonstrated that a consumer-use scanner and a freely-downloadable image analysis software can be used for the data acquisition and elaboration, thus making the developed dot-blot immunoassay methodology a potentially useful tool for commonly-equipped laboratories and for museum and conservation centre laboratories, to carry out a reliable identification of specific proteins in works of art.

Acknowledgements.

This work was supported by "Ministero dell'Istruzione, dell'Università e della Ricerca" (MIUR) grant, PRIN 2008 (2008XXAMZT). The authors wish to thank Sandro Baroni, (Sandro Baroni Restauro, Milano), for kindly providing the samples.

References.

Abramoff MD, Magalhaes PJ and Ram SJ 2004 Image Processing with ImageJ *Biophotonics Int.* **11** 36-42

Arslanoglu J, Schultz J, Loike J and Peterson K 2010 Immunology and art: using antibody-based techniques to identify proteins and gums in artworks; *J. Biosci.* **35** 3-10

Blazkova M, Mickova-Holubova B, Rauch P and Fukal L 2009 Immunochromatographic colloidal carbon-based assay for detection of methiocarb in surface water; *Biosens. Bioelectron.* **25** 753-758

Bonaduce I and Boon JJ 2008 An integrated mass spectrometric and molecular imaging analytical approach to identify and localise constituents in paintings applied to gilded multilayer structures from 14^{th} to 16^{th} C works of art; In: New trends in analytical, environmental and cultural heritage chemistry (eds) Colombini MP and Tassi L (Kerala, India: Research Signpost, Transworld Research Network) pp 389-423

Bonaduce I, Carlyle L, Colombini MP, Duce C, Ferrari C, Ribechini E, Selleri P and Tiné MR 2012 New insights into the ageing of linseed oil paint binder: a qualitative and quantitative analytical study; *PLoS One* DOI 10.1371/journal.pone.0049333

Bonaduce I, Cito M and Colombini MP 2009 The development of a gas chromatographic-mass spectrometric analytical procedure for the determination of lipids, proteins and resins in the same paint micro-sample avoiding interferences from inorganic media; *J. Chromatogr. A* **1216** 5931-5939

Bonaduce I, Colombini MP and Diring S 2006 Identification of garlic in old gildings by gas chromatography–mass spectrometry; *J. Chromatogr. A* **1107** 227-232

Bradford MM 1976 Rapid and sensitive method for the quantitation of microgram quantities of protein utilizing the principle of protein-dye binding; *Anal. Biochem.* **72** 248-254

Cartechini L, Vagnini M, Palmieri M, Pitzurra L, Mello T, Mazurek J and Chiari G 2010 Immunodetection of proteins in ancient paint media; *Acc. Chem. Res.* **43** 867-876

Cennini C 1954 The craftsman's handbook (New York: Dover publications)

Colombini MP and Modugno F 2004 Characterization of proteinaceous binders in artistic paintings by chromatographic techniques; *J. Sep. Sci.* **27** 147-160

Colombini MP, Andreotti A, Bonaduce I, Modugno F and Ribechini E 2010 Analytical strategies for characterizing organic paint media using Gas Chromatography/Mass Spectrometry; *Acc. Chem. Res.* **43** 715-727

Cotte M, Checroun E, Mazel V, Solé VA, Richardin P, Taniguchi Y, Walter P and Susini J 2009 Combination of FTIR and X-RAYS Synchrotron-Based Micro-Imaging Techniques for the Study of Ancient Paintings. A Practical Point of View; *e-Preserv. Sci.* **6** 1-9

Cotte M, Susini J, Solé VA, Taniguchi Y, Chillida J, Checroun E and Walter P 2008 Applications of synchrotron-based micro-imaging techniques to the chemical analysis of ancient paintings; *J. Anal. At. Spectrom.* **23** 820-828

Dallongeville S, Koperska M, Garnier N, Reille-Tailefert G, Rolando C and Tokarski C 2011 Identification of Animal Glue Species in Artworks Using Proteomics: Application to a 18th Century Gilt Sample; *Anal. Chem.* **83** 9431-9437

Dolci LS, Sciutto G, Guardigli M, Rizzoli M, Prati S, Mazzeo R, Roda A 2008 Ultrasensitive chemiluminescent immunochemical identification and localization of protein components in painting cross-section by microscope low-light imaging; *Anal. Bioanal. Chem.* **329** 29-35

Duce C, Ghezzi L, Onor M, Bonaduce I, Colombini MP, Tinè MR and Bramanti E 2012 Physico-chemical characterization of protein–pigment interactions in tempera paint reconstructions: casein/cinnabar and albumin/cinnabar; *Anal. Bioanal. Chem.* **402** 2183-2193

Fremout W, Dhaenens M, Saverwyns S, Sanyvova J, Vandenabeele P and Deforce D 2010 Tryptic peptide analysis of protein binders in works of art by liquid chromatography-tandem mass spectrometry; *Anal. Chim. Acta* **658** 156-162

Fremout W, Dhaenens M, Saverwyns S, Sanyova J, Vandenabeele P, Deforce D and Moens L 2012 Development of a dedicated peptide tandem mass spectral library for conservation science; *Anal. Chim. Acta* **728** 39-48

Gil JRN, Sbihi Y, Alvarez PA, Maache M, Larrubia M, Rojas J and Osuna A 2003 Development of a dot-blot system to detect gluten in food; *Food Agric. Immunol.* **15** 235-242

Gimeno-Adelantado JV, Mateo-Castro R, Domenech-Carbò MT, Bosch-Reig F, Domenech-Carbò A, de la Cruz-Canizares J and Casas-Catalan MJ 2002 Analytical study of proteinaceous binding media in works of art by gas chromatography using alkyl chloroformates as derivatising agents; *Talanta* **56** 71-77

Guillemin N, Meunier B, Jurie C, Cassar-Malek I, Hocquette JF, Leveziel H, Picard B 2009 Validation of a dot-blot quantitative techinque for large scale analysis of beef tenderness biomarkers; *J. Physiol. Pharmacol.* **60** 91-97

Hawkes R, Niday E, Gordon J 1982 A dot-immunobinding assay for monoclonal and other antibodies; *Anal. Biochem.* **119** 142-147

Heginbotham A, Millay V, Quick M 2006 The Use of Immunofluorescence Microscopy and Enzyme-Linked Immunosorbent Assay as Complementary Techniques for Protein Identification in Artists' Materials; *J. Am. Inst. Conserv.* **45** 89-105

Howey JE, Browning MC and Fraser CG 1987 Assay of serum fructosamine that minimizes standardization and matrix problems: use to assess components of biological variation; *Clin. Chem.* **33** 269-272

Kockaert L, Gausset P and Dubi-Rucquoy M 1989 Detection of ovalbumin in paint media by immunofluorescence; *Stud. Conservat.* **34** 183-188

Laemmli UK 1970 Cleavage of structural proteins during the assembly of the head of bacteriophage T4 *Nature* **227** 680-685

Leo G, Bonaduce I, Andreotti A, Marino G, Pucci P, Colombini MP and Birolo L 2011 Deamidation at asparagine and glutamine as a major modification upon deterioration/aging of proteinaceous binders in mural paintings; *Anal. Chem.* **83** 2056-2064

Leo G, Cartechini G, Pucci P, Sgamellotti A, Marino G and Birolo L 2009 Proteomic strategies for the identification of proteinaceous binders in paintings; *Anal. Bioanal. Chem.* **395** 2269-2280

Lluveras A, Bonaduce I, Andreotti A and Colombini MP 2010 A GC/MS analytical procedure for the characterization of glycerolipids, natural waxes, terpenoid resins, proteinaceous and polysaccharide materials in the same paint micro sample avoiding interferences from inorganic media; *Anal. Chem.* **81** 376-386

Matsumoto M, Tsunematsu K, Tsuji A, Kido Y 1997 Enzyme immunoassay using peroxidase as a label and a dip-strip test for monitoring residual bacitracin in chicken plasma; *Anal. Chim. Acta* **346** 207-213

Matteini M and Moles A 2003 La chimica nel restauro. I materiali nell'arte pittorica (Firenze, Italy: Nardini Editore)

Morozova VS, Levashova AI and Eremin SA 2005 Determination of pesticides by enzyme immunoassay; *J. Anal. Chem.* **60** 202-217

Motulsky HJ and Brown RE 2006 Detecting outliers when fitting data with nonlinear regression-a new method based on robust nonlinear regression and the false discovery rate; *BMC Bioinf.* **7** 1-20

Palmieri M, Vagnini M, Pitzurra L, Rocchi P, Brunetti BG, Sgamellotti A and Cartechini A 2011 Development of an analytical protocol for a fast, sensitive and specific protein recognition in paintings by enzyme-linked immunosorbent assay (ELISA); *Anal. Bioanal. Chem.* **399** 3011-3023

Phenix A 1997 The composition and chemistry of eggs and egg tempera; In: Early Italian Paintings: Techniques and Analysis (Symposium, Maastricht, 9-10 October 1996) (eds)

Bakkenist T, Hoppenbrouwers R and Dubois H (Maastricht: Limburg Conservation Institute) pp 11-20

Potenza M, Sabatino G, Giambi F, Rosi L, Papini AM, Dei L 2012 Analysis of egg-based model wall paintings by use of an innovative combined dot-ELISA and UPLC-based approach; *Anal. Bioanal. Chem.* DOI 10.1007/s00216-012-6049-9

Ramirez-Barat B and de la Vina S 2001 Characterization of proteins in paint media by immunofluorescence. A note on methodological aspects; *Stud. Conservat.* **46** 282-288

Rampazzi L, Andreotti A, Bonaduce I, Colombini MP, Colombo C, and Toniolo L 2004 Analytical investigation of calcium oxalate films on marble monuments; *Talanta* **63** 967-977

Rasmussen KL, Lluveras AT, Bonaduce I, Colombini MP, Birolo L, Galano E, Amoresano A, Doudna G, Bond AD, Palleschi V, Lorenzetti G, Legnaioli S, van der Plicht J and Gunneweg J 2012 The constituents of the ink from a Qumran inkwell: new prospects for provenancing the ink on the Dead Sea Scrolls; *J. Archaeol. Sci.* **39** 2956-2968

Read SM and Northcote DH 1981 Minimization of variation in the response to different proteins of the Coomassie blue G dye-binding assay for protein; *Anal. Biochem.* **116** 53-64

Schubert-Ullrich P, Rudolf J, Ansari P, Galler B, Fuhrer M and Molinelli A 2009 Commercialized rapid immunoanalytical tests for determination of allergenic food proteins: an overview; *Anal. Bioanal. Chem.* **395** 69-81

Sciutto G, Dolci LS, Buragina A, Prati S, Guardigli M, Mazzeo R and Roda A 2011 Development of a multiplexed chemiluminescent immunochemical imaging technique for the

simultaneous localization of different proteins in painting micro cross-section; *Anal. Bioanal. Chem.* **399** 2889-2897

Scott DA, Warmlander S, Mazurek J and Quirke S 2009 Examination of some pigments, grounds and media from Egyptian cartonnage fragments in the Petrie Museum, University College London; *J. Archaeol. Sci.* **36** 923-932

Tijssen P 1985 Practice and theory of enzyme immunoassays (Amsterdam: Elsevier)

Tokarski C, Martin E, Rolando E and Cren-Olivé C 2006 Identification of proteins in renaissance paintings by proteomics; *Anal. Chem.* **78** 1494-1502

Toniolo L, D'Amato A, Saccenti R, Gulotta D and Righetti PG 2012 The silk road, Marco Polo, a bible and its proteome: a detective story; *J. Proteomics* **75** 3365-3373

UNI 2001 Italian standard UNI 10925: cultural heritage (Milano, Italy: Ente nazionale italiano di unificazione)

Vagnini M, Pitzurra L, Cartechini L, Miliani C, Brunetti BG and Sgamellotti A 2008 Identification of proteins in painting cross-sections by immunofluorescence microscopy; *Anal. Bioanal. Chem.* **392** 57-64

Van der Weerd J, Brammer H, Boon JJ and Heeren RMA 2002 Fourier transform infrared microscopic imaging of an embedded paint cross-section; *Appl. Spectrosc.* **56** 275-283.

Yamada N, Ozawa S, Kageyama N and Miyano H 2004 Detection and quantification of protein residues in food grade amino acids and nucleic acids using a dot-blot fluorescent staining method *J. Agric. Food Chem.* **52** 5329-5333

Zevgiti S, Sakarellos C, Sakarellos-Daitsiotis M, Ioakimoglou E and Panou-Pomonis E 2007 Collagen models as a probe in the decay of works of art: synthesis, conformation and immunological studies; *J. Pept. Sci.* **13** 121-127

Tables.

Table 1

Ovalbumin quantified by dot-blot immunoassay of pigmented painting laboratory samples. Protein amounts detected in the same samples by colorimetric and thermogravimetric methods are also reported.

sample pigment	protein amount (% ± SD)[a]		immunodetected ovalbumin (% ± SD)[a]
	colorimetric method	TGA method	
Azurite	52.2 ± 3.3	67.0 ± 3.4	308.8 ± 22.0
Red ochre	54.5 ± 0.3	64.4 ± 3.2	142.0 ± 48.8
Minium	37.4 ± 3.7	51.0 ± 2.6	139.5 ± 10.8
Cinnabar	38.2 ± 0.4	n.d.[b]	90.7 ± 14.7
Calcite	22.0 ± 1.4	23.4 ± 1.2	69.8 ± 25.3

[a] Data are reported as percent of weighted sample material ± SD **(**n = 3).

[b] n.d., not detectable (see "Experimental Section").

Table 2

Ovalbumin quantified by applying method of standard additions to the dot-blot immunoassay (MSA-DBA) of fresh and aged pigmented painting laboratory samples.

Sample pigment	Immunodetected ovalbumin[a]			
	ng		RSD%[b]	
	fresh	aged	fresh	aged
Azurite	4.3	4.6	20.9	19.6
Red ochre	4.4	4.3	6.8	7.0
Minium	3.5	3.6	2.9	13.9
Cinnabar	4.0	2.8	25.0	14.3
Calcite	2.2	2.0	31.8	25.0

[a] Values reported represent the amount of ovalbumin immunodetected in 6.8 ng of painting laboratory sample, with the exception of calcite (13.7 ng). No statistically significant differences between fresh and aged painting laboratory samples were determined by Student's *t*-test analysis ($p < 0.05$).

[b] n = 3

Table 3

Ancient samples from Saint Francesco Church in Lodi (Italy): dot-blot immunoassay analysis for ovalbumin.

sample name	ovalbumin presence[a]
13	+ +
18	-
19	+ + +
20	+ / -
22	+
25	+ +
28	+ / -

[a] Evaluation of ovalbumin presence based on the frequency distribution of the sample density from four dot-blot immunoassay replicates in the classes delimitated by the calculated threshold density values.

Table 4

Identification of proteins in gilding samples by proteomic strategies.

Sample	Protein[a] (accession number)	Matched sequence (Oxidation of methionine, and pyro-Glu formation at Gln at the N-terminus of peptides were inserted as variable modifications in the MS/MS Ion Search Program)
13	Ovalbumin (P01012)	^{106}LYAEER^{111} ^{128}GGLEPINFQTAADQAR^{143}
18	n.d.	n.d.
19	Ovalbumin (P01012)	^{220}VASMASEK^{227} ^{265}LTEWTSSNVMEER^{277} ^{128}GGLEPINFQTAADQAR^{143} ^{324}ISQAVHAAHAEINEAGR^{340}
20	n.d.	n.d.
22	Ovalbumin (P01012)	^{128}GGLEPINFQTAADQAR^{143}
25	Ovalbumin (P01012)	^{220}VASMASEK^{227} ^{128}GGLEPINFQTAADQAR^{143} ^{324}ISQAVHAAHAEINEAGR^{340} ^{144}ELINSWVESQTNGIIR^{159}
	Vitellogenin-2 (P02845)	^{1515}MVVALTSPR^{1523}+ Oxidation (M) ^{260}QQLTLVEVR^{268}
28	n.d.	n.d.

[a] n.d., not detectable

Figure legends.

Figure 1

Intra-assay precision profile of response of dot-blot immunoassay at different ovalbumin amounts. Response variability (RSD%) of 4 independent densitometric analyses (rhomb, square, full triangle, empty triangle) carried out on the same membrane containing 3 replicates of each set of the indicated ovalbumin amounts in 6 M urea is reported.

Figure 2

Immunospecificity of the anti-ovalbumin antibody. Developed membrane of dot-blot immunoassay of high amounts of proteinaceous binders and conservation materials for artworks (egg white, EW; casein, CAS; rabbit glue, glue), and bovine serum albumin (BSA), fish gelatine (FG) and ovalbumin (OVA) in 6 M urea. Sample amounts are indicated on the left. The line with negative controls (6 M urea in the absence of sample) is indicated (-).

Figure 3

Quantification of ovalbumin in egg white painting laboratory samples by the application of method of standard additions to dot-blot immunoassay (MSA-DBA). Values reported (white bars) represent the amount of ovalbumin immunodetected in 6.8 ng of sample in 6 M urea with the exception of calcite painting laboratory samples (13.7 ng). Quantification of protein in the same samples by colorimetric (pointed bar) and thermogravimetric (dashed bars) methods are also reported. Error bars represent ± SD from the mean of three independent measurements. The *p*-values obtained by ANOVA analysis were all greater than 0.05, except for minium (0.0028)

for which a post-hoc analysis (Tukey's HSD, $p < 0.05$) was performed: means sharing the same letter are not significantly different from each other.

Figure 1
Click here to download high resolution image

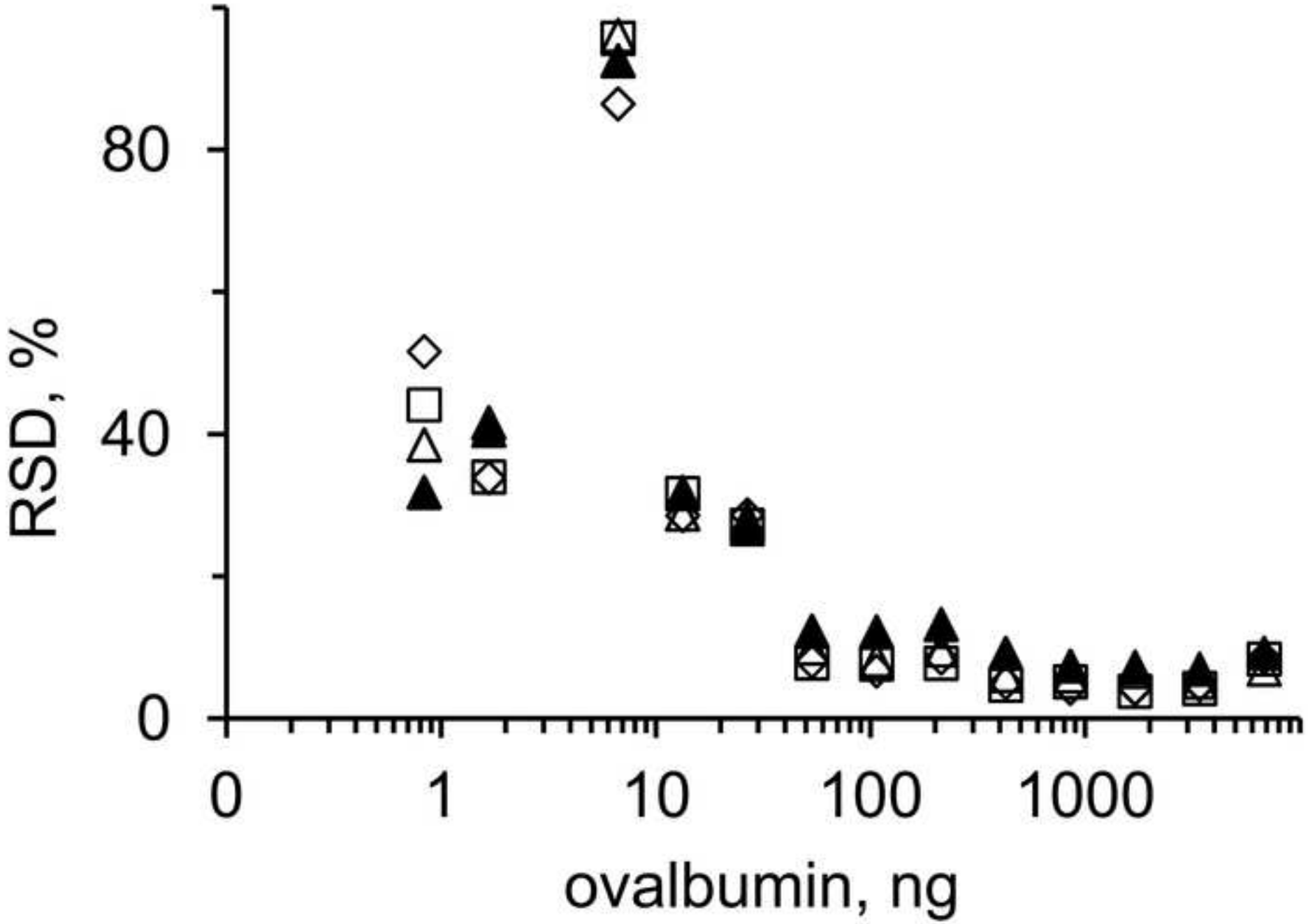

Figure 2
Click here to download high resolution image

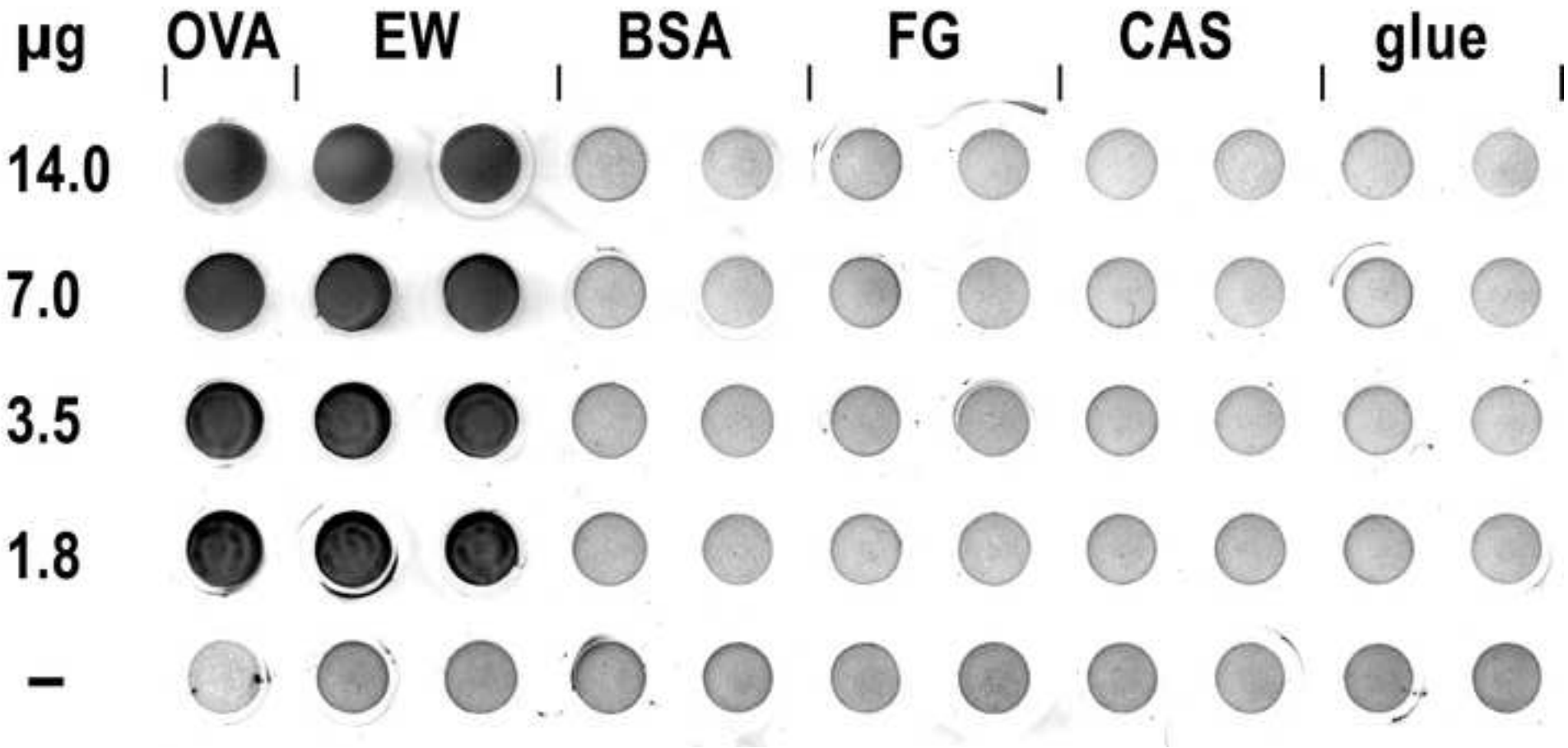

Figure 3
Click here to download high resolution image

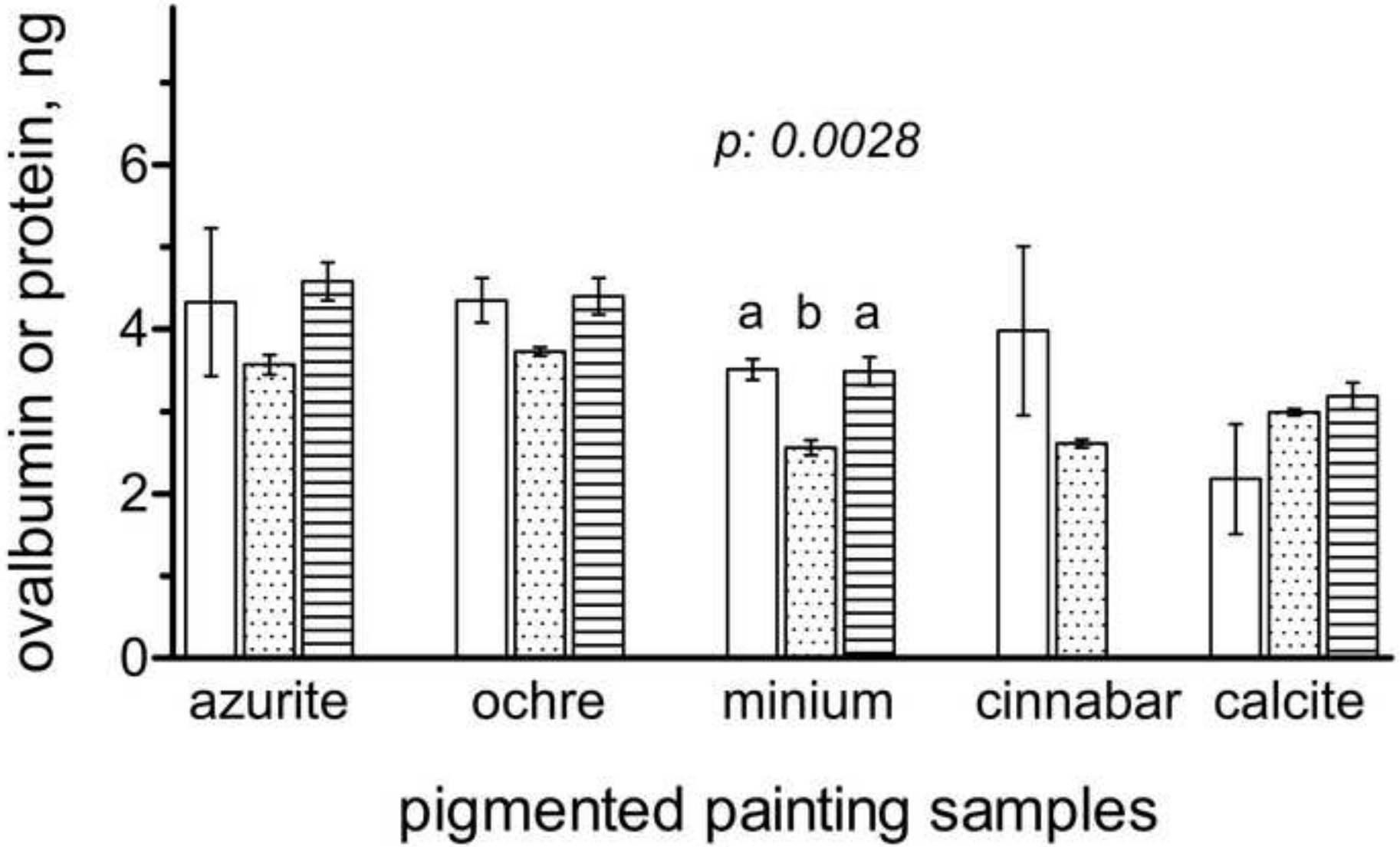

Electronic Supplementary Material

Click here to download Electronic Supplementary Material: Supporting information JBS.doc

Electronic Supplementary Material (source file of figure s_1)
Click here to download Electronic Supplementary Material: figura S_1.tif